



City Research Online

City, University of London Institutional Repository

Citation: Wong, S. S-W. (1998). Collapse behaviour of micro-concrete box girders bridges. (Unpublished Doctoral thesis, City, University of London)

This is the accepted version of the paper.

This version of the publication may differ from the final published version.

Permanent repository link: <https://openaccess.city.ac.uk/id/eprint/30987/>

Link to published version:

Copyright: City Research Online aims to make research outputs of City, University of London available to a wider audience. Copyright and Moral Rights remain with the author(s) and/or copyright holders. URLs from City Research Online may be freely distributed and linked to.

Reuse: Copies of full items can be used for personal research or study, educational, or not-for-profit purposes without prior permission or charge. Provided that the authors, title and full bibliographic details are credited, a hyperlink and/or URL is given for the original metadata page and the content is not changed in any way.

COLLAPSE BEHAVIOUR OF MICRO-CONCRETE BOX GIRDERS BRIDGES

DISSERTATION SUBMITTED TO THE CITY UNIVERSITY
FOR THE DEGREE OF DOCTOR OF PHILOSOPHY

BY

Eur Ing SAMUEL SUN-WING WONG
BSc (Eng) CEng MStructE MICE

DECEMBER 1997

PREFACE

The work described in this dissertation was partly carried out in the Concrete Laboratory in the Cement and Concrete Association, (now British Cement Association), Wexham Spring and also at the Civil Engineering Laboratory of the City University, London. The research Project was carried out under a Co-operative Award in Science and Engineering in conjunction with the Cement and Concrete Association and the Science and Engineering Research Council.

I gratefully acknowledge the advice and constant encouragement from my supervisor Professor L F Boswell, who originally proposed this research project.

I am in debt to many members of the laboratory staff both at the Cement and Concrete Association and at the City University for their skill and assistance in my extensive experimental work. In particular, the help from Mr W A Jones at the University has been of great value.

I would also like to thank my wife, Fung-Luen for her constant encouragement, support and sacrifices made during my time at the University and in particular, for her unfailing patience and tolerance during my extended writing period.

Except where reference is made to the works of others, this dissertation describes my own work.

SUMMARY

The behaviour of micro-concrete in shear has been studied. The experimental result from the shear tests was used to modify an established generalised yield criterion that could be applied to reinforced concrete and prestressed concrete slab elements. The elements form part of a model structure such as box girders in which micro concrete was used as the model material.

The generalised yield line considered stress resultants including transverse bending moment, in-plane normal forces and shear forces along the yield line. The modified yield expression was compared with available experimental results from the literature. Possible collapse mechanisms and local failure modes were studied.

The experimental work on shear included Mattock type push-off shear tests. They were conducted to evaluate the shear behaviour of micro-concrete comparing with the behaviour of normal concrete. Ultimate load tests were carried out on four concrete box girder models. The first test model was to investigate the collapse behaviour of an internal web of a twin-cell simply supported concrete box beam. The second test was on a restrained single cell beam, designed to represent an outer cell of a multi-cell continuous box beam. The third test was on a twin-cell two span continuous prestressed concrete box beam. The final test was conducted on a multi-cell two span continuous reinforced concrete box girder.

The results predicted using the modified yield criterion were compared with those obtained from the experimental work.

The last chapter discussed the suitability of the method for predicting collapse loads was discussed and conclusions drawn.

TABLE OF CONTENTS

| | page |
|---|------|
| <u>Title page</u> | |
| <u>Preface</u> | -1 |
| <u>Summary</u> | -2 |
| <u>Table of Contents</u> | -3 |
| <u>List of Symbols</u> | -7 |
| <u>List of Figures</u> | -10 |
| | |
| <u>Chapter 1. Introduction</u> | -16 |
| | |
| <u>Chapter 2. Shear Behaviour of Micro-concrete</u> | |
| 2.1 Introduction | -19 |
| 2.2 The Mattock Shear Specimens | -20 |
| 2.3 Description of Shear Test | -22 |
| 2.4 Instrumentation | -24 |
| 2.5 Material Used for Shear Specimens | |
| 2.5.1 Concrete | -25 |
| 2.5.2 Reinforcement | -28 |
| 2.5.3 Formwork for Casting of Shear Specimens | -30 |
| 2.6 The Experimental Procedure | -31 |
| 2.7 The Experimental Observations | |
| 2.7.1 Symmetrically Reinforced Specimens | -33 |
| 2.7.2 Non-symmetrically Reinforced Specimens | -36 |
| 2.8 Surface Strain Measurement | -39 |
| 2.9 The Results and Their Interpretations | |
| 2.9.1 Shear Stress versus Normal Displacement | -40 |
| 2.9.2 Shear Displacement versus Normal Displacement | -42 |
| 2.9.3 Shear Stress versus Reinforcement Parameter | -43 |
| 2.9.4 Dimensionless Shear Stress versus Reinforcement Parameter | -44 |

| | | |
|--|---|------|
| 2.9.5 | Results of Non-symmetrically Reinforced Specimens | -45 |
| 2.10 | Summary of the Results of the Mattock Shear Tests | -46 |
| | | |
| <u>Chapter 3 Yield Criterion For Reinforced and Prestressed Concrete</u> | | |
| 3.1 | Introduction | -64 |
| 3.2 | General Plastic Theory | |
| 3.2.1 | Yield Condition and Yield Surface | -65 |
| 3.2.2 | Flow Rule and Normality Rule | -65 |
| 3.2.3 | Lower Bound and Upper Bound Theorem | -66 |
| 3.3 | Yield Criterion of Concrete Elements | |
| 3.3.1 | Yield Criterion of Concrete Element Subjected to Bi-axial Stresses | -67 |
| 3.3.2 | Yield Criterion of Concrete Subjected to Bending and Axial Forces | -69 |
| 3.3.3 | Yield Criterion of Concrete Subjected to Shear and Axial Force | -75 |
| 3.3.4 | Yield Criterion of Concrete Subjected to Bending, Shear and Axial Force | -76 |
| 3.3.5 | Work Equations and Equilibrium Equations | -87 |
| 3.4 | Yield Criterion for Reinforced Concrete | -89 |
| 3.5 | Yield Criterion Applied To Prestressed Concrete | -95 |
| 3.6 | Summary | -97 |
| | | |
| <u>Chapter 4 Ultimate Collapse Analysis Of Concrete Box Girders</u> | | |
| 4.1 | Introduction | -100 |
| 4.2 | Previous Work on Analysis and Design of Concrete Box Girders | -101 |
| 4.3 | Elastic Analysis of Box Girders | |
| 4.3.1 | Structural Actions In Box-beams | -103 |

| | | |
|---------|--|------|
| 4.3.1.1 | Distortion | |
| 4.3.1.2 | Warping | |
| 4.3.1.3 | Shear Lag | |
| 4.3.1.4 | St Venant Torsional Shear Stress | |
| 4.3.1.5 | Local Effect of The Flanges | |
| 4.3.2 | Methods Of Elastic Analysis | -106 |
| 4.4 | Plastic Analysis of Concrete Box Girders | -107 |
| 4.4.1 | Simply Supported Single Cell Box Beams | -109 |
| 4.4.2 | Continuous Single Cell Box Beams | -111 |
| 4.4.3 | Continuous Multi-Cell Box Beams | -112 |
| 4.4.4. | Twisting work of flanges, webs and diaphragms | -113 |
| 4.4.5 | Failure Mechanism in Webs | -114 |
| 4.5 | Summary | -118 |

Chapter 5 Concrete Box Girder Model Experiments

| | | |
|-------|--|------|
| 5.1 | Introduction | -127 |
| 5.2 | Formwork and Material | |
| 5.2.1 | Formwork | -129 |
| 5.2.2 | Micro Concrete | -130 |
| 5.2.3 | Reinforcement | -132 |
| 5.3 | Instrumentation | |
| 5.3.1 | Load Cells and Proving Ring | -135 |
| 5.3.2 | Strain Measurement | -136 |
| 5.3.3 | Deflection Measurement | -137 |
| 5.4 | Idealised Internal Web and Flanges of a Simply Supported Girder | -138 |
| 5.5 | Idealised External Flanges and Web of continuous girder. | -141 |
| 5.6 | Multi-cell Two Span Continuous Reinforced Concrete Box Girder | -143 |
| 5.7 | Multi-cell Two Span Continuous Prestress Concrete Box Girder | -145 |

| | | |
|---------------------------------------|--|------|
| 5.8 | Summary | -147 |
| | | |
| <u>Chapter 6 Experimental results</u> | | |
| 6.1 | Introduction | -184 |
| 6.2 | Comparison of Experimental and Theoretical Results | |
| 6.2.1 | Collapse Loads | -185 |
| 6.3 | Experimental Observations | |
| 6.3.1 | Box Beam B1 | -188 |
| 6.3.2 | Box beam B2 | -192 |
| 6.3.3 | Box Beam B3 | -195 |
| 6.3.4 | Box Beam B4 | -197 |
| 6.4 | Summary | -198 |
| | | |
| <u>Chapter 7 Conclusion</u> | | -239 |
| | | |
| <u>References</u> | | -244 |
| | | |
| <u>Appendix A</u> | Parametric Yield Surface Computation | |
| Appendix B | Collapse Load computation | |
| Appendix C | Further Literature review | |

LIST OF SYMBOLS

Some symbols that are defined locally in the text are not included in the following list.

A dot on top of the symbol indicates rate of change

| | | |
|-----------------|---|--|
| A_c, A_{cr} | - | area of concrete section |
| A_p | - | area of prestressed reinforcement per unit width |
| A_s | - | area of reinforcement per unit width |
| b | - | width of cell considered, width of section |
| D | - | internal work or energy dissipation |
| d | - | depth of section |
| d_1 | - | position of reinforcement layer related to centre line of the slab element |
| E_s | - | Elastic modulus of reinforcement |
| e_0 | - | direct strain at mid layer of section |
| e_i, e_x, e_y | - | direct strain in the i, x, y direction |
| e_n | - | normal strain |
| e_{nt} | - | shear strain |
| e_t | - | tangential strain |
| F_u | - | Yield load of reinforcement |
| f_{cu} | - | 28 day concrete cube strength |
| f_y, f_s | - | yield stress and service stress of reinforcement |
| f_{yp} | - | yield stress of prestressing reinforcement |
| $f(\sigma_i)$ | - | yield condition in stress tensor, where $f=0$ indicates yielding |
| h | - | thickness/depth of section |
| L | - | span length |
| M_c | - | yield moment at the flange web junction |
| M_n, M | - | bending moment normal to shear plane |
| M_p | - | plastic yield moment |

| | | |
|------------|---|---|
| M_t | - | transverse moment across the shear plane |
| m_n | - | non-dimensional moment parametric term |
| N_n, N | - | normal force perpendicular to the failure plane |
| N_{nt} | - | shear force along the failure plane |
| N_t | - | tangential force perpendicular to the failure plane |
| n | - | number of cells |
| n_n | - | non-dimensional normal stress parameter |
| n_{nt} | - | non-dimensional shear stress parameter |
| P_b | - | load required to form mid-span plastic hinges |
| P, P_c | - | collapse load |
| P_d | - | distortional load at collapse |
| $Q,$ | - | shear force along shear plane |
| T_h, T_w | - | twisting moment about the shear plane |
| t | - | thickness of web element |
| t_f | - | thickness of flanges |
| v_{cr} | - | cracking stress |
| U | - | log function of strain rate ration term |
| v_n, v_u | - | shear stress |
| V_u | - | Ultimate Shear Load |
| W_b | - | total work in bottom flanges |
| W_T | - | twisting work in the end diaphragms, flanges and webs |
| W_t | - | total work in top flanges excluding twisting |
| W_w | - | total work in webs excluding twisting |
| w | - | self weight dead load per unit length of member |
| Z_n | - | distance of neutral axis from mid depth of section |
| z | - | depth from mid depth of section |

| | | |
|--------------------------------|---|---|
| α | - | shear ductility reduction factor |
| α' | - | uniform shear strain rate |
| β | - | strain rate ratio at top surface of slab |
| γ | - | strain rate ratio at bottom surface |
| γ_m | - | material strength factor |
| δ | - | strain rate ratio at bottom surface of slab; |
| Δ | - | deflection under point load |
| Δ_n, Δ_x | - | normal displacement across the yield zone; crack width; yield zone width |
| Δ_{nt}, Δ_s | - | shear displacement along the yield zone |
| ϵ_n | - | direct strain normal to yield surface at centre of section |
| ϵ_{nt} | - | shear strain at centre of section |
| ϵ_{Th} | - | tangential strain at centre of section |
| Θ_n | - | bending rotation of yield hinge |
| θ | - | angle of rotation of yield hinges |
| k | - | curvature or curvature rate |
| λ | - | flow rule parametric constant |
| ρ | - | reinforcement ratio A_s/A_c |
| ρ_p | - | prestressing reinforcement ratio A_p/A_c |
| σ_c | - | uni-axial compressive strength of concrete |
| σ_n | - | normal stress, |
| σ_t | - | tangential stress |
| $\sigma_i, \sigma_x, \sigma_y$ | - | stress in i, x, y direction |
| τ, τ_{xy} | - | shear stress |
| Φ | - | yield surface equation |
| ϕ | - | angle of rotation of yield hinges; function of strain rate ration term |

LIST OF FIGURES

- FIGURE 2.1 MATTOCK SHEAR SPECIMEN
- FIGURE 2.2 SYMMETRICAL REINFORCED SPECIMEN
- FIGURE 2.3 UNSYMMETRICAL REINFORCED SPECIMEN
- FIGURE 2.4 STRESS-STRAIN CURVE FOR 1.07mm WIRE
- FIGURE 2.5 LOAD STRAIN CURVE FOR 1/8" WIRE
- FIGURE 2.6 LOAD STRAIN CURVE FOR 6mm REINFORCING BAR
- FIGURE 2.7 TIMBER FORMWORK FOR SHEAR SPECIMEN
- FIGURE 2.8 HALF SIZE SPECIMEN REINFORCING CAGE AND FORMWORK
- FIGURE 2.9 CRACKING ALONG SHEAR PLANE
- FIGURE 2.10 FULL SIZE AND HALF SIZE SPECIMEN
- FIGURE 2.11 TENTH SCALE SPECIMEN IN TENSIO METER
- FIGURE 2.12 NON-SYMMETRICAL REINFORCED SPECIMEN LARGER CRACK WIDTH ON LOW REINFORCED SURFACE
- FIGURE 2.13 NON-SYMMETRICAL REINFORCED SPECIMEN SMALLER CRACK WIDTH ON HIGH REINFORCED SURFACE
- FIGURE 2.14 SHEAR STRESS Vs NORMAL DISPLACEMENT
- FIGURE 2.15 Δ_s Vs Δ_n CURVE (TYPICAL SHEAR DISPLACEMENT Vs NORMAL DISPLACEMENT)
- FIGURE 2.16 SHEAR STRESS Vs NORMAL STRESS
- FIGURE 2.17 NON-DIMENSIONAL SHEAR STRESS Vs NORMAL STRESS
- FIGURE 2.18 NON-DIMENSIONAL SHEAR STRESS Vs BENDING
- FIGURE 3.1 BI-AXIAL YIELD SURFACE OF CONCRETE (SQUARE YIELD CRITERION)

- FIGURE 3.2 TYPICAL YIELD LINE AND STRESS - STRAIN RELATIONSHIP
- FIGURE 3.3 DISPLACEMENT RATES IN A GENERALISED YIELD LINE
- FIGURE 3.4 NORMAL STRAIN DISTRIBUTION
- FIGURE 4.1 DISTORTION OF CROSS SECTION DUE TO SYMMETRICAL LOADING
- FIGURE 4.2 DISTORTION OF CROSS SECTION DUE TO ASYMMETRICAL LOADING
- FIGURE 4.3 WARPING DISPLACEMENT OF BOX BEAM
- FIGURE 4.4 SHEAR LAG IN BENDING
- FIGURE 4.5 BENDING STRESS DISTRIBUTION IN A BOX BEAM CROSS SECTION
- FIGURE 4.6 St VENANT TORSIONAL SHEAR STRESS DISTRIBUTION IN A BOX BEAM
- FIGURE 4.7 TRANSVERSE BENDING STRESS IN TOP FLANGE UNDER HEAVY WHEEL POINT LOAD
- FIGURE 4.8 PUNCHING SHEAR OF TOP SLAB UNDER WHEEL LOAD
- FIGURE 4.9 SINGLE CELL BOX GIRDER COLLAPSE MECHANISM PROPOSED BY SPENCE
- FIGURE 4.10 TYPICAL SINGLE CELL CONTINUOUS BOX BEAM AND IDEALISED COLLAPSE MECHANISM
- FIGURE 4.11 ALTERNATIVE COLLAPSE MECHANISM IN MULTI-CELL BOX BEAMS
- FIGURE 4.12 BRAESTRUP'S SHEAR MECHANISM IN A LOADED WEB
- FIGURE 4.13 FAILURE MECHANISM PROPOSED BY REGAN AND PLACAS
- FIGURE 5.1 TWIN CELL BOX BEAM B1
- FIGURE 5.2 FABRICATION DRAWING FOR BOX BEAM B1, EDGE STEEL TRUSS

- FIGURE 5.3 REINFORCEMENT DETAIL OF 2-CELL BOX B1
- FIGURE 5.4 REINFORCEMENT DETAIL OF BOTTOM FLANGE FOR BEAM B1
- FIGURE 5.5 REINFORCEMENT DETAILS OF END DIAPHRAGMS
- FIGURE 5.6 LAYOUT OF STRAIN GAUGES
- FIGURE 5.7 LAYOUT OF WEB STRAIN GAUGES
- FIGURE 5.8 LAYOUT OF DEMEC GAUGES TO BOTTOM FLANGE
- FIGURE 5.9 LAYOUT OF DEMEC GAUGES TO TOP FLANGE
- FIGURE 5.10 LAYOUT OF DEMEC GAUGES TO LOAD WEB
- FIGURE 5.11 LOCATION OF DISPLACEMENT GAUGES
- FIGURE 5.12 TESTING OF EDGE STEEL TRUSS FRAMES
- FIGURE 5.13 BOTTOM FLANGE AND WEB REINFORCEMENT
- FIGURE 5.14 COMPLETION OF TOP REINFORCEMENT CAGE
- FIGURE 5.15 REINFORCEMENT DETAILS FOR IDEALISED EXTERNAL FLANGE AND WEB ELEMENT B2
- FIGURE 5.16 MID SPAN SECTION FOR BEAM B2
- FIGURE 5.17 LONGITUDINAL SECTION FOR BEAM B2
- FIGURE 5.18 TOP REINFORCEMENT FOR BEAM B2
- FIGURE 5.19 BOTTOM REINFORCEMENT FOR BEAM B2
- FIGURE 5.20 BEAM B2 READY FOR CONCRETING
- FIGURE 5.21 BEAM B2 SET UP READY FOR TESTING
- FIGURE 5.22 TYPICAL PIN SUPPORT WITH LOAD CELL

- FIGURE 5.23 TYPICAL ROLLER SUPPORT WITH LOAD CELL
- FIGURE 5.24 CANTILEVER END RESTRAINT FOR BEAM B2
- FIGURE 5.25 PLAN AND ELEVATION FOR BOX BEAM B3
- FIGURE 5.26 REINFORCEMENT DETAILS FOR BOX BEAM B3
- FIGURE 5.27 DIAPHRAGM REINFORCEMENT DETAIL FOR BEAM B3
- FIGURE 5.28 BOX BEAM B3 BOTTOM CAGE
- FIGURE 5.29 BOX BEAM B3 READY FOR CONCRETING
- FIGURE 5.30 BOX BEAM B3 EXTERIOR FLANGE WEB TEST
- FIGURE 5.31 BOX BEAM B3 INTERIOR FLANGE WEB TEST
- FIGURE 5.32 PRESTRESSED BOX BEAM B4 PLAN AND SECTIONS
- FIGURE 5.33 BOX BEAM B4 TOP FLANGE REINFORCEMENT DETAILS
- FIGURE 5.34 BOX BEAM B4 BOTTOM FLANGE REINFORCEMENT DETAILS
- FIGURE 5.35 BOX BEAM B4 SECTIONS
- FIGURE 5.36 BOX BEAM B4 PRESTRESSING WIRE PROFILE
- FIGURE 6.1 LOAD DEFLECTION CURVE AT CENTRE OF BOX BEAM B1
- FIGURE 6.2 LONGITUDINAL DEFLECTION PROFILE OF BEAM B1
- FIGURE 6.3 TRANSVERSE DEFLECTION PROFILE OF BEAM B1
- FIGURE 6.4 DEFLECTION PROFILE OF BOTTOM FLANGE BEAM B1 LOAD AT 110kN
- FIGURE 6.5 DEFLECTION PROFILE OF BOTTOM FLANGE BEAM B1 LOAD AT 112kN
- FIGURE 6.6 BOTTOM STEEL STRAIN DISTRIBUTION IN BOTTOM FLANGE NEAR CENTRE OF BOX BEAM B1

- FIGURE 6.7 TOP STEEL STRAIN DISTRIBUTION IN BOTTOM FLANGE NEAR CENTRE OF BOX BEAM B1
- FIGURE 6.8 BOTTOM TRANSVERSE STEEL STRAIN DISTRIBUTION IN BOTTOM FLANGE NEAR CENTRE OF BOX BEAM B1
- FIGURE 6.9 TOP TRANSVERSE STEEL STRAIN DISTRIBUTION IN BOTTOM FLANGE NEAR CENTRE OF BOX BEAM B1
- FIGURE 6.10 BOTTOM LONGITUDINAL STEEL STRAIN DISTRIBUTION IN TOP FLANGE NEAR CENTRE OF BOX BEAM B1
- FIGURE 6.11 TOP LONGITUDINAL STEEL STRAIN DISTRIBUTION IN TOP FLANGE NEAR CENTRE OF BOX BEAM B1
- FIGURE 6.12 BOTTOM TRANSVERSE STEEL STRAIN DISTRIBUTION IN TOP FLANGE NEAR CENTRE OF BOX BEAM B1
- FIGURE 6.13 TOP TRANSVERSE STEEL STRAIN DISTRIBUTION IN TOP FLANGE NEAR CENTRE OF BOX BEAM B1
- FIGURE 6.14 LONGITUDINAL WEB STEEL STRAIN DISTRIBUTION NEAR CENTRE SECTION OF BOX BEAM B1
- FIGURE 6.15 LONGITUDINAL STEEL STRAIN DISTRIBUTION AT CENTRE SECTION OF BOX BEAM B1 LOAD AT 110kN
- FIGURE 6.16 LONGITUDINAL SURFACE STRAIN DISTRIBUTION AT CENTRE SECTION OF BOX BEAM B1 LOAD AT 110kN
- FIGURE 6.17 TRANSVERSE STEEL STRAIN DISTRIBUTION AT CENTRE SECTION OF BOX BEAM B1 LOAD AT 80kN
- FIGURE 6.18 TRANSVERSE SURFACE STRAIN DISTRIBUTION AT CENTRE SECTION OF BOX BEAM B1 LOAD AT 80kN
- FIGURE 6.19 BEAM B1 TOP SURFACE CRACK PATTERN
- FIGURE 6.20 BEAM B1 BOTTOM SURFACE CRACK PATTERN
- FIGURE 6.21 LOAD DEFLECTION CURVE AT CENTRE OF BOX BEAM B2
- FIGURE 6.22 DEFORMATION PROFILE OF BEAM B2 AT 120kN

- FIGURE 6.23 LOCAL PUNCHING SHEAR FAILURE UNDER POINT LOAD FOR BEAM B2
- FIGURE 6.24 BEAM B2, BEAM REPAIRED AND LOAD APPLICATION REVISED
- FIGURE 6.25 BEAM B2 TOP VIEW DURING LOAD TEST
- FIGURE 6.26 BEAM B2 LOADED WEB CRACK PATTERN
- FIGURE 6.27 BEAM B2 TOP FLANGE CRACK PATTERN
- FIGURE 6.28 BEAM B2 BOTTOM FLANGE CRACK PATTERN
- FIGURE 6.29 LOAD DEFLECTION CURVE AT CENTRE FOR BEAM B3
- FIGURE 6.30 GENERAL VIEW OF BEAM B3 AFTER LOAD TEST
- FIGURE 6.31 BEAM B3 TOP FLANGE CRACK PATTERN
- FIGURE 6.32 BEAM B3 TOP FLANGE CRACK PATTERN
- FIGURE 6.33 BEAM B3 BOTTOM FLANGE CRACK PATTERN
- FIGURE 6.34 LOAD DEFLECTION CURVE AT CENTRE FOR BEAM B3
LOAD AT EXTERNAL WEB
- FIGURE 6.35 CRACK PATTERN OF LOADED WEB FOR BEAM B3
- FIGURE 6.36 CRACK PATTERN OF LOADED WEB FOR BEAM B3
- FIGURE 6.37 CRACK PATTERN TO TOP FLANGE FOR BEAM B3 LOAD
TO EXTERIOR WEB
- FIGURE 6.38 CRACK PATTERN TO BOTTOM FLANGE FOR BEAM B3
LOAD TO EXTERIOR WEB
- FIGURE 6.39 LOAD DEFLECTION CURVE AT CENTRE FOR BEAM B4
- FIGURE 6.40 LONGITUDINAL AND TRANSVERSE DEFORMATION
PROFILE OF BOX BEAM B4

Chapter 1. Introduction

In order to simulate the ultimate behaviour of concrete box girder bridges using scale models, micro-concrete were often used as a model material for the tests. The advantage of using micro-concrete is that with careful mix design and quality control, it is possible to produce a mix comparable with a prototype concrete in terms of stress and strain characteristics. In addition, the crack patterns and the yield mechanism can be realistically simulated. This is an important aspect in the prediction of the ultimate collapse load.

For concrete box girder models, the ultimate failure mechanism involves regions of high stress concentration causing local crushing and fracture of the slab and wall elements. These failure regions can be idealised as yield lines and plastic zones. Because of the complex nature of box girder and its geometry of deformation, the stress resultants along yield lines forming the collapse mechanism can involve shear moment and normal forces. For the collapse mechanism to fully develop, large deformation is required.

Plastic analysis requires the material to possess adequate ductility. In the case of micro-concrete, the effect of shear transfer along shear yield lines can be affected by large shear deformation. In addition, when the yield line involves a bending moment as well as shear, the rotation of the yield line due to bending reduces the effective depth of the slab elements that can transfer shear. It is, therefore, important to study the effect of using micro-concrete as a model material in the transfer of shear.

Chapter 2 reviewed the shear tests conducted by other researchers. It then described the shear tests carried out by the author. It studied the effect of using micro-concrete for the transfer of shear. The effect of shear ductility was also studied and the experimental result was applied to modify the yield criterion described in Chapter 3.

Plasticity theory and the philosophy of limit analysis provide a simplified method of assessing the collapse load

of a structure by the development of a failure mechanism. This method of analysis is based upon the assumption that the material used will possess sufficient ductility to enable the collapse mechanism to develop fully.

Unreinforced concrete by itself has limited ductility in tension and shear. In compression, it can sustain load for large compressive deformation. When concrete is combined with steel reinforcement, the reinforcement provides the strength in tension and also the ductility after yielding. It is therefore considered realistic to assume that plastic analysis can be applied to this type of structure. Chapter 3 described briefly the concepts of plasticity theory, followed by the general yield criterion applied to unreinforced concrete, incorporating the modification required to account for the shear ductility from Chapter 2. The yield criterion was then extended to reinforced concrete and prestressed concrete elements.

Chapter 4 discussed the ultimate collapse analysis of concrete box girders using the developed yield criterion to predict the collapse load. The box girders studied in this thesis involved distortion of the cross section. Except at the supports, no additional diaphragms were provided at the spans. In order to preserve geometric compatibility in the failure mechanism, in-plane shear strains were required to distort the section. The stress resultants along yield regions involved bending moment, normal forces and in plane shear. The yield criterion discussed in Chapter 3 was extended to evaluate the collapse load of the box girder models. Potential collapse mechanisms for box girders were studied. No attempt was made to look into all the possible collapse modes for the lowest upper bound solution. This was considered justifiable as the collapse mechanisms were based upon observed failure modes from the experiments and also previous research work conducted by others.

The box girder experiments were described in Chapter 5. It was not the intention of this thesis to directly simulate any particular box girder bridge or any particular loading pattern recommended in the codes of practice. For the purpose of designing the section using micro-concrete as the modelling material, the scale of the models was kept to approximately one to ten. The applied loading was also simplified and idealised in order to emphasis the collapse mechanisms.

The transverse strength of the top slab elements in multi-cell concrete box girder models is often limited. The application of large eccentric point loading will result in localised failure. Experiments were therefore conducted to study the failure of local cell directly influenced by the concentrated loading.

In ultimate load analysis, ordinary reinforced and prestressed concrete elements are considered similar if the ultimate yield strength for both reinforcing steel and prestressing steel is the same. Thus, an experiment on a prestressed box girder was conducted and compared with the results of a reinforced box girder.

The experimental results for the box girders were collated in Chapter 6 and compared with theoretical values. The limitations of the theory and its extension to the analysis of full-scale structure are then discussed.

Chapter 7 concluded the thesis and considered the results provided in previous chapters. The problems and limitations of the proposed method of analysis together with its application to the prediction of the behaviour of full-scale structures were discussed. Recommendations were put forwarded for future research.

Chapter 2. Shear Behaviour of Micro-concrete

2.1 Introduction

Micro-concrete models are often used for studying the ultimate collapse behaviour of complex concrete structures. The advantage of using this material is its similarity to the concrete of a prototype structure. Hence, the elastic behaviour can be reproduced realistically. The accurate simulation of the crack patterns and yield lines prior to final collapse allows a more precise prediction of the ultimate collapse load. Although the behaviour of micro-concrete was examined, its behaviour under shear condition had not been studied in great detail. Hence, a series of shear tests were carried out to determine the effect of shear on micro-concrete and its implication upon the yield criterion for the material.

2.2 The Mattock Shear Specimens

The Mattock type shear specimen was selected for the experiment, Figure 2.1. The specimen had two notches on opposite sides near the top and bottom. These notches extended to the centre of the specimen. A compression load was applied on the top along the centre line. This load subjected the area between the notches to a direct shear stress resultant.

Hofbeck Ibrahim & Mattock (1969) and Mattock & Hawkins (1972), used the specimen to investigate the effect of various reinforcement arrangements upon shear capacity. Mattock, Johal & Chow (1975) used similar specimens to investigate shear failure of corbels. In this latter work, the reinforcement was adjusted along the shear plane to sustain the bending moment caused by the eccentric application of the shear force. Rajandran (1972) applied an external bending moment along the shear plane of pre-cracked and uncracked specimens to study failure due to shear and bending moment. Walraven & Reinhardt (1978) tested pre-cracked specimens with reinforcement crossing the shear plane at different orientations. The displacements of crack opening and shear deformation were monitored.

Unreinforced concrete has only very limited tensile capacity and hence low shear strength. Such values are often ignored in ultimate analysis. For the specimens that were investigated by the author, shear reinforcement was provided across the shear plane to prevent the sudden splitting of the specimen when the cracking strength of the shear plane was exceeded. The crack opening and shearing of the symmetrically reinforced specimen were uniform and the stress resultants on the shear plane could be assumed to be uniform shear and normal forces. The normal force could be assumed to be equal to the total yield force of the reinforcement across the shear plane. Previous experiments by Birkeland & Birkeland (1966) and Mattock & Hawkins (1972) indicated that shear strength of symmetrically reinforced specimens were the same with identical reinforcement content irrespective of reinforcement sizes and spacing. The effect of size of specimen and aggregate could be investigated by varying the specimen size and the size of aggregate used in the concrete mix.

The symmetrical arrangement of reinforcement resulted in a uniform compressive stress across the shear plane for these specimens, Figure 2.2. The non-symmetrical arrangement of reinforcement however, caused an internal moment to be induced. This was the result of unequal yielding forces in the reinforcement that produced a self-induced bending moment along the shear plane, Figure 2.3. Thus the failure plane of the specimen was subjected to combine shear, bending and normal forces. The bending moment could be applied externally, but there would be considerable experimental difficulties in maintaining the constant bending moment during the failure of the specimen.

2.3 Description of Shear Test

The shear tests conducted were divided into two groups of symmetrically and non-symmetrically reinforced specimens.

In the first group, the following variables were introduced for symmetrically reinforced specimens.

1. maximum size of course aggregate.
2. reinforcement content across the shear plane.
3. area of shear plane.
4. scale of the specimens.

In the second group, the following variables were introduced for non-symmetrically reinforced specimens.

1. maximum size of aggregate.
2. reinforcement content across the shear plane.
3. position of the reinforcement relative to the central axis of the shear plane giving a different effective depth.

Each specimen was assigned a code that identified the variables. The first letter could be 'F', 'H' or 'T' to signify the size of the specimen, 'F' for full scale, 'H' for half scale and 'T' for tenth scale.

The second letter indicated the size of aggregate used; 'F' for full size 20mm aggregate, 'H' for 10mm aggregate and 'T' for a zone 2 sand mix with maximum grit size of 2mm.

A number was used to indicate the different reinforcement parameter given by $f_y A_s / (bh)$. The number '1' was used to describe specimens with a lower reinforcement ratio and the number '2' for the higher ratio.

The third letter with a number suffix identified the specimen thickness or the reinforcement positions. 'T₁' and 'T₂' were used for the different thickness of symmetrically reinforced specimens. 'D₁' and 'D₂' were for the different effective depths of non-symmetrically reinforced specimens.

A summary of the specimens including all the variables is shown in Table 2.1.

| Specimen No | Size of Specimen | | | Aggregate Size | | | Reinf. Parameter | | Thickness Type | | Effective Depth | | Remarks |
|-------------------|------------------|------|-------|----------------|------|-----|------------------|---|----------------|---|-----------------|---|--|
| | Full | Half | Tenth | 20mm | 10mm | 2mm | 1 | 2 | 1 | 2 | 1 | 2 | |
| FF1 | * | | | * | | | * | | | | | | Equal thickness & Effective Depth |
| FF2 | * | | | * | | | | * | | | | | |
| FH1 | * | | | | * | | * | | | | | | 1 - 2.456 N/mm ² (3 - T6 E.F.) |
| FH2 | * | | | | * | | | * | | | | | |
| FT1 | * | | | | | * | * | | | | | | 2 - 3.768 N/mm ² (5 - T6 E.F.) |
| FT2 | * | | | | | * | | * | | | | | |
| NH1 | | * | | | * | | * | | | | | | Reinf. Parameter 1 - 3.232 N/mm ² (3 - 3mm dia E.F.) |
| NH2 | | * | | | * | | | * | | | | | |
| HT1 | | * | | | | * | * | | | | | | 2 - 5.390 N/mm ² (5 - 5mm dia E.F.) |
| HT2 | | * | | | | * | | * | | | | | |
| TT1 | | | * | | | * | * | | | | | | Reinf. parameter 1 - 4.16 N/mm ² 2 - 6.93 N/mm ² |
| TT2 | | | * | | | * | | * | | | | | |
| FH1T ₁ | * | | | | * | | * | | * | | | | Thickness 1 - 100 mm 2 - 67 mm |
| FT1T ₁ | * | | | | | * | * | | * | | | | |
| FH1T ₂ | * | | | | * | | * | | | * | | | |
| FT1T ₂ | * | | | | | * | * | | | * | | | |
| HT1T ₁ | | * | | | | * | * | | * | | | | Thickness 1 - 50 mm 2 - 25 mm |
| HT1T ₂ | | * | | | | * | * | | | * | | | |
| FF1D ₁ | * | | | | * | | * | | | | * | | Reinf. Parameter 1 - 1.228 N/mm ² 2 - 2.703 N/mm ² |
| FT1D ₁ | * | | | | | * | * | | | | * | | |
| FF2D ₁ | * | | | | * | | | * | | | * | | Effective Depth |
| FT2D ₁ | * | | | | | * | | * | | | * | | |
| FF1D ₂ | * | | | | * | | * | | | | | * | D1 - 53 mm from centre |
| FT1D ₂ | * | | | | | * | * | | | | | * | |
| FF2D ₂ | * | | | | * | | | * | | | | * | D2 - 31 mm from centre |
| FT2D ₂ | * | | | | | * | | * | | | | * | |

Table 2.1: SUMMARY DESCRIPTION OF SPECIMENS

2.4 Instrumentation

Although the specimen instrumentation was simple it was sufficient to obtain the required results.

Demountable portal strain transducers with a gauge length of 100mm were used in conjunction with a digital strain indicator and a switch balance unit. This equipment was developed by the British Cement Association (BCA), formerly Cement and Concrete Association (C & CA). The gauges were set up in sets of three arranged in a rosette pattern across the anticipated shear zone on both faces. "Demec" gauges were also used to supplement the results from the strain transducer when the capacity of the transducer was exceeded.

Electric resistance strain gauges were attached to some of the reinforcement to confirm yielding of the steel during shear failure.

Dial gauges were used to monitor the relative displacements of the shear zone. They were used to measure the rate of displacement during the yielding of the shear reinforcement.

A crack microscope capable of measuring widths to within 0.01mm was used to measure crack widths. The observed values were compared with those obtained from surface strain measurements.

The bearing arrangements were designed to allow minimum resistance to crack opening for the symmetrical reinforced specimens and to the bending rotation for the non-symmetrical reinforced specimens.

The loading machine was hydraulically operated and capable of applying a maximum load of 500kN. The machine possessed a facility for maintaining the load or the displacement. The latter device was useful during the final stages of the experiments when large deformation was experienced with little increase in load.

2.5 Material Used for Shear Specimens

2.5.1 Concrete

Mix designs were carried out to obtain consistent mixes for concrete using different maximum size aggregate of 20mm, 10mm and zone 2 sand. It was found difficult to obtain a mix design producing comparable compressive strength as well as tensile strength. The concrete specimens using sand mix tends to give higher tensile strengths than those with normal size aggregate (20mm, 10mm), even though the compressive strength were comparable. It was decided that the mixes were chosen to achieve similar compressive strength as the main criteria. The variation in tensile strength was noted.

The grading of typical 20mm maximum aggregate concrete and the mix proportion was obtained from the HMSO design pamphlet. The finer mixes were proportioned accordingly. Johnson's (1962) mix-design for concrete models was used as guidance. The grading and proportion of the mixes are shown in Table 2.2.

The aggregates used were oven dried Thames gravel. Absorption was assumed to be 1 %. After batching, the coarse and fine aggregates were allowed to soak for about one hour to ensure a saturated surface dried condition. This process was to ensure control of the moisture content of the aggregate and an accurate assessment of water cement ratio.

Rapid hardening Portland cement was used in the mix. Thus, the specimens could be tested after a short curing period with minimum delay between the different tests.

For each mix, three cubes and three cylinders were taken for compressive strength tests and indirect tensile strength tests. Different size cubes and cylinders were taken corresponding to the different sizes of the shear specimen. The range and size of the control specimens were shown in Table 2.3.

| B.S. sieve | Percentage by weight passing | | | Remarks |
|--------------------|------------------------------|------|------|--|
| | B.S. sieve | | | |
| | 20mm | 10mm | 2mm | |
| 3/4"-3/8" | 38 | - | - | Based on Saturated Surface Dried Aggregate |
| 3/8"-3/16" | 24 | 38 | - | |
| 3/16"-7 | 6 | 24 | - | |
| 7-14 | 6 | 6 | 40 | |
| 14-25 | 7 | 6 | 10 | |
| 25-52 | 9 | 16 | 10 | |
| 52-100 | 7 | 7 | 35 | |
| 100+ | 3 | 3 | 5 | |
| Agg/Cement Ratio | 6.25 | 5.25 | 4.25 | |
| Water/Cement Ratio | 0.63 | 0.63 | 0.63 | |

TABLE 2.2: CONCRETE MIX PROPORTION

| Size of Shear Specimen | Size of control Cube for Compressive Strength | Size of control Cylinder for indirect tensile strength |
|------------------------|---|--|
| Full size | 100x100x100mm | 100mm dia x 200mm |
| Half size | 70x70x70mm | 50mm dia x 100mm (2"x4") |
| Tenth size | 25x25x25mm | 25mm dia x 50mm |

TABLE 2.3: SCHEDULE OF CONTROL SAMPLES

2.5.2 Reinforcement

The region adjoining the shear plane was reinforced such that failure would be restricted to the shear plane only. Hence, only the reinforcement across the shear plane was of interest.

For the large size specimens, 6mm diameter hot roll high yield bars were used. For the thinner and the half scale specimens, 3mm diameter high yield and 2.67mm diameter mild steel wire were used. For the tenth scale specimen, 1mm diameter mild steel wire was used. BCA developed a hand-operated machine for introducing indentations on the surface of mild steel wire. The knurled mild steel wire gave improved bond characteristic and slightly higher yield strength caused by the effect of work hardening.

The strengths of the reinforcement were expressed as total yield loads. Although they could also be expressed as yield stresses, their calculated values depended upon the accuracy of assessing the diameters of the reinforcement. In ultimate load analysis, for the purpose of determining the normal stress across the shear plane, it was sufficient to obtain the total yield force of the reinforcement without actually calculating the area of reinforcement across the shear plane.

Table 2.4 summarised the average yield load and the corresponding yield stress for the various nominal sizes shear reinforcement. The stress strain characteristics of each wire type were plotted in Figure 2.4, 2.5 and 2.6.

| Reinforcement Nominal Diameter mm | Yield Force KN | Yield Stress N/mm ² |
|---|----------------------|--------------------------------------|
| 6.00 (high yield) | 15.35 | 543.00 |
| 3.00 (high yield) | 5.05 | 714.00 |
| 2.67 (annealed) | 1.00 | 179.00 |
| 1.00 (knurled) | 0.20 | 252.00 |

TABLE 2.4: AVERAGE STRENGTH OF REINFORCEMENT

2.5.3 Formwork for Casting of Shear Specimens

Timber formwork was used for casting the full and half size specimens. The formwork was made of hardwood ply board and coated with polyurethane varnish, Figure 2.7. For specimens with different thickness, two different thickness spacers were used by inserted into the formwork to reduce the thickness of the casting. A steel mould was used for the tenth scale specimen.

The formwork and mould for the control specimens were covered with mould oil after assembly for easy stripping.

2.6 The Experimental Procedure

Twenty-six shear specimens were tested. Normally the specimens were load tested to failure fourteen days after casting.

The primary reinforcing cages were prepared before the main casting period. The cages were basically similar for the two rigid zones. The only variable being the amount of shear reinforcement crossing the shear plane. Both ends of the shear reinforcement were bent up to provide the required bond and anchorage. The assembled cage was then positioned into the oiled formwork for casting, Figure 2.8.

Compaction of the wet concrete for the specimen, the control cubes and cylinders were achieved by using a vibrating table. They were then covered with polythene sheeting to cure for one week.

Prior to testing, the specimen surfaces were prepared for the attachment of the strain transducers. The specimen was set up with the appropriate end bearing arrangement in the loading frame for testing, Figure 2.1.

Load was applied in increments of 15kN initially. For each increment, the surface strains and dial gauge readings were recorded. This was repeated until cracks developed along the shear plane. Cracking was usually associated with a sudden increase in the surface strain readings. The same procedure was continued with reducing load steps. Crack widths were measured at each subsequent stage after cracking.

At the ultimate load stage, displacement increments were used instead of load increments. Releasing the pressure valve slowly controlled displacement of the shear plane at this stage until the displacement dial gauge stabilised at a pre-determined rate. The load, strain values and dial gauge readings were recorded. This was continued until the capacity of the measuring instruments was exhausted.

Control cubes and cylinders were tested on the same day for compressive strength and indirect tensile strength.

2.7 The Experimental Observations

2.7.1 Symmetrically Reinforced Specimens

Eighteen specimens were tested. The variables and ultimate shear stresses were summarised in Table 2.5.

Specimens FF1, FH1, FT1 were all identically reinforced. The only variable was the size of aggregate. The initial cracking load and ultimate load were comparable for the three specimens. The initial sets of surface strain measurement were less reliable as a result of the unfamiliar instrumentation. Acceptable results were obtained in later tests, however, after some modification of the measuring technique. Crack widths were observed and measured until it reached approximately 2mm, Figure 2.9.

Specimens FF2, FH2 and FT2 were reinforced with higher shear reinforcement content than the previous set of tests. The specimen FT2 using the sand mix showed a slightly higher cracking strength. The ultimate shear strength of these specimens was very close. From the surface strain, a small twisting curvature was evident. The strain readings from the electric resistance strain gauges indicated yielding of the shear reinforcement.

Specimens FH1T₁, FT1T₁, FH1T₂ and FT1T₂ were reinforced with a similar reinforcement parameter. The variable was the thickness of the specimens. Ultimate shear stresses were comparable. Some small twisting and normal rotation of the shear plane were recorded during the test.

The next set of tests included six specimens HH1, HT1, HH2, HT2, HT1T₁ and HT1T₂. These tests were a repeat of previous sets except that the scale of the specimen was halved. Shear cracking for all the specimens were evident with the crack developing between the notches following the predetermined failure plane, Figure 2.10. In specimen HT1T₂, flexural cracking adjacent to the notches were also observed. The fractures in these areas indicated the reinforcement in the rigid part was insufficient to prevent premature flexural failure.

Attempts were made to test two tenth scale shear specimens TT1 and TT2. The load was applied using the Hounsfield Tensiometer apparatus, Figure 2.11. The specimens failed almost immediately after the shear crack develop. Complete shear failure did not occur for the specimen TT2, instead, flexural failure of this specimen was observed with yield hinges forming at root of the notches. The small size of the tenth scale specimens prevented any acceptable strain measurements being obtained along the shear plane. The results obtained for these two specimens were, therefore, of limited value.

| Specimen No. | Max Agg Size mm | Size of ShearPlane mm x mm | Reinf. arrangement | Cube Strength | | Indirect Tensile Strength N/mm ² | Total Yield Force kN | Reinf. Para. ρf_y N/mm ² | Max. Shear $V_{max} = V_u/A_{cr}$ N/mm ² | Crack. Stress V_{cr} N/mm ² |
|-------------------|--------------------|-------------------------------|--------------------|-------------------|---|--|-------------------------|--|--|---|
| | | | | N/mm ² | a | | | | | |
| FF1 | 20 | 250X150 | 3-T6 EF | 30 | a | 2.61 | 92.10 | 2.46 | 5.20 | 3.87 |
| FH1 | 10 | 250X150 | 3-T6 EF | 32 | a | 2.78 | 92.10 | 2.46 | 6.27 | 4.40 |
| FT1 | 2 | 250X150 | 3-T6 EF | 31.4 | a | 3.18 | 92.10 | 2.46 | 5.47 | 3.60 |
| FF2 | 20 | 250X150 | 5-T6 EF | 31.7 | a | 2.71 | 141.30 | 3.77 | 7.20 | 3.73 |
| FH2 | 10 | 250X150 | 5-T6 EF | 30.3 | a | 2.79 | 141.30 | 3.77 | 7.23 | 4.13 |
| FT2 | 2 | 250X150 | 5-T6 EF | 30.8 | a | 2.98 | 141.30 | 3.77 | 7.09 | 4.80 |
| FH1T ₁ | 10 | 250x100 | 2-T6 EF | 30.9 | a | 2.79 | 61.40 | 2.46 | 5.92 | 4.00 |
| FT1T ₁ | 2 | 250x100 | 2-T6 EF | 30.4 | a | 3.07 | 61.40 | 2.46 | 5.72 | 4.40 |
| FH1T ₂ | 10 | 250x67 | 3-3mm EF | 31.5 | a | 2.76 | 30.30 | 1.81 | 5.81 | 4.78 |
| FT1T ₂ | 2 | 250x67 | 3-3mm EF | 33.4 | a | 2.88 | 30.30 | 1.81 | 5.28 | 4.48 |
| HH1 | 10 | 125x75 | 3-3mm EF | 30.9 | b | 2.79 | 30.30 | 3.23 | 6.18 | 4.80 |
| HT1 | 2 | 125x75 | 3-3mm EF | 34.3 | b | 3.93 | 30.30 | 3.23 | 6.58 | 5.76 |
| HH2 | 10 | 125x75 | 5-3mm EF | 26.9 | b | 2.98 | 50.50 | 5.39 | 7.82 | 4.80 |
| HT2 | 2 | 125x75 | 5-3mm EF | 31.5 | b | 3.55 | 50.50 | 5.39 | 8.00 | 5.87 |
| HT1T ₁ | 2 | 125x50 | 2-3mm EF | 33.7 | b | 3.19 | 20.20 | 3.23 | 6.23 | 4.80 |
| HT1T ₂ | 2 | 125x25 | 5-2.67mm EF | 35.0 | b | 3.44 | 10.00 | 3.23 | 7.58 | 6.40 |
| TT1 | 2 | 25x15 | 3-1.07mm EF | 44.9 | c | 3.36 | 1.57 | 4.16 | 11.50 | - |
| TT2 | 2 | 25x15 | 5-1.07mm EF | 34.7 | c | 3.38 | 2.60 | 6.93 | * | - |

Notes: * Premature Failure

Control Samples

| | cubes | cylinders for indirect tensile strength |
|---|-------|---|
| a | 100mm | 100 dia x 200mm |
| b | 70mm | 50 dia x 100mm |
| c | 25mm | 25 dia x 50mm |

TABLE 2.5: RESULTS OF SYMMETRICALLY REINFORCED SHEAR SPECIMENS

2.7.2 Non-symmetrically Reinforced Specimens

Eight non-symmetrically reinforced specimens were tested. Specimens FF1D1, FT1D1, FF1D2 and FT1D2 were all identically reinforced on only one face. The variables for the specimens were the size of the aggregate and the effective depth.

The pre-cracking and failure behaviour of FF1D1 and FT1D1 were very similar. Before cracking, the tensile strain was measured on opposite faces of the specimen across the shear plane. The unreinforced face of the shear plane opened suddenly after cracking whilst the reinforced face exhibited little damage, and from then on, only a very small increase in load was possible. Further shear displacement of the specimen induced considerable large twisting and normal curvature of the shear plane. The shear load reduced during the final stages of the experiment.

The specimens FF1D2 and FT1D2 both had a smaller effective depth. The reduce effective depth was achieved by placing the shear reinforcement closer to the central axis of the shear plane. This resulted in a reduction of the self-induced bending moment along the shear plane. Similarly, tensile strain was observed on both faces prior to cracking. Cracking occurred simultaneously on both faces. The crack width on the unreinforced face was generally much wider. After cracking, the applied shear load could be increased further by as much as 35kN. From the surface strain measurement, it was evident that twisting and normal curvature occurred across the shear plane. Subsequent load increases caused the crack widths on both faces to develop further. The crack width on the unreinforced face tended to increase more rapidly than that on the reinforced face.

The specimens FF2D1, FT2D1, FF2D2 and FT2D2 were repeats of the previous set with the variable being the amount of reinforcement. A higher reinforcement content was used in these specimens. Different amounts of reinforcement were placed near the opposite faces. From the resistance strain gauge readings on some of the shear reinforcement, the stress level was well within the elastic limit when the first crack appeared. Therefore further increase in loading was possible. Yielding of reinforcement corresponded to the ultimate load of the shear specimen. Again, crack widths

were wider on the face with lower reinforcement content, Figures 2.12 and Figure 2.13. From the surface strain measurements, bending rotation and twisting of the shear plane were present.

A summary of the parameters and results obtained in this test series was provided in Table 2.6.

| Specimen No. | Max Agg. Size mm | Shear plane mm x mm | Reinforcement arrangement | Cube Strength N/mm ² | | Indirect Tensile Strength N/mm ² | Total Yield Force kN | Reinf. Para. ρf_y N/mm ² | Max. Shear $V_{max} = V_u/A_{cr}$ N/mm ² | Crack. Stress V_{cr} N/mm ² |
|-------------------|---------------------|------------------------|------------------------------------|------------------------------------|---|--|-------------------------|--|--|---|
| FF1D ₁ | 20 | 250X150 | 3-T6 (FF ONLY) 53mm from ϕ | 30.5 | a | 2.61 | 46.05 | 1.23 | 3.60 | 3.60 |
| FT1D ₁ | 2 | 250X150 | 3-T6 (FF ONLY) 53mm from ϕ | 32.1 | a | 2.86 | 46.05 | 1.23 | 3.65 | 3.47 |
| FF1D ₂ | 20 | 250X150 | 3-T6 (FF ONLY) 31mm from ϕ | 32.0 | a | 2.69 | 46.05 | 1.23 | 4.20 | 3.47 |
| FT1D ₂ | 2 | 250X150 | 3-T6 (FF ONLY) 31mm from ϕ | 32.2 | a | 3.02 | 46.05 | 1.23 | 4.67 | 3.73 |
| FF2D ₁ | 20 | 250X150 | 2-T6NF, 5-T6FF 53mm from ϕ | 29.2 | a | 2.71 | 101.35 | 2.70 | 5.07 | 3.20 |
| FT2D ₁ | 2 | 250X150 | 2-T6NF, 5-T6FF 53mm from ϕ | 29.6 | a | 2.85 | 101.35 | 2.70 | 6.40 | 4.00 |
| FF2D ₂ | 20 | 250X150 | 2-T6NF, 5-T6FF 31mm from ϕ | 27.4 | a | 2.54 | 101.35 | 2.70 | 6.13 | 3.47 |
| FT2D ₂ | 2 | 250X150 | 2-T6NF, 5-T6FF 31mm from ϕ | 33.9 | a | 2.83 | 101.35 | 2.70 | 6.13 | 4.00 |

a -Cube and indirect tensile strength based on 100mm³ cube and 100mm dia. x200mm cylinder

TABLE 2.6: RESULTS OF NON-SYMMETRICALLY REINFORCED SPECIMENS

2.8 Surface Strain Measurement

The rosette arrangement for the surface strain measurements allowed the following strains to be calculated:

- a. The strain or relative displacement between gauge points in the direction along the gauge.
- b. The normal strain perpendicular to the shear plane. This measurement could be related to the crack width or crack opening of the shear plane after cracking had occurred.
- c. The shear strain or shear displacement after cracking. The shear displacement could be referred to the relative movement of the two rigid portions on each side of the shear plane.
- d. The tangential strain before cracking. After cracking, the tangential strain is small and the tangential displacement would be included in the concentrated displacement.
- e. Normal bending rotation could be calculated from the difference in strain measurement on opposite faces of the shear plane. This could either be expressed as an angle of rotation normal to the shear plane or as a bending curvature.
- f. Twisting rotation could be assessed from the differences in shear displacement along the two faces of the specimen. In the experiment, such twisting rotation was caused by a twisting moment resultant over the shear plane and the experiment arrangement did not restrict such rotation. This moment was due to the eccentric distribution of shear stress caused by the reinforcement arrangement. See Figure 2.3.

If the twisting rotation was restricted on a generalised yield line, there is no contribution to the work done in an upper bound solution from the twisting moment resultant. In a lower bound solution however, the computation of the twisting moment would be more useful where equilibrium conditions were to be maintained.

2.9 The Results and Their Interpretations

The following graphs were plotted from the results of the experiments for the symmetrically reinforced series:

- a. Shear stress versus normal displacement.
- b. Shear displacement versus normal displacement.
- c. Shear stress versus reinforcement parameter.
- d. Dimensionless shear stress versus reinforcement ratio.

2.9.1 Shear Stress versus Normal Displacement

The average shear stress for each specimen was calculated by dividing the applied shear load by the shear area of the specimen. This was only a nominal value since the shear distribution over the shear plane was not uniform. The normal displacement was obtained from the surface strain measurement. Typical shear stress versus normal displacement curves was shown in Figure 2.14.

The resulting curve could be sub-divided into three phases.

The initial cracking phase for all the specimens showed very little normal displacement before cracks developed. The strain measured in the reinforcement was small. When the crack first developed, the steel stress remained within the elastic limit. Slightly higher cracking strength was recorded for specimens using the sand mixed concrete. This was considered to be due to the higher indirect tensile strength of the micro-concrete. Varying the thickness of the specimen did not show a significant difference in the cracking stress. Once cracks started to develop, the strain in the reinforcement increased with increasing crack width corresponding to the increasing shear load.

At the maximum stress phase, most specimens sustained an increase in the applied shear load after cracking. The increase depended upon the amount of reinforcement provided across the shear plane. The higher the reinforcement contents the higher the capacity to resist shear load. The ultimate load usually corresponded to the yielding of the shear reinforcement. Thus, the ultimate shear value corresponded to certain crack widths. The normal crack displacement at which maximum shear stress was attained was

between about 0.3 to 0.4mm for the micro-concrete specimens compared with over 0.5mm for the specimens using a normal concrete mix.

In reinforced concrete design, the code of practice BS8110 (1985) imposed a restriction on crack widths for normal concrete to not exceeding 0.3mm for reasons of durability. This restriction implied that at the ultimate limit state of acceptable design crack width, the shear stress phase did not reach its maximum for the normal concrete mix.

The slope of the curves in this region could be related to the shear stiffness of the cracked concrete. Specimens with higher reinforcement content showed a higher stiffness value.

The peak shear stress achieved for normal mix specimens remained nearly constant for increasing normal displacement up to crack widths of 1.5mm. For micro-concrete specimens however, the peak shear stress was followed closely by a gradual reduction of the shear stress to a lower residual value as the normal displacement continued to increase.

Such difference in behaviour was considered to be due to the different aggregate interlock characteristic of normal and micro-concrete. For the mix with larger size aggregate, the shear crack would pass through aggregate particles. This resulted in larger displacements being required to mobilise the peak shear stress and enabled the shear stress to remain stable at a peak value under further shear displacement.

For a micro-concrete mix, the shear crack tended to pass through the cementing gel. Hence the shear interface would be less rough. The peak stress would be reached as soon as the shear cracks were established. Subsequent shear displacement resulted in further smoothing out of the fine shear zone giving rise to a reduction in the shear capacity. This reduction in shear would continue until a lower but more stable value was reached. Thus it showed a peak and residual stress behaviour not dissimilar to the shear behaviour of compacted cohesionless soil.

2.9.2 Shear Displacement versus Normal Displacement

The measured surface strain values enabled the computation of shear and normal displacements after cracking had developed along the shear plane. The displacements along and across the shear plane were very small before the concrete cracked.

For the specimens using normal size aggregate, the shear and normal displacement graph was almost linear with very little change in direction for the increasing normal displacement.

For specimens using micro-concrete and with similar amounts of reinforcement, the initial slope of the graphs was almost the same up to a normal displacement of 0.4mm. The slope then changed sharply with a much larger shear displacement and a smaller increase in normal displacement. Figure 2.15 shows the plots of shear displacement versus normal displacement.

It was apparent that concrete using a large size aggregate remained ductile for a large normal displacement, whilst concrete using a sand mix was less ductile. This aspect was important in micro-concrete modelling where the properties of concrete sustaining shear could change with increase in crack displacement.

The slope of the curve on the plot for shear displacement versus normal displacement was also of some significance. If the results were plotted on the yield surface curves for the normal and micro-concrete mixes, they appeared to satisfy the normality rule of the theory of plasticity, Figure 2.16.

2.9.3 Shear Stress versus Reinforcement Parameter

The reinforcement parameter was expressed as a stress acting normal to the shear plane. In these experiments, the reinforcement was positioned perpendicular to the shear plane and the crack opening of the shear plane caused yielding of the reinforcement. Such yielding had been confirmed by the strain measurement of the reinforcement using electrical resistance strain gauges. Since there were no other externally applied forces acting normal to the shear plane, the yield forces in the reinforcement gave rise to an equal and opposite compressive stress acting on the concrete shear plane. Dowel action and kinking of the reinforcement could modify the shear values. Since these effects were considered to be negligible (Gambarova (1981), Walraven (1978)), no allowances were deemed necessary.

The graph of shear stress versus reinforcement parameter was equivalent to plotting the shear stress versus normal stress. Both peak shear stress and residual values were plotted on the graph. Curves fitted around the test results resembled the interactive yield curve of shear and normal stress acting together on a concrete element. Separate curves were plotted for the peak stress and the residual shear stresses, Figure 2.16.

The peak stress curve followed closely the yield criterion derived from the so call square yield criterion by Neilson (1964).

$$-\sigma_n (\sigma_c - \sigma_n) + \tau_{xy}^2 = 0 \text{ ----- (2.1)}$$

The residual stress curve could be represented by the following equation proposed by the Author.

$$-\sigma_n (\sigma_c - \sigma_n) + \left(\frac{\tau_{xy}}{\alpha} \right)^2 = 0 \text{ ----- (2.2)}$$

α is the modification factor introduced to account for the reduced ductility in shear of the micro-concrete.

2.9.4 Dimensionless Shear Stress versus Reinforcement Parameter

To account for the variation in the strength of concrete in each specimen, the shear stress and reinforcement normal stress were made non-dimensioned by dividing throughout by the corresponding uni-axial compressive strength σ_c .

$$n_n = \frac{\sigma_n}{\sigma_c} = \rho \frac{f_y}{\sigma_c} \text{ ----- (2.3)}$$

$$n_{nt} = \frac{\tau_{xy}}{\sigma_c} \text{ ----- (2.4)}$$

Equations 2.1 and 2.2 could be written as:

for peak stress,

$$-n_n (1 + n_n) = n_{nt}^2 \text{ ----- (2.5)}$$

and for residual stress:

$$-\alpha^2 n_n (1 + n_n) = n_{nt}^2 \text{ ----- (2.6)}$$

Curves from Equations (2.5) and (2.6) were plotted in Figure 2.17

2.9.5 Results of Non-symmetrically Reinforced Specimens

The graphs of shear versus moment for the non-symmetrically reinforced specimens were of interest, Figure 2.18. The effect of a moment upon shear was to cause a reduction in the shear capacity of the section.

It could be explained by the fact that the bending curvature reduced the effective depth of concrete for transfer of shear. The assumption was that once concrete cracked in the tension zone, the shear contribution in that region would become non-existent. From experimental observation however, after cracking of the specimen, it was still possible to sustain further increase in the applied shear until failure. Modification to the effective depth for shear transfer could be made to account for the size of aggregate used. This could be handled by stipulating a nominal crack width beyond which aggregate interlock would cease to be effective. Hence, within the limiting crack width, part of the tension zone could still carry shear. The extra depth would depend on the size of aggregate used. The coarser the aggregate, the larger would be the effective zone for transferring shear caused by aggregate interlock. The smoother crack surface of a micro-concrete mix would result in a smaller effective depth for shear transfer.

Rajandran (1972) assumed a uniform shear stress over the compression zone above the neutral axis for a specimen subjected to bending. The disadvantage of this assumption was that during failure of a section subjected to shear and moment, the bending curvature increased gradually. This resulted in the crack on the tension side to open further. Hence, the shear contribution changed continuously as the curvature continued to increase. That also indicated the shear stress resultant changes throughout the deformation of the shear plane.

2.10 Summary of the Results of the Mattock Tests

Twenty-six shear specimens were tested, the results for the symmetrically reinforced sections showed that the normality rule of plasticity theory hold true. The size of aggregate in the concrete mix could influence the behaviour of the members in shear. Normal concrete with 10-20mm aggregate showed a peak stress behaviour under shear, whilst micro-concrete showed a residual stress characteristic. Such characteristic was important in small-scale model testing of concrete structures. A modification factor was introduced into the basic shear yield criterion, giving a much closer correlation with the shear behaviour of the material.

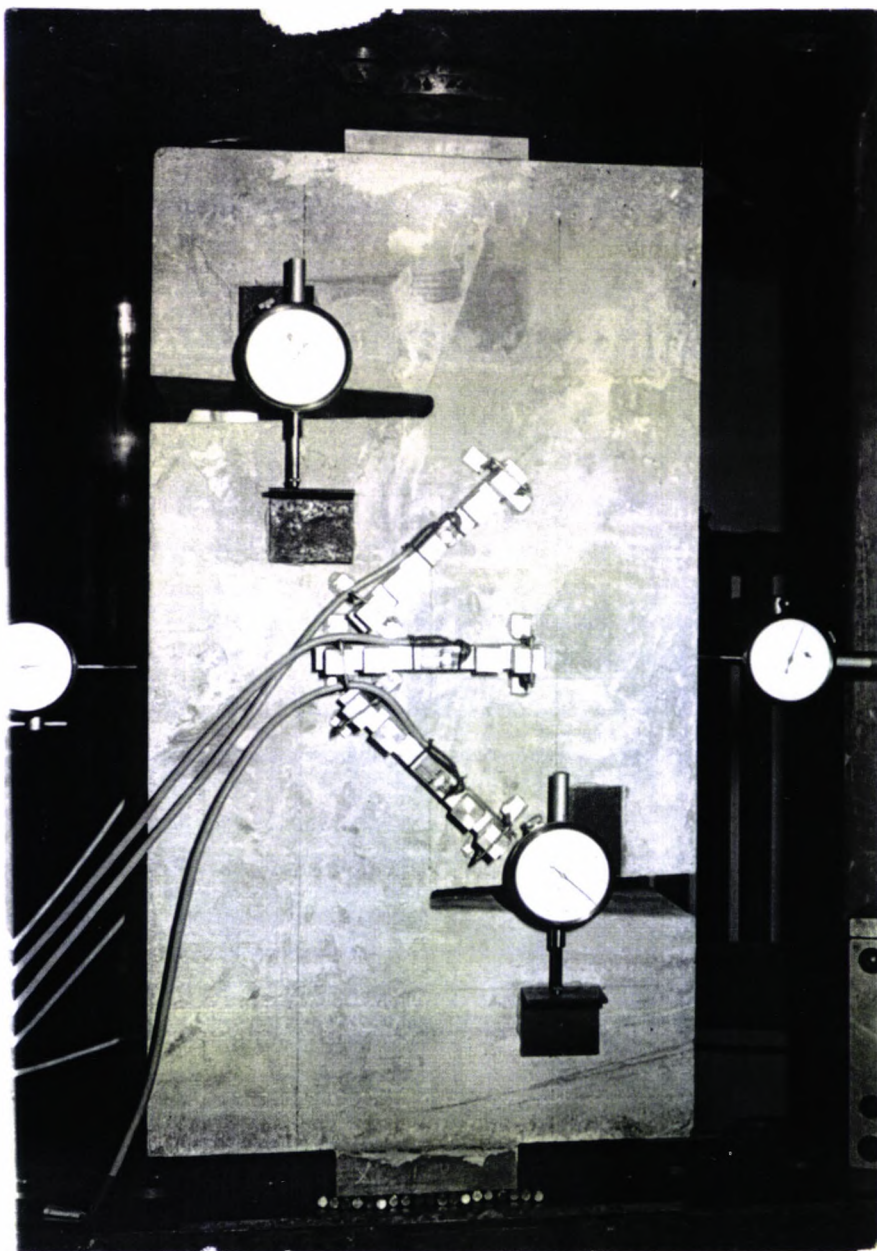


FIGURE 2.1

MATTOCK SHEAR SPECIMEN

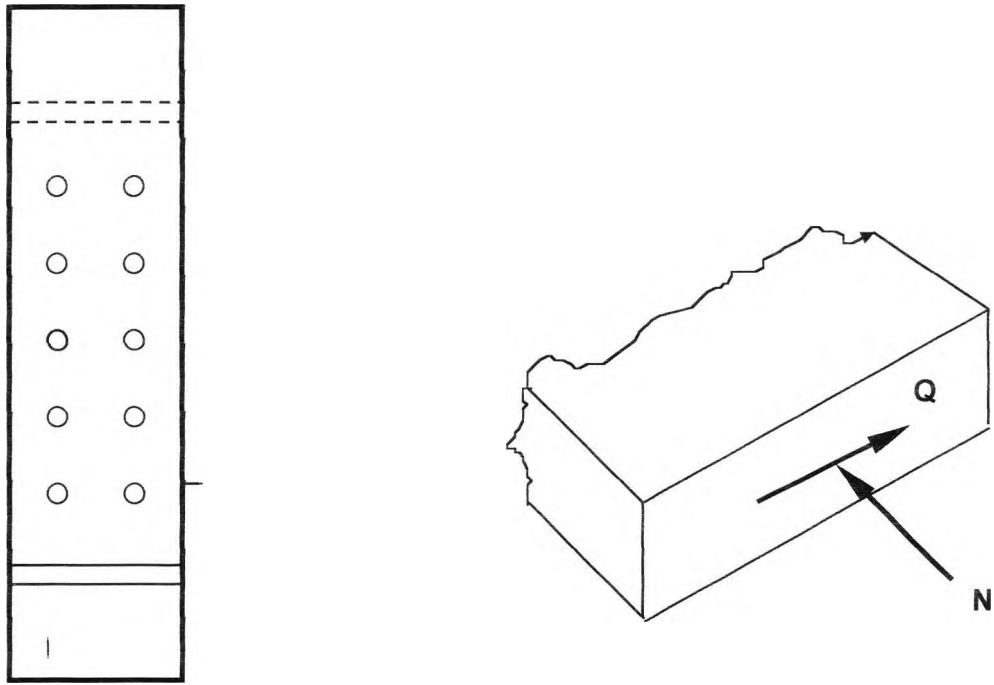


FIGURE 2.2 **SYMMETRICAL REINFORCED SPECIMEN**

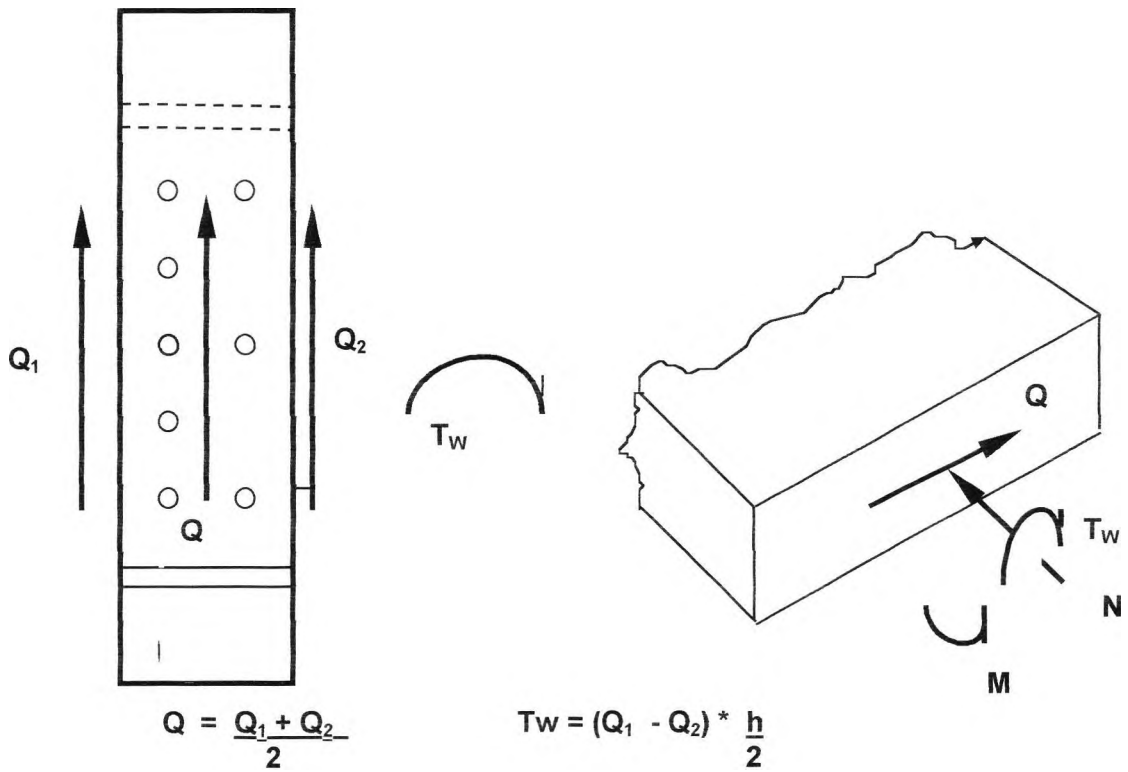


FIGURE 2.3 **UNSYMMETRICAL REINFORCED SPECIMEN**

FIGURE 2.4 STRESS STRAIN CURVE FOR 1.07mm WIRE

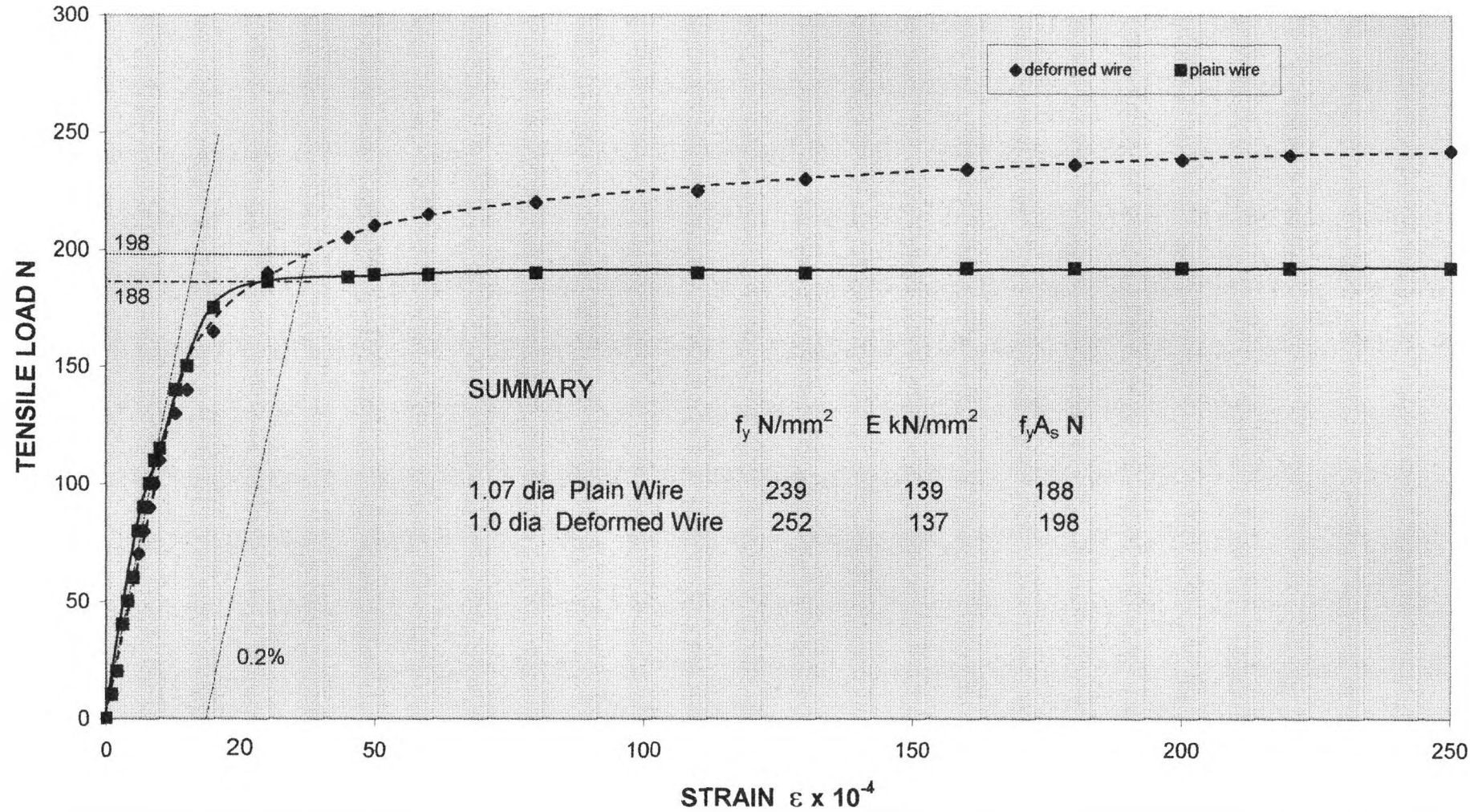


FIGURE 2.5 LOAD STRAIN CURVE FOR 3mm (1/8") WIRE

50

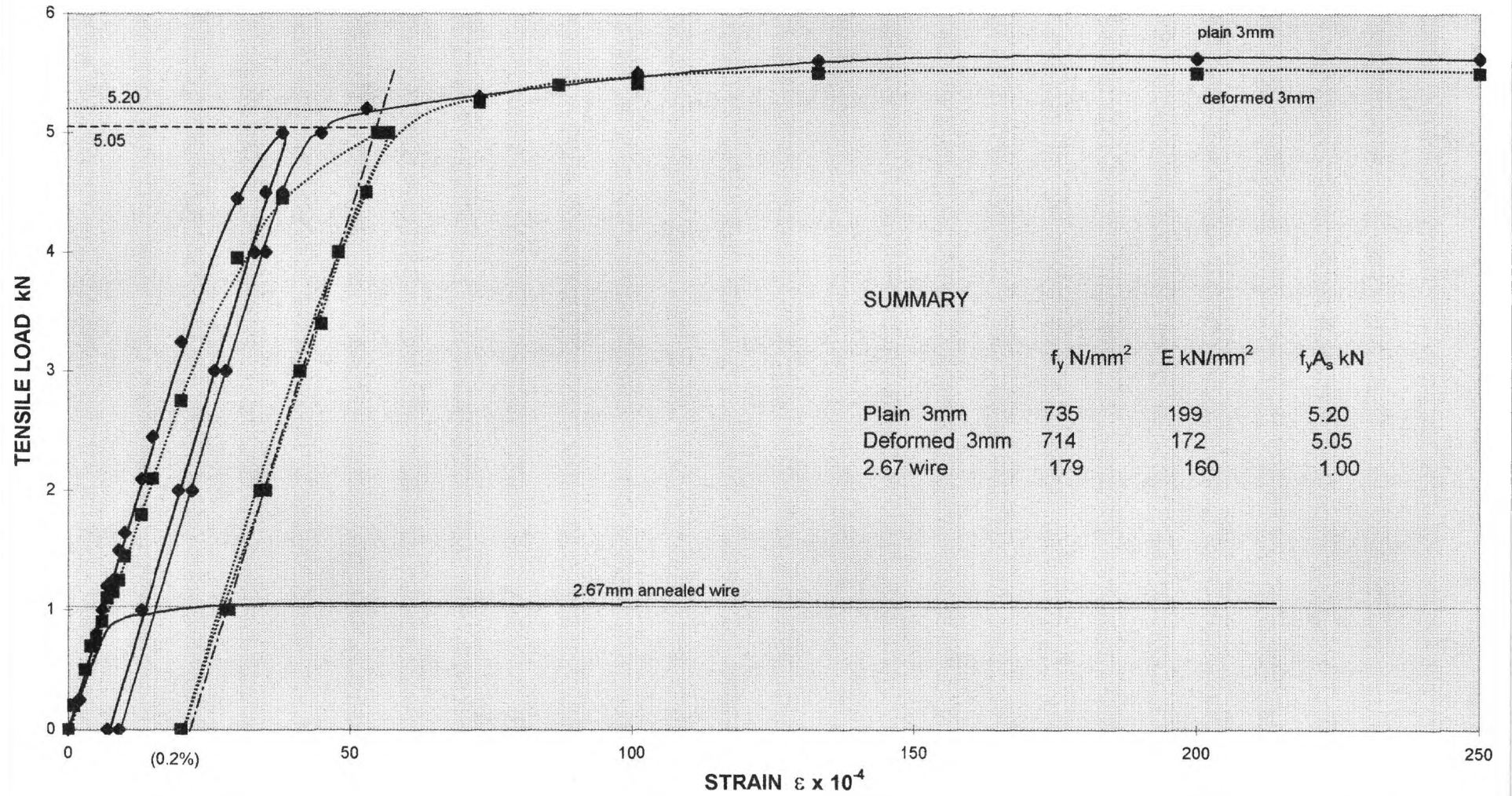
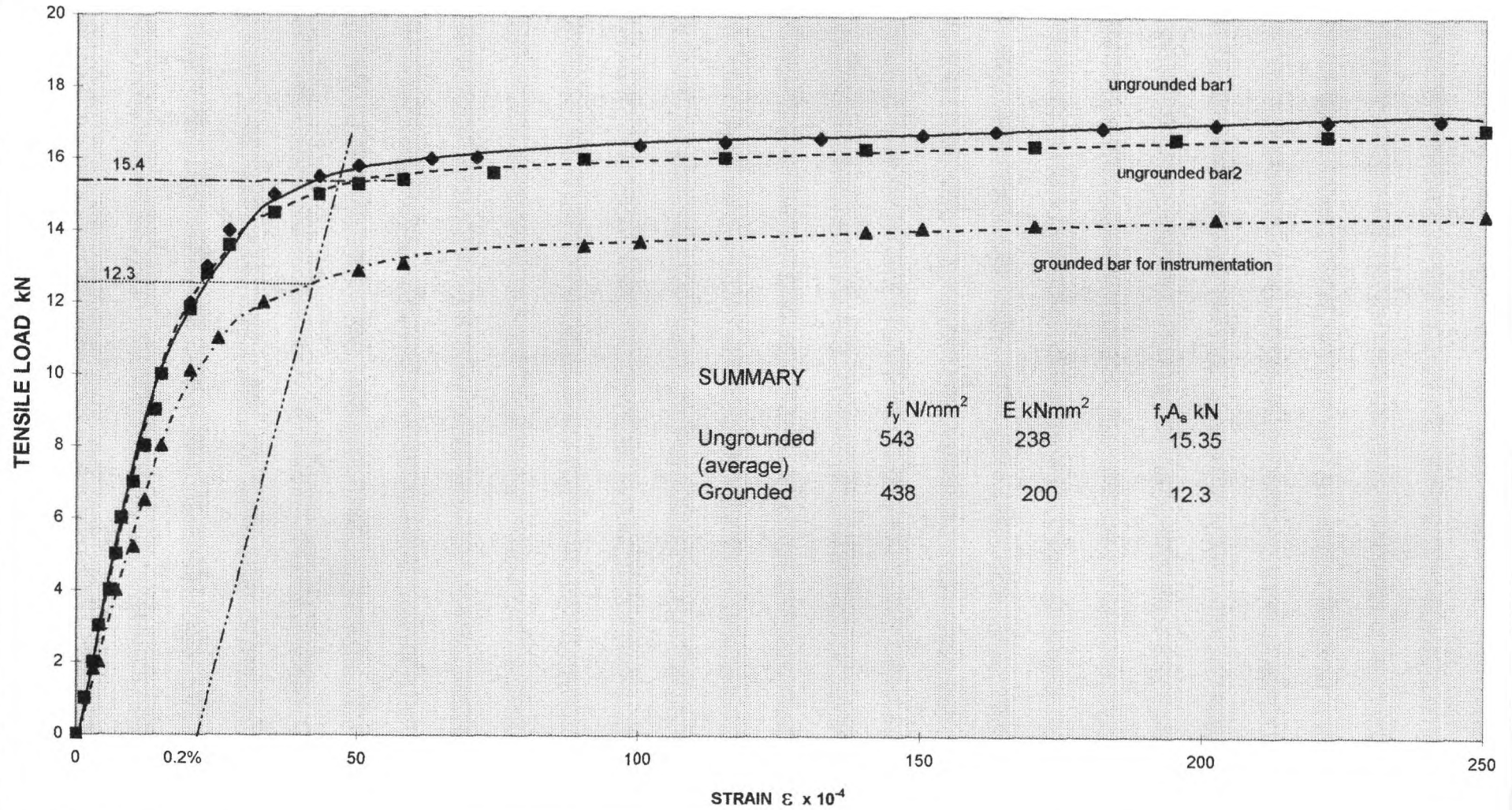


FIGURE 2.6 LOAD STRAIN CURVE FOR 6mm REINFORCING BAR



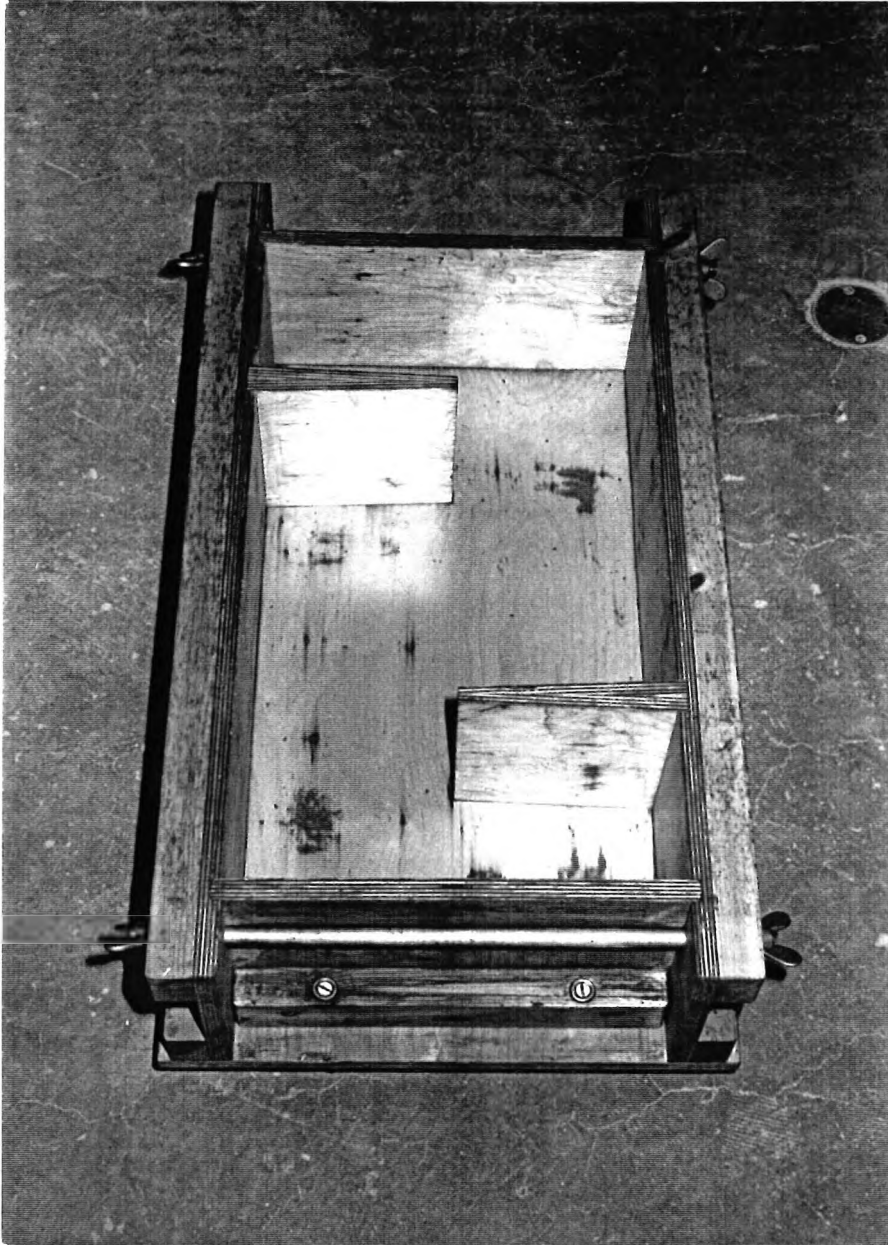


FIGURE 2.7

TIMBER FORMWORK FOR SHEAR SPECIMEN

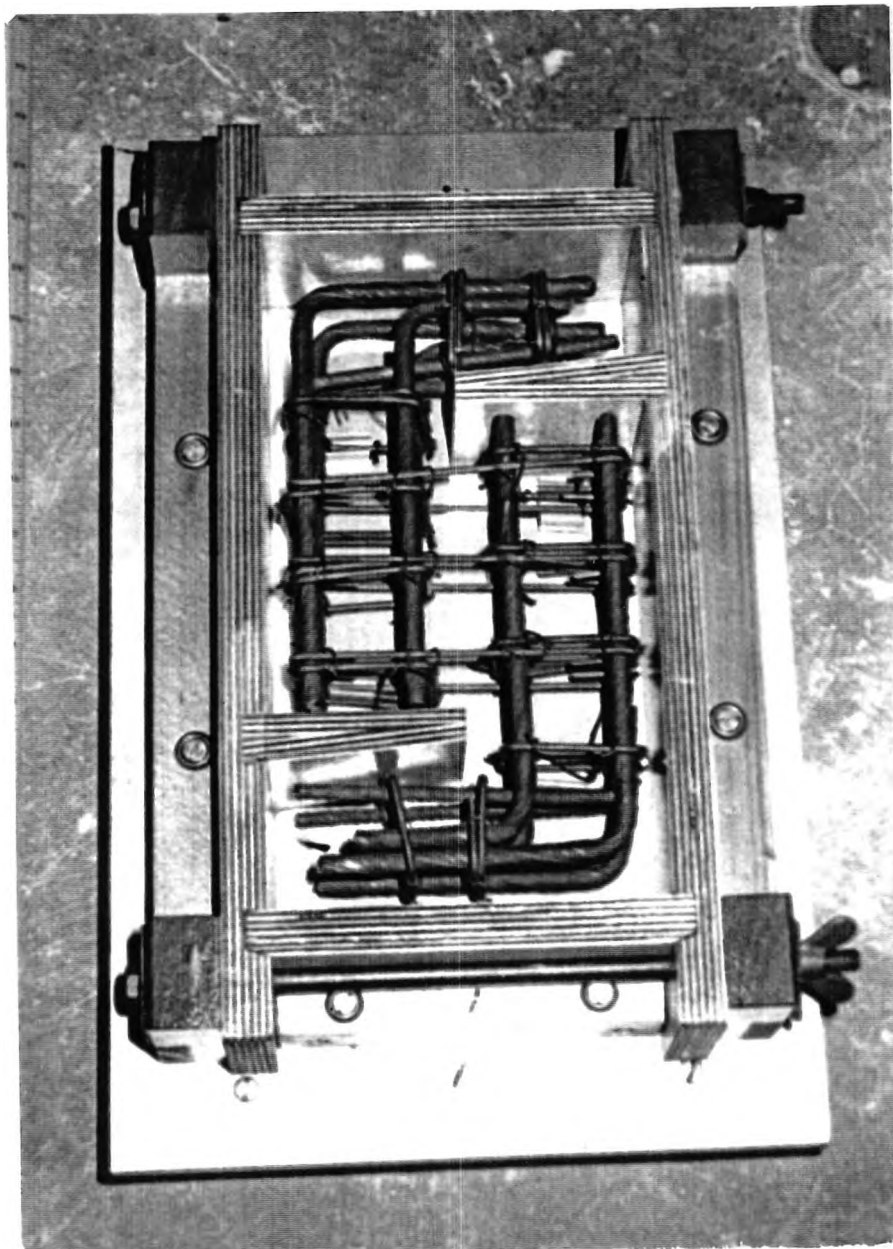


FIGURE 2.8 **HALF SIZE SPECIMEN REINFORCING CAGE AND FORMWORK**

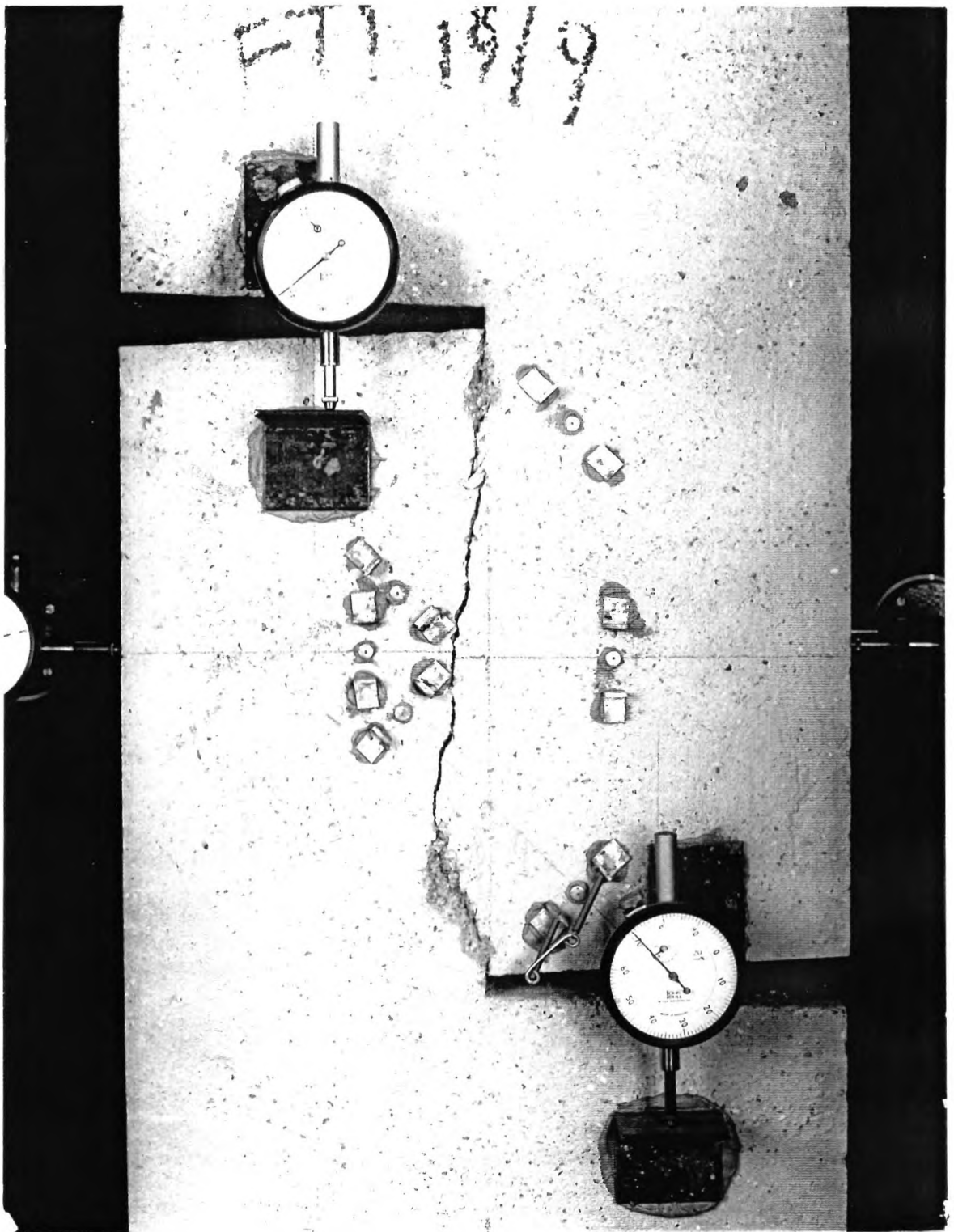


FIGURE 2.9

CRACKING ALONG SHEAR PLANE

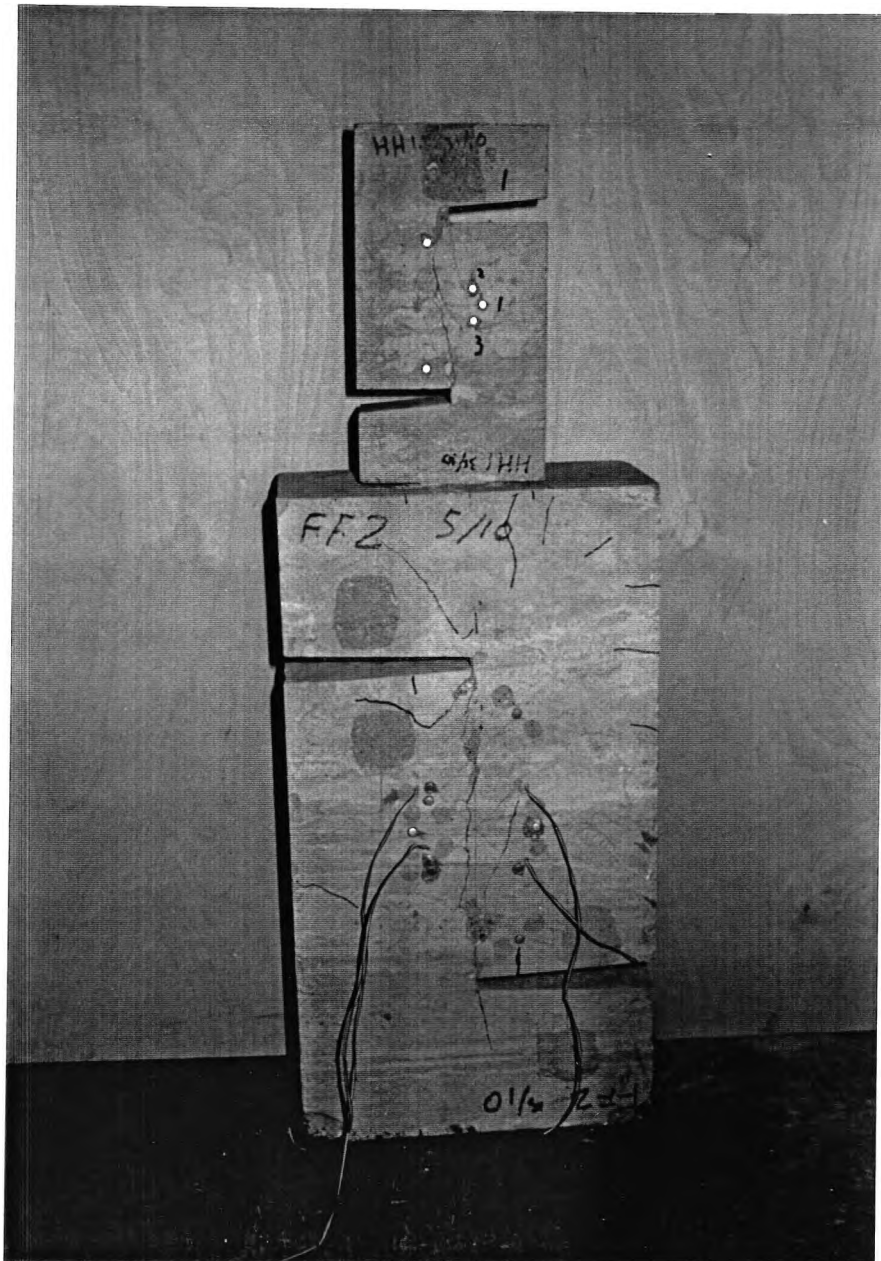


FIGURE 2.10

FULL SIZE AND HALF SIZE SPECIMEN

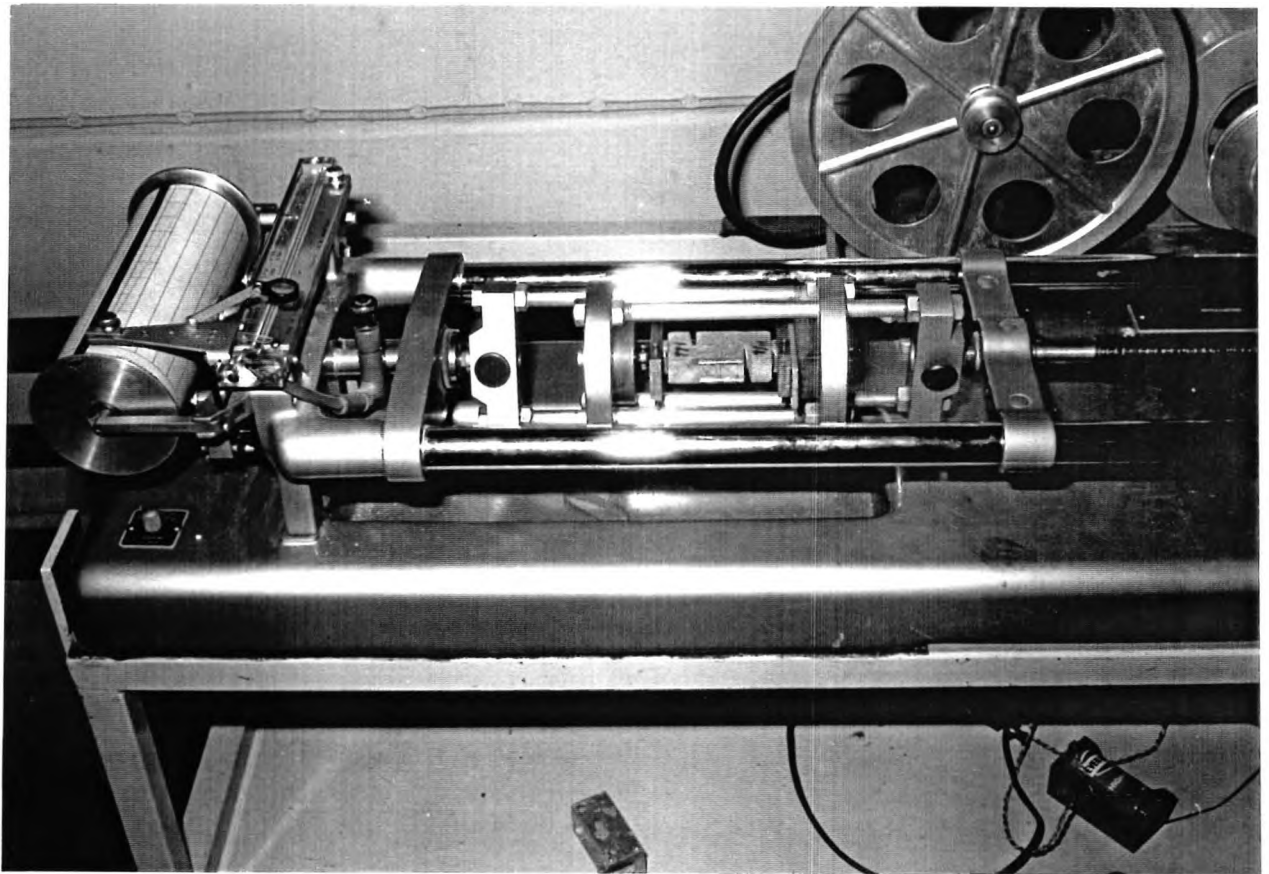


FIGURE 2.11

TENTH SCALE SPECIMEN IN TENSIOMETER

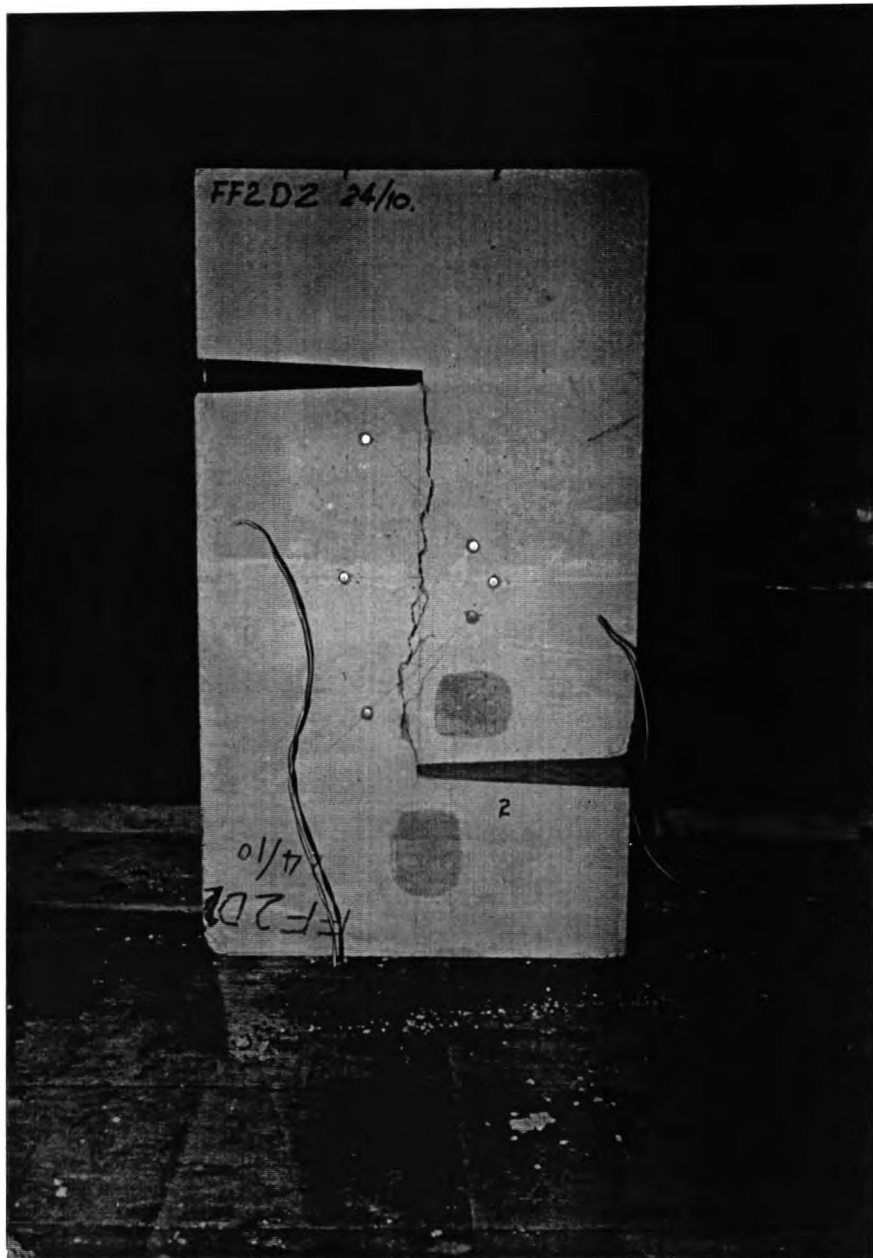


FIGURE 2.12

**NON-SYMMETRICAL REINFORCED SPECIMEN
LARGER CRACK WIDTH ON LOW REINFORCED SURFACE**



FIGURE 2.13

NON-SYMMETRICAL REINFORCED SPECIMEN
SMALLER CRACK WIDTH ON HIGH REINFORCED SURFACE

FIGURE 2.14 SHEAR STRESS Vs NORMAL DISPLACEMENT

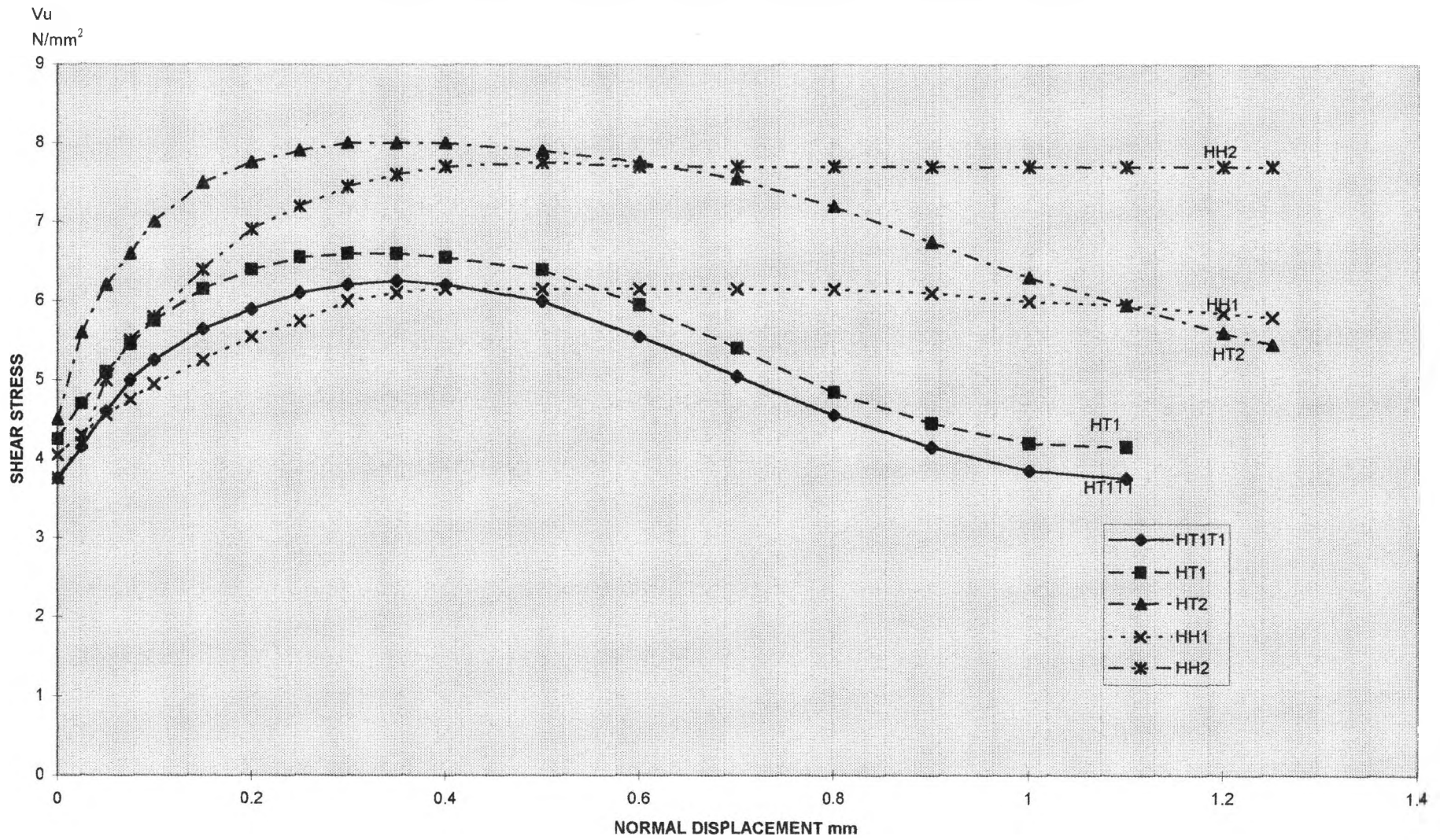


FIGURE 2.15 SHEAR DISPLACEMENT Vs NORMAL DISPLACEMENT

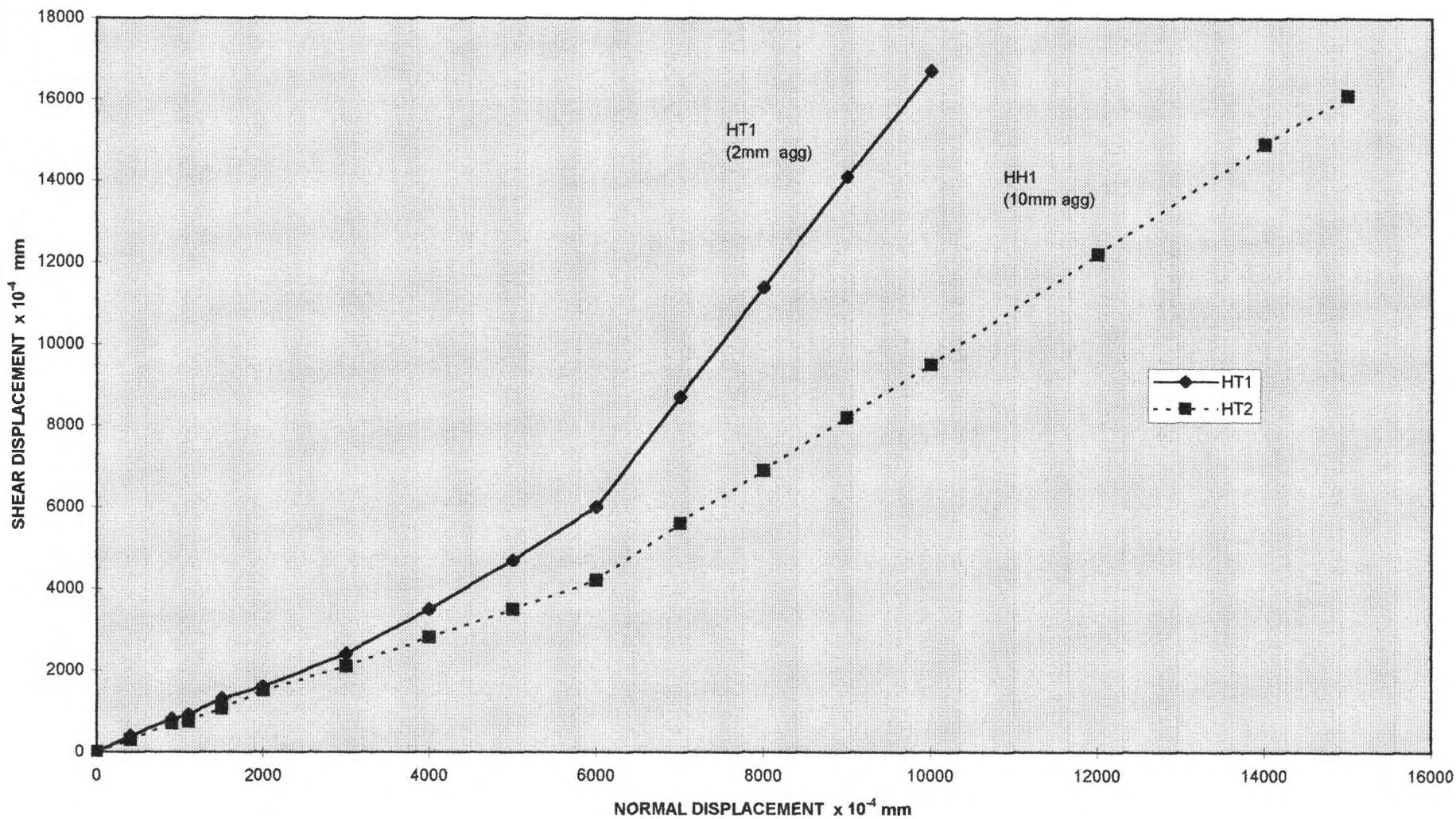


FIGURE 2.16 SHEAR STRESS Vs NORMAL STRESS

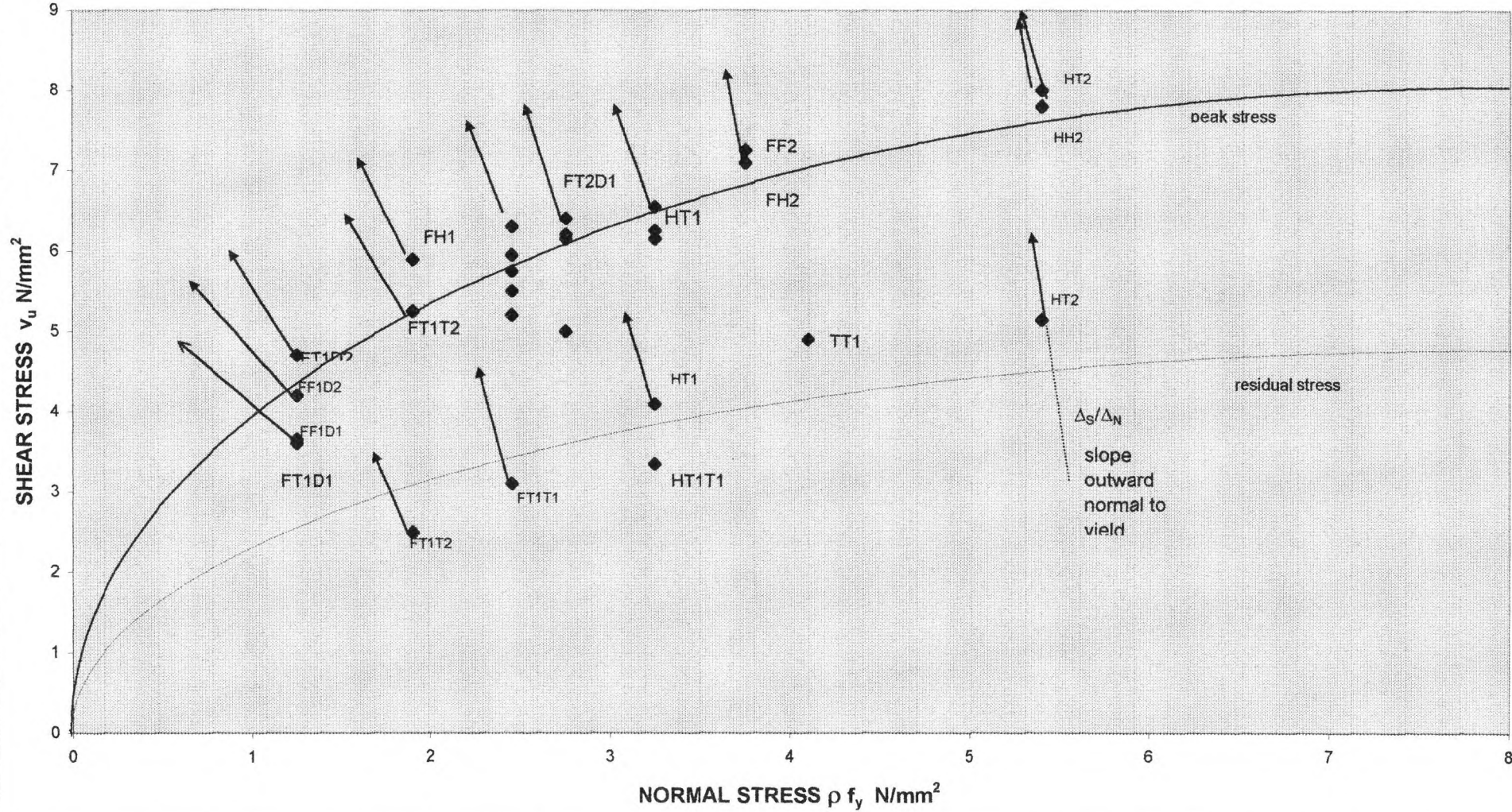


FIGURE 2.17 NON DIMENSIONAL SHEAR STRESS Vs NORMAL STRESS

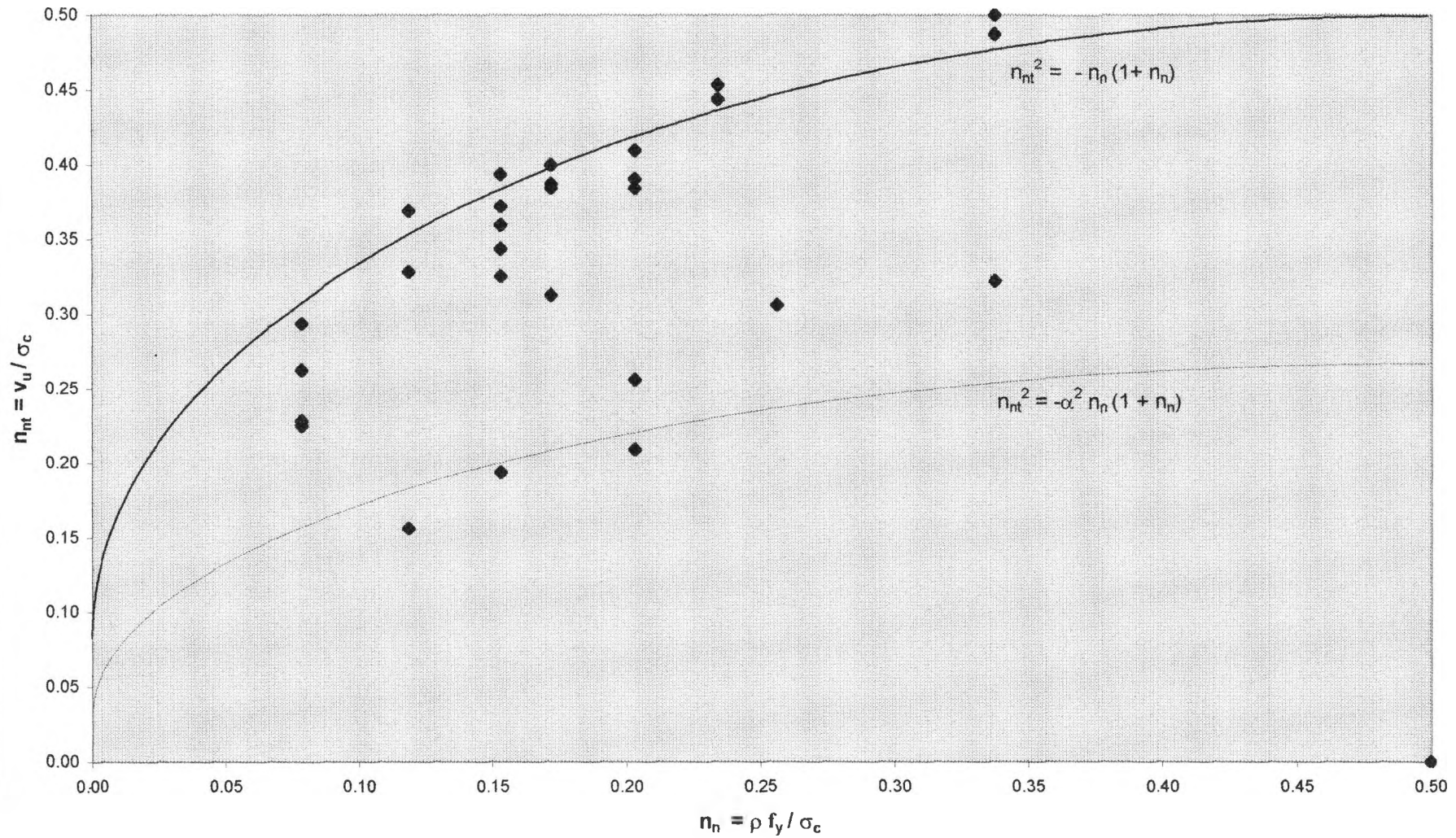
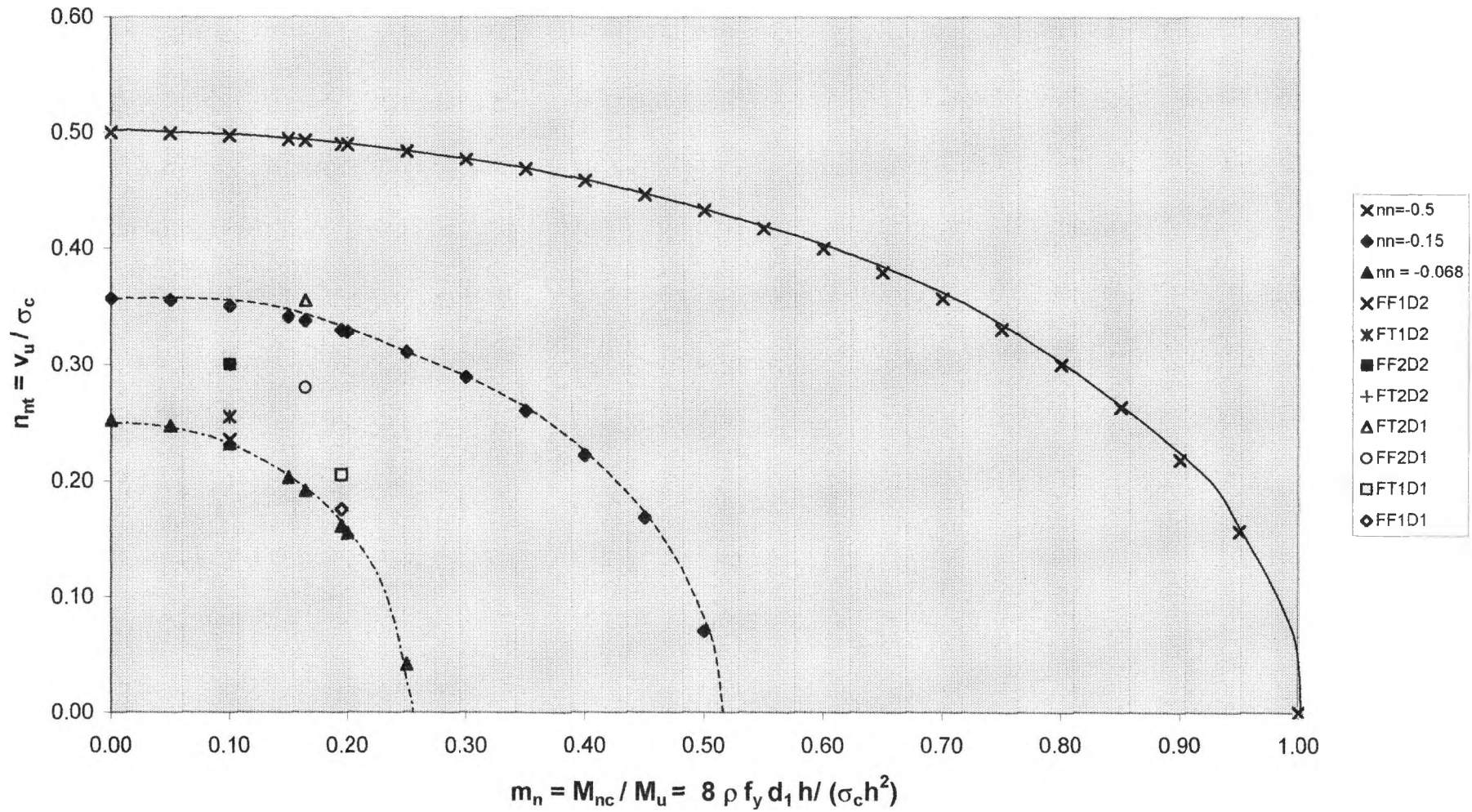


FIGURE 2.18 NON-DIMENSIONAL SHEAR Vs MOMENT



Chapter 3 Yield Criterion For Reinforced and Prestressed Concrete

3.1 Introduction

This chapter outlined the theory of plasticity and discussed how the theory can be applied to an apparent non-ductile concrete material. A generalised yield criterion was proposed which combined bending, shear and axial force resultants. The criterion was developed from a bi-axial stress and a combine axial and shear stress condition. Modification factors were included in the yield criterion to account for the material ductility. The effect of prestressing is discussed and suitable conclusion drawn.

3.2 General Plastic Theory

3.2.1 Yield Condition and Yield Surface

In Plasticity Theory, the yield condition describes the combination of stresses or internal forces that can produce yielding. The yield condition can be given as:

$$f(\sigma_i) = 0 \text{ -----3.1}$$

The above expression describes the yield condition in stress tensor, it can equally be expressed in terms of the moment tensor or force tensor. The sign for the expression is usually adjusted so that $f < 0$ corresponds to status prior to yielding, i.e. only elastic strain has taken place for an elastic plastic material. For perfectly rigid plastic material, no strain is developed. For the stress condition $f = 0$, yielding of the material takes place. The condition $f > 0$ is not possible for perfectly rigid plastic materials. The stresses in the yield condition may include reactions. This is useful in the so-called lower bound solution where the state of equilibrium for the whole structural system has to be maintained. For the case of an upper bound solution with perfectly plastic material and non yielding supports, the reactions do not need to be included in the yield condition since the strain rate will be zero.

The surface or curve corresponding to $f = 0$ is often known as the yield surface or yield curve.

3.2.2 Flow Rule and Normality Rule

By means of the flow rule, the plastic strains can be related to the yield condition as:

$$e_i = \lambda \frac{\partial f(\sigma_i)}{\partial \sigma_i} \text{ -----3.2}$$

If the strain tensor is considered as a vector in the co-ordinate system of the yield conditions, this vector is an outward normal to the yield surface, which is convex.

The internal dissipation or work done can be expressed as:

$$D = \sum_{i=1}^n \sigma_i \epsilon_i \text{ -----3.3}$$

The work equation is a maximum when moving along the top of the yield surface, hence, the rate of change would be zero. All other work equations within the yield surface would be less. At points where the normal to the yield surface cannot be defined, the strain tensor would still be restricted to within limiting values satisfying the general work equation 3.3. Thus, at an apex, the admissible strain rates are permitted to lie within the angle contained by the normal to the adjoining discontinuity of the yield surface.

3.2.3 Lower Bound and Upper Bound Theorems

The lower bound theorem can be defined as a load on the structure resulting in a stress field just on or within the yield surface. In proportional loading, the load will always be less than or equal to the load carrying capacity of the structure.

In the case of an upper bound solution, if the internal work corresponding to an arbitrary kinematic admissible strain field is lower than the external work, the corresponding load is always greater or just equal to the load-carrying capacity of the structure.

For the case of proportional loading, there is only one theoretical load for which a safe stress field and a kinematically admissible strain field can be found. Only under this condition would an exact solution or the true collapse load be determined.

3.3 Yield Criterion of Concrete Elements

3.3.1 Yield Criterion of a Concrete Element Subjected to Bi-axial Stress State

Concrete material has been used advantageously in structures for its relatively high compressive strength. Under uni-axial compression, after the ultimate strength is reached, the test cube or cylinder may exhibit a certain degree of strain softening. Non the less it would still sustain a load near the maximum with increasing strain. It is therefore not unrealistic to treat it as a material with plastic behaviour in compression.

In direct tension however, its strength is very limited, often less than one tenth of the compressive strength. The concrete splits when the maximum tensile strength is reached with a sudden brittle failure. Hence the maximum tensile stress cannot be maintained. Comparing with the compressive strength, the tensile strength of concrete is small and is often ignored. However, the material could still be treated as behaving plastically. Any tensile stress will result in increasing tensile strain for un-reinforced concrete. In practice, either steel reinforcement or an external pre-compression in the form of prestressing resists tensile stress in concrete.

Many other researchers have used the square yield criterion with some degree of success. When concrete element is subjected to bi-axial stress only, if the material was assumed to be rigid plastic having no tensile strength, the yield criterion of concrete subjected to bi-axial stress is shown in figure 3.1.

It is to be noted that the strain rates plotted on the corresponding stress co-ordinates are normal to the yield surface. At the corners O, A, B, C, the strain rates will lie between the two outward normal of the adjacent plane yield surfaces. If the strain rates are known, the state of the stresses in the concrete may be established. Along the flat of a yield surface, however, the complete stress resultants may not be known.

By considering the square yield surface shown in Figure 3.1, the following can be deduced for the strains and stresses.

On the flat surface OA,

$$e_x = +ve; e_y = 0, \quad \sigma_x = 0; 0 \geq \sigma_y \geq -\sigma_c \text{-----} 3.4$$

On the flat surface AB,

$$e_x = 0; e_y = -ve, \quad 0 \geq \sigma_x \geq -\sigma_c; \sigma_y = -\sigma_c \text{-----} 3.5$$

On the flat surface BC,

$$e_x = -ve; e_y = 0, \quad \sigma_x = -\sigma_c; 0 \geq \sigma_y \geq -\sigma_c. \text{-----} 3.6$$

On the flat surface OC,

$$e_x = 0; e_y = +ve, \quad 0 \geq \sigma_x \geq -\sigma_c; \sigma_y = 0 \text{-----} 3.7$$

The general energy equation 3.3 for a concrete element subjected to a biaxial stress state can be written as:

$$D = \sum \sigma_x e_x + \sum \sigma_y e_y \text{-----} 3.8$$

For the state of stress on the yield surface BC, the above energy equation can be reduced to the first term only. It can be shown that the stress in the Y direction need not be known. The reason is that σ_y corresponds to e_y which is zero. Hence the energy dissipation from σ_y is also zero.

An important feature in the upper bound analysis is that only stress resultants that correspond to a plastic strain need be considered in the energy equation.

3.3.2 Yield Criterion of Concrete Subjected to Bending and Axial Forces

In the case of bending, along the so called Johansen yield lines, yielding can be assumed to be concentrated on a narrow zone where the stress resultants reach the yield condition of the constituent material. The area adjacent to the yield line can be assumed to be non-yielding. The strain rates of such a yield line will consist of a normal strain e_n , and a curvature rate k . Whilst the curvature rate k is related to the rotation rate θ of the yield line. The normal strain rate varies linearly with the depth from the mid-depth of the section and the curvature rate.

The curvature rate is taken as positive anti-clockwise. The tensile normal strain is positive (Figure 3.2). For this type of yield line, there is no tangential dislocation of the yield line, therefore, the tangential strain rate should also be zero and,

$$e_n = e_o + k z \text{ -----3.9}$$

$$e_t = 0 \text{ -----3.10}$$

With the strain rates known at any depth, the stress resultants may be determined from the yield surface shown in figure 3.1. The above strain rates correspond to stresses on the flat surface BC and the stresses are in compression. The strain below the neutral axis is tensile, the corresponding stress, therefore, is zero. The transverse strain is zero which indicates non-yielding, and depends on the boundary conditions, thus,

$$\sigma_n = -\sigma_c \quad \text{above neutral axis}$$

$$\sigma_n = 0 \quad \text{below neutral axis}$$

$$0 > \sigma_t > -\sigma_c \quad \text{non-yielding}$$

By summing through the entire depth of the concrete slab section, the normal force resultant can be written as:

$$N_n = -\sigma_c \left(\frac{h}{2} + Z_n \right) \text{-----} 3.11$$

The bending moment can be written as:

$$M_n = -N_n \left[\frac{h}{2} - \frac{1}{2} \left(\frac{h}{2} + Z_n \right) \right] \text{-----} 3.12$$

Substituting 3.11 into 3.12

$$\begin{aligned} M_n &= \frac{\sigma_c}{2} \left[\left(\frac{h^2}{2} \right) - Z_n^2 \right] \\ &= -\frac{N_n}{2} \left(h + \frac{N_n}{\sigma_c} \right) \text{-----} 3.13 \end{aligned}$$

For maximum values of M_n

$$\begin{aligned} \frac{\partial M_n}{\partial N_n} &= 0 \\ \frac{h}{2} + \frac{2N_n}{2\sigma_c} &= 0 \\ N_n &= -\frac{\sigma_c h}{2} \text{-----} 3.14 \end{aligned}$$

∴

$$\begin{aligned} M_{\max} &= \frac{\sigma_c h}{4} \left(h - \frac{h}{2} \right) \\ M_{\max} &= \frac{\sigma_c h^2}{8} \text{-----} 3.15 \end{aligned}$$

Introducing the non dimensionless terms

$$m_n = \frac{8M_n}{\sigma_c h^2} \quad ; \quad n_n = \frac{N_n}{\sigma_c h}$$

3.13 can be written as:

$$m_n = -4 n_n (1 + n_n) \text{-----} 3.16$$

This is the parametric yield surface equation for an unreinforced concrete member subjected to bending and axial forces only.

If the bending curvature reverses, the section below the neutral axis becomes compressive, and equations 3.11, 3.12, 3.13 and 3.16 can be written as:

$$N_n = -\sigma_c \left(\frac{h}{2} - Z_n \right) \text{-----} 3.17$$

$$M_n = N_n \left[\frac{h}{2} - \frac{1}{2} \left(\frac{h}{2} - Z_n \right) \right] \text{-----} 3.18$$

$$\begin{aligned} M_n &= -\frac{\sigma_c}{2} \left[\left(\frac{h^2}{2} \right) - Z_n^2 \right] \\ &= \frac{N_n}{2} \left(h + \frac{N_n}{\sigma_c} \right) \text{-----} 3.19 \end{aligned}$$

$$m_n = 4 n_n (1 + n_n) \text{-----} 3.20$$

The parametric equations 3.16 and 3.20 indicate that for the same axial force, the bending moment can reverse depending on the eccentricity of the applied force. Therefore, for a more general yield surface equation covering both +ve and -ve moment, the combined yield surface equation can be written as:

$$m_n = \pm 4 n_n (1 + n_n) \text{-----} 3.21$$

Squaring and rearranging the equation,

$$\frac{m_n^2}{[4 n_n (1 + n_n)]^2} = 1 \text{-----} 3.22$$

For +ve bending curvature, i.e., $k \geq 0$

$$m_n = -4 n_n (1 + n_n)$$

and for $k \leq 0$,

$$m_n = 4 n_n (1 + n_n)$$

Since concrete may be considered not to resist tensile forces, the normal stress would have a value between 0 and $-\sigma_c$, or in non-dimensional parametric term $0 \geq n_n \geq -1$.

3.3.3 Yield Criterion of Concrete Subjected to Shear and Axial Force

Mohr's stress circle can be applied to concrete subjected to axial force and shear. The maximum stress would be equals $-\sigma_c$ and the maximum shear stress occurs when axial stress equals $-\frac{1}{2}\sigma_c$. Equation for the shear and normal stress can be written as:

$$\tau^2 = -\sigma_n (\sigma_c + \sigma_n) \text{-----} 3.23$$

This yield criterion holds true if the concrete possesses sufficient shear ductility at the peak shear stress. However, from the shear tests involving the sand mix, (Chapter 2) the shear stress reduced rapidly to a residual value. Hence the yield condition could be modified to include a shear reduction factor α . This can be represented by the equation of an ellipse. The equation including the modification factor can be written as:

$$\tau^2 = -\alpha^2 \sigma_n (\sigma_c + \sigma_n) \text{-----} 3.24$$

The modification factor α has been deduced from the experimental results given in Chapter 2.

Equation 3.24 can be written as a yield surface equation as follows:

$$\Phi = \tau^2 + \alpha^2 \sigma_n (\sigma_c + \sigma_n) = 0 \text{-----} 3.25$$

The strain rates tend to take up a specific direction when the concrete element fails due to shear and normal forces. According to the flow rule of plasticity (equation 3.2). The normal and shear strain rate can be written as:

$$e_n = \lambda \frac{\partial \Phi}{\partial \sigma_n} = \lambda [\alpha^2 (\sigma_c + 2\sigma_n)] \text{-----} 3.26$$

and
$$2e_{nt} = \lambda \frac{\partial \Phi}{\partial \tau} = 2 \lambda \tau \text{-----} 3.27$$

Therefore, the slope of the outward normal to the yield surface can be expressed as:

$$\frac{2e_{nt}}{e_n} = \frac{2\tau}{\alpha^2(\sigma_c + 2\sigma_n)} \text{-----3.28}$$

and the tangent to the yield surface on the τ - σ_n plane is given by :

$$\frac{\partial \tau}{\partial \sigma_n} = \frac{-\alpha^2(\sigma_c + 2\sigma_n)}{2\tau} \text{-----3.29}$$

It can be seen that the resultant of the strain rate is an outward normal to the yield surface which satisfies the condition of orthogonality, and hence the normality rule of plasticity.

$$\frac{\partial \tau}{\partial \sigma_n} \cdot \frac{2e_{nt}}{e_n} = -1 \text{-----3.30}$$

Introducing a strain rate ratio $\gamma = \frac{e_n}{2e_{nt}}$

3.28 can be written as:

$$\tau = \frac{\alpha^2(\sigma_c + 2\sigma_n)}{2\gamma} \text{-----3.31}$$

Substituting into 3.24 and rearranging,

$$\sigma_n = \frac{-\sigma_c}{2} \left[1 - \frac{\gamma}{\sqrt{\gamma^2 + \alpha^2}} \right] \text{-----3.32}$$

$$\tau = \frac{\sigma_c}{2} \frac{\alpha^2}{\sqrt{\gamma^2 + \alpha^2}} \text{-----3.33}$$

The tangential stress may also be determined from the Mohr circle of stress:

$$\sigma_t = \frac{-\alpha_c}{2} \left[1 - \frac{\gamma(1 - 2\alpha^2)}{\sqrt{\gamma^2 + \alpha^2}} \right] \text{-----3.34}$$

Equations 3.32, 3.33 and 3.34 indicate that the normal and shear stresses can be determined if the strain rates are known.

Substituting the non-dimensional parametric terms

$$n_{nt} = \frac{\tau}{\sigma_c} \quad \text{and} \quad n_n = \frac{\sigma_n}{\sigma_c}$$

Equation 3.24 can be written as:

$$n_{nt}^2 = -\alpha^2 n_n (1 + n_n)$$

$$\text{or} \quad \frac{n_{nt}^2}{-\alpha^2 n_n (1 + n_n)} = 1 \text{-----3.35}$$

This is the parametric yield surface equation for concrete subjected to normal and shear forces.

3.3.4 Yield Criterion of Concrete Subjected to Bending, Shear and Axial Force

It is possible for bending, shear and axial stress resultants to act along a yield line in a more complex collapse mechanism. The corresponding displacement vectors along such generalised yield lines would be the normal and shear displacement together with the rotation rate. Figure 3.3

For an infinitesimal yield zone width $\Delta x \rightarrow 0$, the corresponding homogeneous strain rates could be written as:

$$e_n, e_{nt}, e_{tt} \text{ and } k.$$

As before e_{tt} could be taken as zero since it occurs on both sides of the yield zone within the rigid non-yielding region. If e_n is taken as +ve for tensile strain, a normal strain distribution throughout the depth of a section can be shown thus in figure 3.4

At any depth z from the centre axis of the section, the corresponding strain rates are:

$$e_n = e_o + k z \text{-----} 3.36$$

$$2e_{nt} = 2\varepsilon_{nt} = \text{constant} \text{-----} 3.37$$

$$e_{tt} = \varepsilon_{tt} = 0 \text{-----} 3.38$$

Hence the strain rate ratio $\gamma = e_n / (2e_{nt})$ at each layer of the concrete is known. The associated concrete stresses can also be established using the relationship in equations 3.32, 3.33 and 3.34

$$\sigma_n = \frac{-\sigma_c}{2} \left[1 - \frac{\gamma}{\sqrt{(\gamma^2 + \alpha^2)}} \right] \text{-----} 3.39$$

$$\tau = \frac{\sigma_c}{2} \frac{\alpha^2}{\sqrt{(\gamma^2 + \alpha^2)}} \text{-----} 3.40$$

$$\sigma_t = \frac{-\sigma_c}{2} \left[1 - \frac{\gamma(1 - 2\alpha^2)}{\sqrt{(\gamma^2 + \alpha^2)}} \right] \text{-----} 3.41$$

With the stresses known at each layer dz of the concrete, the total normal force, shear force and bending moment resultant can be evaluated by integrating through the entire depth of the section.

$$\text{Normal Force: } N_n = \int_{-h/2}^{h/2} \sigma_n dz \text{ -----3.42}$$

$$\text{Shear Force: } N_{nt} = \int_{-h/2}^{h/2} \tau dz \text{ -----3.43}$$

$$\text{Bending : } M_n = \int_{-h/2}^{h/2} \sigma_n z dz \text{ -----3.44}$$

$$\text{Tangential Force: } N_t = \int_{-h/2}^{h/2} \sigma_t dz \text{ -----3.45}$$

$$\text{Tangential Moment: } M_t = \int_{-h/2}^{h/2} \sigma_t z dz \text{ -----3.46}$$

$$\text{Twisting Moment: } T_n = \int_{-h/2}^{h/2} \tau z dz \text{ -----3.47}$$

Equations 3.42, 3.43 and 3.44 are the primary stress resultants that will affect the yield criterion. Whilst the last three equations 3.45, 3.46 and 3.47 are secondary resultants which although do not affect the yield criterion, contribute to the overall equilibrium condition along the yield line.

The force resultants of equations 3.42 to 3.47 can be computed by substituting the strain rate ratio γ of equations 3.36, 3.37 by the following:

$$\text{at } z=h/2 \quad \beta = \gamma_{\text{top}} = \frac{\epsilon_n + \frac{k_n \cdot h/2}{2e_{nt}}}{2e_{nt}} \text{-----3.48}$$

$$\text{at } z=-h/2 \quad \delta = \gamma_{\text{bot}} = \frac{\epsilon_n - \frac{k_n \cdot h/2}{2e_{nt}}}{2e_{nt}} \text{-----3.49}$$

substituting and rearranging;

$$\frac{\epsilon_n}{2e_{nt}} = \frac{\beta + \delta}{2} \text{-----3.50}$$

$$\frac{k_n}{2e_{nt}} = \frac{\beta - \delta}{h} \text{-----3.51}$$

$$z = \frac{h}{\beta - \delta} \left(\gamma - \frac{\beta + \delta}{2} \right) ; \quad dz = \frac{h}{\beta - \delta} \cdot d\gamma \text{----3.52}$$

therefore equation 3.42 can be written as

$$N_n = -\frac{\sigma_c h}{2(\beta - \delta)} \int_{\delta}^{\beta} \left[1 - \frac{\gamma}{\sqrt{(\gamma^2 + \alpha^2)}} \right] \cdot d\gamma$$

Integrating in respect of γ and introducing :

$$\chi = \sqrt{(\beta^2 + \alpha^2)} - \sqrt{(\delta^2 + \alpha^2)}$$

and also substituting for the non dimensional parametric term:

$$n_n = N_n / \sigma_c h$$

$$n_n = \frac{1}{2} \left[\frac{\chi}{(\beta - \delta)} - 1 \right] \text{-----3.53}$$

Similarly for the shear force, equation 3.43 becomes:

$$N_{nt} = -\frac{\sigma_c h a^2}{2(\beta - \delta)} \int_{\delta}^{\beta} \left[\frac{1}{\sqrt{(\gamma^2 + a^2)}} \right] \cdot d\gamma \text{ -----3.54}$$

putting $\text{Sinh}^{-1} \frac{\gamma}{a} = y$ and $\frac{\gamma}{a} = \text{Sinh } y = \frac{e^y - e^{-y}}{2}$

therefore $e^{2y} - 2 \frac{\gamma}{a} e^y - 1 = 0$

solving the binomial equation;

$$e^y = \frac{\gamma}{a} + \sqrt{\left(\frac{\gamma^2}{a^2} + 1 \right)}$$

hence, $y = \log_e \frac{\gamma}{a} + \sqrt{\left(\frac{\gamma^2}{a^2} + 1 \right)}$

Also; $\frac{d\gamma}{a} = \text{Cosh } y \, dy$

$$\text{Cosh } y = \sqrt{1 + \text{Sinh}^2 y} = \frac{\sqrt{(\gamma^2 + a^2)}}{a}$$

therefore the integral term in equation 3.54 can be written as:

$$\int_{\delta}^{\beta} \left[\frac{1}{\sqrt{(\gamma^2 + a^2)}} \right] \cdot d\gamma = \int \frac{a \text{Cosh } y \, dy}{a \text{Cosh } y} = \int dy = y$$

introducing $U = \log_e \frac{\beta + \sqrt{(\beta^2 + a^2)}}{\delta + \sqrt{(\delta^2 + a^2)}}$

and the non dimensional parametric term given by:

$$n_{nt} = N_{nt} / \sigma_c h$$

the following is obtained:

$$\underline{\underline{n_{nt} = \frac{\alpha^2 U}{2(\beta - \delta)} \text{ -----3.55}}}$$

For the bending moment, equation 3.44 can be written as:

$$\begin{aligned}
 M_n &= -\frac{\sigma_c h^2}{2(\beta-\delta)^2} \int_{\delta}^{\beta} \left[1 - \frac{\gamma}{\sqrt{(\gamma^2 + \alpha^2)}} \right] \cdot \left(\gamma - \frac{\beta + \delta}{2} \right) \cdot d\gamma \\
 &= \frac{\sigma_c h^2}{2(\beta-\delta)^2} \left\{ \frac{\beta + \delta}{2} \int_{\delta}^{\beta} \left[1 - \frac{\gamma}{\sqrt{(\gamma^2 + \alpha^2)}} \right] \cdot d\gamma + \int_{\delta}^{\beta} \frac{\gamma^2}{\sqrt{(\gamma^2 + \alpha^2)}} \cdot d\gamma \right. \\
 &\quad \left. - \int_{\delta}^{\beta} \gamma \cdot d\gamma \right\}
 \end{aligned}$$

The first integral term can be compared with that for N_n . For the second term may be considered by using the expression:

$$y = \text{Sinh}^{-1} \gamma/\alpha \quad \text{i.e.} \quad \text{Sinh } y = \gamma/\alpha$$

$$\begin{aligned}
 \int_{\delta}^{\beta} \frac{\gamma^2}{\sqrt{(\gamma^2 + \alpha^2)}} \cdot d\gamma &= \int a^2 \text{Sinh}^2 y \cdot dy \\
 &= \frac{a^2}{2} \int (\text{Cosh} 2y - 1) \cdot dy \\
 &= \frac{a^2}{2} \left(\frac{\text{Sinh} 2y}{2} - y \right) \\
 &= \frac{a^2}{2} \left(\text{Sinhy} \cdot \text{Coshy} - y \right) \\
 &= \frac{a^2}{2} \left[\frac{\gamma \sqrt{(\gamma^2 + \alpha^2)}}{\alpha^2} - \text{Sinh}^{-1} \frac{\gamma}{\alpha} \right] \Big|_{\delta}^{\beta}
 \end{aligned}$$

Introducing $\phi = \beta \sqrt{(\beta^2 + \alpha^2)} - \delta \sqrt{(\delta^2 + \alpha^2)}$ and the non-dimensional parametric term given by

$$m_n = M_n / (\sigma_c h^2 / 8)$$

$$\begin{aligned}
M_n &= \frac{\sigma_c h^2}{2(\beta-\delta)^2} \left[\frac{\beta+\delta}{2} (\beta-\delta-\chi) + \frac{1}{2} \cdot \phi - \frac{U \cdot \alpha^2}{2} - \frac{\beta^2-\delta^2}{2} \right] \\
&= \frac{\sigma_c h^2}{2(\beta-\delta)^2} \left[\frac{1}{2} \cdot \phi - \frac{U \cdot \alpha^2}{2} - \frac{\beta+\delta \cdot \chi}{2} \right] \\
m_n &= \frac{2}{(\beta-\delta)^2} \left[\phi - U \cdot \alpha^2 - (\beta+\delta) \cdot \chi \right] \text{-----3.56}
\end{aligned}$$

The Tangential force in equation 3.45 can be written as

$$N_t = -\frac{\sigma_c}{2} \int_{-h/2}^{h/2} \left[1 - \frac{\gamma(1-2\alpha^2)}{\sqrt{(\gamma^2 + \alpha^2)}} \right] \cdot dz$$

for non-dimensional parametric term

$$n_t = \frac{1}{2} \left[\frac{\chi(1-2\alpha^2)}{(\beta-\delta)} - 1 \right] \text{-----3.57}$$

The Tangential moment in equation 3.46 can be expressed as:

$$\begin{aligned}
M_t &= -\frac{\sigma_c}{2} \int_{-h/2}^{h/2} \left[1 - \frac{\gamma(1-2\alpha^2)}{\sqrt{(\gamma^2 + \alpha^2)}} \right] \cdot z \cdot dz \\
&= -\frac{\sigma_c h^2}{2(\beta-\delta)^2} \int_{\delta}^{\beta} \left[1 - \frac{\gamma(1-2\alpha^2)}{\sqrt{(\gamma^2 + \alpha^2)}} \right] \cdot \left(\gamma - \frac{\beta + \delta}{2} \right) \cdot d\gamma
\end{aligned}$$

which may be reduced to the following by noting the integral in previous equations and writing in parametric form

$$m_t = \frac{2}{(\beta-\delta)^2} \left[\phi - U \cdot \alpha^2 - (\beta+\delta) \cdot \chi \right] (1-2\alpha^2) \text{-----3.58}$$

Finally, the twisting moment of equation 3.47 can be written as

$$M_{tw} = -\frac{\sigma_c h^2 \alpha^2}{2(\beta-\delta)^2} \int_{\delta}^{\beta} \frac{1}{\sqrt{(\gamma^2 + \alpha^2)}} \cdot (\gamma - \frac{\beta+\delta}{2}) \cdot d\gamma$$

which can be reduced to the non-dimensional form expressed as

$$\underline{m_{tw} = \frac{4\alpha^2}{(\beta-\delta)^2} \left[\chi - \left(\frac{\beta+\delta}{2} \right) \cdot U \right]} \text{-----3.59}$$

The center of action of the force resultants can be written as:

$$Z_n = \frac{M_n}{N_n} = \frac{\sigma_c h^2 / 8 \cdot m_n}{\sigma_c h \cdot n_n} = \frac{m_n h}{n_n 8} \text{-----3.60}$$

$$Z_{nt} = \frac{M_{tw}}{N_{nt}} = \frac{\sigma_c h^2 / 8 \cdot m_{tw}}{\sigma_c h \cdot n_{nt}} = \frac{m_{tw} h}{n_{nt} 8} \text{-----3.61}$$

$$Z_t = \frac{M_t}{N_t} = \frac{\sigma_c h^2 / 8 \cdot m_t}{\sigma_c h \cdot n_t} = \frac{m_t h}{n_t 8} \text{-----3.62}$$

It should be noted that when the curvature rate is zero, $\gamma = \beta = \delta = \text{constant}$ and the normal force equation becomes:

$$n_n = \frac{1}{2} \left[\frac{\beta}{\sqrt{(\beta^2 + \alpha^2)}} - 1 \right] \text{-----3.53a}$$

which is independent of the depth z.

The shear force equation becomes:

$$n_{nt} = \frac{\alpha^2}{2\sqrt{(\beta^2 + \alpha^2)}} \text{-----3.55a}$$

and the bending moment reduces to zero. Table 3.1 gives a summary of the parametric stress resultants.

TABLE 3.1 SUMMARY OF PARAMETRIC STRESS RESULTANTS

| | $\beta \neq \delta$ | $\beta = \delta$ |
|-----------------------------|--|---|
| Normal Force n_n | $\frac{1}{2} \left[\frac{\chi}{\beta - \delta} - 1 \right]$ | $\frac{1}{2} \left[\frac{\beta}{\sqrt{\beta^2 + \alpha^2}} - 1 \right]$ |
| Shear Force n_{nt} | $\frac{\alpha^2 U}{2(\beta - \delta)}$ | $\frac{\alpha^2}{2\sqrt{\beta^2 + \alpha^2}}$ |
| Normal Moment m_n | $\frac{2[\phi - U \cdot \alpha^2 - (\beta + \delta) \cdot \chi]}{(\beta - \delta)^2}$ | 0 |
| Tangential Force n_t | $\frac{1}{2} \left[\frac{\chi(1 - 2\alpha^2)}{\beta - \delta} - 1 \right]$ | $\frac{1}{2} \left[\frac{\beta(1 - 2\alpha^2) + 1}{\sqrt{\beta^2 + \alpha^2}} \right]$ |
| Tangent. Moment m_t | $\frac{2[\phi - U \cdot \alpha^2 - (\beta + \delta) \chi](1 - 2\alpha^2)}{(\beta - \delta)^2}$ | 0 |
| Twisting Moment m_{tw} | $\frac{4\alpha^2}{(\beta - \delta)^2} \left[\chi - \frac{\beta + \delta}{2} \right] \cdot U$ | 0 |

Where: $n_n = N_n / \sigma_{ch}$, $n_{nt} = N_{nt} / \sigma_{ch}$, $m_n = M_n / (\sigma_{ch}^2 / 8)$,
 $n_t = N_t / \sigma_{ch}$, $m_t = M_t / (\sigma_{ch}^2 / 8)$ and $m_{tw} = M_{tw} / (\sigma_{ch}^2 / 8)$

$$\chi = \sqrt{\beta^2 + \alpha^2} - \sqrt{\delta^2 + \alpha^2}$$

$$U = \log_e \frac{\beta + \sqrt{\beta^2 + \alpha^2}}{\delta + \sqrt{\delta^2 + \alpha^2}}$$

$$\phi = \beta \sqrt{\beta^2 + \alpha^2} - \delta \sqrt{\delta^2 + \alpha^2}$$

$$\beta = \gamma_{top} = \frac{\epsilon_n}{2} + \frac{k_n h/2}{2\epsilon_{nt}} \quad (\text{strain ratio at top.})$$

$$\delta = \gamma_{bot} = \frac{\epsilon_n}{2} - \frac{k_n h/2}{2\epsilon_{nt}} \quad (\text{strain ratio at bottom.})$$

It is important to note that although the tangential force, tangential moment and the twisting moment can be determined from the surface strains, they will not influence the overall yield criterion in the upper bound solution. The reason is that their corresponding strain rates are zero, hence they do not contribute work in the energy dissipation equation. The stress resultants, which influence the yield criterion in this type of generalised yield line, would be the normal force, normal moment and the longitudinal shear. They may be determined by the surface strain rates e_n , e_{nt} and the curvature rate k_n .

It can be seen from the above expressions that the stress resultants are functions of the normal strain and shear strains on the top and bottom surfaces of the section. If $e_n/2e_{nt}$ were expressed as $\text{Cot}\theta$, θ would be the angle between the outward normal on the yield surface and the e_n axis. By substituting values of θ between 5° and 175° in steps of 5° , this variation applies to the top and bottom surface to give different values of β and δ . By adopting a value of 0.55 for the shear stress reduction coefficient α derived from Chapter 2, all the parametric stress resultants around the entire yield surface can be computed. (See Appendix A). At the same time, the eccentricities of the force resultants can also be evaluated from equations 3.60-3.62.

It has already been established earlier in section 3.3.3 that for normal force and shear force alone, the 'exact' yield surface equation 3.35 is:

$$\frac{n_{nt}^2}{-\alpha^2 n_n (1 + n_n)} = 1$$

Also in section 3.4 for normal force and bending moment, the yield surface equation 3.22 is:

$$\frac{m_n^2}{[4 n_n (1 + n_n)]^2} = 1$$

The yield criterion for the combine bending, shear and axial force resultant can be approximately written as:

$$\frac{m_n^2}{[4 n_n (1 + n_n)]^2} + \frac{n_{nt}^2}{-\alpha^2 n_n (1 + n_n)} = \Phi_1 \text{ ----3.63}$$

The above equation represents an ellipse, which is similar to that proposed by Cookson (1976).

By substituting the three primary parametric stress resultants computed earlier into the approximate yield surface equation 3.63, it is found that the maximum error for the equation is 9.6% compare to unity.

Cookson (1976) introduced two further approximate yield surface equations to deal with bending dominant and in-plane force dominant cases. Converting to terms compatible to the above and also introducing the α term, the two criterion proposed by Cookson can be written respectively as follows:-

$$\frac{m_n}{-4n_n(1 + n_n)} + \frac{n_{nt}^2}{-2\alpha^2 n_n(1 + n_n)} = \Phi_3 \text{ -----} 3.64$$

$$\frac{m_n^2}{2[-4n_n(1 + n_n)]} + \frac{n_{nt}}{\alpha\sqrt{[-n_n(1 + n_n)]}} = \Phi_4 \text{ -----} 3.65$$

Equations 3.64 and 3.65 are parabolic curves, which give good correlation at certain part of the yield surface when the stress resultants are well defined. The error level is reduced to less than 4% from the unity factor. As the parametric stress resultants vary with the strain ratios at different parts of the structure, it would be difficult to predetermine the range over which the above expressions are applicable. Further more, the equations are only valid for positive values of m_n and n_{nt} . If the yield surface equations are used together, there is also a corner on the yield surface where the two meet. This can further complicate the calculation since the strain rate at such corners of the yield surface is not defined. In the collapse mechanism of a complex structure such as a box girder bridge, there would be a wide range of shear displacement and curvature ratios. It would be useful if a continuous curve can be formulated to fit as close as possible to the exact yield surface.

The actual yield surface appears to lie between the elliptical surface of equation 3.63 and the equation of a rectangle with its side being tangents to the principle stress resultants.

The equation of rectangle can be written as:

$$(x/a)^2 + (y/b)^2 - (x/a)^2(y/b)^2 = 1$$

And the equation of ellipse can be written as:

$$(x/a)^2 + (y/b)^2 = 1$$

Hence, for a curve lying between the above two equations, the following holds:

$$(x/a)^2 + (y/b)^2 - k(x/a)^2(y/b)^2 = 1 \quad ; \quad 0 \leq k \leq 1$$

Similarly, an improvement of the elliptical equation 3.63 can be made by adding a third term which is a constant times the product of the first two terms of the equation. By trying different values of k together with the values of the stress resultants, it was found that $k=1/3$ gave an error of fit of less than 1.4%.

The modify general yield surface equation can be written as:

$$\frac{m_n^2}{[4n_n(1+n_n)]^2} + \frac{n_{nt}^2}{-\alpha^2 n_n(1+n_n)} + \frac{m_n^2 n_{nt}^2}{48\alpha^2 n_n^3(1+n_n)^3} = \Phi_2 \text{-----3.66}$$

Although a better approximation may be obtained by including a higher order for the third term in the above equation 3.66, the equation would be too cumbersome to be of practical use.

The parametric stress resultants given by equations 3.53 to 3.59 as well as the yield functions Φ_1 , Φ_3 , Φ_4 and Φ_2 given by equations 3.63, 3.64, 3.65 and 3.66 are calculated on spread sheets by substituting different values of β and δ . The results are included in Appendix A.

3.3.5 Work Equations and Equilibrium Equations

It is useful in the ultimate load analysis but not always necessary to have an explicit form of yield surface equation. It was demonstrated in Section 3.3.4 that it is possible to compute the stress resultants from the displacement rates. In a generalised yield line such as that shown in Figure 3.3, the displacement rates are Δ_n , Δ_{nt} and Θ_n and the corresponding stress resultants are N_n , N_{nt} and M_n . It is also possible to compute the values of the secondary stress resultants, i.e., tangential force, tangential moment and twisting moment from the basic displacement rates. As there are no corresponding displacement rates for these secondary stress resultants, they do not contribute to the internal energy dissipation equation. Thus the internal energy equation 3.3 can be written as:

$$D_i = \sum (N_n \cdot \Delta_n + N_{nt} \cdot \Delta_{nt} + M_n \cdot \Theta_n)$$

The summation is to be carried over all the yield lines and plastic hinges.

In a collapse mechanism that is kinematically admissible, it is possible to relate the displacement rates along the various yield lines to a specific displacement on the structure. The external work equation is then the product of the external applied forces and their associated displacements. i.e.

$$D_e = \sum P \times \Delta$$

By equating the external work with the internal dissipation, it is possible to establish the ultimate collapse load of the particular mechanism. It is to be noted that such solution only represent an upper bound condition since there may be other collapse mechanisms which can give a lower value of collapse load.

Although the secondary stress resultants do not contribute to the energy dissipation, they are useful in establishing the equilibrium condition. In this case, if a system of stress resultants, which do not violate the yield

criterion can be established and which are statically admissible with respect to the external applied forces, then such solution would always give a lower load than the actual collapse load. This represents the lower bound solution.

3.4 Yield Criterion for Reinforced Concrete

The relevant equilibrium equation can be modified for reinforced concrete by simply adding the contribution from the reinforcement.

Therefore,

$$\text{Normal Force} \quad N_n = N_{nc} + N_{ns} \text{-----} 3.67$$

$$\text{Shear Force} \quad N_{nt} = N_{ntc} + N_{nts} \text{-----} 3.68$$

$$\text{Normal Moment} \quad M_n = M_{nc} + M_{ns} \text{-----} 3.69$$

$$\text{Twisting Moment} \quad T_n = T_{nc} + T_{ns} \text{-----} 3.70$$

$$\text{Tangential Force} \quad N_t = N_{tc} + N_{ts} \text{-----} 3.71$$

$$\text{Tangential Moment} \quad M_t = M_{tc} + M_{ts} \text{-----} 3.72$$

The yield criterion for reinforcement is assumed to be $\pm f_y$. The assumption is that the steel bar can only sustain uniaxial stress along the reinforcement. Dowel action and the effect of the reinforcing bar kinking across yield lines are often small and can be ignored without significant errors. This simple criterion implies that for positive values of strain rate (tensile), the associated stress in the steel would be $+ f_y$; and for negative strain (compressive), $- f_y$. When the strain rate is zero, the stress is unidentified but may be limited to

$$- f_y \leq f_s \leq + f_y.$$

In an ordinary reinforced concrete slab, the reinforcement is usually provided in two orthogonal directions near both the top and bottom surfaces. For a yield line forming at an angle θ from the x and y axis, the steel contribution can be determined. Introducing reinforcement parameters ρ_{xi} and ρ_{yi} for the i^{th} layer in both the x and y direction, which are equal to,

$$\rho_{xi} = \frac{A_{xi}}{h} \frac{f_y}{\sigma_c} \frac{\text{sign } |e_{xi}|}{|e_{xi}|} \text{-----} 3.73$$

$$\rho_{yi} = \frac{A_{yi}}{h} \frac{f_y}{\sigma_c} \frac{\text{sign } |e_{yi}|}{|e_{yi}|} \text{-----} 3.74$$

Where the last term of the above expressions determines whether the steel stresses are in tension or compression.

The steel contribution, therefore, can be written as:

$$\text{Normal force: } N_{ns} = \sigma_{ch} \sum_1^i (\rho_{xi} \cos^2\theta + \rho_{yi} \sin^2\theta)$$

$$\text{Shear force: } N_{nts} = \frac{\sigma_{ch}}{2} \sum (\rho_{xi} - \rho_{yi}) \sin 2\theta$$

$$\text{Bending moment: } M_{ns} = \sigma_{ch} \sum (\rho_{xi} d_{xi} \cos^2\theta + \rho_{yi} d_{yi} \sin^2\theta)$$

$$\text{Twisting: } T_{ns} = \frac{\sigma_{ch}}{2} \sum (\rho_{xi} d_{xi} - \rho_{yi} d_{yi}) \sin 2\theta$$

$$\text{Tangential force: } N_{ts} = \sigma_{ch} \sum (\rho_{xi} \sin^2\theta + \rho_{yi} \cos^2\theta)$$

$$\text{Tangential moment: } M_{ts} = \sigma_{ch} \sum (\rho_{xi} d_{xi} \sin^2\theta + \rho_{yi} d_{yi} \cos^2\theta)$$

Where d_{xi} and d_{yi} are the position of the reinforcement layers related to the centre line of the slab element.

These expressions could then be added to the relevant concrete stress resultants to give the modified yield criterion for reinforced concrete.

Therefore, the three main force resultants, normal force, shear and bending moment of ordinary reinforced concrete using equations 3.53, 3.55, and 3.56 can be considered with the reinforcement to give the yield criterion for reinforced concrete as:

$$N_n = \sigma_{ch} \sum (\rho_{xi} \cos^2\theta + \rho_{yi} \sin^2\theta) + \sigma_{ch} \frac{1}{2} \left[\frac{\chi}{(\beta-\delta)} - 1 \right] \quad \text{---3.75}$$

$$N_{nt} = \frac{\sigma_{ch}}{2} \sum (\rho_{xi} - \rho_{yi}) \sin 2\theta + \sigma_{ch} \frac{\alpha^2 U}{2(\beta-\delta)} \quad \text{-----3.76}$$

$$M_n = \sigma_{ch} \sum (\rho_{xi} d_{xi} \cos^2\theta + \rho_{yi} d_{yi} \sin^2\theta) + \frac{\sigma_{ch}^2}{4(\beta-\delta)^2} [\phi - U \cdot \alpha^2 - (\beta+\delta) \cdot \chi] \quad \text{-----3.77}$$

It is to be noted that when computing the shear contribution due to the reinforcement, dowel action is neglected.

An alternative approach is to substitute the steel stress resultants into the approximate yield surface equation 3.63 and after rearranging, this equation becomes,

$$4\sigma_c^2 \alpha^2 (M_n - M_{ns})^2 - (N_{nt} - N_{nts})^2 (N_n - N_{ns}) (\sigma_c h + (N_n - N_{ns})) - \alpha^2 (N_n - N_{ns})^2 (\sigma_c h + (N_n - N_{ns}))^2 = 0 \quad \text{-----3.78}$$

For the case of zero shear strain rate, the yield line only subjects to a normal strain rate and a curvature rate, i.e.,

$$e_{nt} = 0 ; N_{ntc} = 0.$$

equation 3.78 became,

$$4\sigma_c^2 \alpha^2 (M_n - M_{ns})^2 = \alpha^2 (N_n - N_{ns})^2 (\sigma_c h + (N_n - N_{ns}))^2$$

After rearranging, the Bending moment equation,

$$M_n = M_{ns} \pm \frac{1}{2\sigma_c} (N_n - N_{ns}) (\sigma_c h + (N_n - N_{ns})) \quad \text{-----3.79}$$

If there is no support restraint, $N_n = 0$, $N_{nc} = -N_{ns}$

$$\begin{aligned} M_n &= M_{ns} \pm \frac{1}{2\sigma_c} (-N_{ns}) (\sigma_c h - N_{ns}) \\ &= \sigma_c h \sum (\rho_{xi} dx_i \cos^2 \theta + \rho_{yi} dy_i \sin^2 \theta) \\ &\quad \pm \frac{-\sigma_c h^2}{2} [(\sum (\rho_{xi} \cos^2 \theta + \rho_{yi} \sin^2 \theta) \\ &\quad + \sum (\rho_{xi} \cos^2 \theta + \rho_{yi} \sin^2 \theta)^2)] \quad \text{-----3.80} \end{aligned}$$

Johansen's general step yield criterion may be written as

$$M_{nj} = M_x \cos^2\theta + M_y \sin^2\theta \text{ -----3.81}$$

and

$$M_n = M_{nj} \pm N_{nts}^2/2\sigma_c \text{ -----3.82}$$

Equation 3.82 indicates that the basic moment should be modified by the shear contribution of the reinforcement.

For $\theta = 0$ or 90° and for an isotropically reinforced slab, the 2nd term in equation 3.82 vanishes to give

$$M_n = M_{nj}$$

Jain and Kennedy (1974) concluded that for practical reinforcement in slabs, the error in neglecting the 2nd term is about 2% and should be acceptable.

If N_n is not equal to zero as a result of a restraint from the slab boundary condition inducing a normal force across the yield line, the normal force term N_n should be included. Hence, equation 3.82 can be written as:

$$\begin{aligned} M_n &= M_{nj} \pm \frac{N_{nts}^2}{2\sigma_c} \pm \frac{1}{2\sigma_c} (N_n^2 + N_n\sigma_{ch}(1 - \frac{N_{ns}^2}{\sigma_{ch}})) \\ &= M_{nj} \pm \frac{1}{2\sigma_c} (N_{nts}^2 + N_n^2 + N_n(\sigma_{ch} - N_{ns}^2)) \text{ ----3.83} \end{aligned}$$

For no curvature rate, $\Theta_n = 0$, the yield criterion for reinforced concrete derived from equation 3.35 can be written as:

$$(N_{nt} - N_{nts})^2 = -\alpha^2(N_n - N_{ns})(\sigma_{ch} + N_n - N_{ns}) \text{ ----3.84}$$

This is the same as for the approximate general yield criterion when $M_{nc} = 0$.

If the above is applied and it is assumed that the reinforcement is symmetrical about the centre of the section and is perpendicular to the yield line, then

$$N_{nts} = 0, \text{ and } N_{ns} = \sigma_{ch} \sum \rho_{xi}$$

and equation 3.84 became:-

$$N_{nt}^2 = -\alpha^2 (N_n - \sigma_{ch} \sum \rho_{xi}) (\sigma_{ch} + N_n - \sigma_{ch} \sum \rho_{xi}) \text{-----} 3.85$$

$$\left(\frac{N_{nt}}{\sigma_{ch}} \right)^2 = -\alpha^2 \left(\frac{N_n}{\sigma_{ch}} - \sum \rho_{xi} \right) \left(1 + \frac{N_n}{\sigma_{ch}} - \sum \rho_{xi} \right)$$

In the above, dowel action and kinking of the reinforcement has been ignored.

Converting the above expression to Mattock's term where

$$\frac{N_{nt}}{\sigma_{ch}} = \tau_n \text{----- mean shear stress}$$

$$\frac{N_n}{\sigma_{ch}} = -\sigma_n \text{----- mean normal stress}$$

$$\sigma_c \sum \rho_{xi} = \rho f_y$$

hence,

$$\left(\frac{\tau_n}{\sigma_c} \right)^2 = \alpha^2 \left(\frac{\sigma_n + \rho f_y}{\sigma_c} \right) \left(1 - \frac{\sigma_n + \rho f_y}{\sigma_c} \right) \text{-----} 3.86$$

for $\alpha = 1$, there is no shear reduction and the expressions are the same.

For combined bending and shear , $N_n = 0$ and,

$$\frac{(M_n - M_{ns})^2}{2\sigma_c [N_{ns} (\sigma_{ch} - N_{ns})]^2} + \frac{N_{nt}^2}{-\alpha^2 (-N_{ns}) (\sigma_{ch} - N_{ns})} = 1$$

in which $N_{nts} = 0$ since dowel action is ignored.

The above expression became, when there is no applied shear,

$$M_n = M_{ns} \pm \frac{N_{ns}(\sigma_{ch} - N_{ns})}{2\sigma_c}$$

In which σ_c is equal to $0.6 f_{cu}$ where f_{cu} is the cube strength. This expression is the same as the one derived from the simplified stress block used in BS8110, (1985). The partial safety γ_m for both the concrete and reinforcing material has not been included.

3.5 Yield Criterion Applied To Prestressed Concrete

The effect of prestressing enhances the elastic stress strain characteristic of the structure by making better use of the material and mobilising a larger effective compression area of the concrete section. It also enables better control of deflection and limits crack widths of the member. This method of construction is often used for large span floors or long-span beams. In order to obtain the maximum benefit of prestressing, the steel strands and concrete used should be of higher strength than those for ordinary reinforced concrete. The higher compressive stress induced in the concrete from prestressing improves the shear strength of the prestressed members.

In prestressing design, the prestressing tendons are usually stressed up to 70-80% of the yield value. Such stresses result in a high initial strain in the stressing tendon and the concrete. It is this initial pre-straining which reduces the deflection under working load condition. Since the strains are within the elastic state and are small compared to the plastic strain at yield, they can be ignored under the rigid plastic assumption. The prestressing tendon and any other longitudinal tension reinforcement would eventually reach their yield value when the bending element is reaching its ultimate load. In ultimate load analysis, different yield stress for the prestressing tendon compared to that for the ordinary reinforcing steel is immaterial. The higher yield value for the prestressing tendons only result in a later onset of yielding compare to that of the ordinary reinforcement. Provided that the concrete section does not prematurely reach failure, it could be treated as ordinarily reinforced with an equivalent higher reinforcement content. The prestressing steel can be absorbed into the reinforcement term on the right of equations 3.75 to 3.76.

Introducing the prestressing term $\rho_p = A_p f_{yp} / \sigma_{ch}$:-

$$N_n = \sigma_{ch} \Sigma (\rho_{xi} \cos^2 \theta + \rho_{yi} \sin^2 \theta + \rho_p \cos^2 \theta_p) + \sigma_{ch} \frac{1}{2} \left[\frac{\gamma}{(\beta - \delta)} - 1 \right] \quad \text{----3.87}$$

$$N_{nt} = \frac{\sigma_{ch}}{2} \Sigma [(\rho_{xi} - \rho_{yi}) \sin 2\theta + \rho_p \sin 2\theta_p] + \sigma_{ch} \frac{\alpha^2 U}{2(\beta - \delta)} \quad \text{--3.88}$$

$$M_n = \sigma_{ch} \Sigma (\rho_{xi} d_{xi} \cos^2 \theta + \rho_{yi} d_{yi} \sin^2 \theta + \rho_p d_p \cos^2 \theta_p) + \frac{\sigma_{ch}^2}{4(\beta - \delta)^2} [\phi - U \cdot \alpha^2 - (\beta + \delta) \cdot \chi] \quad \text{-----3.89}$$

An alternative approach is to treat the applied prestress as an externally applied force, which is independent of the reinforcing. Thus modifying the left-hand side of equations 3.72. This assumption implies that the external force needs to be maintained during the continue yielding of the section and ignores the plastic behaviour of the prestressing steel. Thus,

$$N_n = A_p f_{yp} \cos^2 \theta_p = \sigma_{ch} \Sigma (\rho_{xi} \cos^2 \theta + \rho_{yi} \sin^2 \theta) + \sigma_{ch} \frac{1}{2} \left[\frac{X}{(\beta - \delta)} - 1 \right] \quad \text{-----3.90}$$

$$N_{nt} = 2 A_p f_{yp} \sin \theta_p \cos \theta_p = \frac{\sigma_{ch}}{2} \Sigma [(\rho_{xi} - \rho_{yi}) \sin 2\theta] + \sigma_{ch} \frac{\alpha^2 U}{2(\beta - \delta)} \quad \text{-----3.91}$$

$$M_n = A_p f_{yp} d_p \cos^2 \theta_p = \sigma_{ch} \Sigma (\rho_{xi} d_{xi} \cos^2 \theta + \rho_{yi} d_{yi} \sin^2 \theta) + \frac{\sigma_{ch}^2}{4(\beta - \delta)^2} [\phi - U \cdot \alpha^2 - (\beta + \delta) \cdot \chi] \quad \text{-----3.92}$$

3.6 Summary

This chapter described how a yield criterion for reinforced and prestressed concrete could be developed from plasticity theory. It has been shown that the normality condition has been satisfied. The yield conditions were studied for elements subjected to simple uni-axial forces through to elements under more generalised resultants involving combine bending moment, axial forces and in plane shear forces. The stress resultants can be related to the non zero concentrated strain rates Δ_n , Δ_{nt} and Θ_n . An additional modification term was introduced for micro concrete to allow for the shear ductility. The yield conditions can also be expressed in non-dimensional parametric form. For reinforced elements, the yield conditions can be modified by the super-position of the yield forces from the reinforcement and the local equilibrium condition. The effect of dowel action was ignored without any significant error.

For prestressed elements, the applied prestress could be treated as an externally applied axial force, which also satisfy the equilibrium condition of the local section of the element. One important feature is the application of the theory to locations where axial forces, shear and bending moments can occur such as the flange web junction of T-beams and box girder elements. In the following chapter, the application of the theory to box girders is presented.

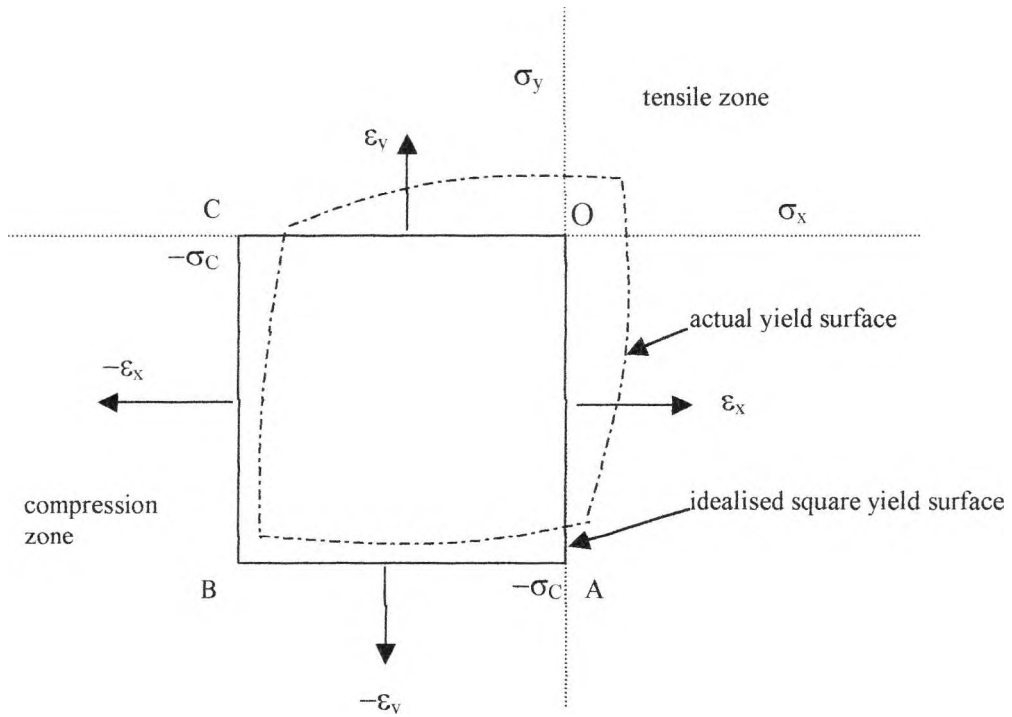


FIGURE 3.1 BI-AXIAL YIELD SURFACE OF CONCRETE (SQUARE YIELD CRITERION)

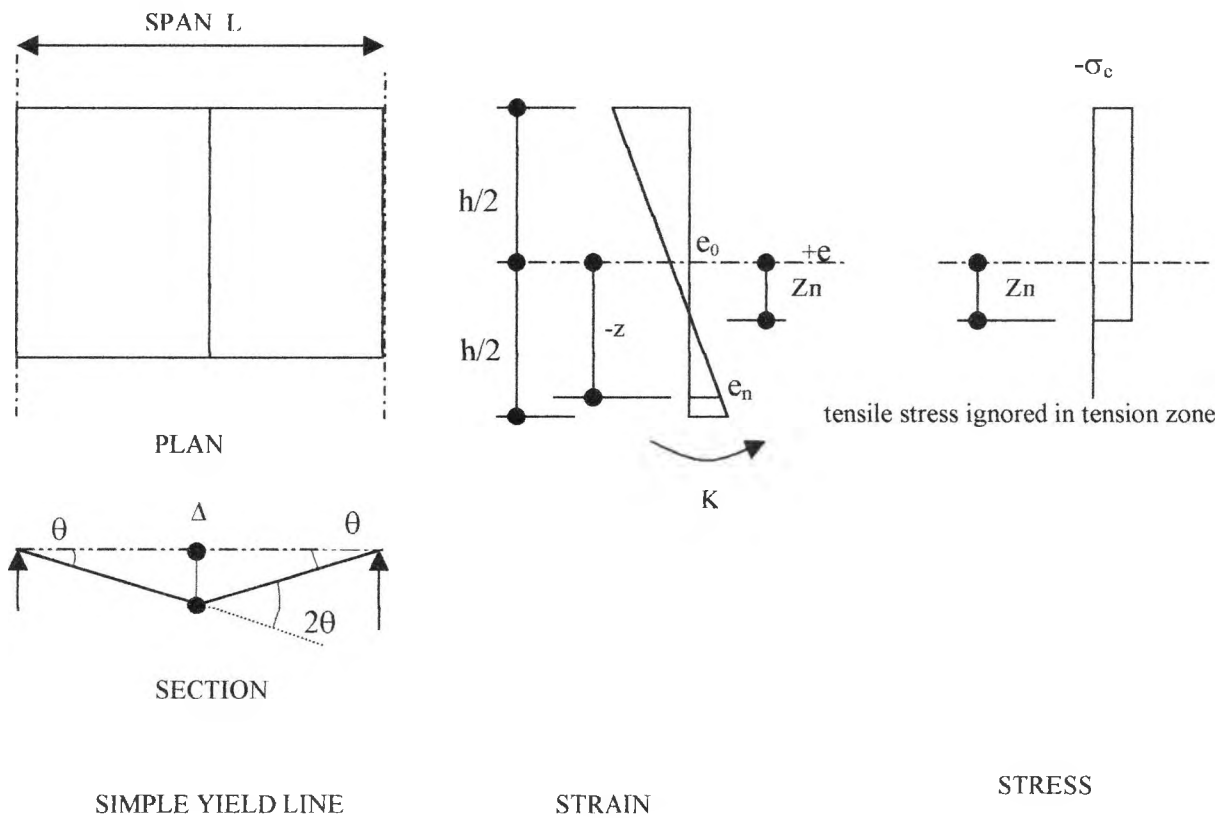


FIGURE 3.2 TYPICAL YIELD LINE AND STRESS-STRAIN RELATIONSHIP

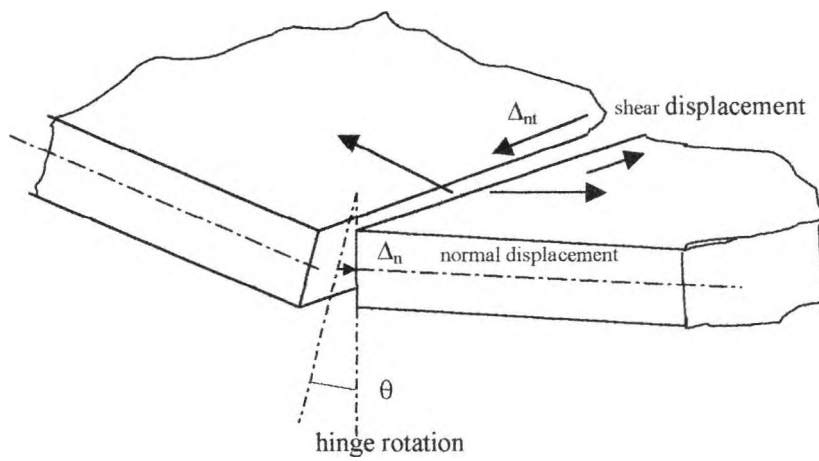


FIGURE 3.3 DISPLACEMENT RATES IN A GENERALISED YIELD LINE

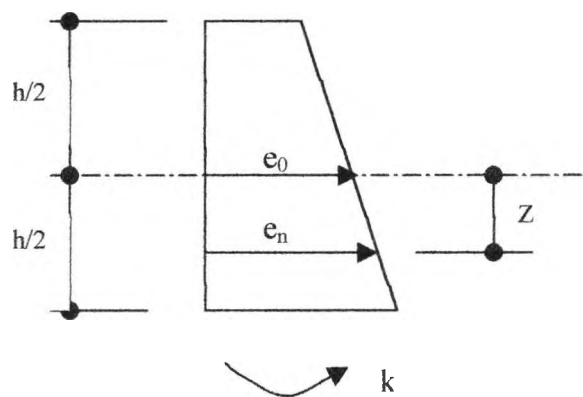


FIGURE 3.4 NORMAL STRAIN DISTRIBUTION

Chapter 4 Ultimate Collapse Analysis of Concrete Box Girders

4.1 Introduction

Concrete box beams have been used extensively in recent years mainly for bridge deck structures. The box shape section provides high torsional stiffness, which enable the distribution of eccentric loading to other sections of the structure. The geometry of the section makes efficient use of materials, which provide economy and also good architectural appearance.

The distortion of the cross section under eccentric load can reduce its efficiency. Although intermediate diaphragms can help to keep its geometric shape, their use is avoided where possible. Diaphragms can restrict the passage of services and are more costly to construct. In practice, diaphragms are only provided over supports or at locations where heavy point loads are anticipated. In general, it is often more economical to increase thickness and/or the transverse bending strength of the slab by providing additional reinforcement and to add stiffening fillets at the wall and slab junctions. The strengthening will not completely eliminate distortion, unlike the situation where regular spaced diaphragms are provided.

The stress distribution for a box beam which is allowed to distort would include transverse bending, torsion and warping stress as a result of out of plane bending of the flanges and webs of the box member. The current design practice is based upon allowing the section to deform under load.

4.2 Previous Work on Analysis and Design of Concrete Box Girders

Swan (1972) carried out a survey of the characteristic and geometry of 173 bridges built before 1972. The statistic assembled assisted bridge designers in initial sizing and profiling of bridges.

Trikha and Edwards (1972) developed a finite element program to study the behaviour of concrete box girders. It used an iterative process to predict the strain distribution under increasing load, first cracking, development of the crack pattern and eventually a collapse mechanism. At the end of each load increment, the stiffness of the member is modified to take into account for the cracking and non-linearity of the element.

Lampert (1972) carried out theoretical studies of non-deformable box beams subjected to torsion and bending utilising the space truss theory. The theory assumed the longitudinal and transverse reinforcement and the concrete elements acts as ties and struts of an imaginary space truss. As the concrete was assumed to be incompressible, the theory was only suitable for lightly reinforced sections. The truss model gave a lower bound solution under plastic theory.

Maisal and Swan (1973) reviewed nearly 300 references on the analysis and design of thin wall beams and in particular box girder structures. The methods of analysis were mostly elastic ranging from simple beam theory to the more complex involving finite elements, finite strips and folded plates requiring computer methods.

Spence (1973) studied the failure mode of single cell box beams subjected to eccentric loading. The section was allowed to deform with the flanges and webs twisted out of plane in order to satisfy geometric compatibility. Spence assumed rigid plastic material with concrete having infinite compressive strength. By ignoring the energy dissipation from the twisting of the flanges, webs and diaphragms, he managed to get a close correlation between theoretical and experimental load carrying capacity of the member.

Swann and Williams (1973) put forward proposals for the reinforcement design of the box girder sections under bending, shear and torsion. The transverse bending can be dealt with separately by super-position. This approach is usually on the safe side since the worst conditions for the combine stresses do not always occur together.

Cookson (1976) further extended Spence's work to cover multi-cell simply supported box beams. A generalised yield criterion involving in plane shear and axial force was developed to describe the failure of slab elements. Twisting work compared to the others was small and could be neglected without involving significant error. Cookson acknowledged the caution of using the theory to models with small size aggregate, which restrict the transfer of in plane shear along the shear plane. The theory is also restricted to small transverse shear stresses; hence the yield criterion was not appropriate for punching shear, thick slabs and column supports.

Various experimental works were carried out on box girder models. Some were direct scale models of actual box girder bridges. Swann (1970) tested a concrete model of the Western Avenue box girder bridge. Sommerville (1965) tested a model of the Mancunian Way. Scordelis (1975) experimented with a model multi-cell two span straight high way box beams. Scordelis and Larsen (1977) also tested models of curved box beams in California. There were also tests carried out on single box girder models of various scales. Swann and Williams (1973) tested box members, which were restricted from the distortion of the cross section under eccentric loading. They tested 16 prestressed single cell box beams and 2 other ordinary reinforced beams. Trikha and Edward (1972) tested a number of simply supported single cell prestressed boxes. Spence (1973) also carried out tests on simply supported single cell boxes. By varying the eccentricity of loading, he was able to study the different failure mechanisms involving flexural and distortion of the section. Cookson (1977) continued Spence's work by carrying out tests on 4 model box beams including a single cell beam; a twin cell beam with ordinary reinforcing; a twin cell beam with profiled post-tensioning and a segmental prestressed beam with straight stressing wires.

4.3 Elastic Analysis of Box Girders

Maisal and Roll (1974) carried out an extensive survey of other references and selected two methods of elastic analysis for box beams with side cantilevers. Torsional warping and distortional warping can be dealt with adequately by formulations developed by Vlasov and the beam on elastic foundation theory. The simplified method was such that the analysis can be handled without the aid of a computer. There are also other methods such as grillage theory, folded plate theory and finite strip method, shell theory and finite element method which would require the extensive use of the computer. With the improvement of computer power in the last few years, the restriction on elements and size of problem is no longer a significant constraint. Engineers and researchers are now less reluctant to use the more complex methods since the results can be obtained more readily and more accurately, in particular when a change of parameters and loading patterns can be handled quickly and efficiently. William, Cassell and Boswell(1992) have recently developed a program for the design of curved prestressed concrete box beams.

4.3.1 Structural Actions in Box-beams

In the case of solid members, the assumption of plane sections remains plane hold true. For box beams with internal diaphragms and with thick walls and flange sections, the effect of distortion and warping would be small and are often neglected. The current trend of design and construction is to reduce the thickness of the box beam walls and bottom slabs in order to minimise self-weight. In addition, internal diaphragms are eliminated to allow the uninterrupted passage of services or for extra lanes of traffic inside the box girder. To compensate for the lost of the diaphragm, introducing haunches or fillets often enhances the transverse strength. Even so, distortion of the section is usually larger than that of the section with diaphragms. The effects of distortion of the cross section and warping and twisting of the flange and web elements of the box beam need to be considered.

4.3.1.1 Distortion

The cross section of a box member will deform under either symmetrical or asymmetrical loading if there are no transverse diaphragms (figure 4.1 and figure 4.2). The effect of transverse bending of the top or bottom slab and walls results in elastic deformation which changes the shape of the cross section. Any eccentric loading can be resolved into a combination of symmetrical and asymmetrical loading. Such deformation, if significant, can reduce the torsion stiffness of the section.

4.3.1.2 Warping

Warping is the out of plane displacement of the elements. The longitudinal displacement of the section when twisted causes a torsional warping displacement even though there may be transverse diaphragms. Additional warping can result under distortion, which is sometimes known as distortional warping displacement (figure 4.3). The warping displacement influences the longitudinal stresses. If such displacement is being restricted, as in the case of built in conditions or in the case of continuous sections, significant additional longitudinal stress can develop. Such stresses can be significant depending upon the geometry of the section and the nature of the loading.

4.3.1.3 Shear Lag

Under symmetrical loading, the differential longitudinal straining of the flanges and the web give rise to an additional warping stress. Such stresses can be created under the effect of bending (figure 4.4, figure 4.5). The warping stress created depends upon the dimension and the relative stiffness and transverse strength of the flanges. Wide flange box beams would have a more significant effect than narrow flange sections under the influence of shear lag.

4.3.1.4 St Venant Torsional Shear Stress

The theory of St Venant torsion assumes that there is no constraint for the warping of the section and therefore, no warping stress. The shear effect created for a thin walled box section is that the shear stress around the perimeter of the section is constant and forms an equal and opposite torque to the external applied torsional moment. For thicker sections, the shear stress across the thickness of the flange and web elements varies (figure 4.6).

4.3.1.5 Local Effect of The Flanges

On bridge structures, the effect of transverse bending under large wheel loads has to be assessed and evaluated (figure 4.7). The slab under the large point load should also be check for local punching shear (figure 4.8).

4.3.2 Methods of Elastic Analysis

There are various methods of elastic analysis for box sections. The simple beam theory deals with the ordinary bending and shear of the section. However, it does not give the transverse bending and shear effect from eccentric loading. By super-position, the effects of warping, distortion shear lag and local effect can be assessed separately. Maisal and Roll summarised the various methods of analysis, which deal with the different effects of structural actions mentioned in section 4.3.1. Their method does not need the aid of computer. The more comprehensive methods of analysis include grillage theory, folded plate theory, finite strip theory, finite element theory and Shell Theory. These methods can deal directly with the various structural actions. The complexity, however, requires more powerful computer capability. With the increasing power of the present day computers, the more general methods can now be easily handled.

4.4 Plastic Analysis of Concrete Box Girders

In the collapse analysis of a complex structure, the failure mode often depends upon the way loading is applied and the geometry of the structure. For localised loading, failure is often restricted to a local mechanism. Whether the failure mechanism extends into other regions depends upon the strength of the transverse members such as the top and bottom flanges. As in all upper bound analysis, there are possibilities of other mechanisms, which have lower values. It may, however, be possible to design the structure against premature failure such as local punching shear under heavy point loads and local crushing at flange web junctions.

It is important to ensure that for experimental work, local failures do not inadvertently occur. Fillets can be added to the internal corners of the box members to improve the local shear and bending capacity of the section. At the location where concentrated loads are applied, the local punching shear should be checked and spreader plates should be provided to reduce local shear stress to within acceptable level.

The collapse mechanism of concrete box girders without intermediate diaphragms will involve distortion of the cross section. Spence (1973) studied distortion mechanisms without shear deformation for single cell box beams with infinite strength for concrete (figure 4.9). Cookson (1977) further extended the work to account for the finite strength of concrete and to deal with continuous and multi-cell boxes (figure 4.10, figure 4.11).

In-plane shear will normally develop when only part of the entire section is distorted. Such shear could develop either in the flanges or webs of the box member depending upon the relative strength of the elements. This shearing of the section may spread uniformly over the region where yielding is deemed to have occurred. Alternatively, such yield can be assumed to concentrate along the discontinuity, which forms the generalised yield lines (figure 4.12, figure 4.13).

In the analysis of the box members, the load obtain by the work equation would be an upper bound solution. Morley (1967) proposed that if a corresponding equilibrium condition can be found, the upper bound value would be a minimum. Morley made the following assumptions for the analysis and design of box members:

1. The collapse mechanism consists of yield lines and rigid portions and or yield zones.
2. There will at least be one variable parameter in the mechanism that defines the geometry.
3. The yield line thus formed is assumed not to move. That is, the yield mechanism does not change in the course of yielding.

In order that plasticity theory can be applied for the collapse analysis of the box girder structure, it is important that the material should have sufficient ductility to enable redistribution of stresses within the structure without premature failure. Premature failures are unintentional sudden failure modes, which occur before the complete development of the assumed mechanism. To avoid such failures, it would be prudent to ensure that the applied loading is sufficiently spread and adequate reinforcing is provided in the critical sections against such premature failures.

In experiments, depending on the size of the model, the scaled down material could have a different characteristic in shear ductility when compared with that of the prototype structure. Appropriate modifications can be incorporated to account for the different shear ductility of the model material.

4.4.1 Simply Supported Single Cell Box Beams,

Spence (1973) assessed the collapse load of a single cell box beam by assuming infinite concrete strength. As a result the neutral axis for bending is located at the top surface of the top flange. This gives an over estimate of the collapse load when compared with the experiments. Cookson (1976) incorporated the finite strength of concrete, which gave a better approximation of the collapse load. For geometrical compatibility, it is necessary for twisting to occur in all the flanges and webs of the section. However, the twisting work is often small and negligible and does not influence significantly the work equation.

The work equation for the pure bending can be written as:

$$P_b * \theta L / 2 + w L^2 * \theta / 2 = M_p * 2\theta \text{ -----4.1}$$

Where P_b is the pure bending imposed live load at collapse
 w is the self-weight dead load per unit length
 M_p is the mid span plastic yield moment

For distortional loading that causes partial collapse of the structure, figure 4.9, the corresponding work equation can be written as:

$$P_d * \theta * L / 2 + w * L^2 * \theta / 4 = \frac{1}{2} * M_p * 2\theta + 4 * M_c * L * \phi + W_T \text{ -----4.2}$$

Where P_d is the distortional live load at collapse

M_c is the yield moment at the flange web junction

W_T is the twisting work in the end diaphragms, flanges and webs.

Substituting 4.1 into 4.2 and rearranging,

$$P_d = P_b / 2 + 4 M_c * L / b + 2 * W_T / L / \theta \text{ -----4.3}$$

The last term on the right hand side of the above expression is small compared to the other two terms. For geometric compatibility, twisting of the flanges and web elements is required. The twisting elements are still well within their elastic limits when the bending plastic hinges and the corner plastic hinges have already been subjected to much larger strain value. In the experiments, where the flange strength was limited, ignoring the twisting work does not result in significant error. Whilst in real structures, where the top flanges are usually thicker and have been designed to support substantial loads from the traffic, the twisting work would be more significant especially in elastic analysis.

4.4.2 Continuous Single Cell Box Beams

In long span multi-span beams, localised failure of single span is one of the mechanisms to be considered. Introducing movement joint at support bearings can usually relieve the longitudinal strain. If the support and end restraints prevent the free movement of the structure, a longitudinal force will be induced, which in turn increases the bending capacity of the yield lines in the flanges, as well as the webs. There are two types of mechanism for the failure of the web. The first one is the classical bending yield hinge shown in figure 4.10. The second type is the load web assumed failure shear zones shown in figure 4.11.

Whether the web elements will fail by the bending mechanism or the shear mechanism will depend on the strength and reinforcing of the section. For the collapse mechanism shown in figure 4.12, it would be possible to determine the displacement rates of the various elements forming the mechanism. The displacement would include rotation of the corner hinges at the flanges and web junction, the rotation of the plastic hinges or shear deformation of the loaded web, and the twisting of the various flanges and web elements for maintaining kinematic compatibility. The collapse load can be written as:

$$P_c = P_b / 2 + 4 M_c * L / b + 2 * W_T / (L \theta) \text{-----} 4.4$$

which is similar to the single span box beam in 4.4.1

In this case, P_b is the load required to form plastic hinges at mid span and the adjoining supports without any longitudinal restraint. M_c is the corresponding yield moments in the flange web junctions; W_T is the twisting work in the flanges, but not the internal diaphragms since there is no twisting of the diaphragms.

Any longitudinal restraint would result in additional compressive forces which would modify the yield moments across the yield hinges by arching actions resulting in a higher value of P_b . Any longitudinal forces may also affect the transverse yield lines.

4.4.3 Continuous Multi-Cell Box Beams

The collapse load for multi-cell box beams can be assessed by a similar approach to that used in earlier sections. The collapse mechanism is shown in figure 4.11. The collapse load can be written as follows:

$$P_c = P_b / 2 + n * M_c * L / b + 2 * W_T / (L \theta) \text{-----4.5}$$

Where n is the number of longitudinal hinges in the mechanism; P_b is the pure flexural bending collapse load; M_c is the corner moment capacity and W_T is the twisting work.

Such hinges can be formed in either the flanges or the webs. Their formation will depend upon the relative strength of the elements. Similar to the last section, any longitudinal restraint would result in arching action giving a larger collapse load than unrestrained members.

4.4.4. Twisting work of flanges, webs and diaphragms

From the collapse loads of the box beams, the twisting work is now defined. The displacement function due to twisting which is the out of plane displacement, can be written as:

$$w = k * x * y \quad \text{-----4.6}$$

The associated twisting work may be written as

$$D = \sum M_p * k/2 \quad \text{-----4.7}$$

Where the plastic moments M_p are moment vectors which include hogging and sagging moments in the two directions. The total twisting work, therefore, should be summed over the all the elements subjected to twisting including the top and bottom, flanges, each of the webs and diaphragms. Hence,

$$W_T = \sum D * \text{Area.} \quad \text{-----4.8}$$

When the member is allowed to expand under applied loading, the restraining forces are released; the membrane action may be taken as zero. The yield moments for the slab elements may be assessed based on the assumption of no membrane forces. The same reasoning may be applied to the bending moments at corners where membrane forces may be assumed to be zero. Where the restraint caused the membrane force to build up, the membrane action may become significant and may not be ignored. In general, the deformation due to twisting remains elastic for large plastic deformation of other parts of the structure. In rigid plastic analysis however, no deformation was supposed to have occurred prior to all the yield hinges approaches yield. This does pose a slight dilemma since twisting is required to maintain geometric compatibility. The elastic work from twisting is ignored.

The twisting work compared with the other elements of work is however relatively small. Its omission therefore, does not give rise to significant errors.

4.4.5 Failure Mechanism in Webs

There are several mechanisms that can satisfy the geometric compatibility required for the failure of the webs. The shear mechanism for the webs can be in the form of distributed shear stresses concentrated in generalised yield lines. The beam shear mechanism proposed by Regan and Placas (1970) involved rotation of a hinge nears the end of the beam towards the top of a crack (figure 4.13). However, such mechanisms can only be valid if all the webs failed simultaneously in the same format. For multi-cell box beams or the failure of individual webs, it appears to be more appropriate to use Breastrup's shear mechanism. (1974) Breastrup's mechanism involved zones of uniform shear strain rates at both ends of the webs and a rigid region near the centre (figure 4.12). Such mechanisms do not involve rotation of the webs, hence they can be applied to single or multi-cell beams. The work done in the uniform shear strain rate end zones can be written as

$$W_c = \frac{\sigma_c * \alpha'}{2 \sin \theta} (1 - \cos \theta) * t \quad \text{-----4.9}$$

where α' is the uniform shear strain rate in the shear zone and t is the thickness of the web element

The shearing of the web also mobilises the yielding of any shear reinforcement. The vertical component of the shear strain rate can be written as $\alpha' \cot \theta$ and the work done for the shear reinforcement can be given as

$$W_s = \alpha' * \cot \theta * A_s * f_y \quad \text{-----4.10}$$

Where A_s is the area of reinforcement per unit width of the section and

f_y is the yield strength of vertical reinforcement.

The total work of the two sections in the shear zone of the web, therefore, can be summarised as

$$W_w = 2[A_s * f_y * \cot \theta + \frac{\sigma_c}{2 \sin \theta} * (1 - \cos \theta) * t] * \alpha' * h * r \quad \text{-----4.11}$$

If the web is external and there is no cantilever, it only requires both the top and bottom flanges to deform to maintain geometric compatibility. The resulting yield mechanism in the top and bottom flanges would involve longitudinal yield lines along the flange web junction and transverse yield lines at the centre and near both ends. The two halves of the flanges on both sides of the centre line would also require twisting. If the deflection under the edge point load is Δ , and the yield moment in both directions of the top flange and bottom flanges are M_t and M_b respectively, the total work done for the top flange would be the sum of work along the yield hinges. The work-done in the twisting region can be written as

$$W_t = 2 M_t * \Delta [2 + b/r + r/b] \quad \text{-----4.12}$$

Similarly, the work equation for the bottom flange can be written as

$$W_b = 2 * M_b * \Delta [2 + b/r + r/b + 2 h/b * \cot \theta] \quad \text{----4.13}$$

The total work including top and bottom flanges and the web is

$$W = W_w + W_t + W_b \quad \text{-----4.14}$$

Thus equating internal dissipation and the external work done by the point load,

$$P_c = 2h[A_s * f_y * \cot \theta + \frac{\sigma_c}{2 \sin \theta} (1 - \cos \theta) * t] + 2(M_t + M_b) * [2 + b/r + r/b] + 4M_b h/b \cot \theta \quad \text{-----4.15}$$

For minimum values of P_c , using partial differentiation and back substitution:

$$P_c = 2 \sigma_c * h * t * \sqrt{[\phi(1-\phi)]} + 8 * (M_t + M_b) \quad \text{-----4.16}$$

$$\text{Where } \phi = \frac{A_s f_y + a M_b/b}{\sigma_c * t} \quad \text{-----4.17}$$

The mechanism within the top and bottom flanges could vary from what was originally assumed depending on the reinforcement content. Punching shear could also occur under the point load in conjunction with the web-shearing mode. The external work in the above expression had ignored the work done by the self-weight of the element.

The collapse mechanism could be also applicable to the loading of internal webs. In this case the membrane force could become significant.

If adequate reinforcement were provided in the web to prevent shear failure in the web, the shearing failure would be forced towards the flanges of the flange web junction. Such concentration of the deformation at the flanges result in the deformation rates of δ_n , $2\delta_{nt}$ and θ_n . The work equation may be itemised as follows:

1. the generalised yield line in the top flange,
2. the generalised yield line in the bottom flange,
3. the mid span hinges in the web,
4. the corner hinges along the flange web junction,
5. twisting work in the top and bottom flanges and
6. mid span flange and web discontinuity.

Cookson derived an expression for evaluating the total work done in the discontinuity along the flange web junction using the yield surface equations similar to 3.78. By using the method of iteration and partial equilibrium along the shear discontinuity, the minimum upper bound for the mechanism was found to be

$$\begin{aligned}
 P = & 4 \frac{\sigma_c}{L} bd^2 \cdot \text{Sinh}^{-1} \left(\frac{L}{2a_t} \right) + d \cdot C_{1t} \left[1 + \left(\frac{L}{2a_t} \right)^2 \right]^{1/2} + \frac{L \cdot M_{yts}}{2b} \\
 & + 4 \frac{\sigma_c}{L} b(h-d)^2 \cdot \text{Sinh}^{-1} \left(\frac{L}{2a_b} \right) + (h-d) \cdot C_{1b} \left[1 + \left(\frac{L}{2a_b} \right)^2 \right]^{1/2} \\
 & + \frac{L \cdot M_{ybs}}{2b} + 2 \frac{\sigma_c}{L} t_w d^2 + \frac{4F(s-d)}{L} + (M_t + M_b) \left(\frac{L}{2b} + \frac{4+2b}{L} \right)
 \end{aligned}$$

-----4.18

Where,

$$C_1 = \sqrt{[N_{ys} (\sigma_c \cdot t_f - N_{ys})]} \quad \text{-----4.19}$$

$$C_2 = C_1^2 / (2\sigma_c) \quad \text{-----4.20}$$

t_f is the flange thickness ; C_{1t} and C_{2t} refer to the top flange; C_{1b} and C_{2b} refer to the bottom flanges respectively.

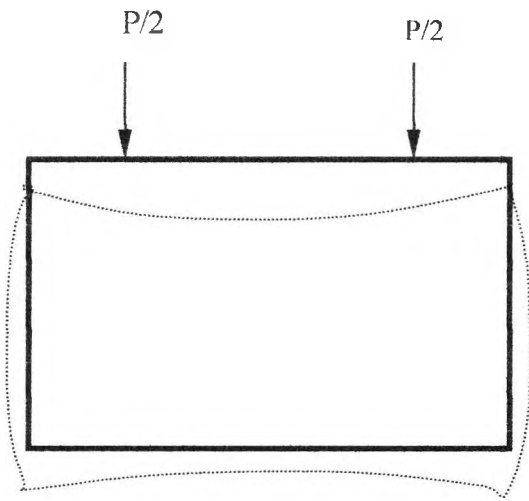
$$a_t = bdC_{1t}/C_{2t} \quad \text{-----4.21}$$

$$a_b = b(h-d)C_{1b}/C_{2b} \quad \text{-----4.22}$$

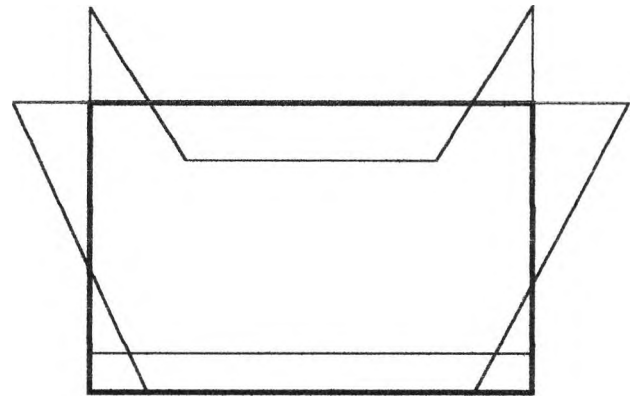
A possible alternative mechanism that may occur for single span box beams involves the shear, distortion of the top and bottom flanges. For continuous beams, however, the restraining effect of the adjacent spans is likely to prevent this mechanism from developing. For this reason, such a mechanism is not given further consideration.

4.5 Summary

This chapter describes briefly the behaviour of box girders under load and the available methods of elastic analysis. The ultimate collapse analysis using the yield criteria developed in chapter three has been presented. Geometrically compatible collapse mechanisms are discussed for the upper bound solution of concrete slab structures. The stress resultants along and across the yield boundaries are assessed. By equating the work done by the external applied load and the total internal energy dissipation along the various yield zones, it is possible to calculate the collapse loads. Since the solution is an upper bound value, there are other possible collapse mechanisms which could give a lower figure. However, by choosing a mechanism, which is close to the actual collapse pattern, it is possible to obtain a collapse load, which is near to the lowest upper bound solution. The solution for prestressed box beams would be similar to the ordinary reinforced sections, except the reinforcement content should be modified to incorporate the effect of prestressing. In the following chapter, the experiments that have been conducted on four box beams are described.

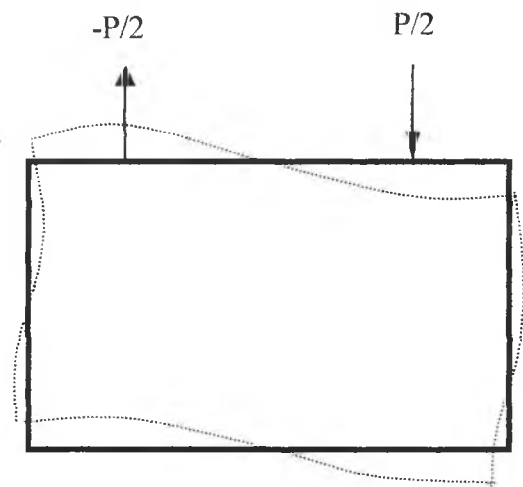


DEFORMATION

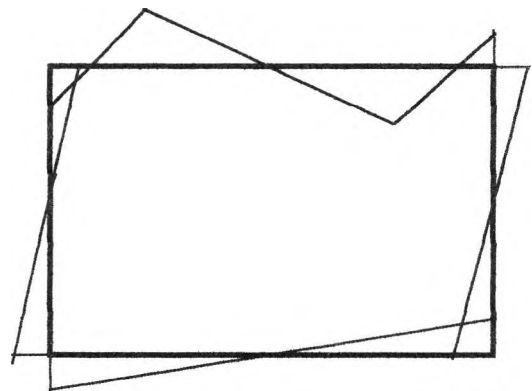


TRANSVERSE BENDING
STRESS DISTRIBUTION

**FIGURE 4.1 DISTORTION OF CROSS SECTION DUE TO SYMMETRICAL
LOADING ON TOP SLAB OF BOX BEAM**



DEFORMATION



TRANSVERSE BENDING
STRESS DISTRIBUTION

**FIGURE 4.2 DISTORTION OF CROSS SECTION DUE TO ASYMMETRICAL
LOADING ON TOP SLAB OF BOX BEAM**

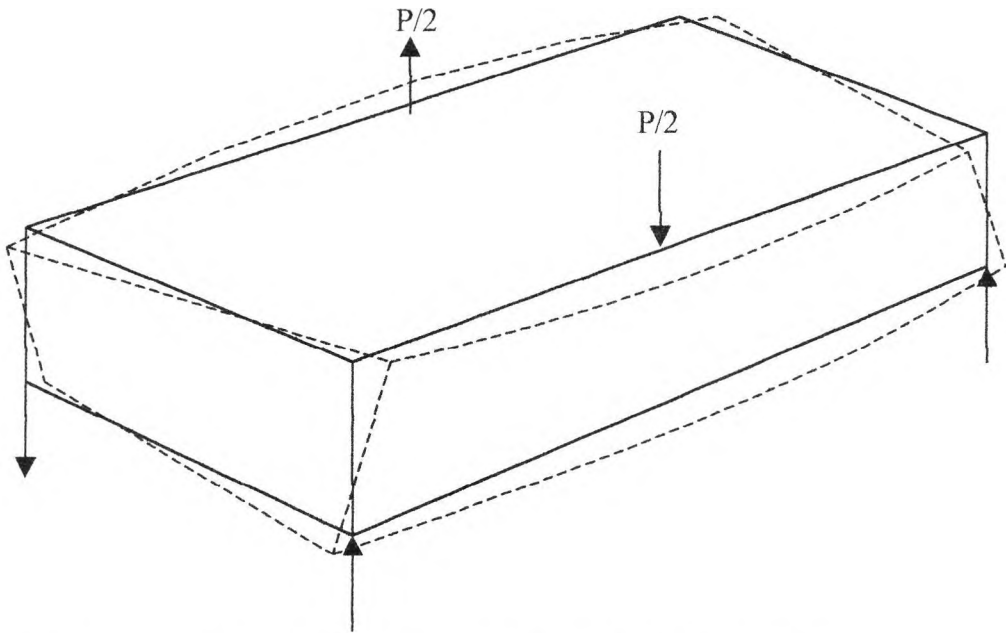


FIGURE 4.3 **WARPING DISPLACEMENT OF BOX BEAM**

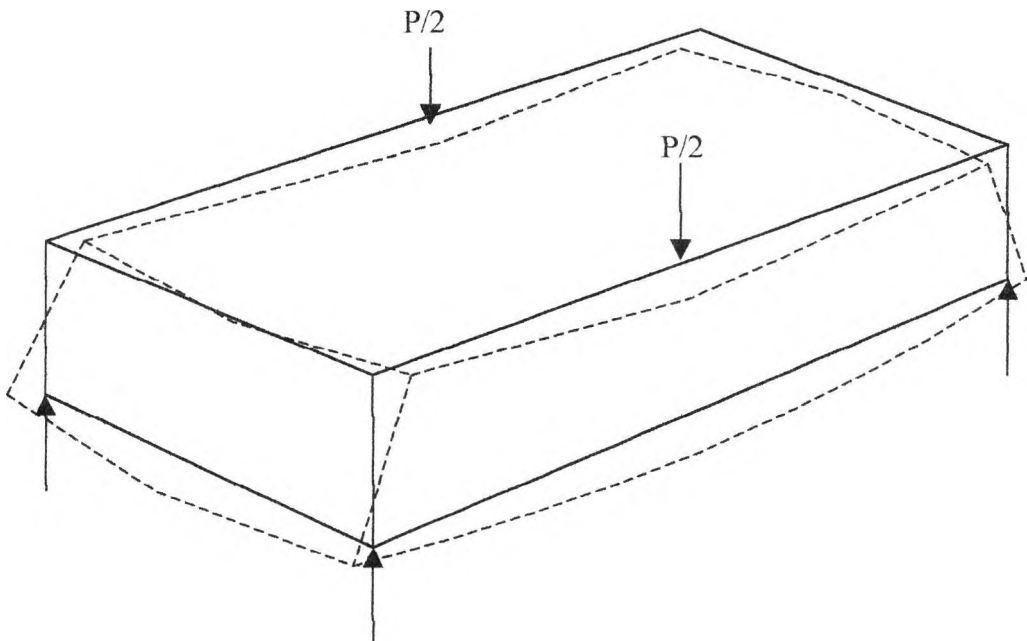
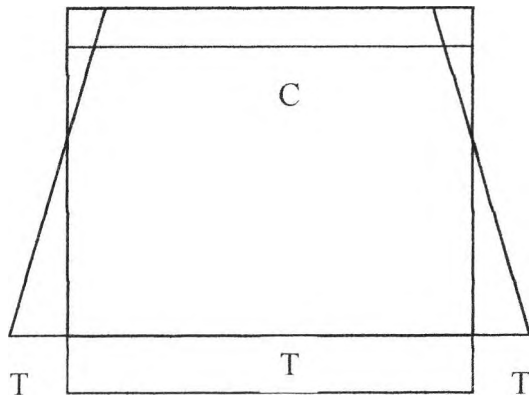
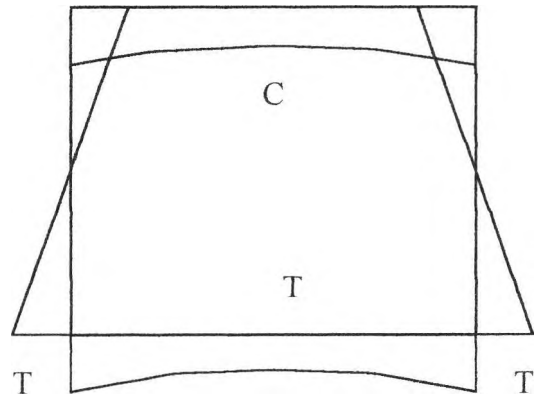


FIGURE 4.4 **SHEAR LAG IN BENDING OF BOX BEAM**



Bending stress distribution in a box beam cross section using ordinary bending Theory



Bending stress distribution in a box beam cross section considering the shear-lag effect

FIGURE 4.5 **BENDING STRESS DISTRIBUTION IN A BOX BEAM CROSS SECTION**

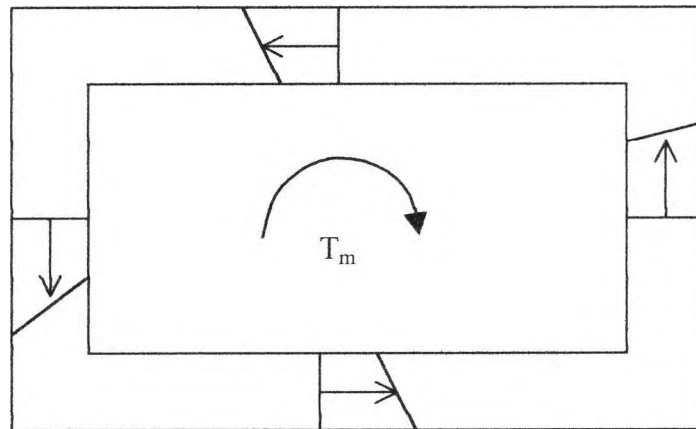


FIGURE 4.6 **St VENANT TORSIONAL SHEAR STRESS DISTRIBUTION IN A BOX BEAM**

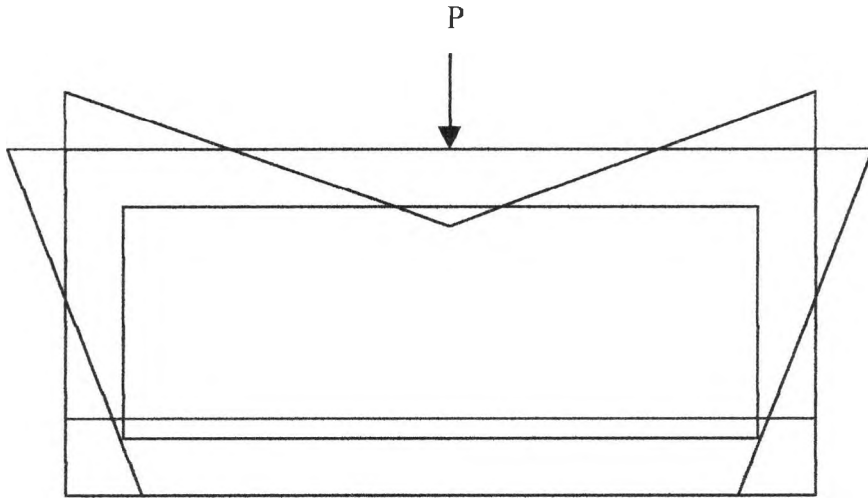


FIGURE 4.7 **TRANSVERSE BENDING STRESS IN TOP FLANGE UNDER HEAVY WHEEL POINT LOAD**

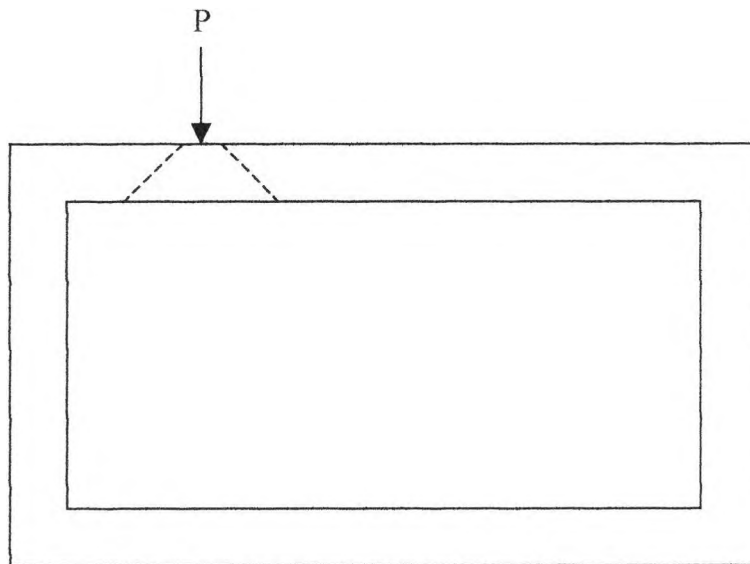
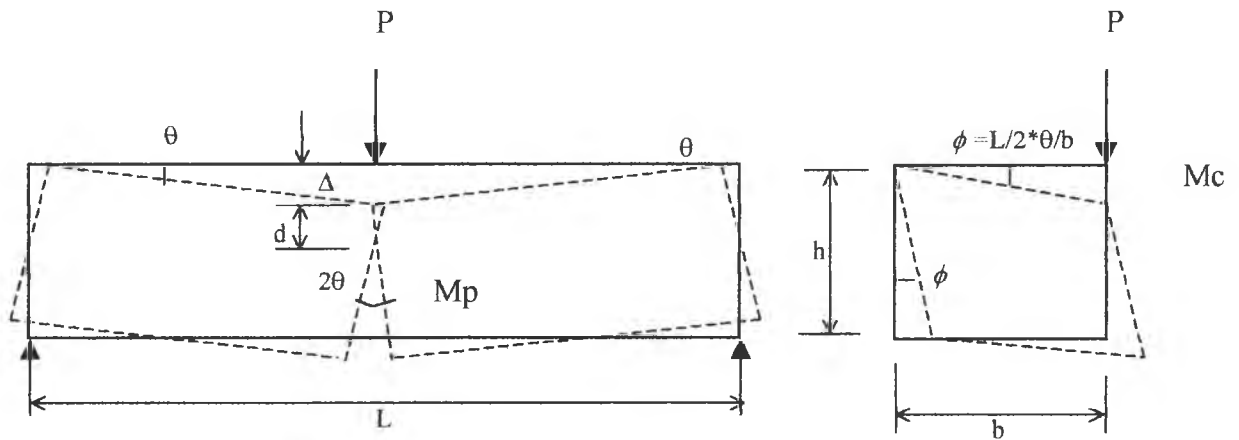
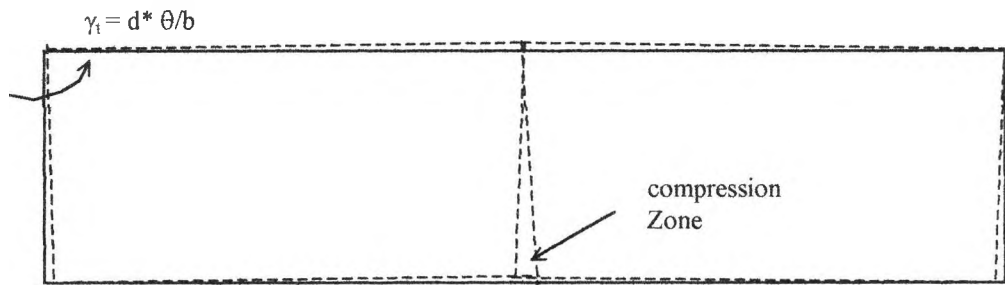


FIGURE 4.8 **PUNCHING SHEAR OF TOP SLAB UNDER WHEEL LOAD**

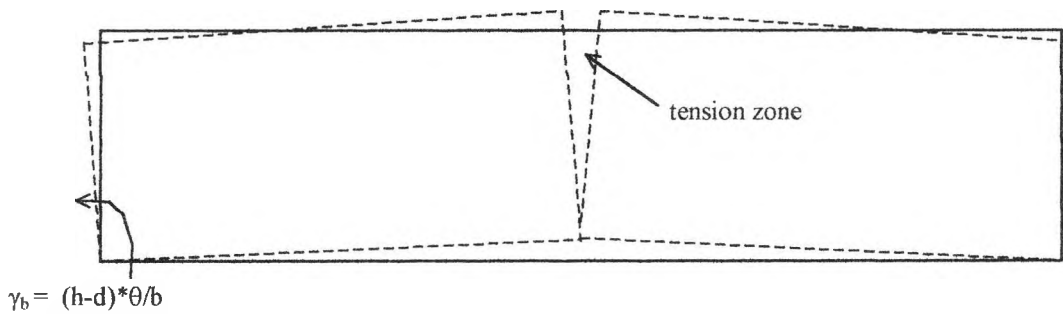


DEFORMATION OF LOADED WEB

DISTORTION OF SECTION NEAR CENTRE



TOP FLANGE DEFORMATION



BOTTOM FLANGE DEFORMATION

FIGURE 4.9 SINGLE CELL BOX GIRDER COLLAPSE MECHANISM

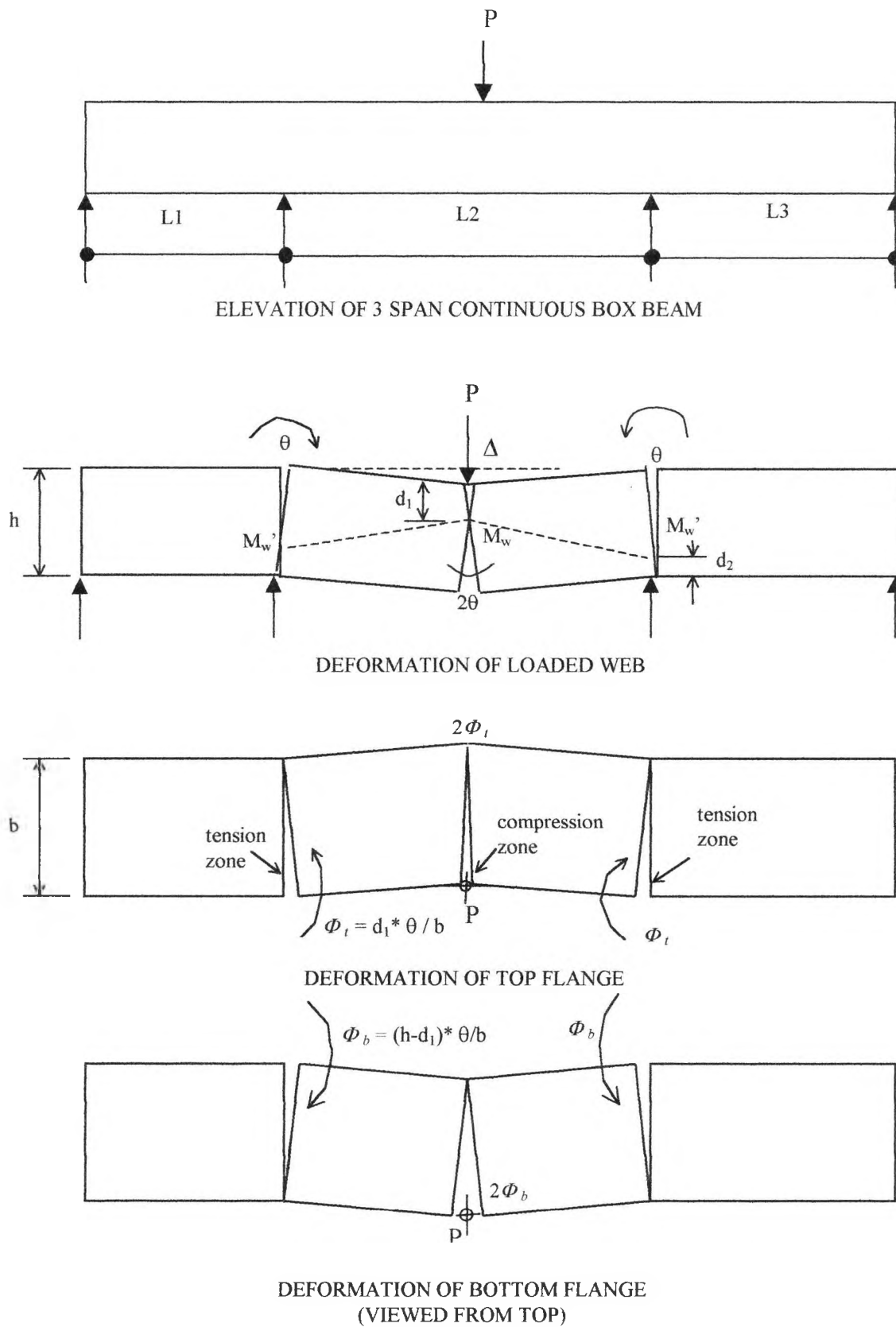


FIGURE 4.10 TYPICAL SINGLE CELL CONTINUOUS BOX BEAM AND IDEALISED COLLAPSE MECHANISM

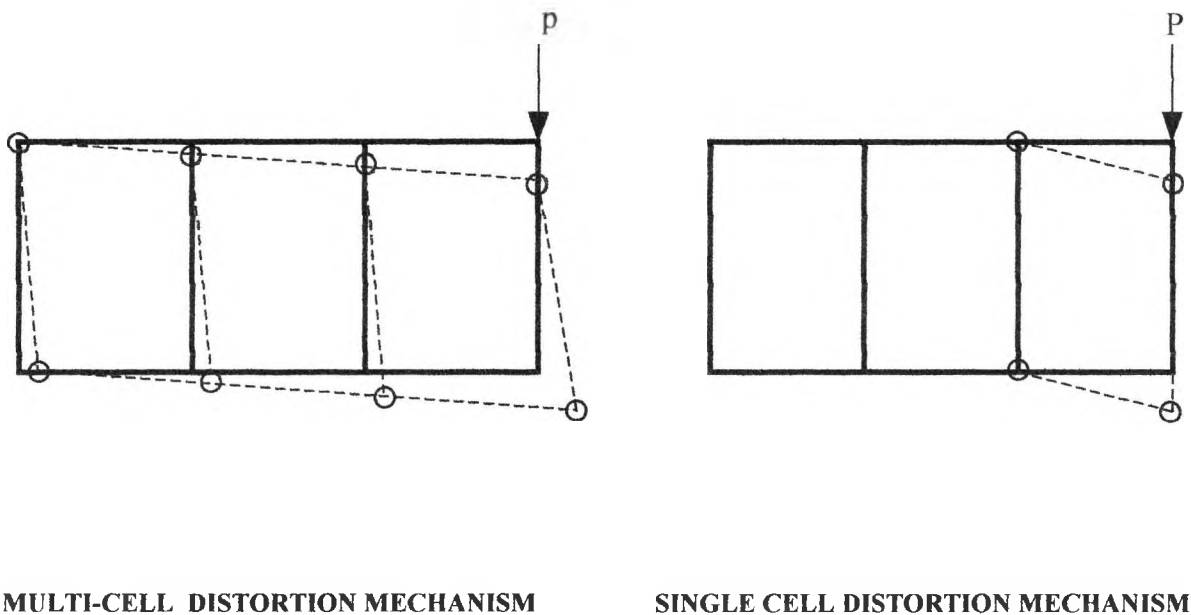
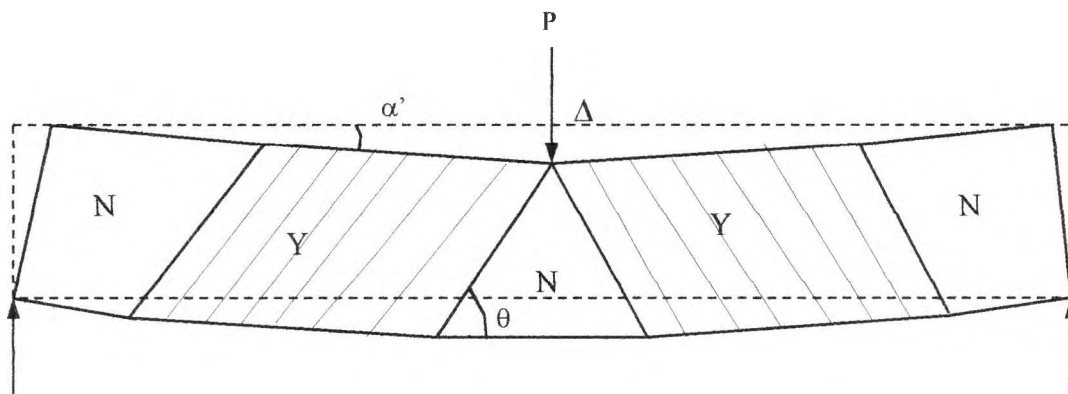
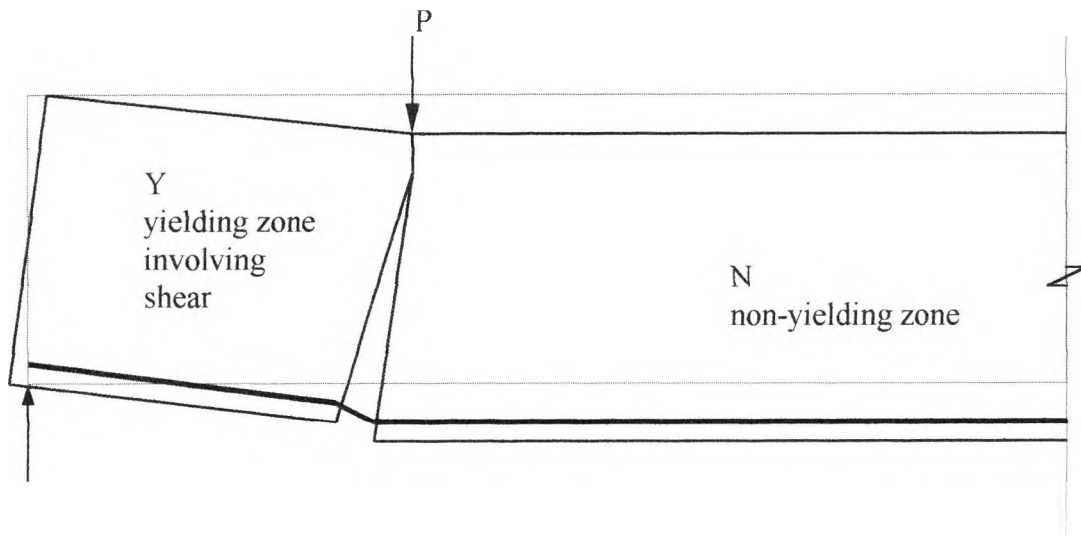


FIGURE 4.11 ALTERNATIVE COLLAPSE MECHANISM IN MULTI-CELL BOX GIRDER



Mechanism requiring no longitudinal extension
 Y- indicates yield region
 N- represents non-yielding region

FIGURE 4.12 BRAESTRUP'S SHEAR MECHANISM IN LOADED WEB



BENDING WITH SHEAR MECHANISM

FIGURE 4.13 FAILURE MECHANISM PROPOSED BY REGAN AND PLACAS

Chapter 5 Concrete Box Girder Model Experiments

5.1 Introduction

Following the preliminary shear experiments described in Chapter 2, four box girder models tests were carried out. It was not the intention in this study to model any particular real box girder structure but merely an attempt to verify the validity of assumptions made for the collapse mechanisms and the corresponding collapse loads. This information could then be used to study the behaviour of actual structures. The average scale of the model structures was chosen as 1:10.

The objective of the first model was to study the collapse behaviour of a typical internal flange and web junction of a simply supported twin-cell box beam B1. The load was applied to an internal web until failure of the section. The two external web members were welded steel frames made from structural channel and Tee sections. The bending and shear capacities of these frames were chosen to be comparable with those of the concrete web members. The load deflection characteristic of the steel frames was studied. The open steel frame on each side allows the observation of crack development of the centre web and made the measurement of strain and crack widths possible.

In the second experiment studied the failure of the external flange and web of an idealised model of a multi-cell continuous box beam B2 was studied. The load was applied to the centre of the outer web. The adjoining cells were idealised by a solid reinforced concrete beam with comparable bending and torsional strength. Providing an external reaction and restraints simulated continuity over the adjoining span.

The objective of the third experiment was to study the collapse behaviour of a three-cell two span continuous reinforced concrete box beam B3. The two spans, including their end diaphragms, were initially cast separately and then connected by a central in-situ diaphragm. The central and end diaphragms prevent distortional deformation at the supports and helped to distribute the reactions more uniformly across the section at the supports. The loading arrangement allowed two separate tests to be carried out at different locations in the two spans.

The last test was conducted on a prestressed concrete double cell two span continuous box beam B4. The beam was cast in two halves with the un-bonded prestressing wires in their correct position. The prestressing wires were then linked together, prior to concreting the diaphragms, using special wire couplers. The prestressing wires were then stressed from both ends after adequate strength was gained, usually after 21 days. Diaphragms were only provided over the supports. Two load cases were considered in the experiment and the loads were applied over the two adjoining spans at selected positions.

This chapter describes the various aspects of formwork, materials and instrumentation, including strain measurement and deflection measurement for the box beam models. The four box girder model tests are described and review of the experimental results is provided.

5.2 Formwork and Material

5.2.1 Formwork

The formwork for the internal cores was made from 15mm plywood. The top and bottom pieces were chamfered to give a 15mmx15mm fillet at the corner of the core. There were internal blocking pieces to maintain the external dimension of the core. Externally, the core formwork was wrapped in thin gauge polythene sheeting to enable easy stripping of the formwork. The side and soffit forms were also made from 15mm ply. The base of the form was of sufficient width to allow the widest three-cell box girder to be cast. Prior to the placement of the reinforcing cage, the formwork was coated with mould oil. The side forms were adequately braced by short strutting pieces to ensure that the width of the section was maintained. Three core forms were made for casting the three-cell box beam.

Permanent timber forms were used for the internal face of the end diaphragms. These were then tied to the external form with spacer blocks in between to ensure that a constant thickness of the diaphragm is maintained. These forms were left in place and were not considered to affect the strength of the box member.

5.2.2 Micro Concrete

The micro concrete mix used for the shear tests was modified and adapted for the concrete box girders. Initially, it was the intention to sieve a Zone 2 sand material. Any larger particles retained on the No 7 sieve to be discarded. Therefore, the maximum size of the graded sand was 2.36mm. The sieved material was used as the aggregate. However, it was felt that difference between the sieved and unsieved zone 2 sand were not great. Further more, because of the quantity of concrete required for each box beam, it was decided to use a Zone 2 sand as the coarse and fine modelling material without sieving. A plasticizer was used to improve the workability of the mix without increasing the water cement ratio. The mix proportion for the micro concrete were as follows:

| | |
|-------------------------|-------|
| Aggregate cement ratio: | 2.8 |
| Water cement ratio: | 0.48 |
| Workability: | High |
| Cement: | O P C |
| Aggregate: | |

Sieved Zone 2 sand

| | |
|--------------|-----|
| 7-14 sieve | 11% |
| 14-25 sieve | 25% |
| 25-52 sieve | 46% |
| 52-100 sieve | 15% |
| 100+ | 3% |

| | |
|---------------------------|-----------------|
| Plasticizer (Celloplast): | 2.8ml/kg cement |
| Average moisture content: | 3% |

The concrete compressive strength was determined from 100mm cubes, and split cylinder indirect tensile strength from 150mm diameter x 300mm cylinders.

The micro-concrete was compacted by externally mounted vibrators. Two external vibrators were mounted on top of each model. In all cases, the concrete compacting was satisfactory except for one span of the three-cell continuous box beam B3. Some honey combing was discovered in the bottom flange near the centre and it was conceived that this would affect the twisting and shear strength contributed by the bottom flange. The area was repaired by removing as much of the honey combing as possible and replacing with the same micro-concrete mix of the original model material.

Additional cubes were cast for determining the strength of the concrete at transfer for the prestressed box girder experiment. Concrete cylinders were also cast to assess the tensile strength of concrete using split cylinder tests.

5.2.3 Reinforcement

Generally, the mesh reinforcement used was a 25mm x 25mm square mesh with 3mm diameter steel wire. The mesh was also tested in conditions where welding was required. This condition was expected in the two span box beams B3 where continuous reinforcement over supports was required. For beam B3, the two spans were cast separately and joined together with an insitu diaphragm. The continuity of reinforcement was achieved by lap welding the top reinforcement. Tensile tests on the welded laps indicated a slight difference in ultimate strength. The elastic strain elongation was less than that of the non-welded specimen. This indicated that welding has reduced the ductility of the wire as expected. The reduction, however, was not significant for the purpose of the model tests. In a prototype structure, however, welding the reinforcement on site has to be carefully monitored to ensure that the welding operation has not significantly altered the yield strength of the reinforcement.

The additional reinforcement used was 4.1mm high tensile plain wire. Some of the wire had been work hardened by twisting. Tensile tests indicated that work hardening by twisting only gives slightly higher yield strength.

For the post-tension box girder experiment B4, a single 5.1mm diameter prestressing steel wire used. No attempts were made to scale down the full size prestressing strands, which were usually 7 wires bundled to form a larger diameter cable. In the experiment, the surface of the wire was covered by insulation tape to simulate the unbonded condition. Depending on the design, the prestressing strands may be grouted to give a bonded condition for the prototype structure. The bonded condition would reduce the stress relaxation of the strands and the losses from the effect of creep. In addition, it also offers some degree of protection against corrosion.

Each type of reinforcement was tensile tested to determine the stress strain characteristic and the results are summarised in table 5.1.

| Type of reinforcement | A_s mm ² | F_u kN | f_y N/mm ² | E_s kN/mm ² |
|-----------------------|-----------------------|----------|-------------------------|--------------------------|
| 3mm mesh | 7.07 | 3.5 | 495 | 45 |
| 4mm twisted | 12.57 | 6.29 | 500 | 209 |
| 4mm unworked | 12.57 | 6.10 | 485 | 222 |
| 5mm prestress | 19.63 | 28.46 | 1450 | 208 |

TABLE 5.1 REINFORCEMENT CHARACTERISTIC

In table 5.1, the area of reinforcement ' A_s ' was based upon the nominal diameter since the actual diameter varied slightly. The yield stresses were therefore, only based upon the nominal diameter. In ultimate load analysis, it is more appropriate to use the total yield force for the reinforcement, F_u .

It was noted that the difference in tensile strength between the twisted and unworked 4mm wire was small. The small gain in tensile strength did not warrant the additional effort in work hardening the large quantity of wires required for the experiments. It was, therefore, decided to use the plain wires for all the box girder experiments.

In general, the reinforcement in the top and bottom flanges of the box beams consisted of two layers of mesh. Additional 4mm longitudinal wires were placed within the mesh to increase the section's reinforcement content to the design requirement. The web reinforcement consisted of two layers of mesh. The top and bottom legs of the web mesh were bent over 90° and lapped with the mesh in the top and bottom flange.

In the idealised internal flange and web beam model B1, the reinforcing mesh was welded to the steel lattice beams on either side. Additional diagonal reinforcement was provided to strengthen the corners and to avoid premature failure of the corner junctions.

For the restrained outer cell model B2, ordinary high tensile steel reinforcement was used in the solid portion. The design stresses were based upon CP110 with f_y varying between 425 and 460 N/mm² depending on the diameter of the

reinforcement used. No tensile tests were carried out for this reinforcement. The current concrete code BS8110 (1985) allows stresses of 460N/mm^2 irrespective of diameter. The difference in stresses for the two codes, however, did not invalidate the ultimate capacity of the solid region.

The reinforcing for the three cell boxes B3 was similar to that of the other box beams. Since the two spans were cast separately, continuity of the top reinforcement was achieved by ensuring adequate anchorage and lap of the reinforcement within the centre diaphragm. When this was not possible, the mesh reinforcement from the two sides was joined together by welding in order to provide continuity.

The two-cell prestressed post-tension box beam B4 also had similar basic reinforcement cages as the other beams. The difference in reinforcement was that fifty percent of the main tension reinforcement in the bottom flanges and top reinforcement over the central support was substituted by 9 number of 5mm prestressing wires. The stressing wires were positioned within the webs and profiled to follow as much as possible the bending moment diagram. The prestressing wires were greased and wrapped with PVC tapes to represent an unbonded condition. The two spans were cast separately and then joined together by an insitu pour over the central support. The prestressing wires were joined at the centre diaphragm by special couplers before the diaphragm concrete was cast. Stressing of the wire was carried out from both ends. The prestressing wire was stressed to 75% of the ultimate value.

Allowances were made for the creep and shrinkage loss, and slippage of wire at the stressing anchors. Although the wires were greased and wrapped to minimise friction loss during stressing, additional losses due to friction and wire profile were inevitable.

5.3 Instrumentation

5.3.1 Load Cells and Proving Ring

A total of twelve load cells were needed for the different experiments. The aluminium load cells were individually calibrated up to 50kN capacity with a sensitivity of 50N/digit during the calibration. The 75mm high, 40mm diameter load cells were used for monitoring reactions under various loading arrangements. In general, the load cells were positioned under each web. In those cases when a reversal of reactions was expected, load cells were also placed on top of the box beam and reacted against the load frame.

Loading was applied via a 250kN capacity proving ring. The ring was attached to a hydraulic jack with a pressure gauge that was fixed to the reaction frame at one end. The opposite end was fixed to a screw jack with a ball reaction mount against the structure. The pressure gauge from the hydraulic jack also acted as a check against the load indicated from the proving ring. The hydraulic ram provided load control, whilst the screw jack provided deflection control during the plastic deformation part of the load deflection curve.

The load was applied to the outer web at mid span for the single cell box beam B2. Hence, the box beam was subjected to eccentric loading that gave rise to bending and torsional effects. The load was applied to an internal web as well as an outer web for the multi-cell beams B3 and B4.

The initial load was applied as a single point load over a spreader plate for the idealised external flange and web model B2. The flange and web junction under the point load failed by local punching shear, unexpectedly. In order that the experiment could continue, the crushed area was repaired. The load was rearranged and applied through a spreader beam onto two reaction pads. This slightly altered the bending moment applied to the beam. However, by splitting the single point load into two, it reduced the effect of direct punching failure. Subsequently, the same load arrangement was adopted for the other tests.

5.3.2 Strain Measurement

Strain was measured on the reinforcement and concrete during each loading cycle. Electrical resistance strain gauges were used to monitor the strain in the reinforcement as well as the load cells. 100mm Demec gauges were used to measure strain on the concrete surface. Where the element was subjected to combined shear and axial stresses, the Demec gauge points were arranged in a rosette pattern to determine the principal stresses. In addition, the gauges were also used to monitor the development of cracks across the fracture section.

The electrical resistance strain gauges (ERS) were attached to the surface of selected reinforcing rods and individually identified and tested before the concrete was cast. The strain gauges were calibrated using an aluminium cantilever beam with a point load at the end. The simple geometry and stress and strain at the root of the cantilever bar was known. Hence the corresponding strain in the gauge could be calibrated in this way. The data logger recorded the change of the resistance as a result of straining with paper printouts for subsequent interpretation and analysis.

A 100 mm Demec gauge was used to measure the surface strain of the concrete. A rosette arrangement of measuring points was set up so that the principle strains could be established. When cracks developed across the rosette, the measurement over the cracks could trace the development of the crack widths during the history of loading. Strains were measured on the top and bottom flanges and the webs at selected locations.

A considerable amount of strain data was obtained from the various model tests. The flange web junction test B1 used 156 strain gauges and 102 Demec gauge readings from the various rosette arrangements. The restraint outer cell test B2 used 56 strain gauges and 68 Demec gauge readings. The two span continuous box B3 used 112 strain gauges and 99 Demec gauge readings. Most of the results merely confirmed the yielding of the reinforcement and the concrete resulting in the measurement of the development of the cracks. In the last prestressed concrete model B4, no attempt was made to measure the strains. Only the deflection profiles along and across the section of the model were monitored.

5.3.3 Deflection Measurement

The deflected profile of the beam sections was monitored during the tests using dial gauges. The locations of the deflection gauges were such that both the longitudinal and transverse deflection could be plotted. Gauges were also placed on the sides and end faces of the beams. The lateral displacement values enabled the assessment of the twisting and warping distortion of the cross section.

Dial gauges were used for the deflection measurements. The gauges were set up on independent scaffolding frames to minimise disturbance. Typical deflected profiles of the various experimental beams will be described in the next chapter.

5.4 Idealised Internal Web and Flanges of a Simply Supported Girder

The experiment B1 was conducted to investigate the collapse behaviour of idealised internal flanges and the web of a simply supported double cell box beam. The box beam model scale was 1:10. Welded steel lattice frames made of structural channel for the top and bottom chords and the structural tee sections for the diagonal members replaced the two external webs. The open frame outer webs enabled the observation and measurement of strain and crack development of the internal web throughout the test. Figures 5.1 to 5.5

The two lattice steel frames, which represented the external webs, were fabricated from 76x38 steel channel and 38x38 structural tee-sections with welded connections throughout. Preliminary tests were carried out to assess the load deflection behaviour. These tests were carried out on the individual frame prior to the fixing of the reinforcing caging. Figure 5.12.

The preliminary tests of the two steel frames involved applying a point load of up to 30kN at selected positions along the span. The corresponding deflections at selected nodes along the span were then recorded. By plotting load verses deflection for each node point, the flexibility matrix was obtained experimentally. It was intended to determine the stiffness matrix by inverting the flexibility matrix using the following relationship.

$$\delta = F \times p \quad \text{where } \delta = \text{Deflection Matrix} \\ F = \text{Flexibility Matrix} \\ p = \text{Force Matrix}$$

The expression could also be written as

$$P = K \times \delta \quad K = \text{Stiffness Matrix,} \\ \text{which is the} \\ \text{inverse of } F$$

and: $K = F^{-1}$

There were limitations to the above method. The flexibility matrix was based on the selected load points and locations where measurement of deflection took place. Therefore, the stiffness matrix obtained by inversion was

also of limited use. In spite of this deficiency, however, the method would still give some indication of the effect of other loads applied to the structure simultaneously. In Lower bound solutions, this information would be useful.

In designing the steel lattices, the members used were so proportioned that the bending and shear capacity was comparable to that of a concrete web element. The steel lattice beam had however a higher stiffness, and produced a smaller deflection. In ultimate load condition, the collapse mechanism would be restricted to yield lines between the webs and flanges. Also, since the material behaviour is assumed to be rigid plastic, the elastic behaviour of the outer web is not likely to influence the failure behaviour of the overall box girder. The overall collapse analysis for the interior flange and web junction would still be valid.

The reinforcement cages were added after the preliminary tests on the steel lattice beams. Figure 5.13. The edge of the reinforcement mesh was welded to the top and bottom of the frame. Additional wires were added as the main longitudinal reinforcement on which strain gauges were attached. The assembly was ready to receive the micro-concrete after inserting the two internal formworks. Figure 5.14

The model span was 3.5m, and the width was 736mm. There were two cells of 330mm centre to centre. The thickness of top and bottom flange slabs was 25mm. The thickness of the internal web was 30mm and the overall depth of the section was 250mm. This represents a span depth ratio of 14, which would be within the range of span depth ratios in Swann's surveys of constructed bridges.

The model was supported on precast concrete plinths at each end. Loading was applied to the centre of the central web via the proving ring and a 300kN capacity hydraulic ram jacking against a reaction frame, The frame legs were anchored down by holding down bolts to the laboratory's strong floor.

Calibrated load cells were used under each web end support. This enabled the measurement of the distribution of the support reactions. In addition a larger load cell

was used under the proving ring to verify the applied loading.

A total of 156 strain gauges were used in both the longitudinal and transverse reinforcement to determine the distribution and development of the strain throughout the test. There were 60 gauges in the top flange, 60 gauges in the bottom flange and 36 gauges in the centre web. Figures 5.6 and 5.7.

100mm Demec gauges were also used for surface strain measurement in different rosette arrangements on the top and bottom flanges and also the internal web surfaces. There were three types of rosette arrangements. The "R" type comprised of 6 gauge points set out to measure strain in three directions at 0° , 45° and 135° , thus enabling the principle strain and development of crack width to be determined. In the "T" Rosette, there were four gauge points set out at 0° and 90° , thus measuring only the longitudinal and transverse strain only. The original intention was also to have some "I" rosettes with 6 gauge points arranged in an "I" format on the web to determine the flexural strain. There was a total of 20 "R" rosettes and 12 "T" rosettes on the top and bottom flanges and outer surfaces of the beam. The "I" rosettes for the webs were abandoned because of access difficulties. The readings from the 20 "R" rosettes, 12 "T" rosettes and 84 Demec gauge readings for each load step are shown in Figures 5.8 to 5.10.

Thirty dial gauges were mounted on independent frames to monitor deflection. Eighteen of those were arranged to measure vertical deflection of the webs and 6 gauges at the each end for the horizontal movement of the end diaphragms, Figure 5.12.

The crack patterns were marked on the member and photographed and compared with anticipated crack patterns and the assumed collapse mechanism.

5.5 Idealised External Flanges and Web of a Continuous Girder.

This experiment B2 was conducted to investigate the collapse behaviour of the external flanges and web of a multi-cell continuous concrete box girder. When the applied loading was concentrated on the outer web, it was conceivable that failure of such a structure would be localised and limited to the outer cell only. It was, therefore, considered appropriate to study the failure of the outer cell only of the structure. The remainder of the structure was idealised by replacing the other cells with a solid rectangular beam that would resist both bending and torsion. Continuity was established by providing a vertical restraint at the free end of the beam. The restraint gave rise to a hogging moment to the end thus simulating a continuous moment over the support. Figure 5.15 to 5.17

In general, the dimensions of the flanges and web were similar to the ordinary twin cell boxes, which have been tested. The overall length of the beam was 4.1m with a 3.5m cellular span and a 500mm solid cantilever end span. The simply supported end diaphragm was 100mm thick. The overall width of the beam was 555mm with a 30mm external web, a 300mm void and the 255mm solid section. The design for the bending and torsional resistance of the solid element was to ensure that failure would be restricted to the outer cell only. The reinforcing for the solid section was made up of 25mm and 16mm diameter high yield bars with 6mm links. The mesh reinforcement from the cellular section lapped onto the cage of the solid element. Additional 4.1mm wire top reinforcement was provided over the short cantilever end for the continuity reinforcement and also at the bottom of the simple span, Figure 5.18 to 5.19. The concreting for the beam was completed in two pours thus enabling the internal formwork core to be removed prior to the second pour forming the end diaphragm, Figure 5.20.

The beam was then set up on the precast concrete plinths on load cells with the reaction frames for loading and holding down ready for testing, Figure 5.21. The simply supported end was placed on rocker bearings that allowed rotation only, Figure 5.22. The centre support was on roller bearings that allowed both rotational and lateral movement, Figure 5.23. The cantilever end restraint was supported also by roller bearings, Figure 5.24.

A concentrated point loading was applied to the outer web. Demec gauge was used to measure the surface strain. Arrays of 15 "R" rosettes, 6 "T" rosettes and 11 linear gauge points making a total of 68 gauge readings for each load step were provided. The strains in the reinforcement were measured by electrical strain gauges. A total of 56 strain gauges were used. It was possible to correlate the Demec readings with those from the strain gauge readings. The deflection at various points were also monitored and recorded to determine the deflection profile under loading through to failure. Twenty dial gauges were used for the deflection measurement.

During the test, a premature local failure of the flange web junction under the point load occurred. The mode of failure appeared to be a punching shear of the flange and local crushing of the web. This type of failure should have been avoided by increasing the contact bearing area. In the prototype structure, where loading would be from traffic, such large local concentration of point loading would not be applied. In order that the experiment could be continued with the original assumed failure mechanism, the model structure was repaired. The applied loading was rearranged with the load applied over 2 points at 450mm apart. The bearing plate size was also increased. Loading was then applied gradually in load steps in the elastic range until yielding started and then by deflection steps until a distinct collapse mechanism was established. It was noted that the collapse mechanism under this loading condition would only result in the formation of yield lines and plastic hinges within the outer web and top and bottom flanges of the outer cell. The repair did not affect the experiment.

The crack patterns were marked and noted after the completion of the test.

5.6 Multi-cell Two Span Continuous Reinforced Concrete Box Girder

The box beam model B3 consisted of two continuous spans of three cells constructed in reinforced micro-concrete. The reinforcing and geometry was basically similar to the idealised models carried out for the internal flange web model and the idealised external flange web model. The overall width of the member was 1020mm. The two equal spans were 3500mm, Figures 5.25 to 5.27. The model was cast in three operations. The two spans were cast separately and then they were connected together by an insitu centre diaphragm, Figures 5.28 and 5.29.

Two basic load tests were carried out on the box beam. The primary test applied a single point load to the outer web near the centre of one span, Figure 5.30. The test was conducted until the ultimate load was reached, and the ultimate load remained constant as the deflection increased. The strain gauge, Demec gauge and dial gauge readings were recorded for analysis. The test was carried out to compare the results with those obtained during the idealised outer cell experiment B2.

A total of 112 electrical resistance strain gauges were used on the reinforcing bars at two sections of the member. There were 56 gauges at the centre and 56 gauges near the central support. The gauges were arranged in such a way that both longitudinal and transverse reinforcement in the top and bottom flanges and in the webs were monitored. Prior to the load test, it was discovered that 15 of the gauges were damaged. Hence, no reliable strain readings were obtained from these gauges.

The surface strain was also monitored by Demec gauge readings. On the top surface, there were 7 one-directional gauges, 6 transverse gauges and 8 three-directional gauges. On the bottom surface, there were 6 transverse gauges and 8 three-directional gauges. 4 three-directional gauges and 8 one-directional gauges measured the surface strains of both outer webs. There were a total of 99 gauge readings for each load stage.

Twelve load cells were used under the web supports to monitor the reaction distributions. Rocker bearings were

used at the centre support and roller bearings were used for the two outer diaphragms. The load cell strain gauge outputs were connected to the data logger for recording.

37 dial gauges monitored the deflection profile of the beam section. There were 8 gauges at the end diaphragm, 8 gauges at each of the quarter span of the loaded span and 5 additional gauges were used on the opposite span along the loaded web.

The loads for the second test were applied over an interior web near the centre of the adjoining span, Figure 5.31. They were applied during the elastic range until the collapse mechanism was established. The test was conducted to verify the validity of the assumption that the yield mechanism was concentrated within the loaded zones of an interior web. In the test, only the deflection profile was monitored and the crack patterns noted. Hence, no attempt was made to measure the strain distribution throughout the structure.

The crack patterns were highlighted and recorded on photographs, Figures 5.30 and 5.31.

5.7 Multi-Cell Two Span Continuous Prestress Concrete Box Girder

The final experiment B4 was carried out on a twin cell two span prestressed box beam. The geometry was generally similar to the other box beams. The beam width was 690mm with three 30mm webs and two 300mm cells. The two span lengths were 3500mm, Figures 5.32 to 5.35. Half of the main top and bottom longitudinal reinforcement was omitted and the equivalent substituted by prestressing wires. A total of nine 5mm prestressing wires were used with three wires concentrated in each of the three webs, Figure 5.36. The wires were coupled over the centre support and, therefore, stressed from both ends. They were stressed in such a sequence that the unbalance force across the section was minimised. To avoid local crushing of the concrete surface under the stressing anchors, 12mm thick steel bearing plates were used to spread the stressing forces uniformly. The positioning of the stressing wire in the webs allowed adequate anchorage to be developed. The ultimate bending moment capacity of the stressing system reduced because of the reduced effective depth of the stressing forces. The prestressing wire profile was such that some of the dead and live load bending moments were resisted by the prestressing system. The wires were wrapped in Denso tapes to simulate an un-bonded condition. The prestressing wires were joined together by special wire couplers over the centre support prior to the casting of the centre diaphragm since the two spans were cast separately.

After the centre diaphragm concrete had cured for at least 28 days, the stressing wires were effectively post-tension to 19.9kN from both ends. This prestressing force represented 70% of the yield strength of the wire. The actual applied stressing force to each wire was up to 24.2kN, however, which was as much as 85% of the yield strength. This was necessary to overcome the frictional losses and anchorage losses during stressing. In a prototype structure, the prestressing strains would normally be grouted inside the tendon duct to reduce the effect of strand relaxation and anchorage slip of the prestressing system. In addition, the effect of creep and shrinkage in the concrete may also be reduced. Grouting would also provide corrosion protection to the strands. On motorway bridges where de-icing salts are often used, if the salt solution find its way into unbonded stressing cable ducts, serious corrosion problems may go undetected.

The end diaphragms were 100mm thick whilst the centre diaphragm was increased to 200mm to accommodate the special prestressing wire couplers. The box beam was set up on three concrete plinths with two load cells on each. Rocker bearings were used over the centre support thus allowing rotation, but not longitudinal movement. The two ends were placed on roller supports which allowed both longitudinal movement as well as rotation.

Symmetrical loading was applied initially to allow the beam to bed properly onto the supports. For the ultimate load case, the loading was applied over the centre of an exterior web. Four additional load cells were used on top of the member to measure the upward reaction should possible uplift under the eccentric loading conditions occur.

No attempt was made to measure the surface strain by Demec gauges or the strain in the reinforcement. The deflected profiles along and across the member were monitored by 16 deflection transducers, which were placed along and across the section. Crack patterns were also noted.

5.8 Summary

This chapter has described the experimental details of the four box beams. To facilitate the development of discussion in the next chapter, the main features of the four tests can be summarised as follows in Table 5.2.

| Beam | Concrete Strength N/mm ² | Longitudinal Reinforcement in typical cell | Remarks |
|------|--|--|---|
| B1 | 40 | 14-3mm T & B flngs 28-4.1mm Bot flng | Idealised internal flange and web study, external steel lattice frames as webs, simply supported, symmetrical loading at mid Span. |
| B2 | 45 | 8-3mm T & B flngs 16-4.1mm Bot span 16-4.1mm Top over Cont. support. | Idealised external flange and web study, adjoining multi-cells idealised by solid concrete beam, simulated continuity, eccentric loading at mid span. |
| B3 | 57 | 16-3mm T & B flngs 32-4.1mm Bot span 32-4.1mm top over Cont. support. | 3 cells 2 span continuous box beam study, eccentric loading to external webs and symmetrical loading to interior webs. |
| B4 | 56.3 | 14-3mm T & B flngs 14-4.1mm bot flng 3x22.6kN prestress per web. | 2 cells 2 span post-tension box beam study, eccentric loading to adjacent spans. |

TABLE 5.2 SUMMARY OF BOX GIRDER EXPERIMENTS

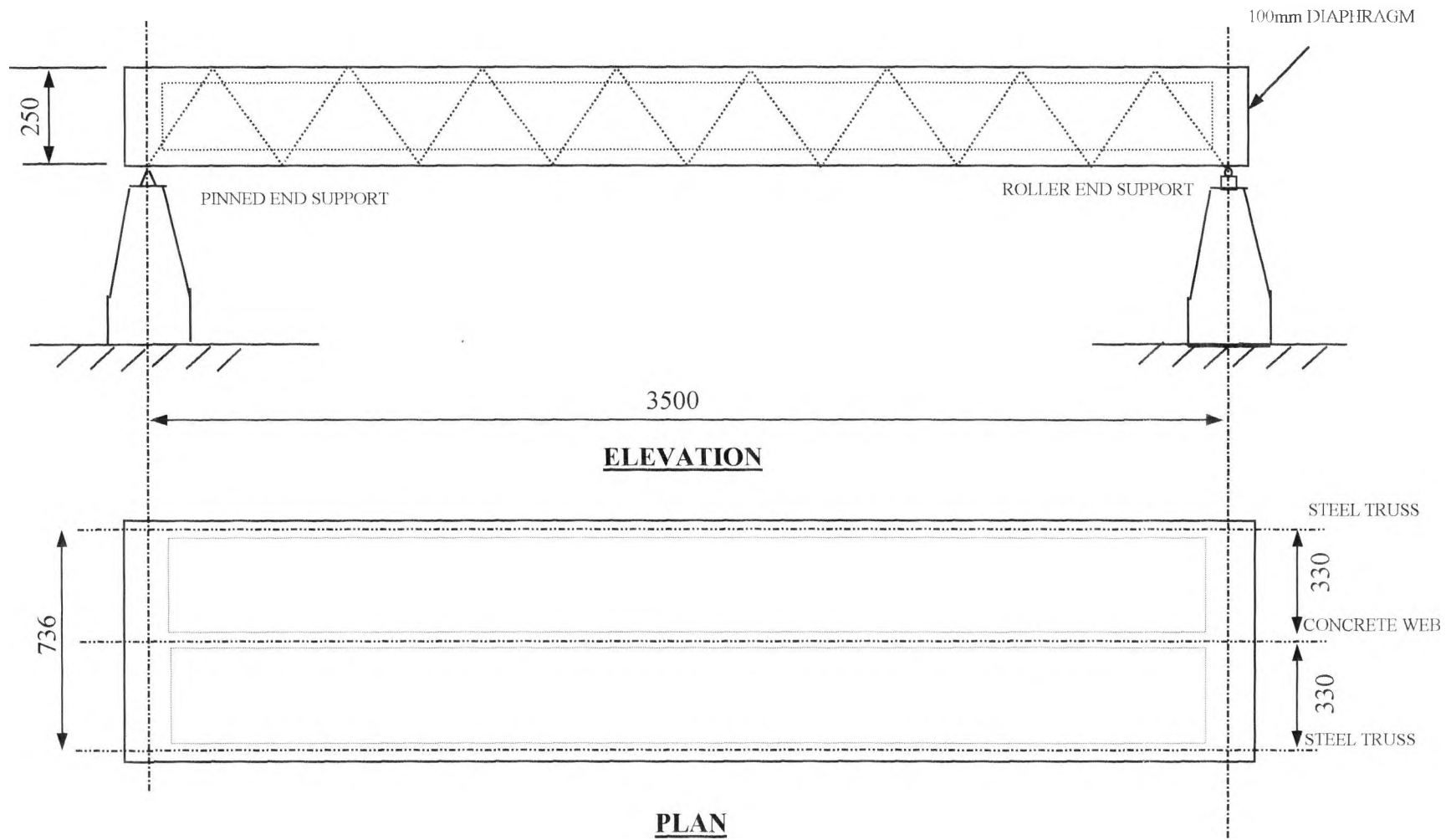
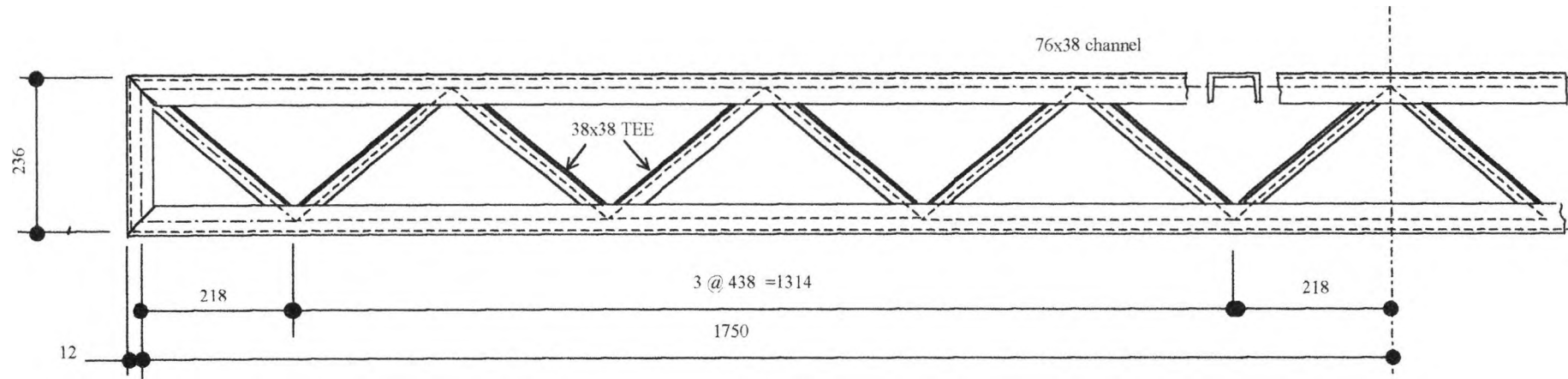


FIGURE 5.1 **TWIN CELL BOX BEAM B1**



DETAIL OF HALF SPAN NUMBER OF TRUSS 2 THUS

NOTES: All Joints to be welded 6mm fillet weld

Material Summary:

| | | |
|---------------|-------|---------|
| 76x38 channel | 4 No. | 3524mm |
| | 4 No. | 236mm |
| Total Length | | 15040mm |
| 38x38 Tee | 32 No | 310 mm |
| Total Length | | 9920mm |

FIGURE 5.2 FABRICATION DRAWING FOR BOX BEAM B1 EDGE STEEL TRUSS

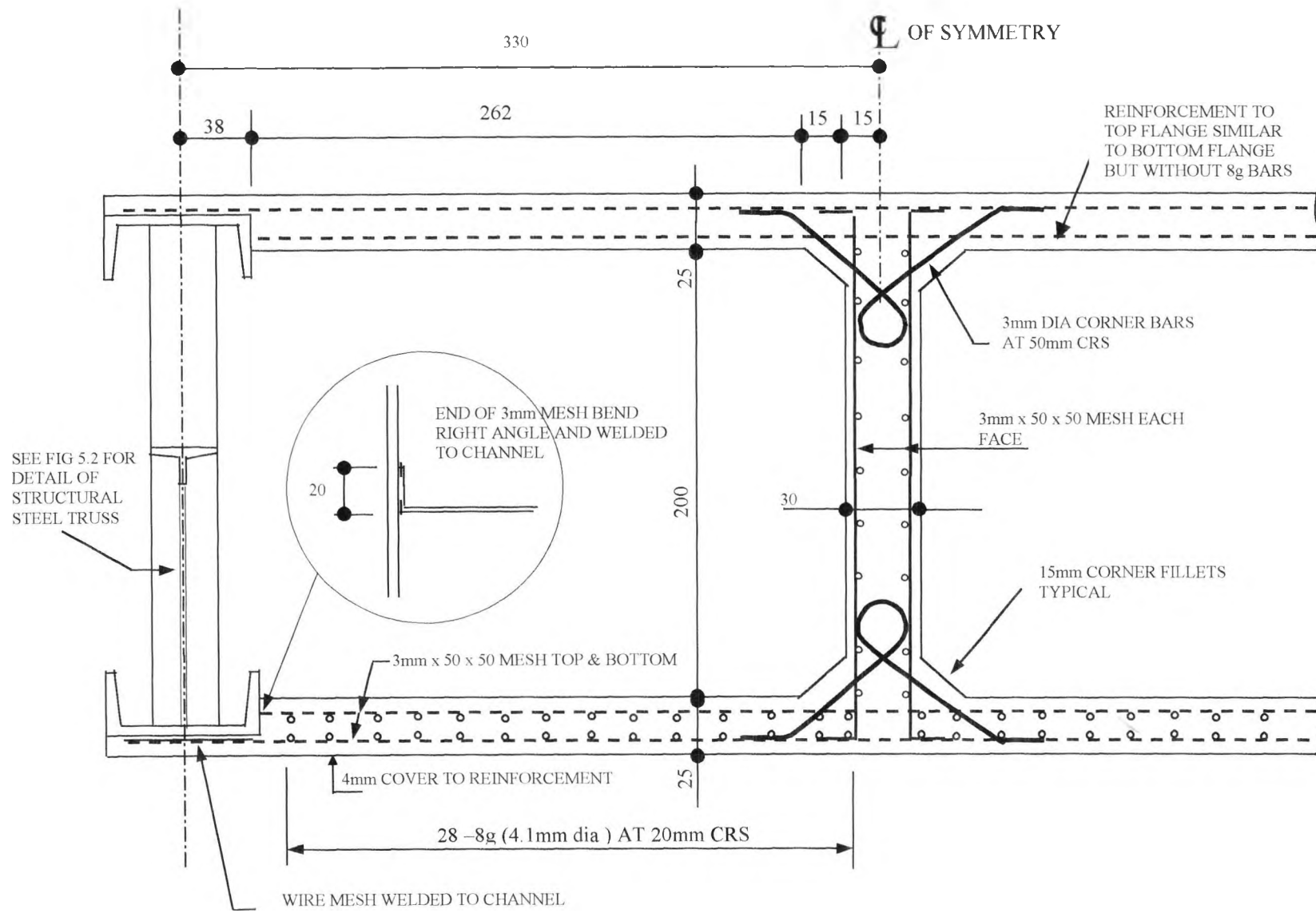


FIGURE 5.3 REINFORCEMENT DETAIL OF 2 CELL BOX BEAM B1

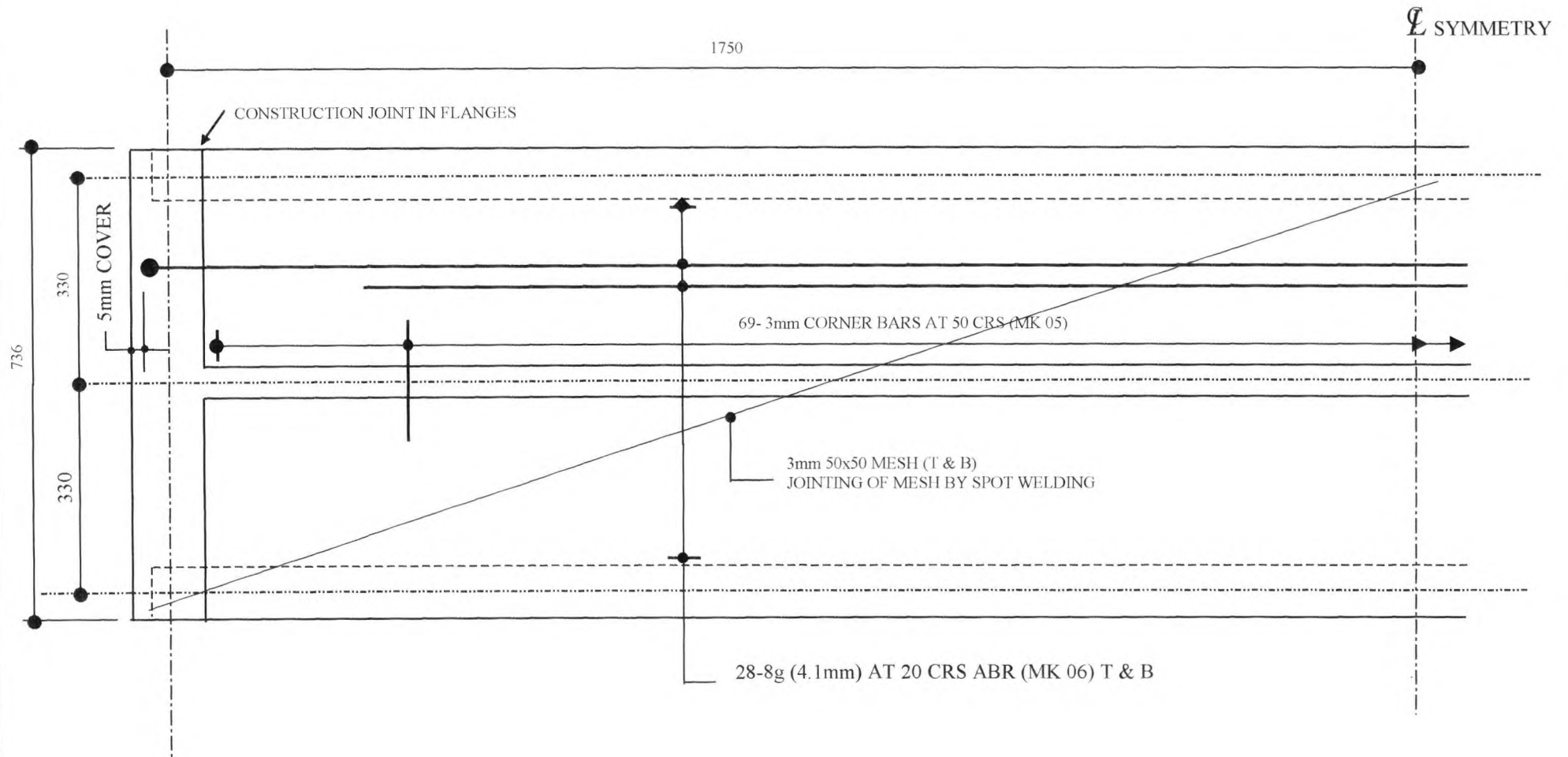


FIGURE 5.4 REINFORCEMENT DETAIL OF BOTTOM FLANGE FOR BEAM B1 (TOP FLANGE REINFORCEMENT SIMILAR EXCEPT OMIT 8g WIRES)

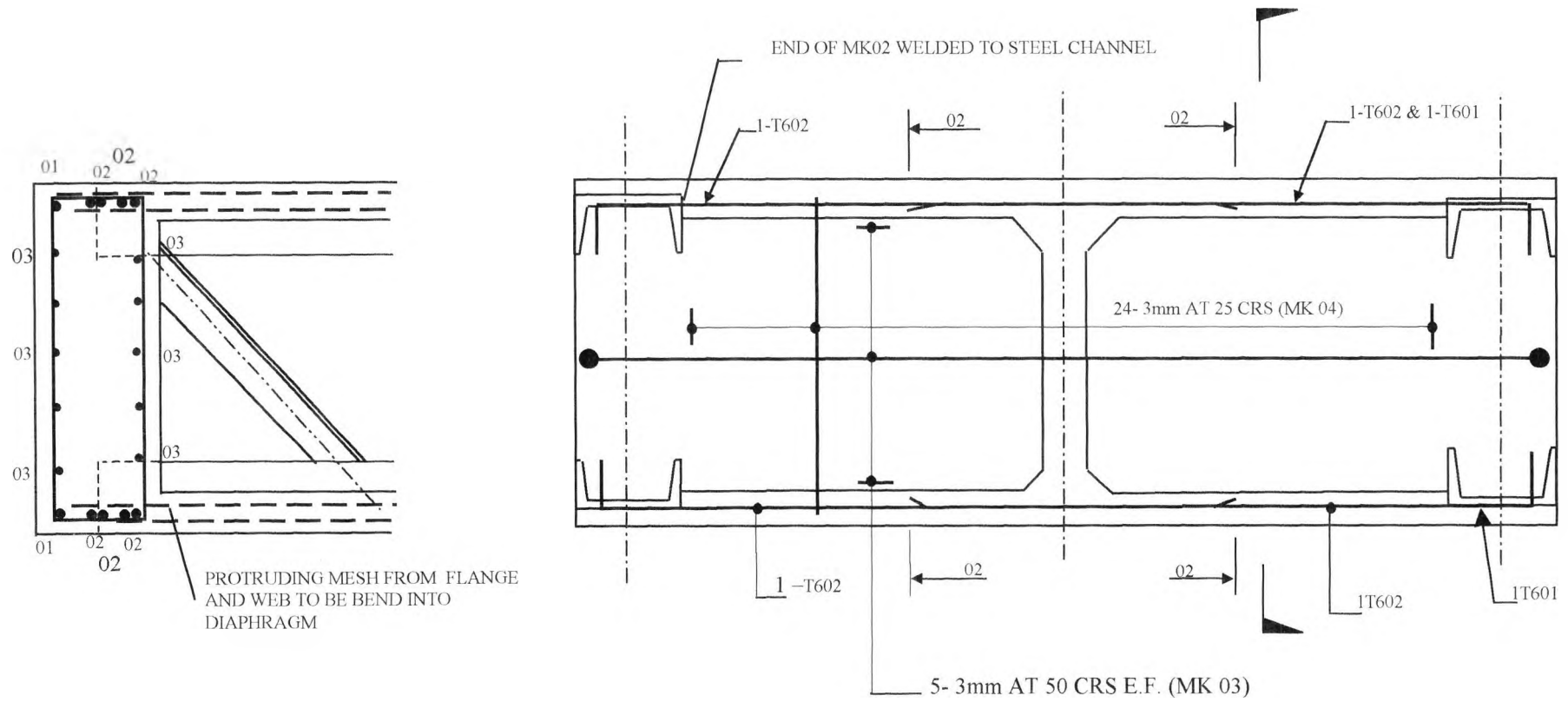
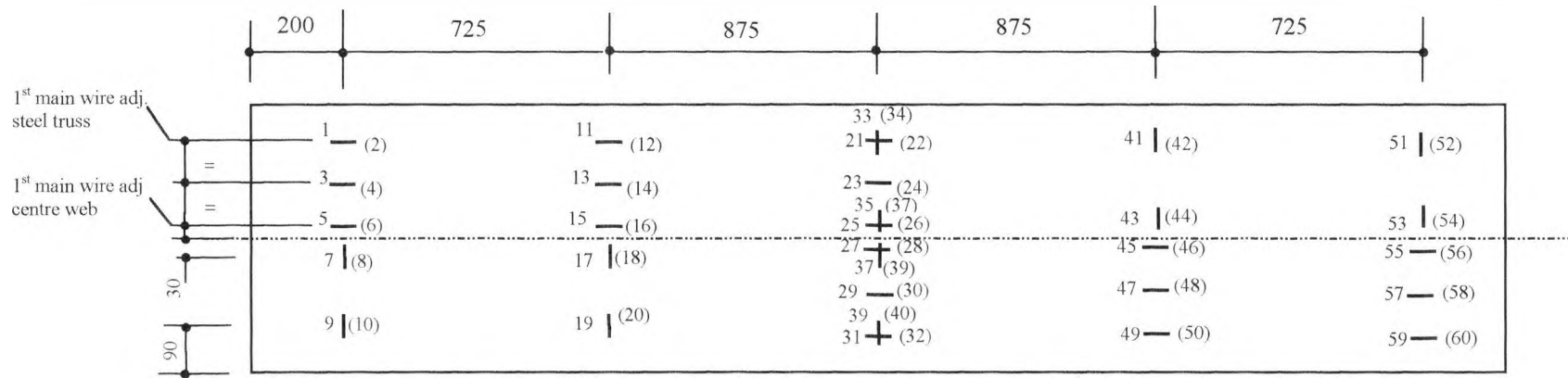
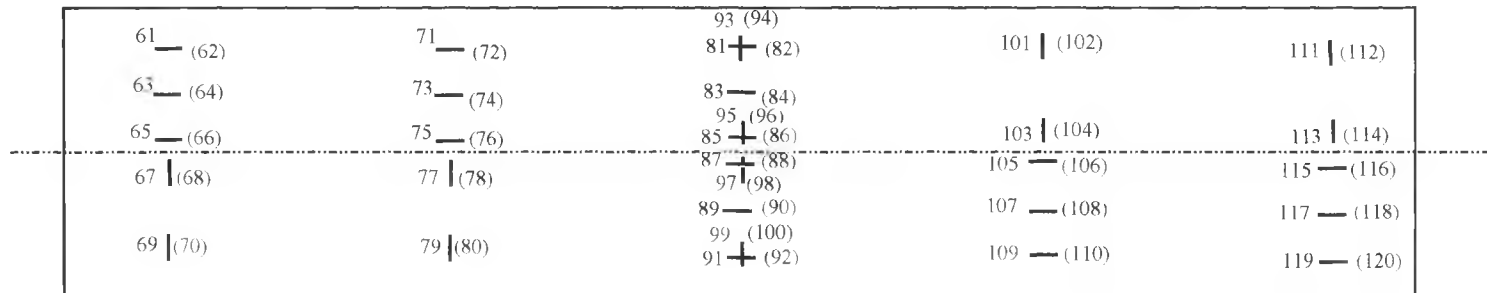


FIGURE 5.5 REINFORCEMENT DETAILS OF END DIAPHRAGMS

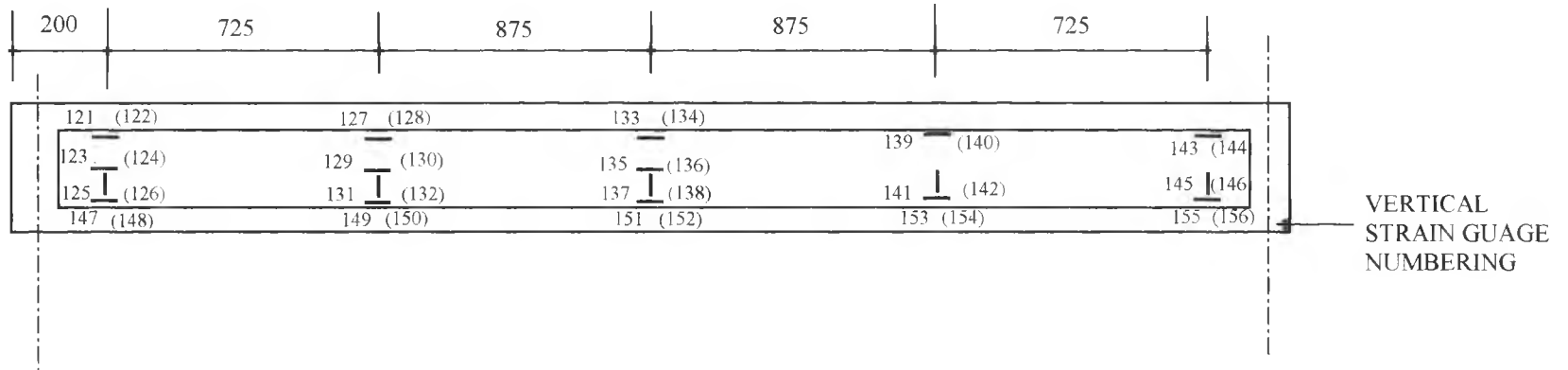


BOTTOM FLANGE LOCATION AND NUMBERING OF E.R.S.
(ODD NUMBER BOTTOM LAYER, EVEN NUMBERS TOP LAYER)
TOTAL NUMBER OF GAUGES IN BOTTOM FLANGE 60



TOP FLANGE LOCATION AND NUMBERING OF E.R.S.
(ODD NUMBERS BOTTOM LAYER EVEN NUMBERS TOP LAYER)
TOTAL NUMBER OF GAUGES IN TOP FLANGE 60

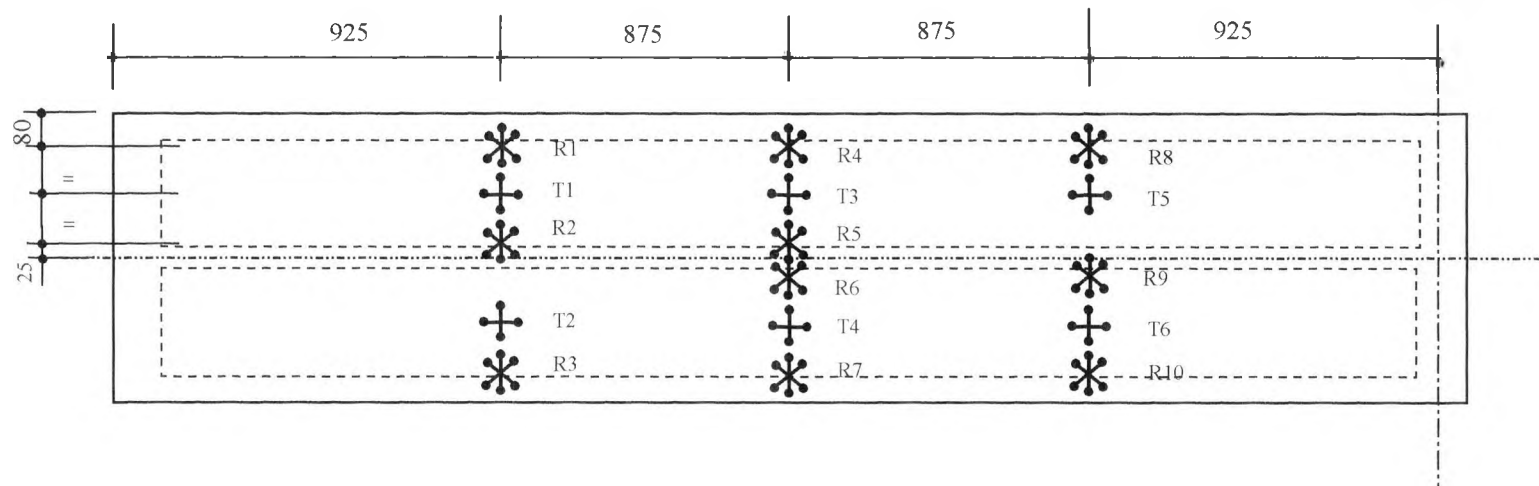
FIGURE 5.6 LAYOUT OF STRAIN GAUGES FOR BOX BEAM B1



LOADED WEB LOCATION AND NUMBERING OF E. R. S.
 (ODD NUMBER FAR FACE, EVEN NUMBERS NEAR FACE)
 TOTAL NUMBER OF GAUGES IN WEB 36

TOTAL NUMBERS OF ERS REQUIRED IN FLANGES AND WEB REINFORCEMENT 156

FIGURE 5.7 LAYOUT OF STRAIN GAUGES IN WEB OF BOX BEAM B1



BOTTOM FLANGE BOTTOM FACE DEMEC GAUGE LOCATIONS

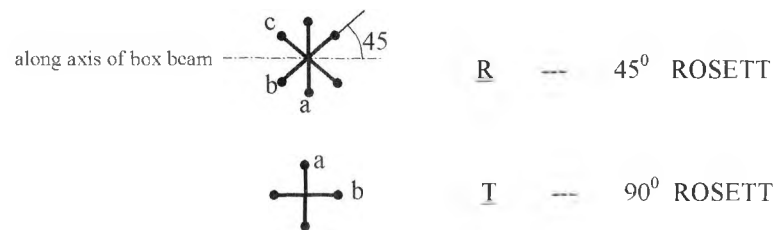
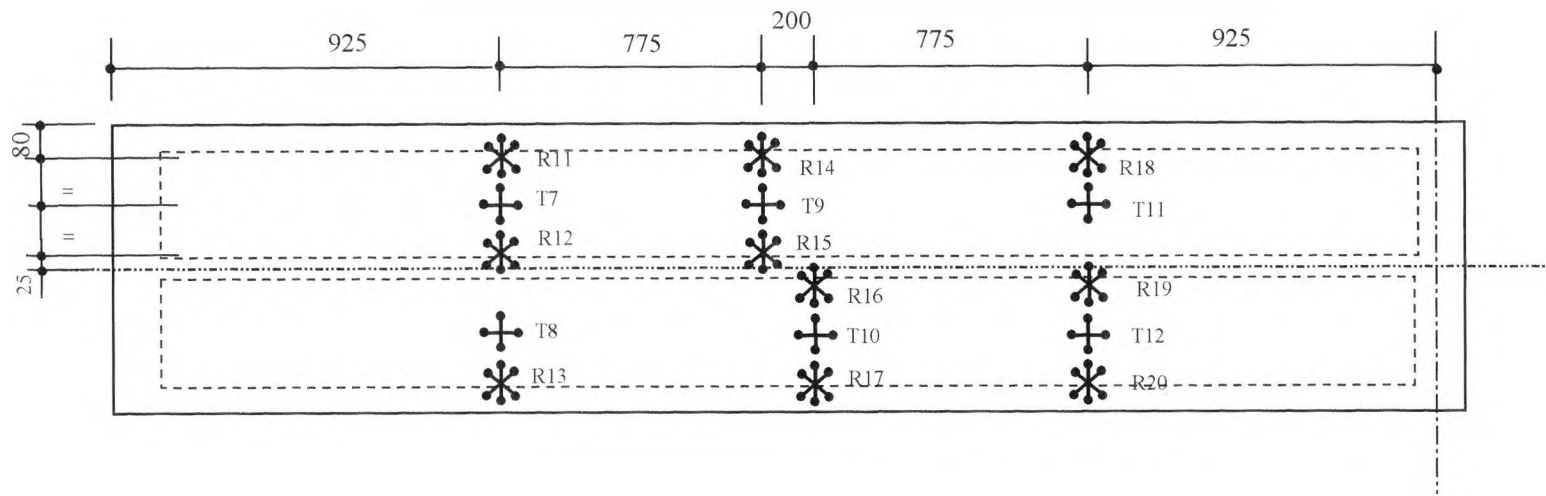


FIGURE 5.8 LAYOUT OF DEMEC GAUGES TO BOTTOM FLANGE OF BOX BEAM B1



TOP FLANGE TOP FACE DEMEC GAUGE LOCATIONS

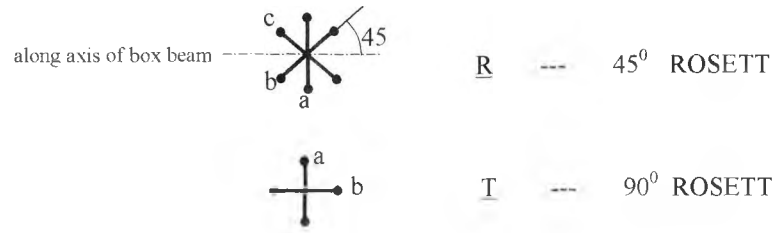
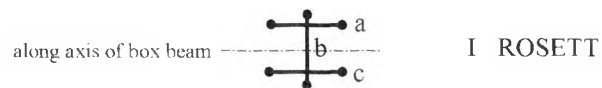
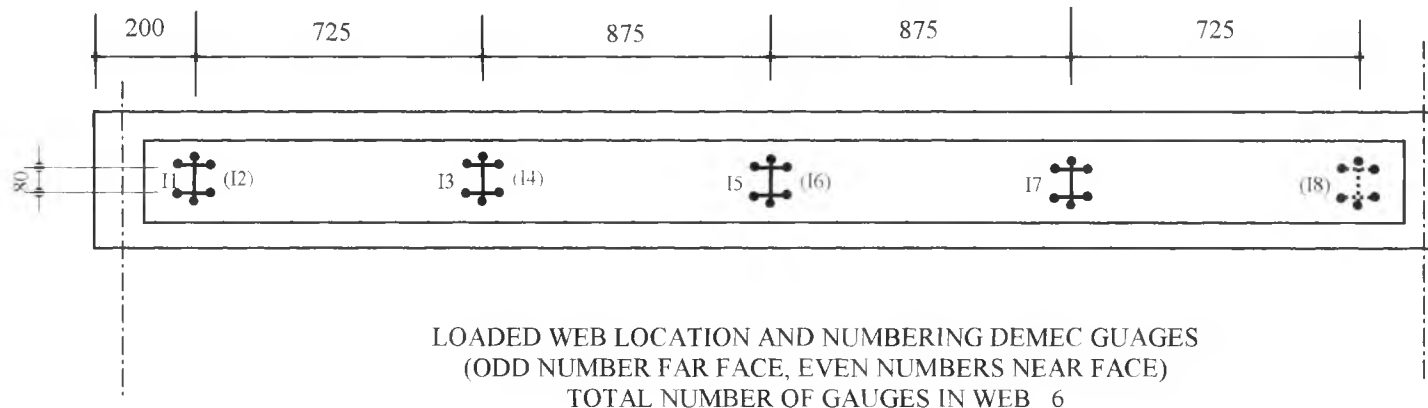


FIGURE 5.9 LAYOUT OF DEMEC GAUGES TO TOP FLANGE OF BOX BEAM B1



| READINGS REQUIRED | | | |
|-------------------------|----|-----|-----------------|
| TOTAL No OF 'R' ROSETTS | 20 | 60 | 3 READINGS EACH |
| TOTAL No OF 'T' ROSETTS | 12 | 24 | 2 READINGS EACH |
| TOTAL No OF 'I' ROSETTS | 6 | 18 | 3 READINGS EACH |
| TOTAL DEMEC READINGS | | 102 | |

FIGURE 5.10 LAYOUT OF DEMEC GAUGES IN LOADED WEB OF BOX BEAM B1

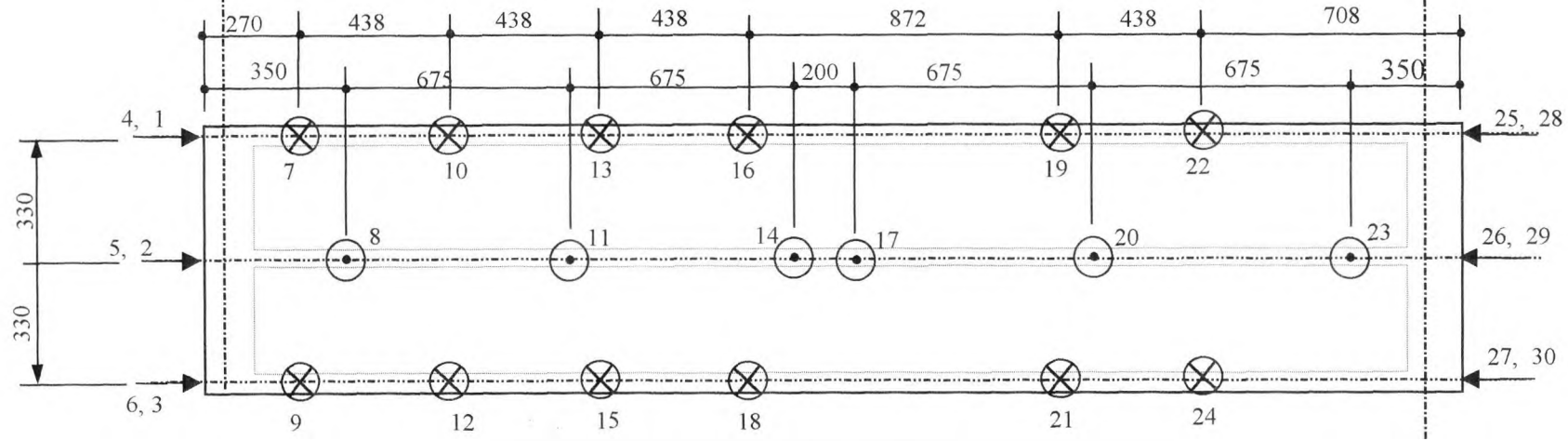
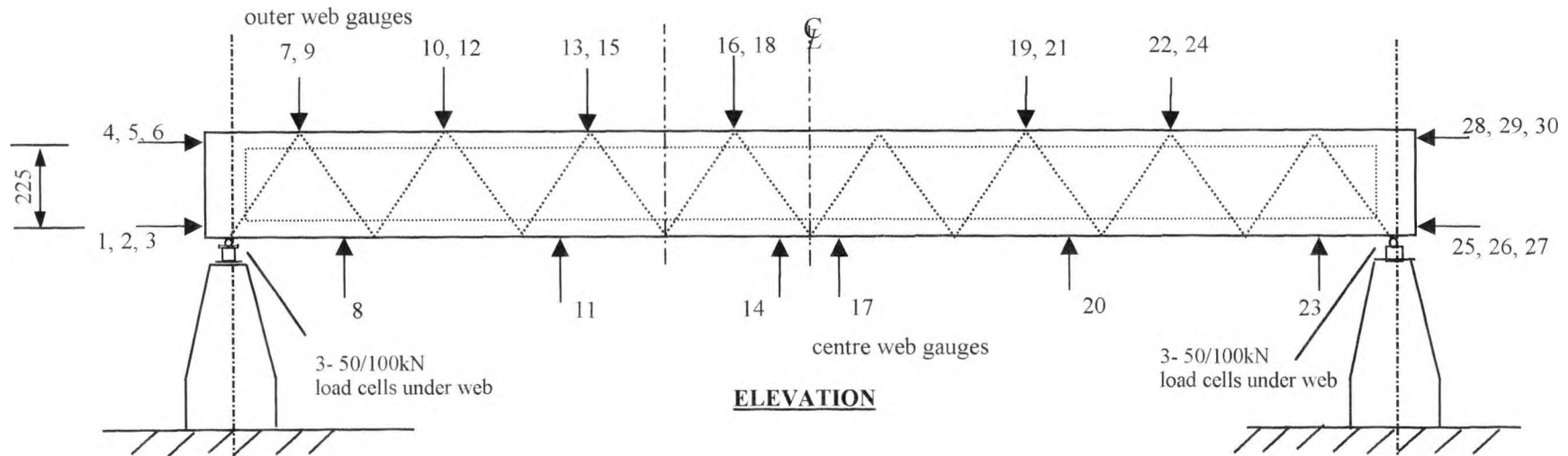


FIGURE 5.11 LOCATION OF DISPLACEMENT GAUGES FOR BOX BEAM B11

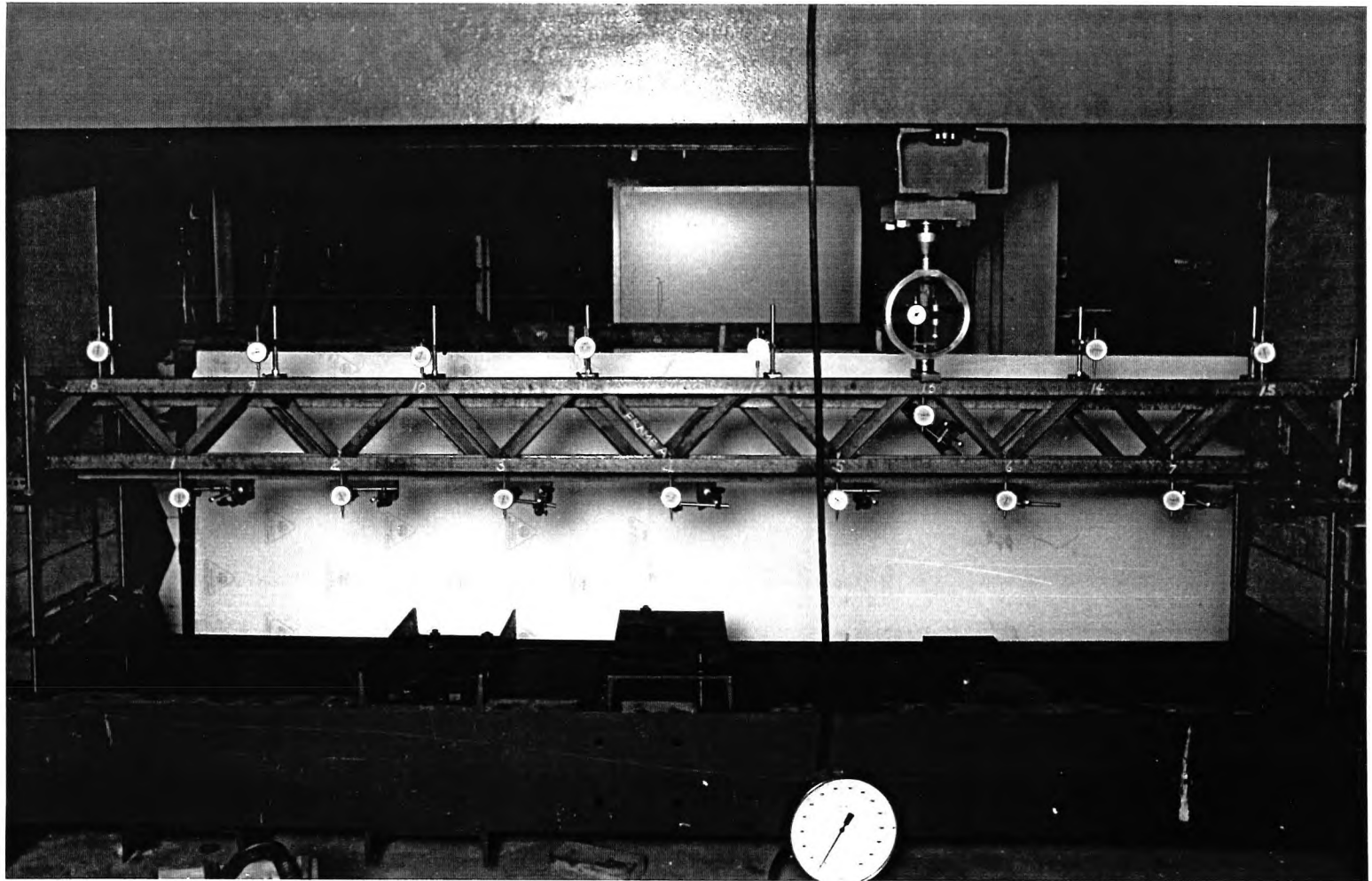


FIGURE 5.12 **TESTING OF EDGE STEEL TRUSS FRAMES**

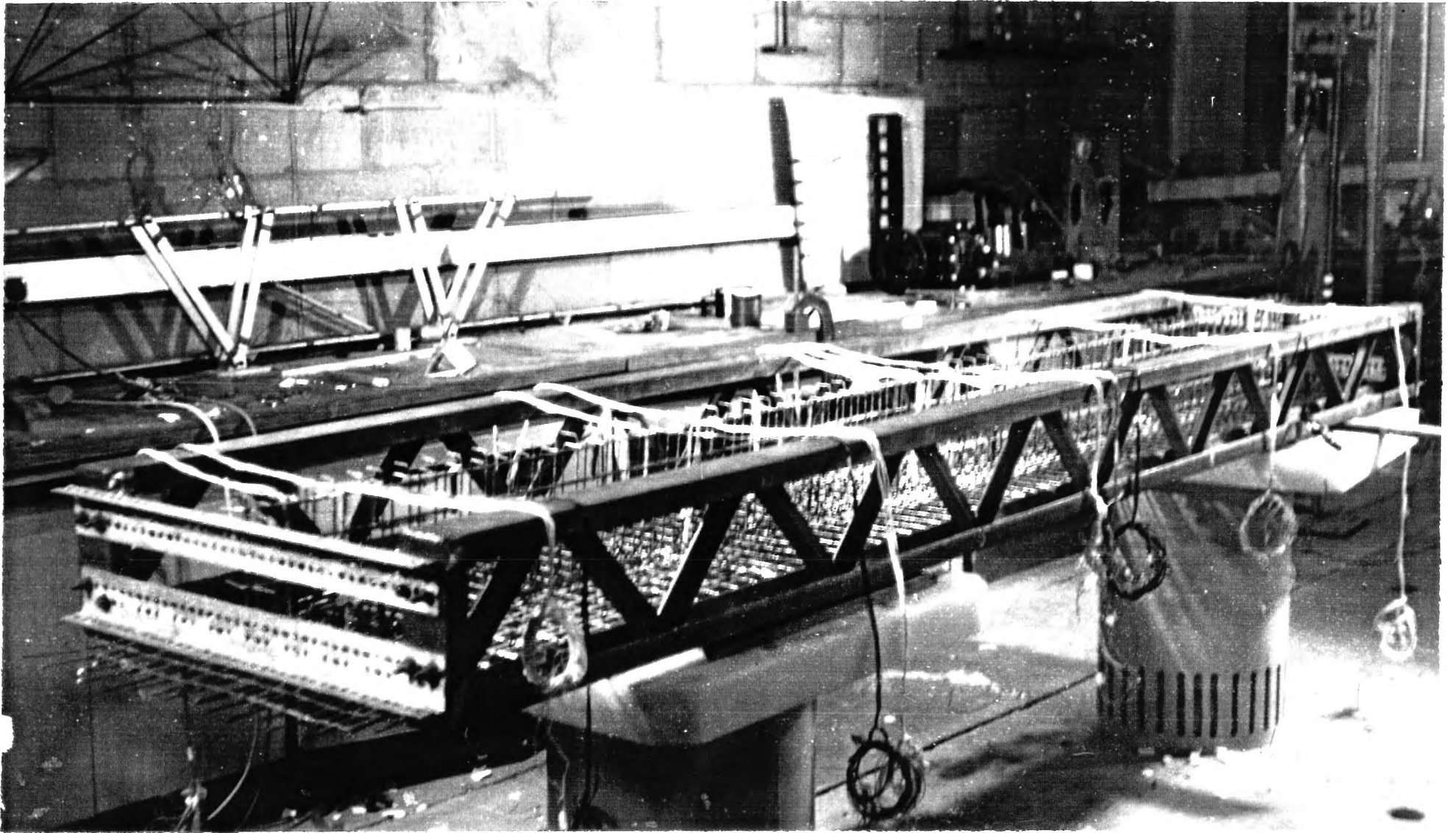


FIGURE 5.13

BOTTOM FLANGE AND WEB REINFORCEMENT

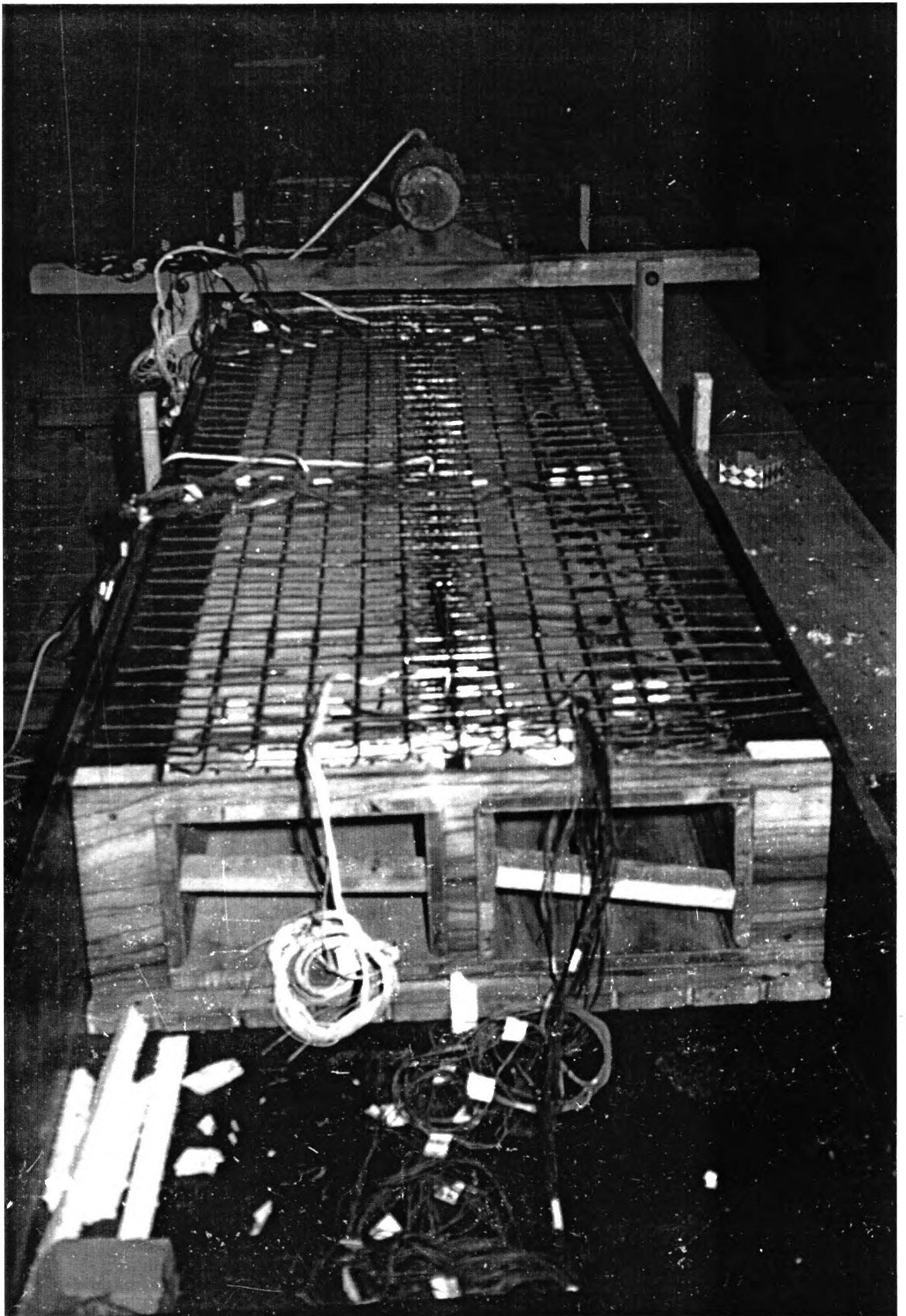


FIGURE 5.14

COMPLETION OF TOP REINFORCEMENT CAGE

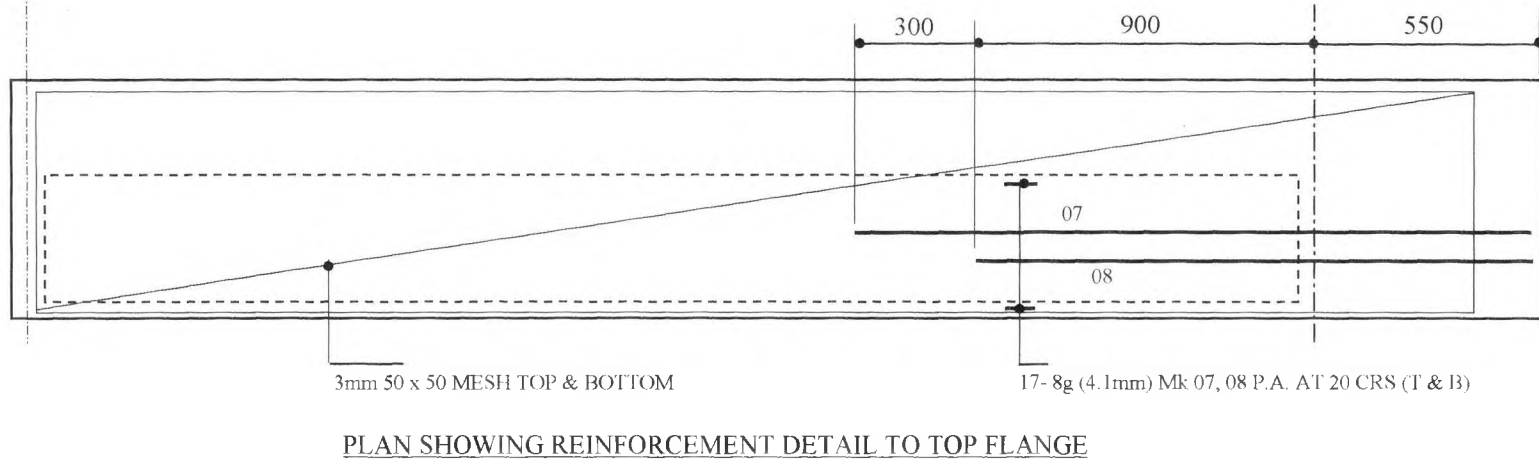
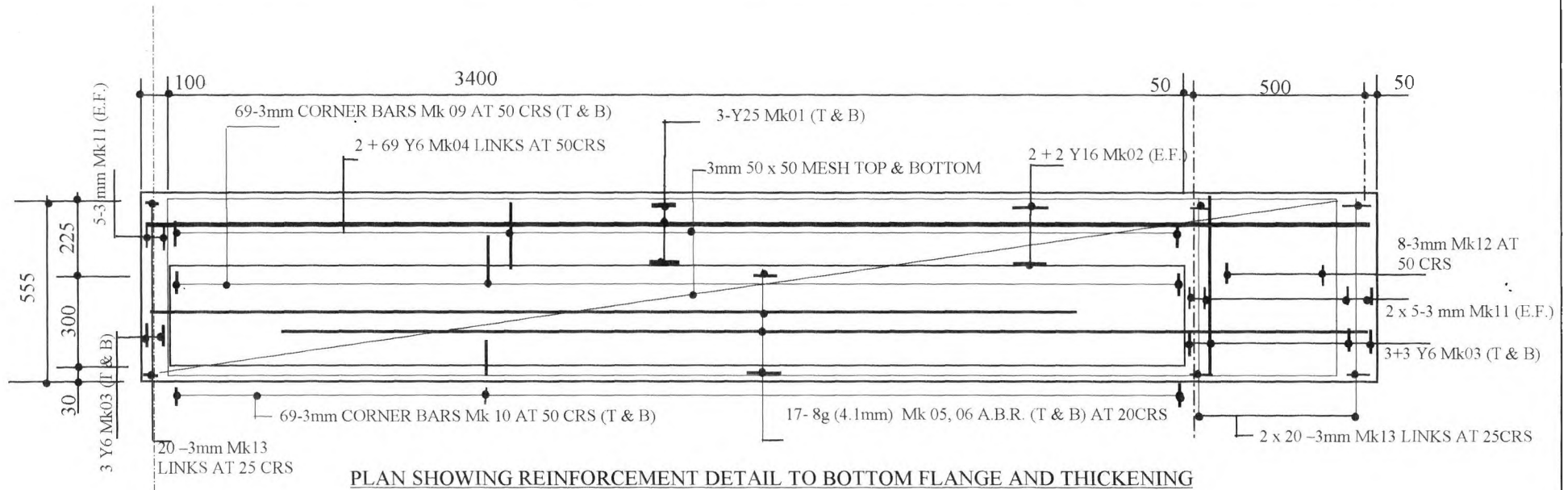


FIGURE 5.15 REINFORCEMENT DETAILS FOR IDEALISED EXTERNAL FLANGE AND WEB ELEMENT B2

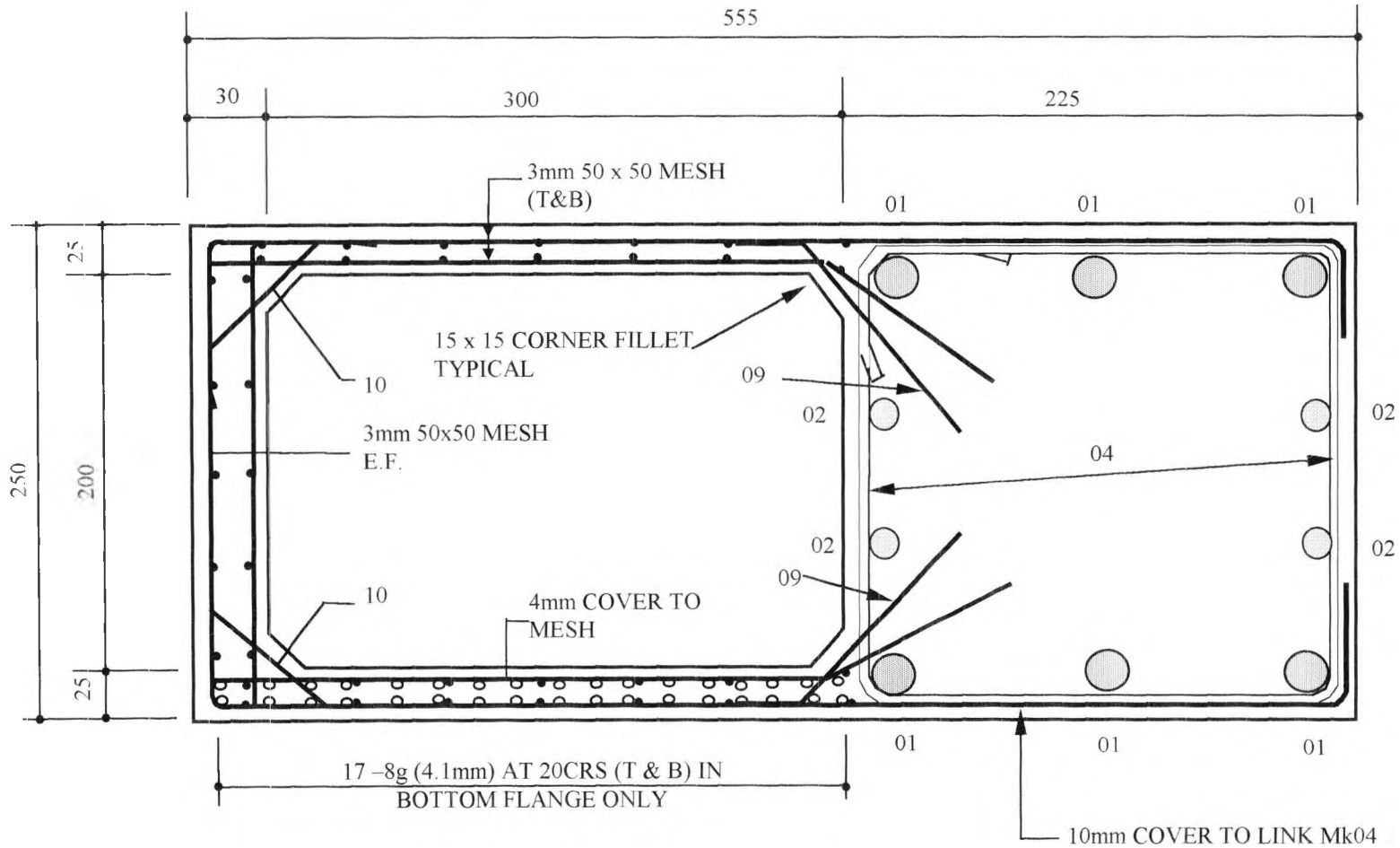


FIGURE 5.16 MID SPAN SECTION FOR BEAM B2

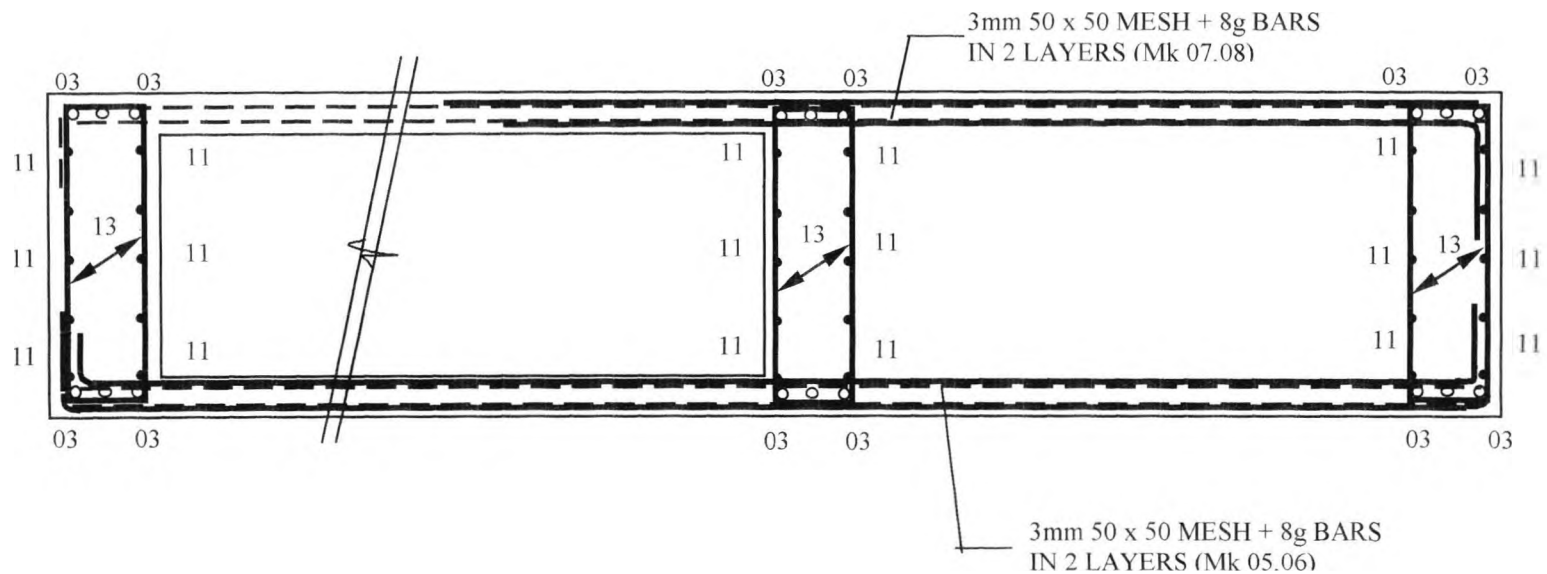


FIGURE 5.17 LONGITUDINAL SECTION FOR BEAM B2

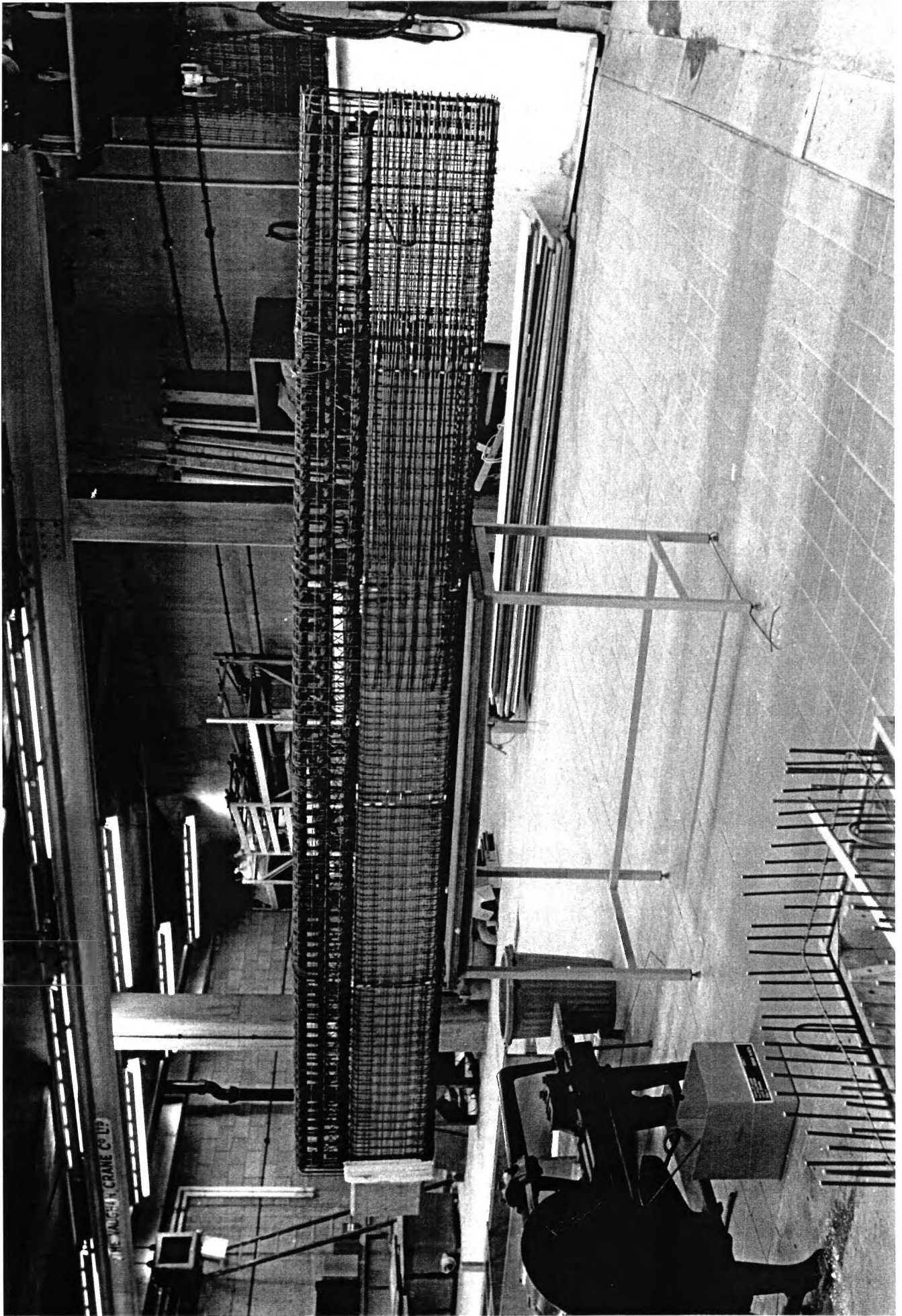


FIGURE 5-18 TOP REINFORCEMENT FOR REAR DECK

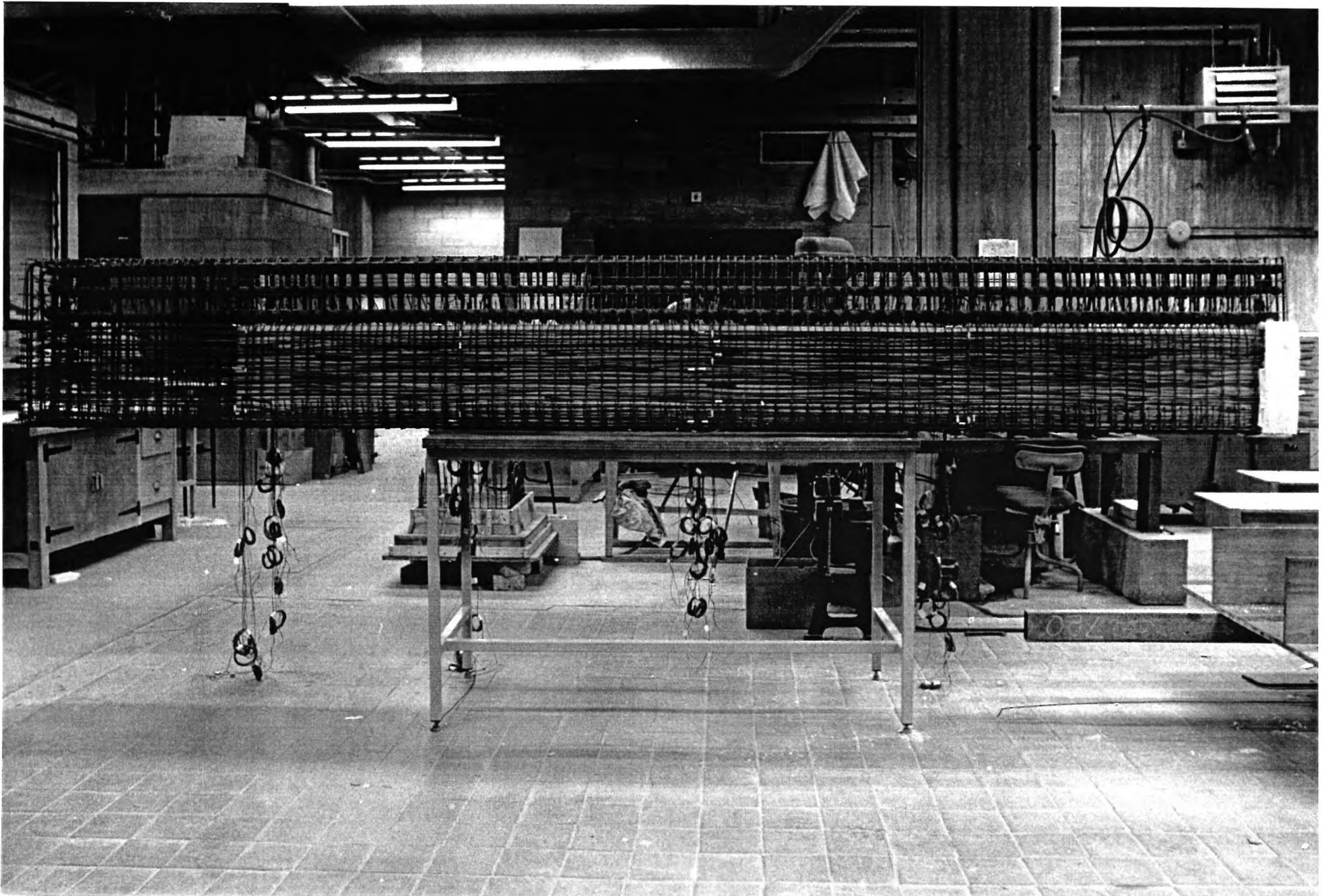


FIGURE 5.19 BOTTOM REINFORCEMENT FOR BEAM B2

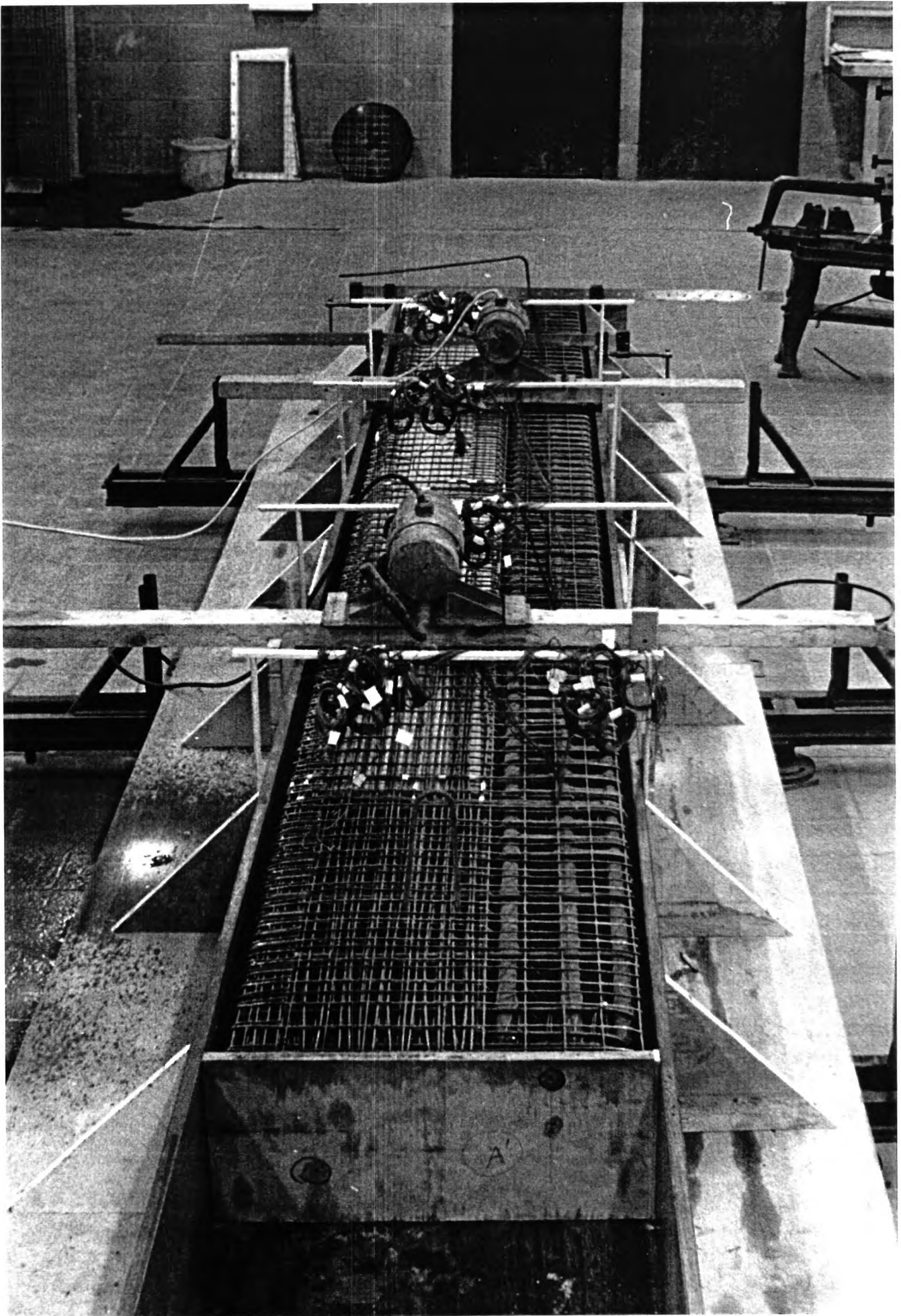


FIGURE 5.20

BEAM B2 READY FOR CONCRETING

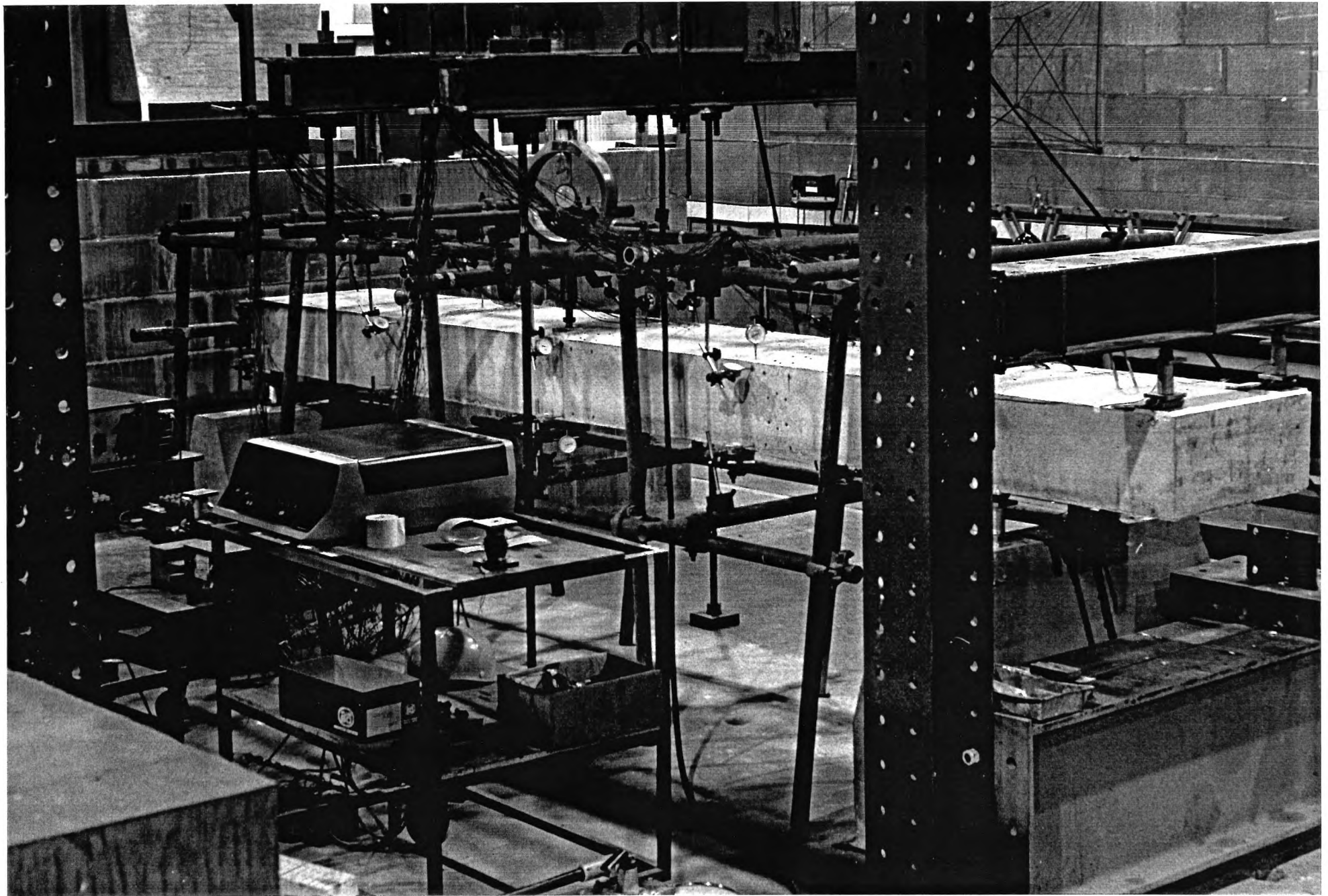


FIGURE 5.21 BEAM B2 SET UP READY FOR TESTING

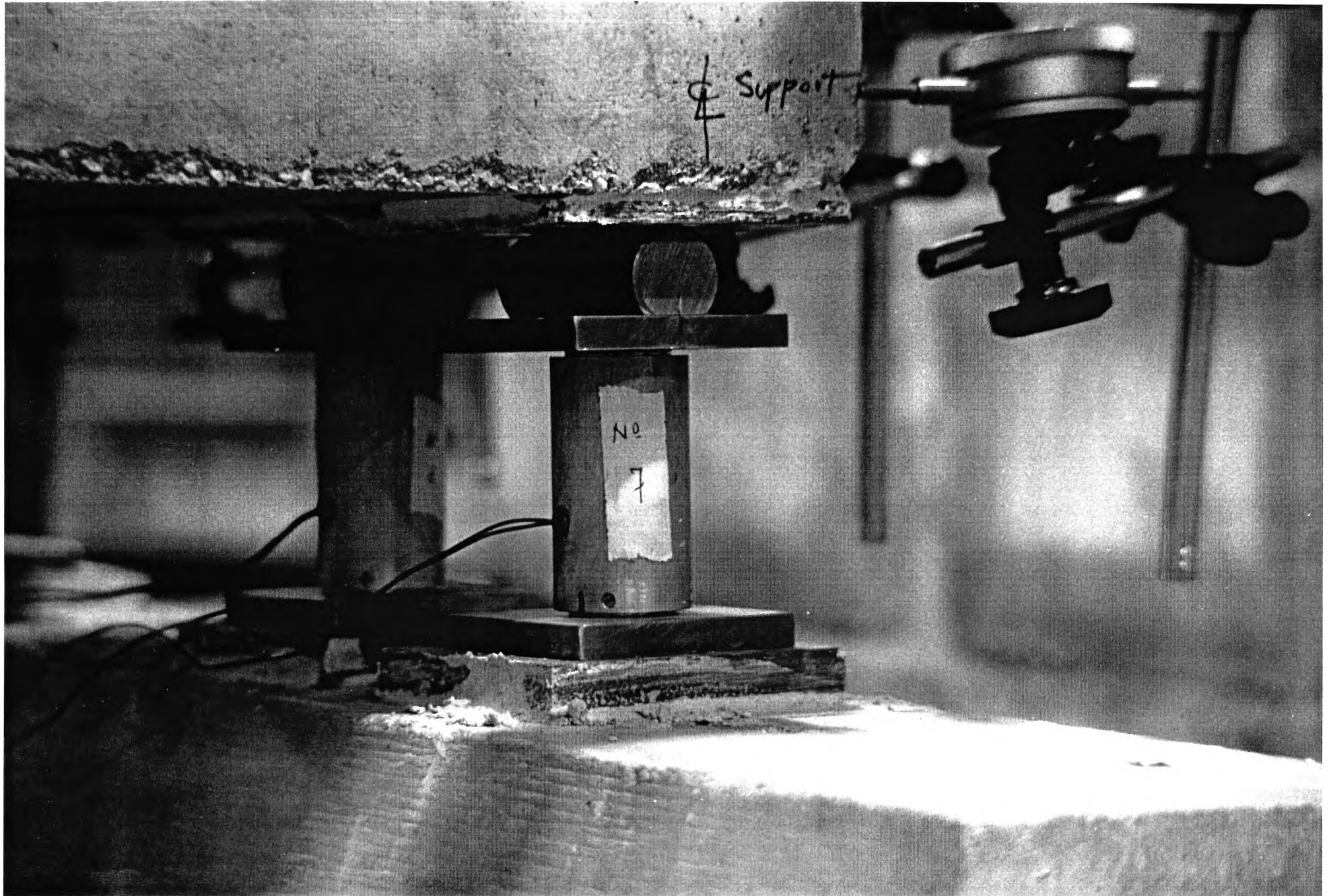


FIGURE 5.22 TYPICAL PIN SUPPORT WITH LOAD CELL

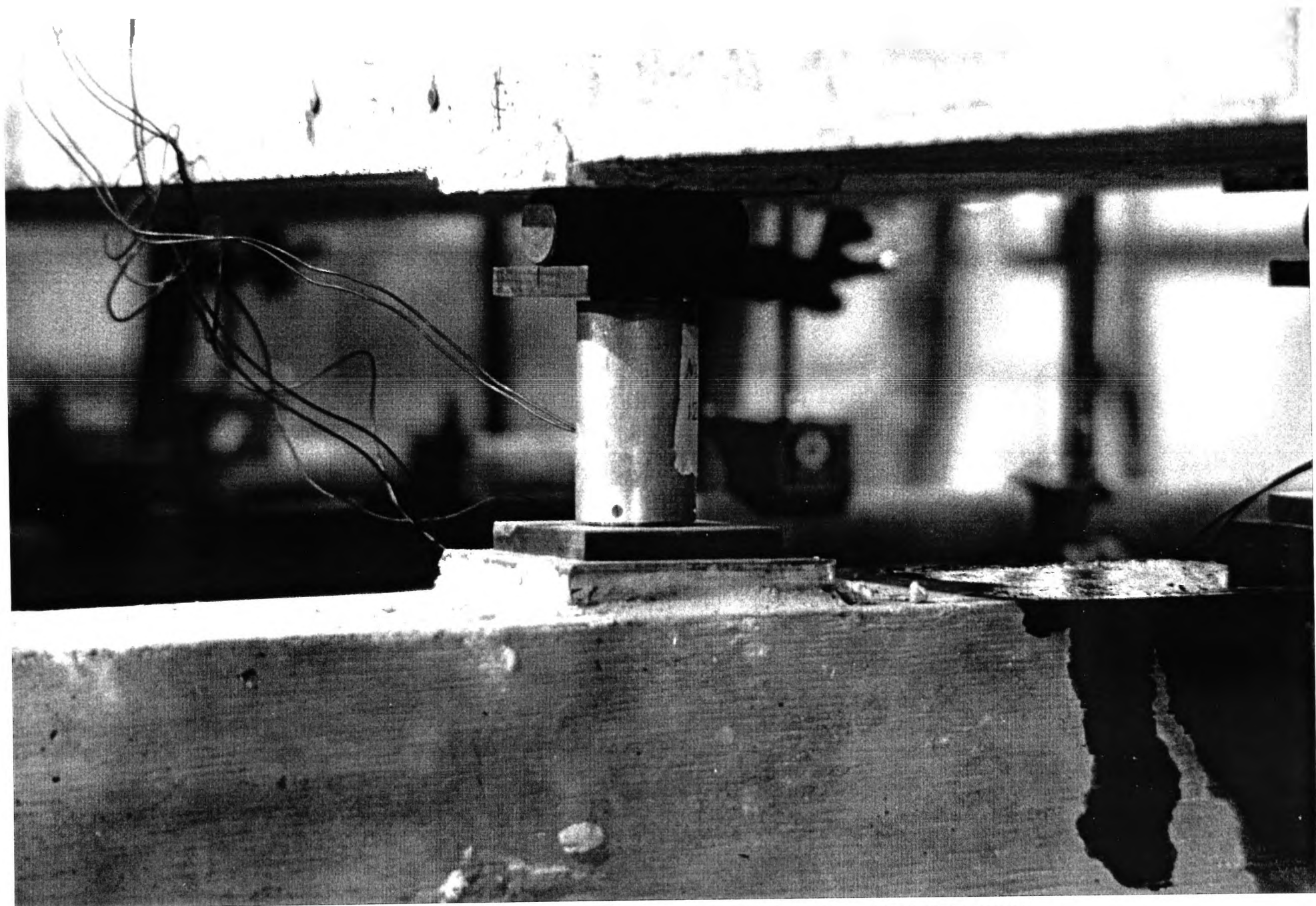


FIGURE 5.23 TYPICAL ROLLER SUPPORT WITH LOAD CELL

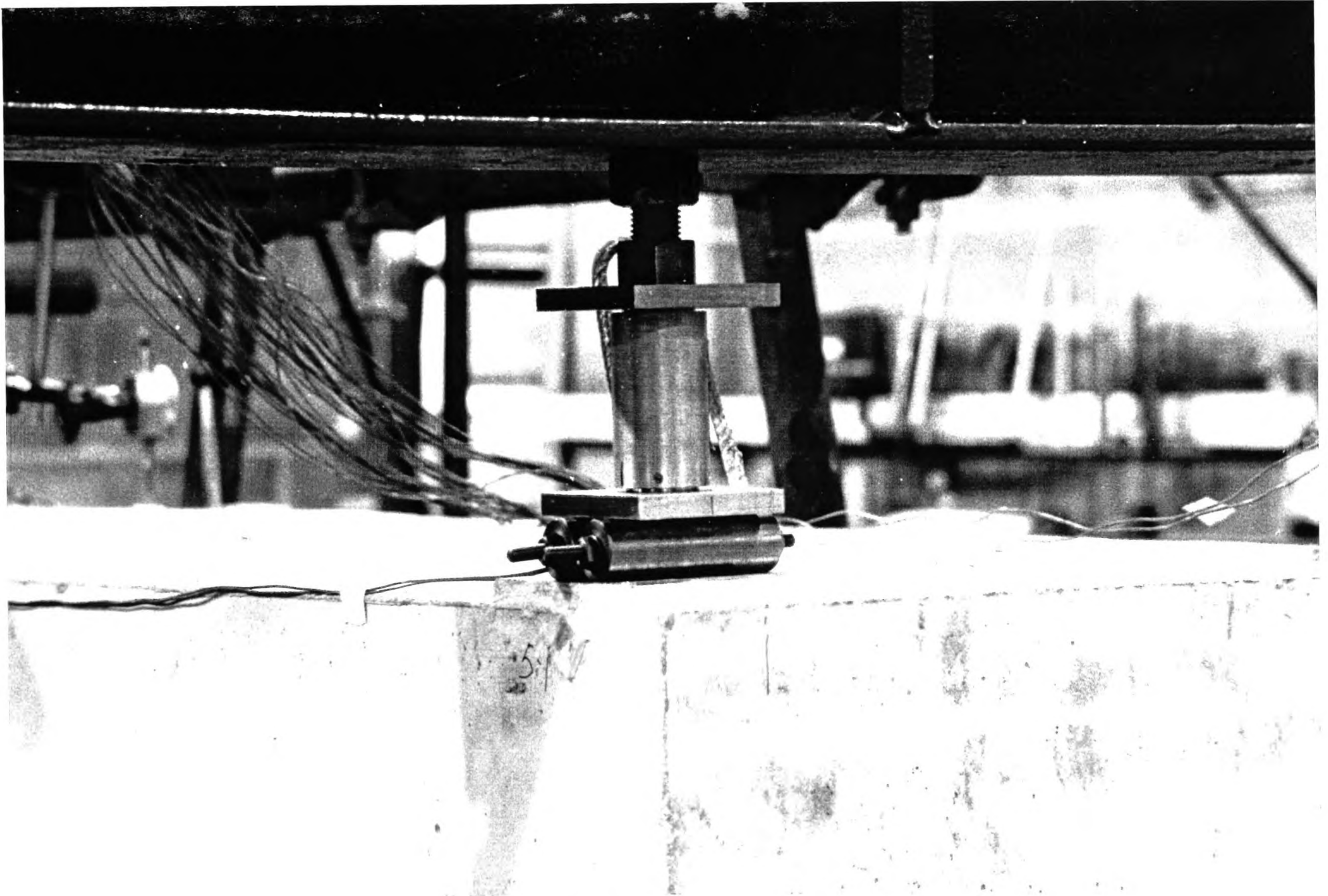


FIGURE 5.24

CANTILIVER END RESTRAINT FOR BEAM B2

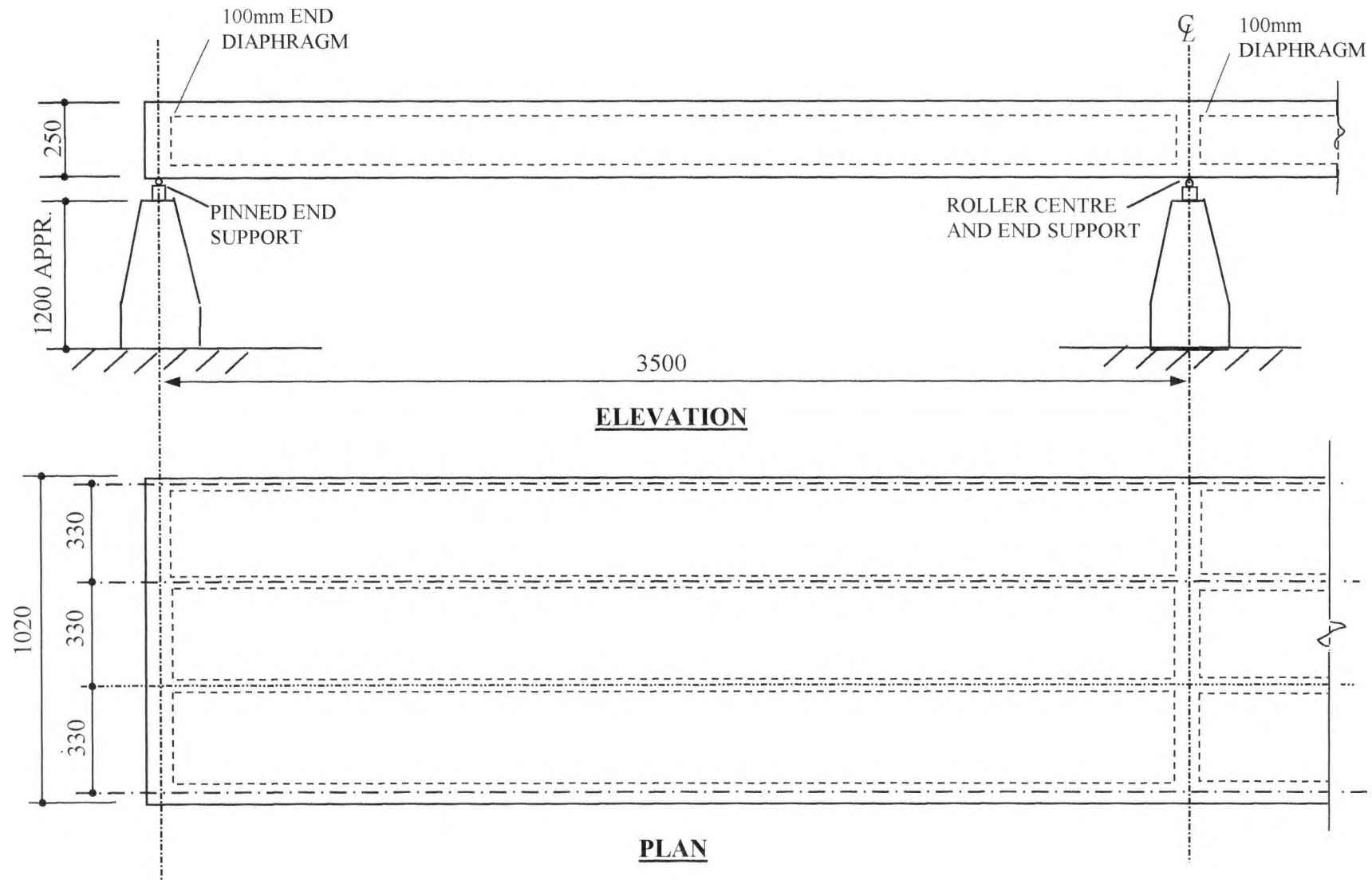


FIGURE 5.25 PLAN AND ELEVATION OF TRIPPLE CELL BOX BEAM B3

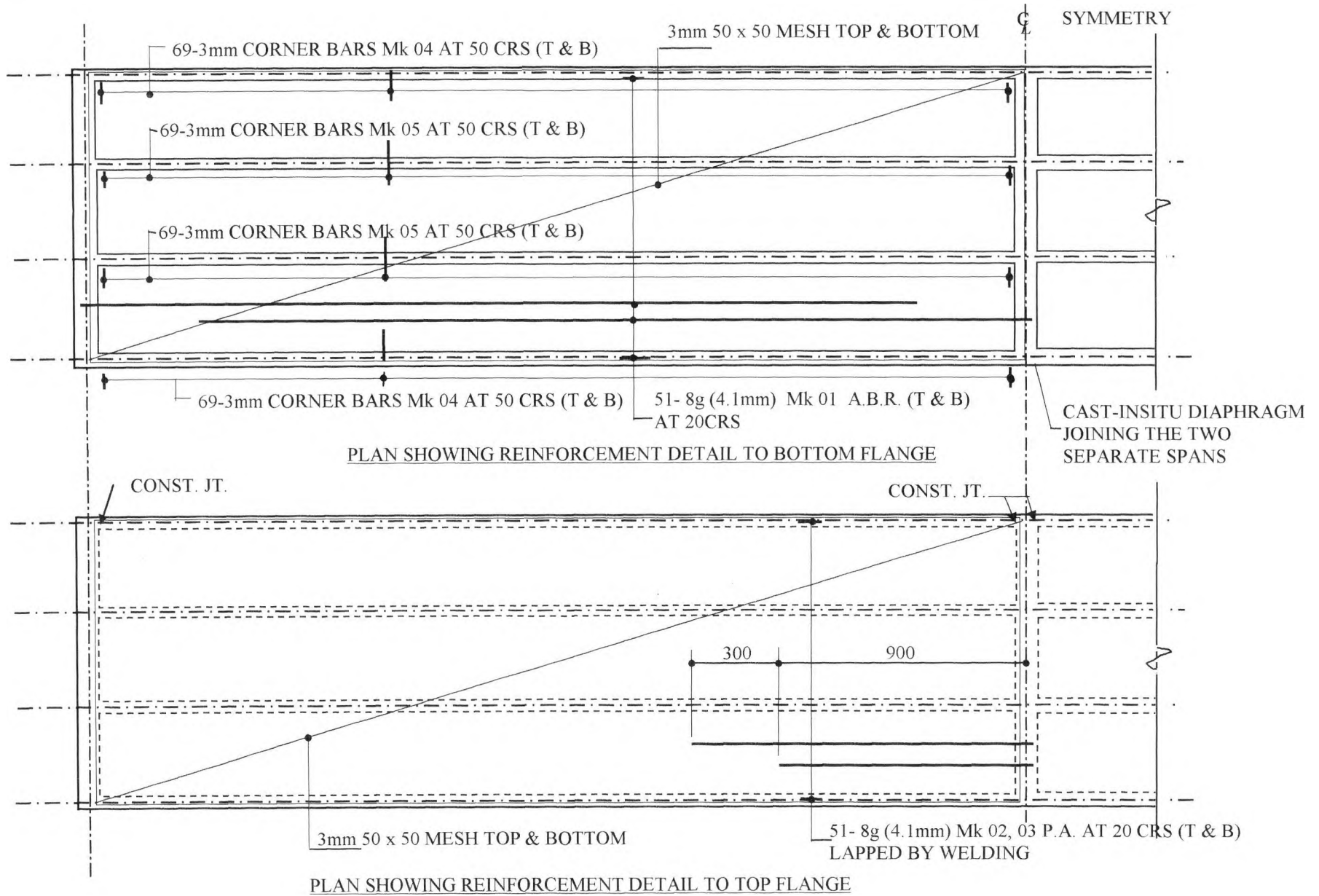
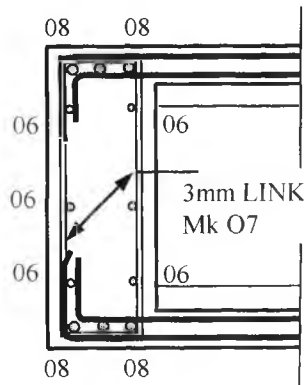
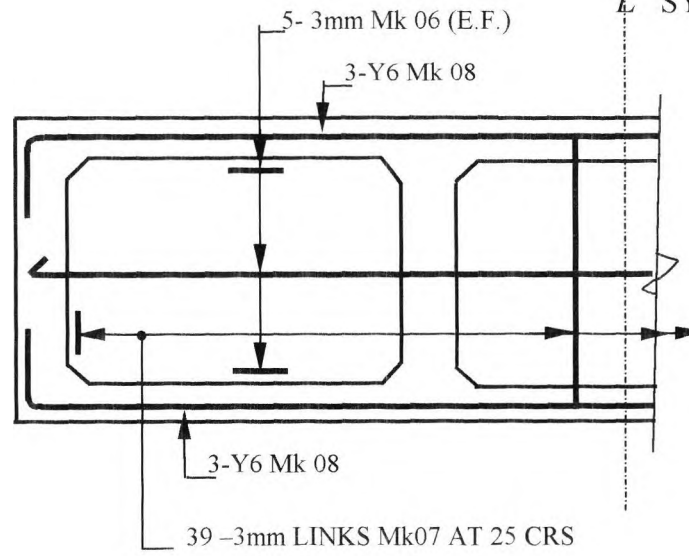


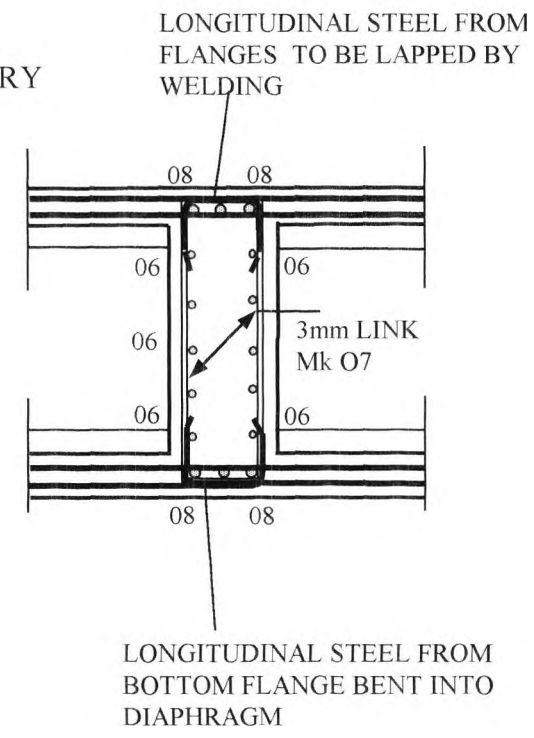
FIGURE 5.26 REINFORCEMENT DETAILS FOR TRIPPLE CELL BOX BEAM B3



END DIAPHRAGM



REINFORCEMENT DETAILS TO DIAPHRAGMS
3 No. THUS



CENTRE DAIPHRAGM

FIGURE 5.27 DIAPHRAGM REINFORCEMENT DETAILS FOR BEAM B3

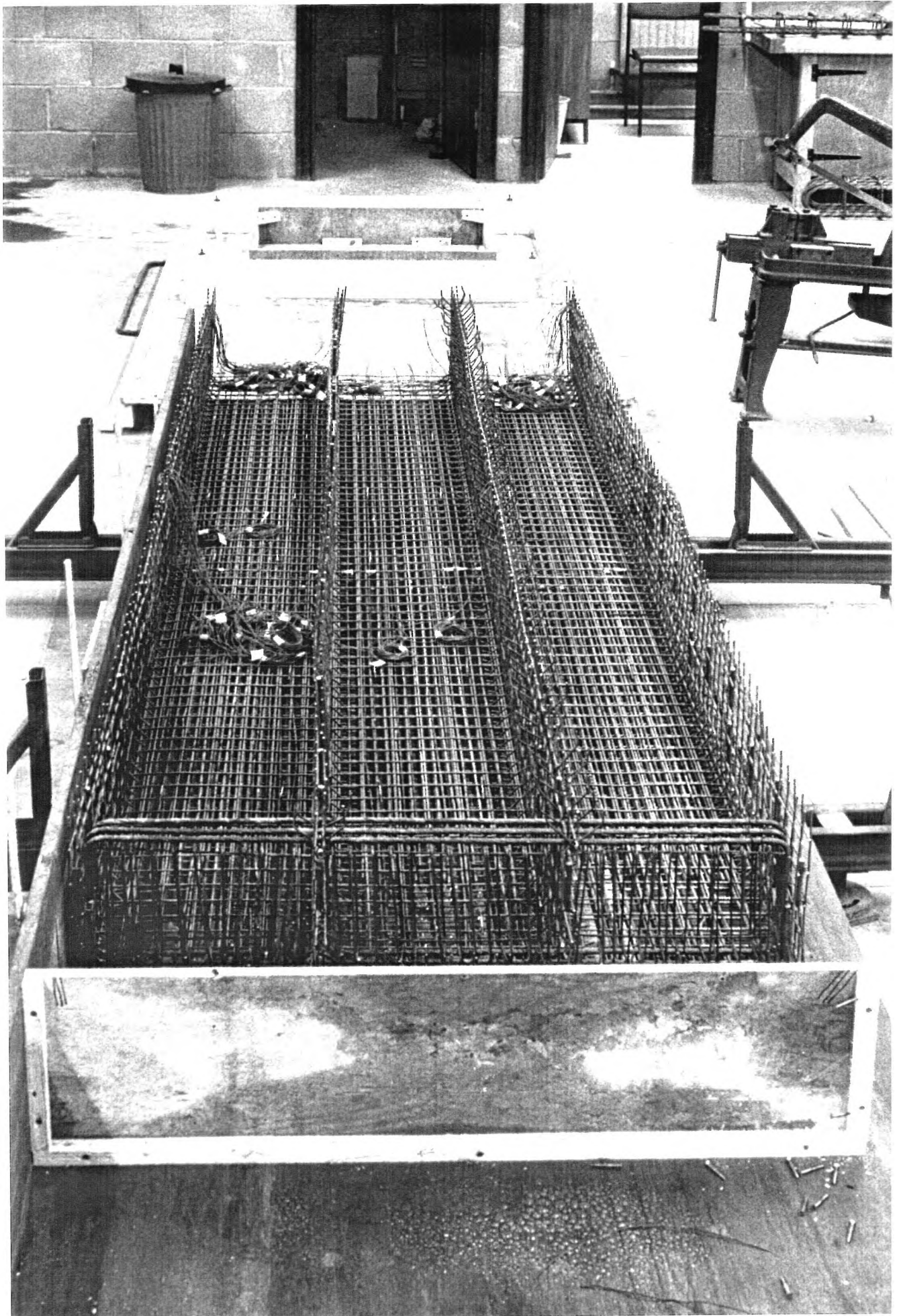


FIGURE 5.28

BOX BEAM B3 BOTTOM CAGE

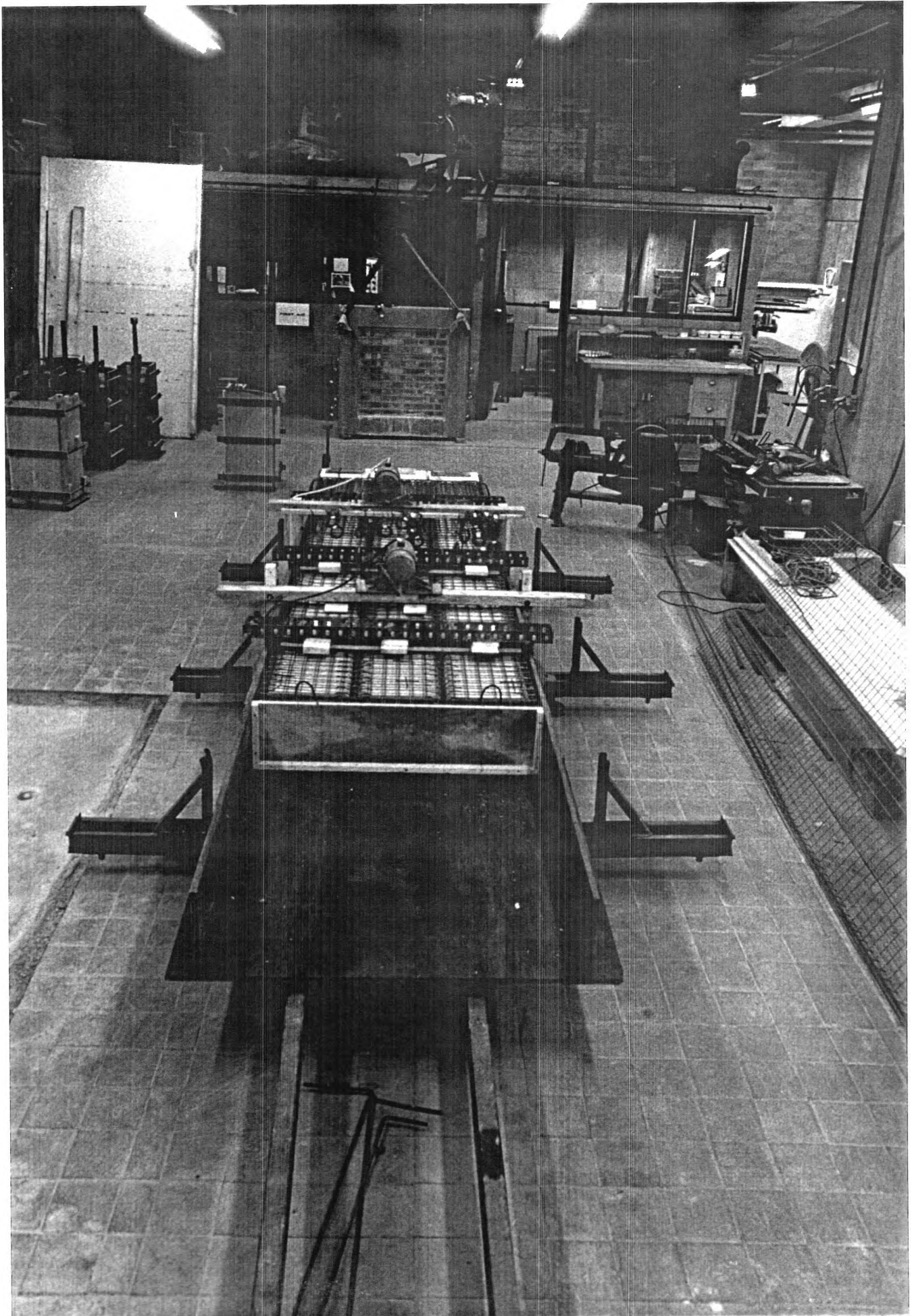


FIGURE 5.29

BOX BEAM B3 READY FOR CONCRETING

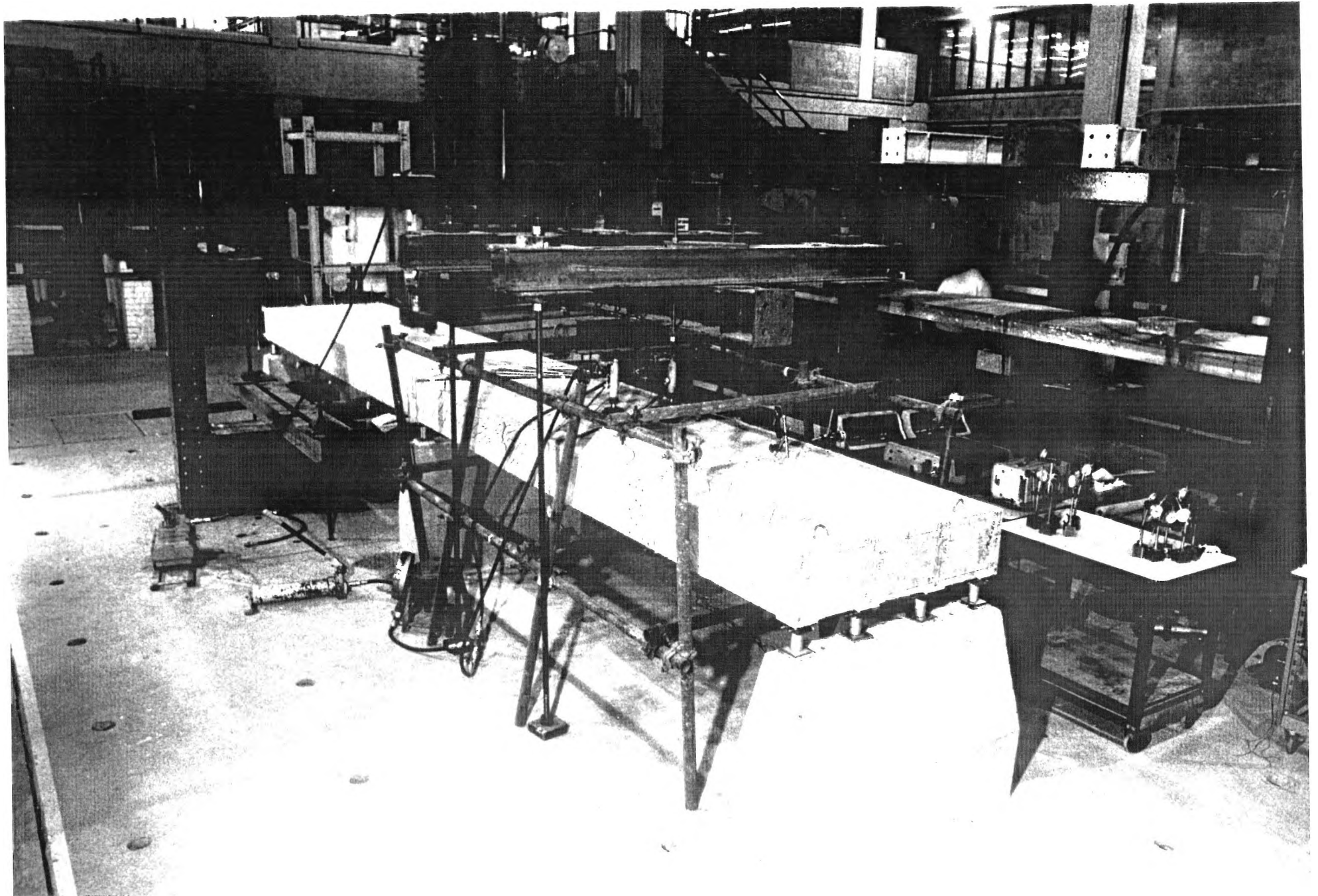


FIGURE 5.30

BOX BEAM B3 EXTERIOR FLANGE WEB TEST

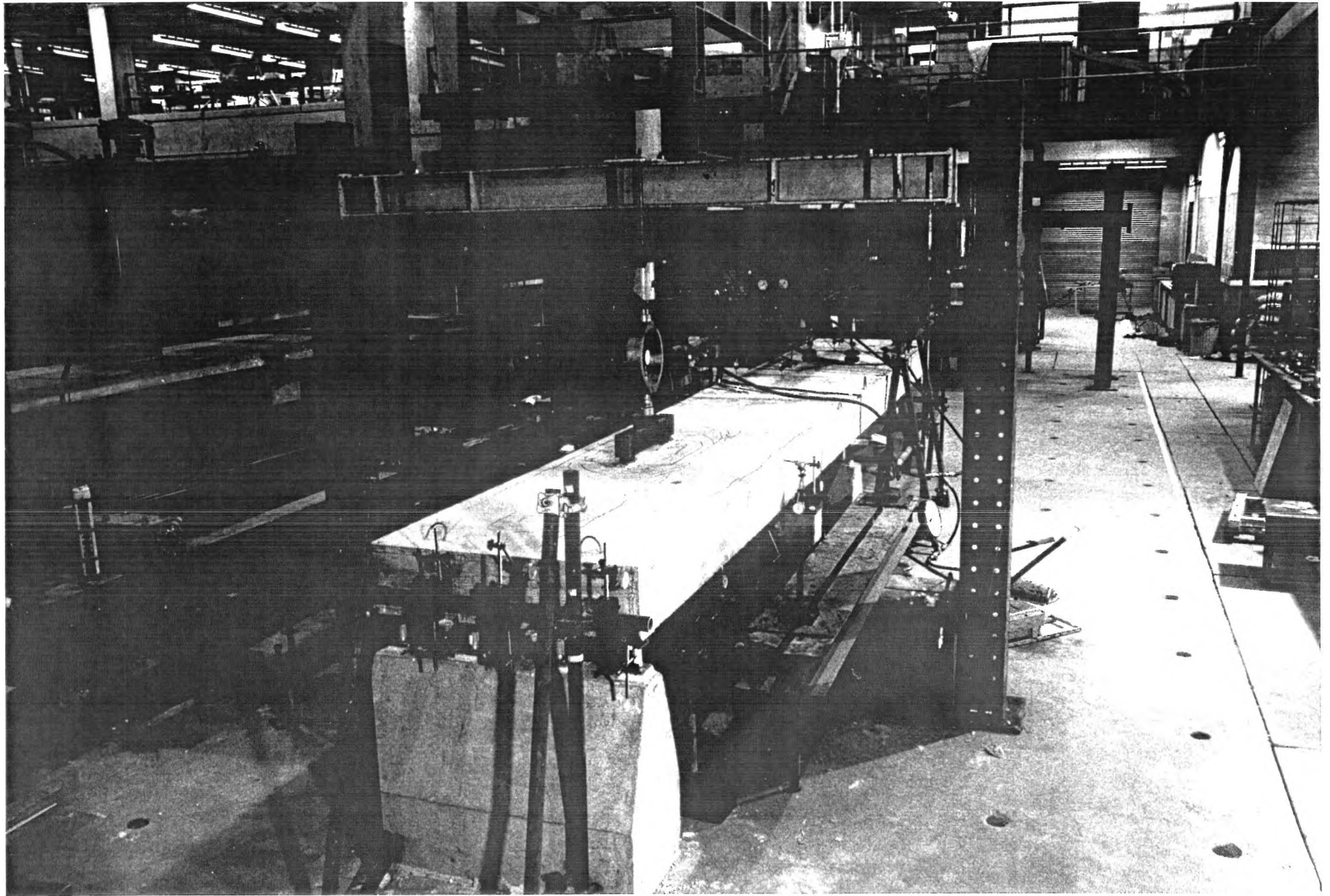


FIGURE 5.31 BOX BEAM B3 INTERIOR FLANGE WEB TEST

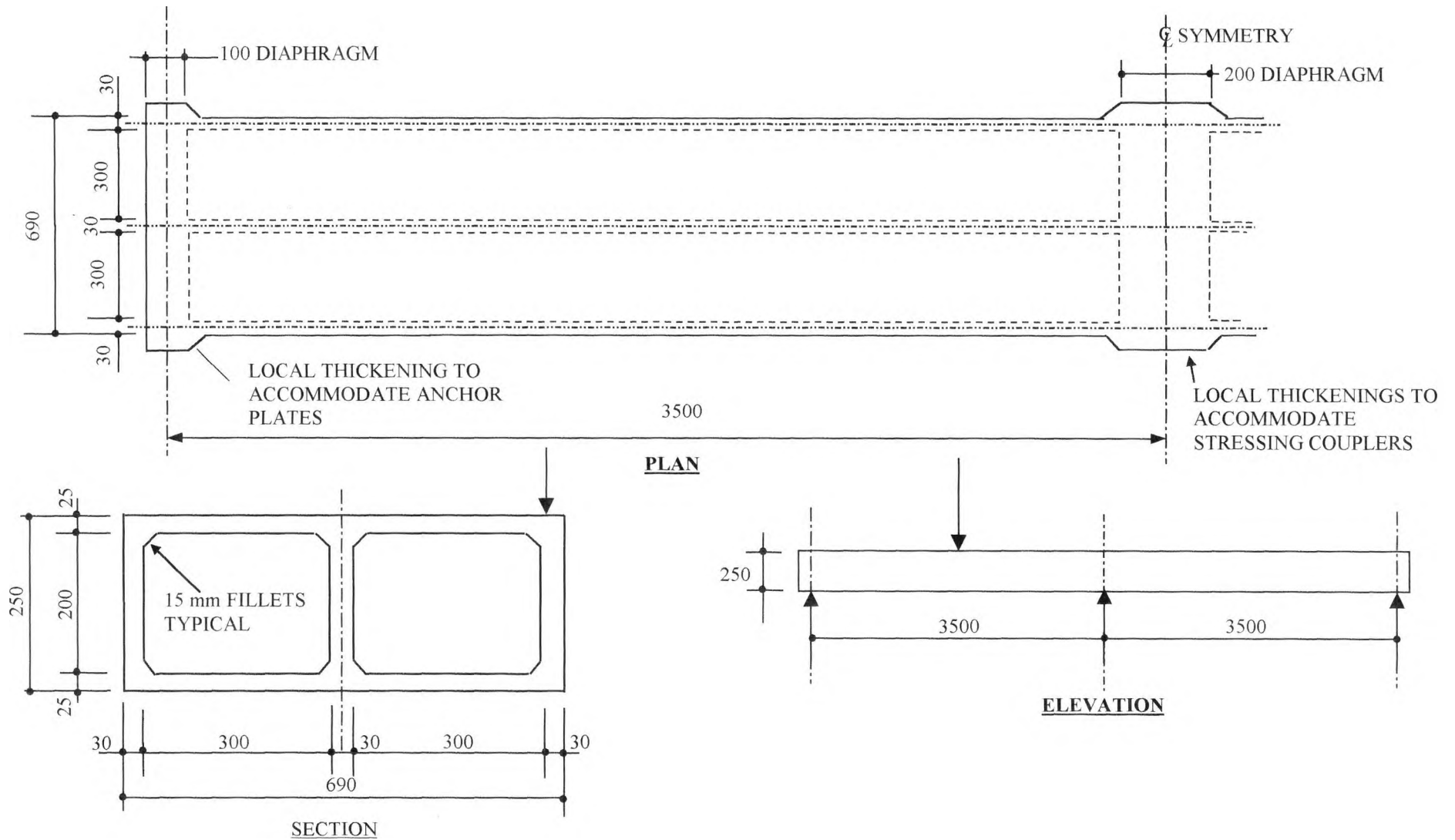


FIGURE 5.32 PRESTRESSED BOX BEAM B4 PLAN ELEVATION AND SECTION

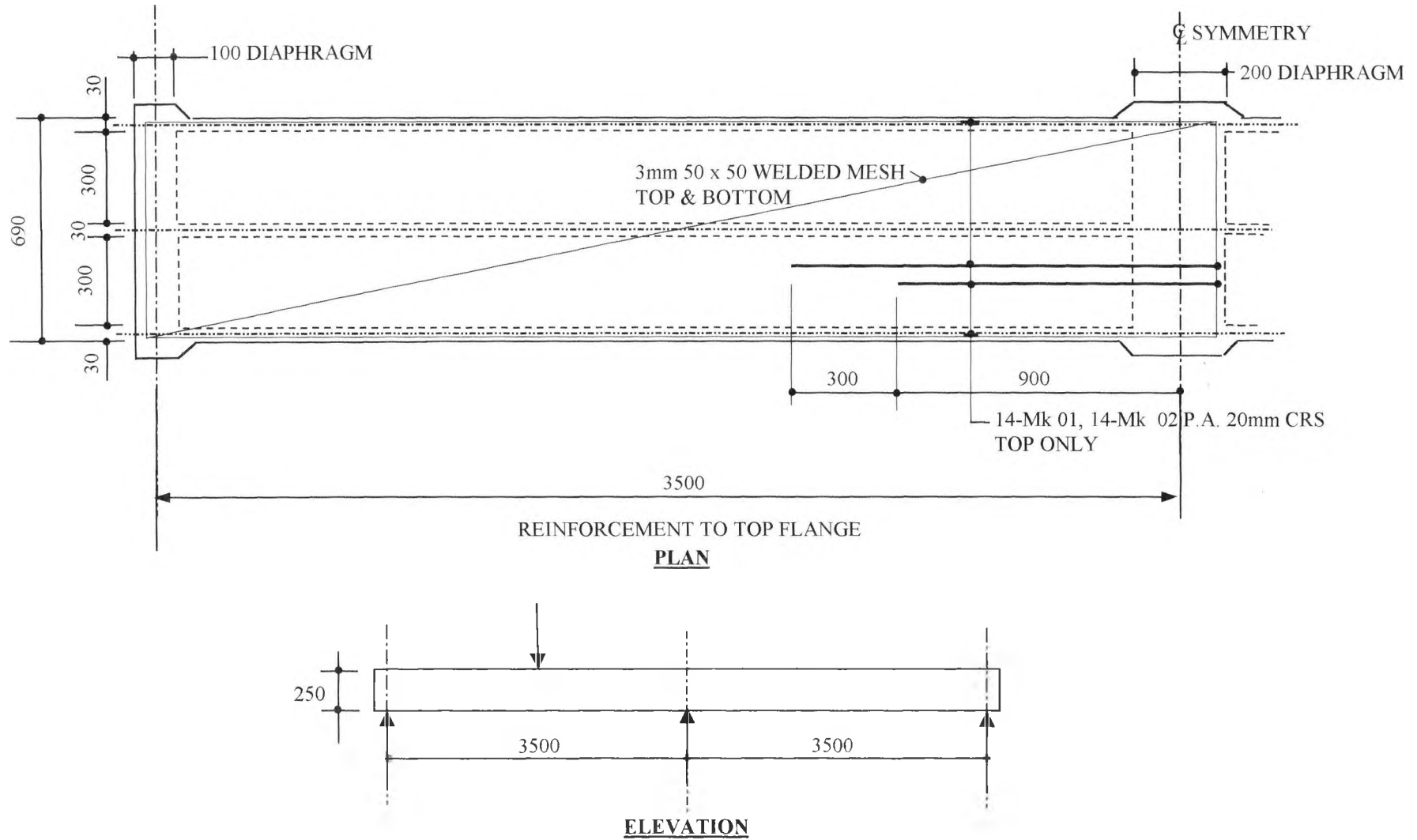


FIGURE 5.33 PRESTRESSED BOX BEAM B4 REINFORCEMENT DETAIL FOR TOP FLANGE

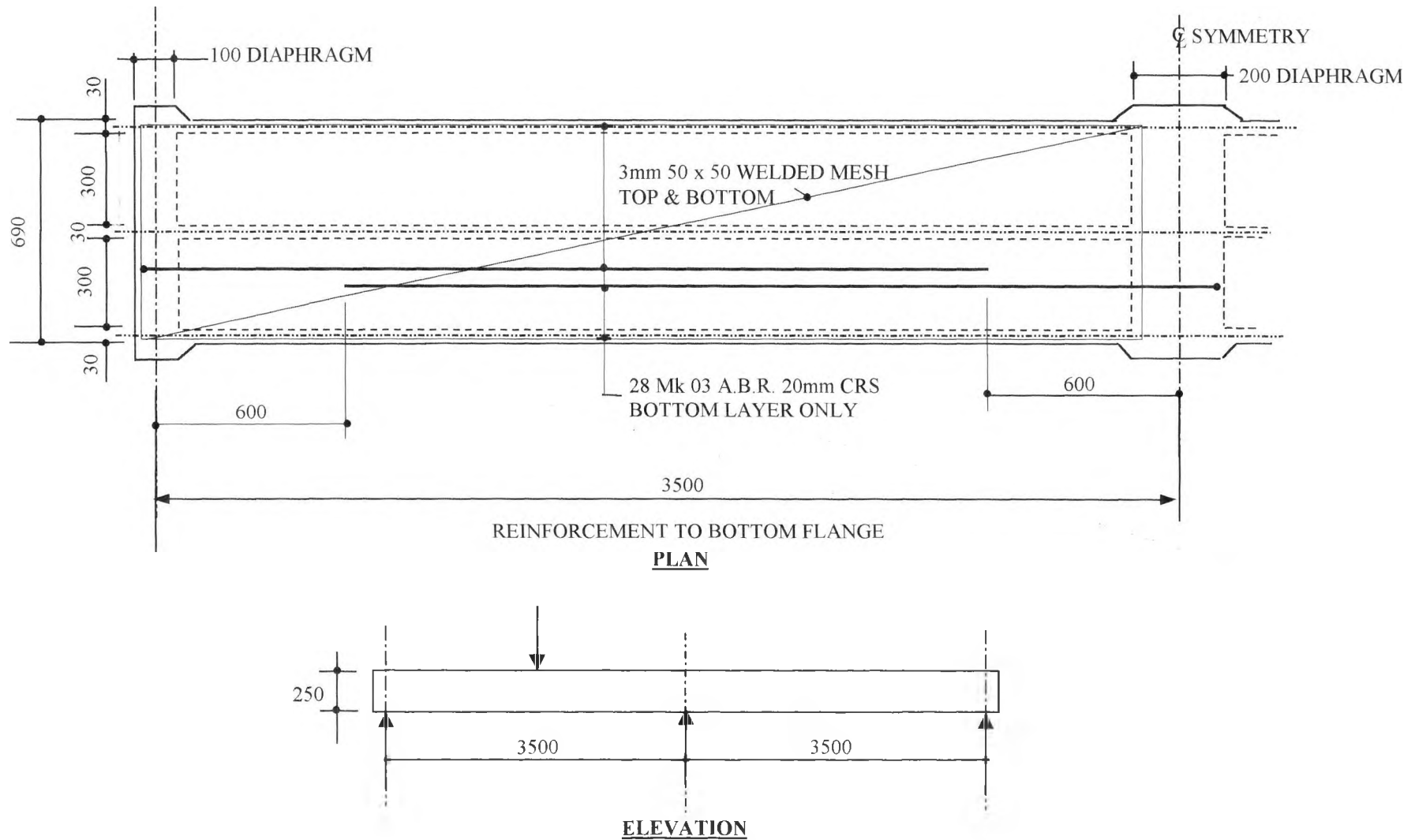
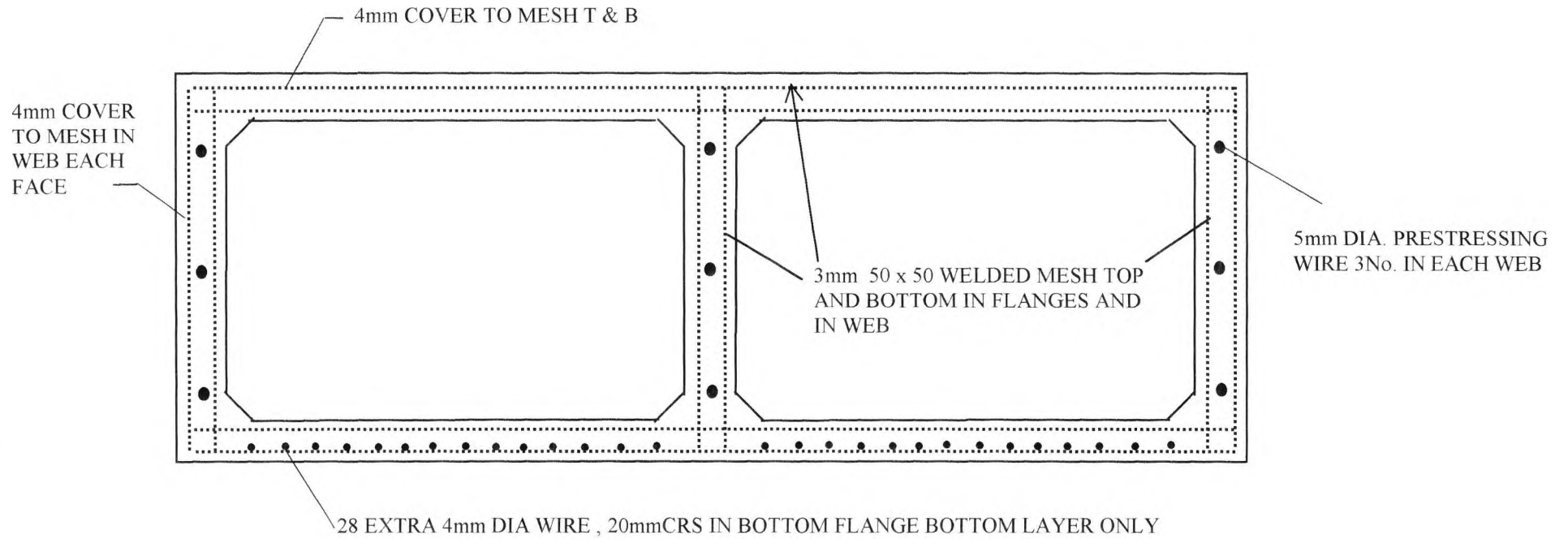


FIGURE 5.34 PRESTRESSED BOX BEAM B4 REINFORCEMENT DETAIL FOR BOTTOM FLANGE

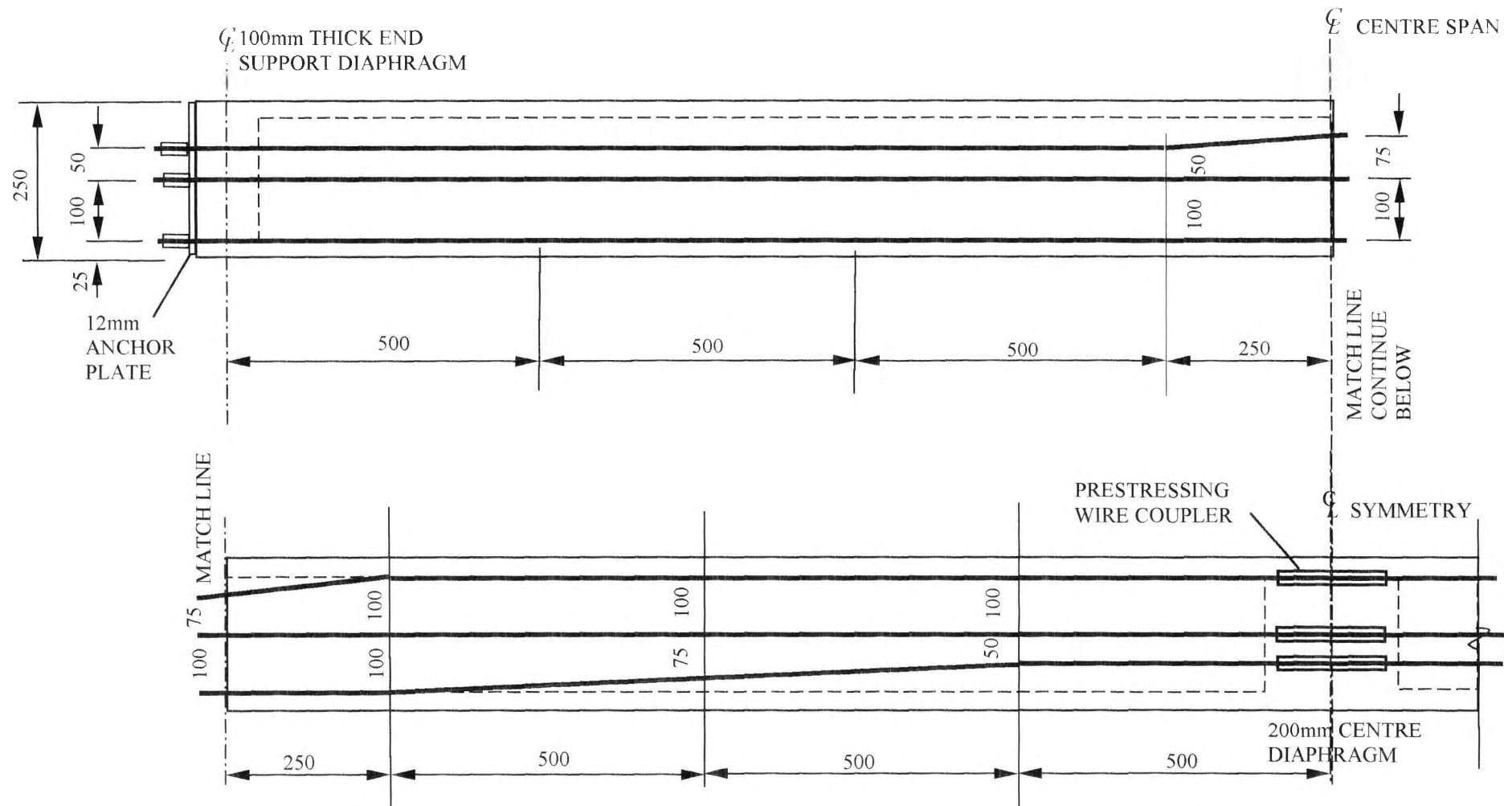


TYPICAL REINFORCEMENT FOR CROSS SECTION

3mm 50 x 50 MESH CUTTING LIST

| | No Thus | Length mm | Width mm |
|---------------------------|---------|-----------|----------|
| Top Flange Top Mesh | 4 | 3800 | 900 |
| Bottom Flange Bottom Mesh | 4 | 3800 | 900 |
| Top Flange Bottom Mesh | 4 | 3800 | 750 |
| Bottom Flange Top Mesh | 4 | 3800 | 750 |
| Web Mesh | 12 | 3800 | 300 |

FIGURE 5.35 PRESTRESSED BOX BEAM B4, REINFORCEMENT SECTION



5mm DIA PRESTRESSING WIRE PROFILE, ALL WEBS SIMILAR,
 MAXIMUM PRESTRESSING FORCE 19.9kN PER WIRE

FIGURE 5.36 BOX BEAM B4 PRESTRESSING WIRE PROFILE

Chapter 6 Experimental results

6.1 Introduction

In the following chapter, the test results were discussed. These results included collapse loads, the observed crack patterns, deflection and strain readings for the box beams. The crack patterns and deformations were related to the assumed collapse mechanisms. The experimental collapse loads were compared with the theoretical values derived from the earlier chapters. The results of similar experiments by other researchers were also compared with those obtained by the author. The discrepancy between the experimental values and expected theoretical values were discussed. Limitations of the experiments and the proposed theory particularly regarding the assumption of rigid plastic theory were examined and summarised at the end of the chapter.

6.2 Comparison of Experimental and Theoretical Results

6.2.1 Collapse Loads

The upper bound collapse loads for the box beams described in the last chapter were assessed using the theoretical expressions derived from Chapter 4. In the case of simply supported members, the theoretical collapse load was itemised under the different structural actions. The assumed collapse mechanism involved shear and or bending in the loaded web; transverse bending of the flange web junctions adjoining to the loaded web; twisting of the top and bottom flanges and the end diaphragms. The location of the transverse yield hinges depended upon the relative bending capacity of the flanges and the web. The tendency was for the yield line to form on the weaker of the two elements. In the experiments, the flange transverse strength was weaker; hence, the yield lines were expected to develop in the flanges.

For continuous box beam, additional internal work was required to cause yielding of the diaphragm over the support region. Hence, additional yield lines across the top and bottom flanges over the continuous support would be required to enable the formation of the collapse mechanism.

In upper bound analysis, it was often possible to have a different collapse mechanism that gave a lower collapse load. In such cases, the structure could fail at a lower value under an alternative unexpected mechanism. To prevent premature failure, it was sometimes possible to reinforce the structure locally to ensure that the assumed mechanism could fully develop. However, sometimes it was not possible to adequately strengthen local regions to avoid failure because of the geometric configuration and/or the limitation imposed by the relevant design code. In such cases, it would be more economical to modify the section geometry.

During testing the idealised outer cell box B2, a punching shear together with local crushing of the loaded web occurred. Because the failure was only local, the failure load was much lower than the predicted value. In order that the failure pattern follows more closely to the assumed mechanism, the loading and reaction system was modified after repairing the local damage. The final failure pattern was comparable to the assumed mechanism and the repair had little effect on the eventual failure.

Computation of both transverse and longitudinal bending capacity of the section was based on a rectangular stress block for the concrete with 0.6 times the ultimate cube strength and the yield load of the reinforcing steel. The yield forces in the steel were taken as 3.5kN for each 3mm wire in the mesh reinforcement; 6.1kN for each additional 4.1mm wire and 28.46kN for each 5mm prestressing wire. In the current concrete code BS8110 (1985), further material factor γ_m applied to both concrete and steel reinforcement to account for the possible variation in the material strength and stress profile across the section. The factors were 1.5 for concrete and 1.15 for reinforcing steel respectively. This could be represented by the concrete stress block being adjusted to 0.4 times the cube strength and 0.87 times the yield stress for the reinforcement. The collapse load was compared with the unfactored theoretical load. For the prestressed beam, the prestressing force was only taken as 0.7 of the yield strength of the stressing wires to allow for prestressing loss due to anchorage slip and creep of the concrete.

The upper bound collapse loads for the box beams were determined from the geometry of the assumed collapse mechanism. The total work done in the mechanism included contributions from the generalised yield hinges in the top and bottom flanges; bending and shearing of the loaded web; transverse yield hinges across the flange and support diaphragm region in the case of multi-cell continuous sections. Although twisting work was included in the work equation, the twisting deformation was small compared to those for bending and shear. Whilst the yield hinges in the yield zones are approaching yield and giving rise to large plastic deformation, the twisting component was still within the elastic limit. Hence the ultimate twisting work was small when compared to the work done in the generalised yield lines. An alternative was to introduce additional yield lines over the slab elements to satisfy the geometric compatibility without any twisting regions. If at the same time, an equilibrium condition could be achieved, the result would tend towards a lower upper bound solution depending on how accurate the equilibrium status had been satisfied.

Three theoretical collapse loads were computed, a deformable section without shear; a deformable section with shear; a deformable section with modification to the shear capacity based on the factor derived from chapter 2, the computation was included in Appendix B and summarised in Table 6.1.

| Member | Theoretical Collapse Loads (kN) | | | Experimental Collapse Load (kN) |
|--------|---------------------------------|----------------------|--|---------------------------------|
| | No Shear/ Distortion | Shear/ Distortion | shear/ distortion with shear modification | |
| B1 | 124.04 | 169.8 | 137.4 | 113.00 |
| B2 | 129.9 | 149.7 | 113.9 | 123.50 |
| B3 a | 160.1 | 199.0 | 163.2 | 155.00 |
| b | 130.4 | 168.7 | 132.9 | 115.00 |
| B4 | 96.10 | 121.6 | 85.2 | 87.50 |

B1 Simply supported twin cell box beam, Idealised internal flange web beam section

B2 Continuous multi-cell box beam, Idealised external flange and web beam section

B3 Two span Continuous three cell box beam

 a. Test on Internal flanged web section

 b. Test on external flange web section

B4 Prestressed two span double cell box beams.

 Test on external flange web section

TABLE 6.1 EXPERIMENTAL AND THEORETICAL COLLAPSE LOAD

For computation of collapse loads see Appendix B

6.3 Experimental Observations

6.3.1 Box Beam B1

Loading of the composite beam was by a single point load applied at the centre of the central web, which was induced by jacking against the proving ring. An initial load of 20kN was applied and then unloaded. The procedure was then repeated with load increments of 20kN up to 80kN. At each stage of unloading, there appeared to be a permanent set. This could be the result of some plastic deformation of the member. In addition, the supports could adjust themselves to take up any initial bedding slack. At each load stage, the automatic data logger recorded the steel strain and concrete strain at various locations. Surface strains at various locations were also measured. At the same time, any crack development was noted. After unloading from 80kN, the box beam was reloaded and subjected to gradual increases until failure. At the final stage, when the applied loading reached a maximum, the deflection of the centre section increased rapidly. The other sections remained stable. This indicated local yielding of the member. The strain values in both steel and concrete at the yield section increased rapidly. The load deflection characteristics of the box beam can be represented by the curves shown on Figure 6.1. The deflection profile of the longitudinal and transverse sections of both outer webs and the centre web were plotted. The results for the loads plotted against deflection are summarised in Figures 6.2 to 6.5. It can be seen that the box beam was behaving elastically prior to the formation of the collapse mechanism. Once the ultimate load of the section is reached, and the mechanism formed, deformation for the loaded centre web increased rapidly whilst the other webs deflect very little subsequently. The rate of deformation from this point onward can be considered. Deformation may be considered to be concentrated on the yield lines and plastic hinges with the other non-yielding parts as rigid regions.

The strain values both on the reinforcement and the concrete surfaces were measured. Figure 6.6 shows the distribution of the strain values in the bottom longitudinal reinforcement in the bottom flange. It can be seen that the strain value is highest immediately under the loaded web and reduces gradually towards the outside non-loaded webs. It is inevitable that the reinforcement under the load web approached yielding first and

progressively reduced towards the outside web.

Similarly, figure 6.7 showed the strain distribution of the longitudinal reinforcement for the top layer reinforcement of the bottom flange. Again the strain under the loaded web was the highest with gradual reduction towards the outer webs.

Figure 6.8 showed the strain distribution of the transverse reinforcement in the bottom flange. As expected, the reinforcement immediately under the loaded web yielded first, followed by the yielding of the reinforcement at the outer flange web junction forming the transverse mechanism. The transverse bending of the bottom flange resulted in a yield line forming under the loaded web.

The transverse deformation caused compression of the top surface of the bottom flange. This was demonstrated by the strain distribution of the transverse reinforcement in the top layer of the bottom flange, Figure 6.9.

Figures 6.10 and 6.11 showed the compressive strain distribution of the longitudinal reinforcement for the top flange. As expected, the compressive strain value for the top layer steel had sustained a higher value than the bottom layer.

The transverse strain distribution for the top and bottom layers of reinforcement for the top flange were shown in Figures 6.12 and 6.13. The distribution was similar to that recorded in the bottom flange, Figures 6.8 and 6.9. Thus the strain values in the material verified that the required transverse yield mechanism had developed.

Figure 6.14 showed the longitudinal strain distribution for the web reinforcement in the loaded web. It was interesting to note that the web reinforcement near the bottom had reached yielding whilst the strain values in the top and centre reinforcement remained more or less constant.

Figure 6.15 provided a summary of the longitudinal strain values for the different elements of the box beam at

the centre section under the load of 110kN. This was compared with the longitudinal strain measurement by Demec gauges on the outer surface of the top and bottom flanges shown in figure 6.16.

Figure 6.17 summarised the transverse strain values of the reinforcement in both the top and bottom flanges near the centre section at a loading of 80kN. This indicated that transverse yielding of the flanges was starting. Figure 6.18 showed the transverse strain on the concrete surface at the same section under the same loading. There were close correlation between the steel strain and the concrete surface strain values.

At yield, the crack widths at the yield hinges increased after the applied load reached a peak value. At this stage, the maximum load could not be sustained. Since the load was applied via a proving ring, the relaxation of the structure under the yield mechanism could result in a reduction of the applied loading from the reaction frame. In order that further observations could be made, the box beam was subsequently governed by deflection control. Under such condition, maximum load was maintained as much as possible on the structure whilst the deformation was recorded.

First appearance of cracks was noticed when the load reached about 30kN. The propagation and distribution of the shear cracks in the loaded web and the top and bottom flanges were observed. Figure 6.19 showed the cracks on the top flange. The main longitudinal cracks were along the flange web junction adjoining the external webs. Although some cracks extended to near the two end diaphragms, the majority of the cracks were concentrated in about 50% of the top flange section.

The bottom flange cracking was shown in Figure 6.20. It could be observed that cracking had developed near the centre of the section. The yield pattern extended outward towards the end diaphragms and also the outside web forming the classical yield line pattern for a rectangular slab. It could also be seen that the underside of the top flange showed similar crack patterns as that shown on the bottom flange. The Demec gauge points for the bottom flange could also be seen in the figure.

Although the assumption for the yield lines was that they were concentrated in the failure zones forming the collapse mechanism, the actual crack patterns were more uniform radiating from the point of initial yielding.

The crack patterns on the loaded web also originated from the centre of the section where the bending moment was highest. The cracks were vertical or near vertical and were typical flexural cracks. The cracks near the support developed at a higher load value of 60kN. At still higher load values, the bending cracks at the centre spread out towards the support, whilst the shear crack at the support spread towards the centre. The strain values measured indicated that the web section deformed linearly with the applied loading. At the maximum yield load of 110kN, the strain value at the quarter point remained static whilst the strain in the centre section increased rapidly forming a yield hinge in the centre of the section allowing large deformation to occur. At this stage, the region with shear cracks near the support increased extending towards the centre and began to merge with the centre yield hinges.

At this stage, limiting the deformation of the mechanism controlled the experiment. The test was continued until the deformation limit of the measuring gauges was exceeded. It was interesting to note that deformation was only confined to the yield zone and mechanism. The other part of the structure remained static. Therefore, if deformation rate rather than deformation were considered, the assumption of the material having a rigid plastic behaviour was valid.

6.3.2 Box beam B2

This box beam simulated a typical edge cell of a multi-cell continuous box beam. It was expected that failure would only be confined to the local span and local cell of the multi-cell box beam. The other cells beyond the first cell were idealised by a solid reinforced concrete beam. Applying external reactions and restraint simulated the continuous support boundary condition.

Initially, a single point load was applied via the proving ring to the centre of the outer web. The bearing plate under the proving ring was a 75x75mm square plate bedded on the top surface. It was expected that the section would be subjected to torsional effects from the eccentric loading. The load was applied gradually. The observed deformation and strain measurement indicated that the box beam behaved in almost linear elastically after initial bedding down of the supports and at the load point.

The web and top flange under the point load began to fail by web crushing and punching shear of the top flange when the applied load reached 94kN, Figure 6.23. This was considerably less than the predicted collapse load. This load appeared to be a premature collapse load of a non-predicted collapse mechanism. It was then decided to halt the experiment temporarily.

In order that the assumed collapse mechanism could be further developed, attempts were made to repair the local crushed area of the web and flange. The applied loading was also modified to reduce the effect of the high concentrated load on the beam flange. This was to ensure that failure by punching shear and web crushing would not occur.

A new spreader beam was introduced under the proving ring. The spreader beam was 600mm long x 100mmx75mm, solid steel. Two additional bearing plates under each end of the spreader beam enabled the applied load to be halved figure 6.24. The spreader beam also allowed the load to be applied outside the original crushed zone.

The test was resumed with the new loading arrangement

after the crushed section were repaired and gained adequate strength, figure 6.25.

The deflections of the entire section at quarter and centre spans of the beam were monitored. The load against deflection characteristic of the different sections was plotted. The result of the load deflection plot for the centre section is shown in Figure 6.21.

These graphs appear to confirm the assumption that failure was only confined to the outer web and the top and bottom flanges close to the overall zone of failure. It could also be observed that the flanges and the web having reached yield then deformed at a rapid rate. The force resultants within other non-yielding regions remained almost static, figure 6.21. The maximum recorded failure load was 123.5kN compared to the lowest theoretical value of 110.6kN.

The longitudinal deflection profile of the loaded web and the solid section was plotted. It could be seen that once the failure load was reached, a rapid increase in the deflection under the load occurred. The transverse and longitudinal deflected profiles were shown in Figure 6.22.

The strain measurement of the reinforcing steel indicated yielding of the reinforcement in the yield zones. Yielding was noted in the following locations near the centre section:

- (a) transverse top reinforcement crossing the junction of the top and bottom flanges and the inner web,
- (b) transverse bottom reinforcement crossing the junction of the top and bottom flanges and the loaded web and
- (c) the longitudinal reinforcement in the lower section of the loaded web.

Elsewhere, the reinforcement behaved elastically until the centre sections started to yield. The strain in the non-yielding sections remained the same, whilst the yielding section continued to deform at a much greater

rate. The surface strain measured by using the Demec gauges may be correlated with the strain values obtained by the electrical resistance strain gauges.

The crack and marked pattern on the flanges and web were recorded during the load test. They were then highlighted after the completion of the experiment.

Figure 6.26 showed the crack pattern on the front of the loaded web. It was noticeable that the diagonal shear cracks on the loaded web were relatively uniform on both sides of the centre section. Further crushing of concrete at the repaired section coupled with yielding of the reinforcement at the centre showed the typical characteristics of the formation of a hinge. There were also longitudinal cracks near the bottom and mid height of the web. These could have been the result of local buckling failure of the web element.

Figure 6.27 showed the failure crack patterns on the top flange. The main longitudinal crack lines ran along the flange web junctions both at the side and at the interior web. The central patched section was the area of repair after the earlier punching failure. The diagonal shear crack patterns were the result of the twisting of the two halves of the flange. Twisting was required to maintain deformation compatibility of the section at failure. The cracks were confined in the loaded cell only and did not extend to adjacent areas.

Figure 6.28 represented the cracks and failure patterns developed in the bottom flange of the box beam. The diagonal cracks due to twisting appeared to radiate from the point of load application. These cracks merged with the longitudinal crack formed between the bottom flange and loaded web junction. There were some similarity between the crack patterns for this box beam and the one shown in Figure 6.20 where two adjoining cells were loaded.

6.3.3 Box Beam B3

Two tests were carried out on this beam. The first test was for a concentrated load applied to the centre of an interior web. The load deflection behaviour for the four webs near the centre span was plotted in Figure 6.29. It could be seen that the box beam section behaved almost linearly elastically up to 100kN. Deflection values appeared to be higher directly under the applied load. This indicated that the transverse section of the box beam showed signs of distortion. Above 100kN, cracks became more prevalent and deformation increased more rapidly under the applied load. Yielding of the section was evident when the applied load reached 155kN when the deflection of the loaded web increased rapidly, whilst the other webs increased at a much lower rate.

The crack patterns were marked on all the visible surfaces. Figure 6.30 showed the crack pattern on the external web, which indicated that this web had also been subjected to considerable amount of indirect loading transferred by the transverse bending stiffness of the top and bottom flanges.

Figures 6.31 and 6.32 showed the crack pattern observed on the top flange. There was distinct similarity between this crack pattern and that of the box beam B1, which was also subjected to similar load configuration. Longitudinal cracks along the remote flange web junction were also visible at the later part of the loading test. This indicated that the large distortion of the cross section had caused yielding of section away from the loaded section. Transverse cracks over the centre support for the continuous beam were also observed. These cracks over the support correspond to the continuous moment over the centre support.

Figure 6.33 showed the crack pattern in the bottom flange. The flange web junction under the loaded web could be seen to have yielded and as a result, severe cracks along the two edges of the loaded web were evident. Some evidence of twisting of the flanges on both sides of the loaded web could be observed. This was similar to the crack pattern for beam B1.

The second load test was to apply the single point load on an exterior web of the adjoining undamaged span after the completion of the first test. The load deflection curves for the loaded web together with the other three webs were plotted in Figure 6.34. The maximum yield load achieved was 115kN in the experiment compared to 123.5kN for beam B2 and 110.6kN in theory. From the load deflection curve in Figure 6.34, it was found that the loaded web deflected more readily than the remaining unloaded webs. Also, the loaded web deflected rapidly once the yield load was reached. It could be observed that the whole section also subject to torsional deformation, which was due to the eccentric arrangement of the loading. Crack patterns were recorded after the completion of the tests.

Figures 6.35 and 6.36 showed the crack pattern in the loaded web. The main feature of the crack pattern was the development of shear cracks on the loaded web. It was interesting to note that the higher shear near the central support compared to the exterior support had resulted in more severe cracking near the centre support. The other crack patterns were similar to those for beam B2.

Figure 6.37 showed the familiar fan shape crack pattern of the top flange and yielding had occurred along the flange web junction. There was also evidence of twisting of the top flange similar to that of beam B2.

Figure 6.38 showed the crack pattern for the bottom surface of the beam. It could be seen that the crack pattern was mainly restricted to the outer most cells under the concentrated load. This crack pattern was quite similar to the corresponding pattern for beam B2 in Figure 6.28.

6.3.4 Box Beam B4

Initially, the prestressed box beam was loaded with symmetrical point loading at the centre of one span in order to bed down the supports. Load cells were placed underneath the diaphragms as well as on top of the adjoining supports to provide holding down action. The threaded bolts above the top load cells were tightened to introduce a small pre-loading so as to eliminate the initial slack of the top supports. Hence any top reactions could be recorded. The central deflection and support reactions were monitored. The loads were taken up to 30kN before unloading and the response of the box was almost linear elastic within this load range.

The central point load was then shifted to the centre of the outer web. Transducers were used to monitor the load and deflection profiles. The beam was then subjected to gradually increasing loading and unloading cycles until failure at 87.5kN. Failure in this case was a local web crushing and web buckling. The failure mode started when the loads reached about 80kN. Once web crushing and buckling started, only a small increase of load to the ultimate load was possible. This was sufficient evidence that the box beam had reached its ultimate load capacity.

The ultimate load test results that were reported in section 6.2.2 were for a load applied at the centre of an external web. The load deflection curve plotted in Figure 6.39 was very flat, which indicates that the elastic stiffness of the beam was lower than the other non-prestressed beams. A typical longitudinal and transverse deflection profile was shown in Figure 6.40.

In designing the prestressed box beam, the amount of prestressing was proportioned such that it replaced some of the main reinforcement. The theoretical load carrying capacity, therefore, was similar to the other box beams. During the construction of the prestressed box beam, there had been problems with adequate compaction of the micro-concrete using the external vibrators. As a result, the yield load obtained was considerably lower.

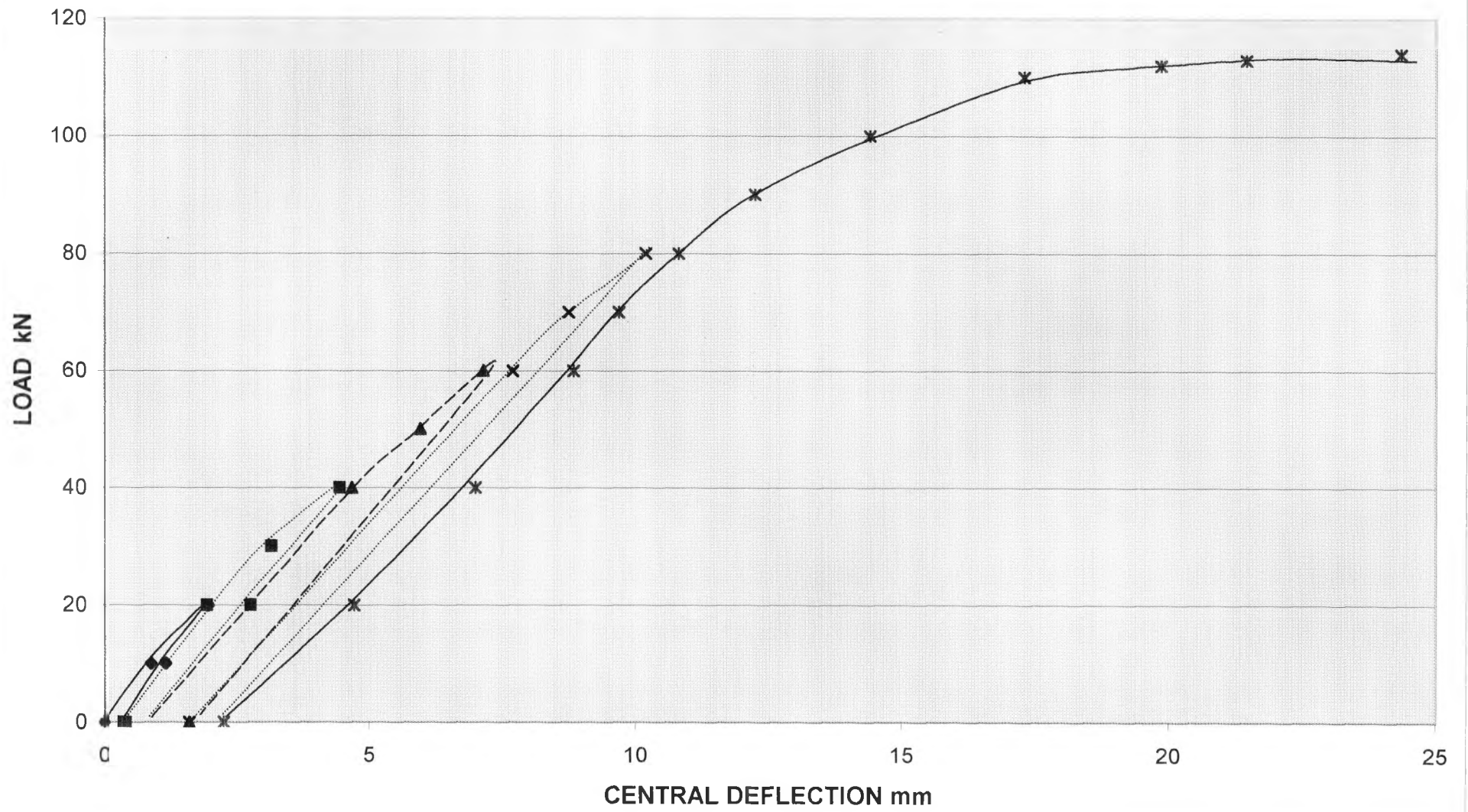
6.4 Summary

This chapter described the experimental results for the four box beams. The collapse load based on no shear distortion mechanism and that based on shear distortion with shear modification compared well with the experimental values. The collapse load based on shear distortion tends to over estimate the actual collapse load. The shear modification allowed the adjustment of the shear component of the collapse load in the shear distortion mode. The deformations appeared to compare well with prediction. For simple structures, rigid plastic theory gave a reasonable upper bound solution since the elastic deformation was small compared with the full plastic deformation. For complex structures, the value of the elastic deformation could be quite significant, in particular, with a mechanism involving shear distortion. Hence the collapse load was often over-estimated. This could be taken into account in predicting the deformation characteristic and ultimate collapse load of the models. The yield lines, when associated with an equilibrium condition of the stress field boundaries, gave reasonable prediction of the collapse load. Account should be taken of the reduction in shear ductility along the yield lines and in hinges, forming the collapse mechanism.

The experimental result for the prestressed box beam was lowered than the initial predicted value. It was apparent that the effect of poor compaction had reduced the elastic stiffness of the prestressed box beam. The bottom flanges were in tension at the centre of the loaded span. Although the lower concrete strength did not significantly affect the flexural strength of the section, it would never the less reduce the web buckling and crushing capacity causing premature failure of the section. In order to account for the lower strength due to poor workmanship, the effective material strength is taken as only 80% of the theoretical value. It highlighted the problems that could be encountered in the construction of the actual prestressed beams where reinforcement was congested. A higher level of site supervision would be required for this type of structure to ensure adequate compaction of the concrete could be achieved.

The next chapter provides a conclusion for the theoretical and experimental works that were carried out and discusses the limitations of the theory that were developed.

FIGURE 6.1 LOAD DEFLECTION CURVE AT CENTRE OF BOX BEAM B1



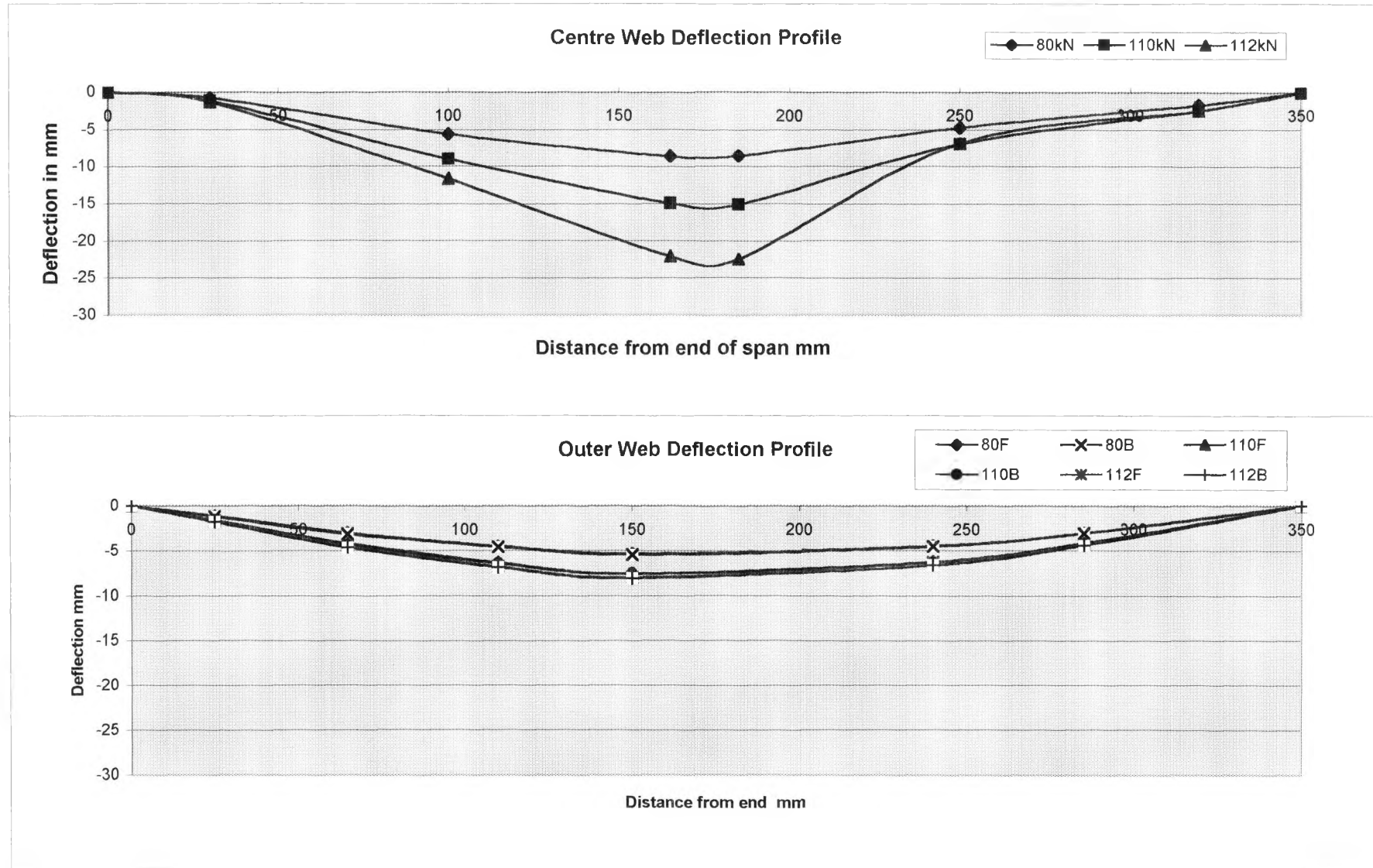
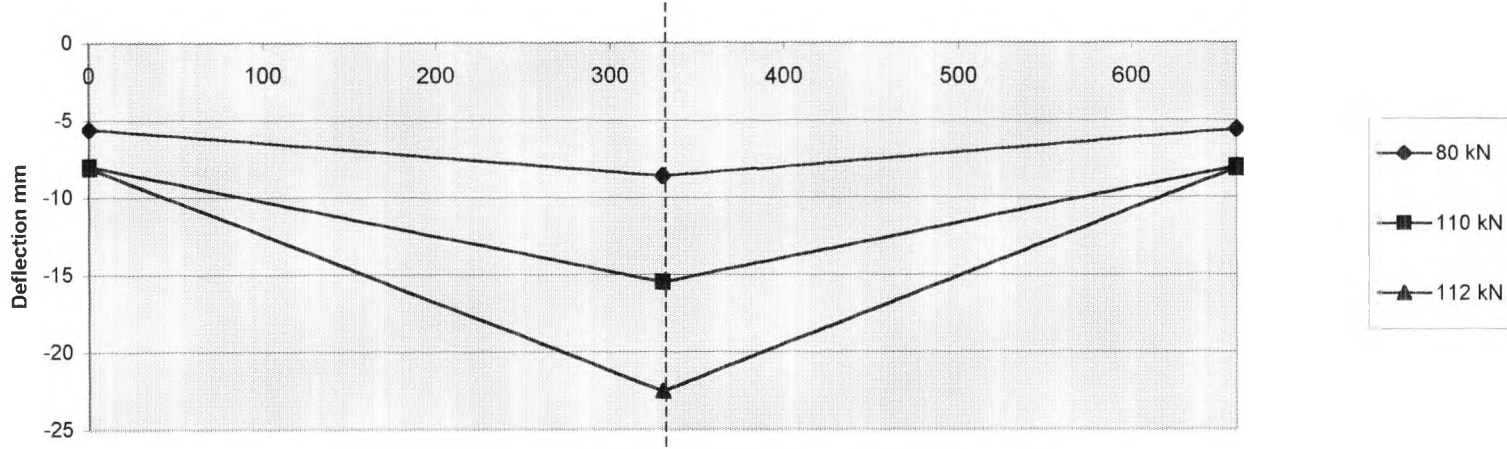


FIGURE 6.2 LONGITUDINAL DEFLECTION PROFILE OF BEAM B1 X 10⁻³mm

Section Near Centre Span



Section Near Quarter Span

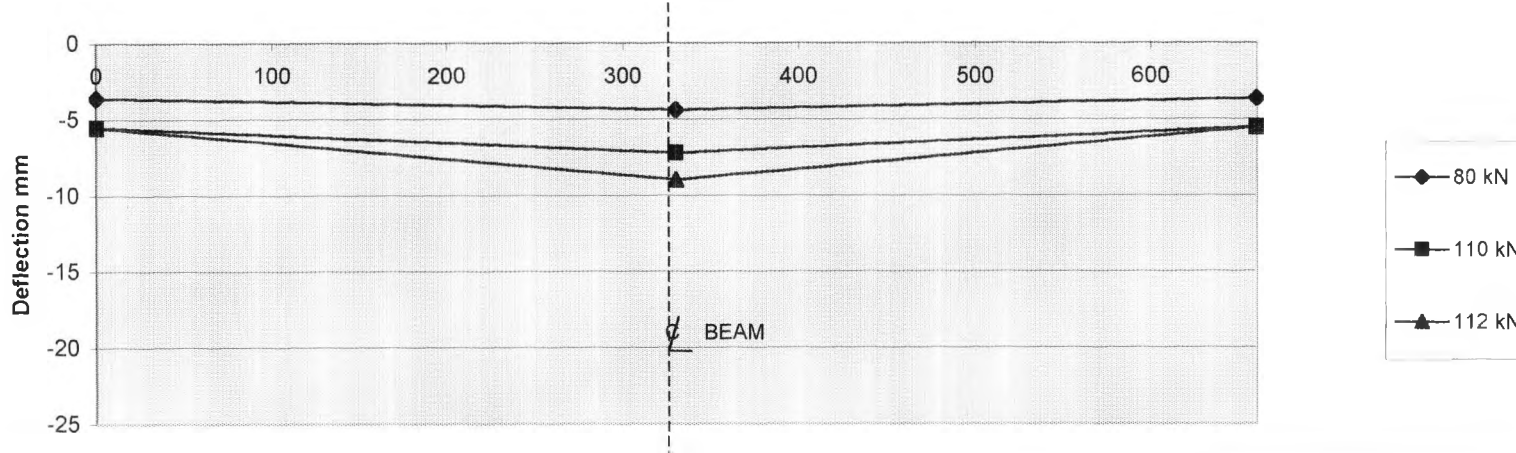


FIGURE 6.3 TRANSVERSE DEFLECTION PROFILE OF BEAM B1 mm

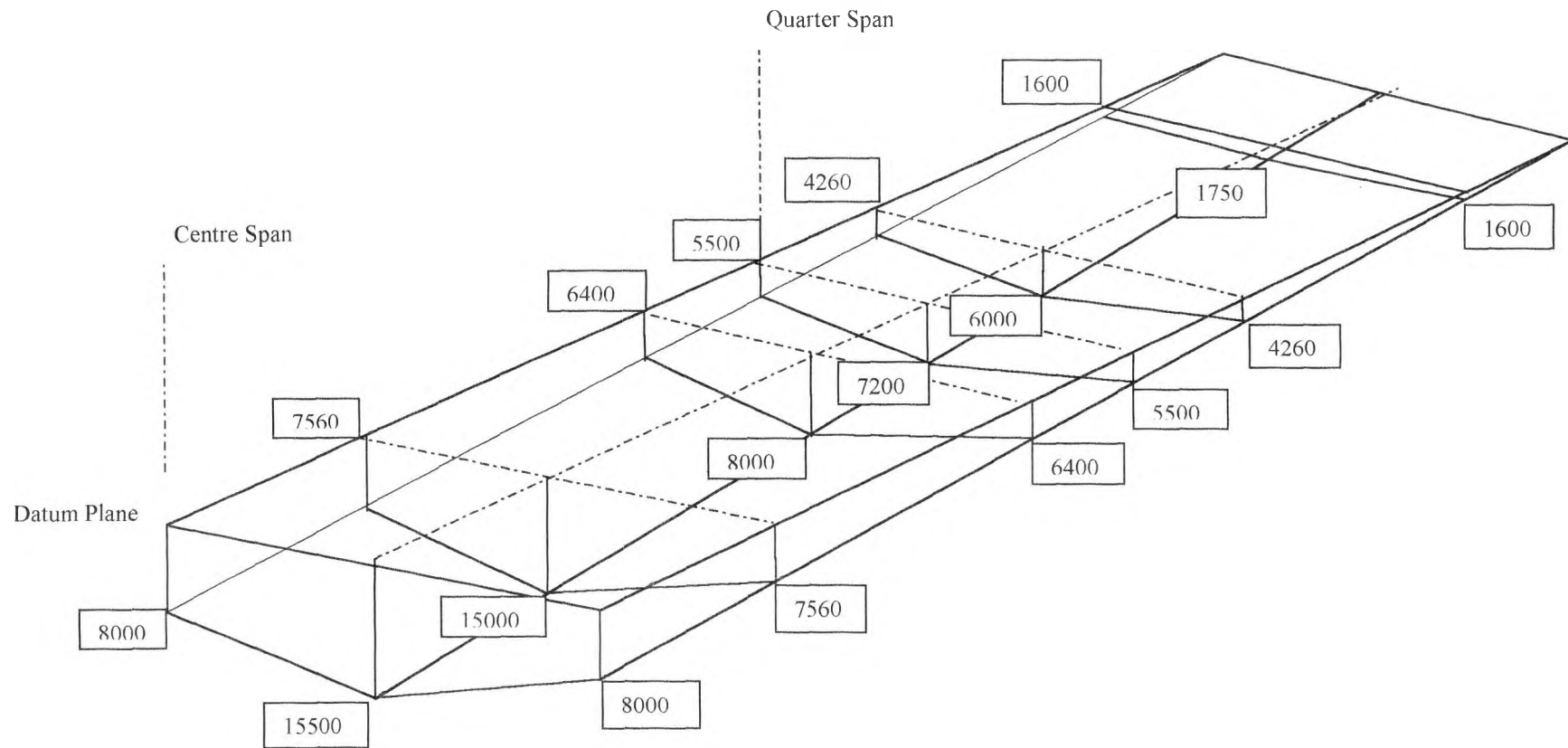


FIGURE 6.4 DEFLECTION PROFILE OF BOTTOM FLANGE BEAM B1 $\times 10^{-3}$ mm LOAD AT 110kN

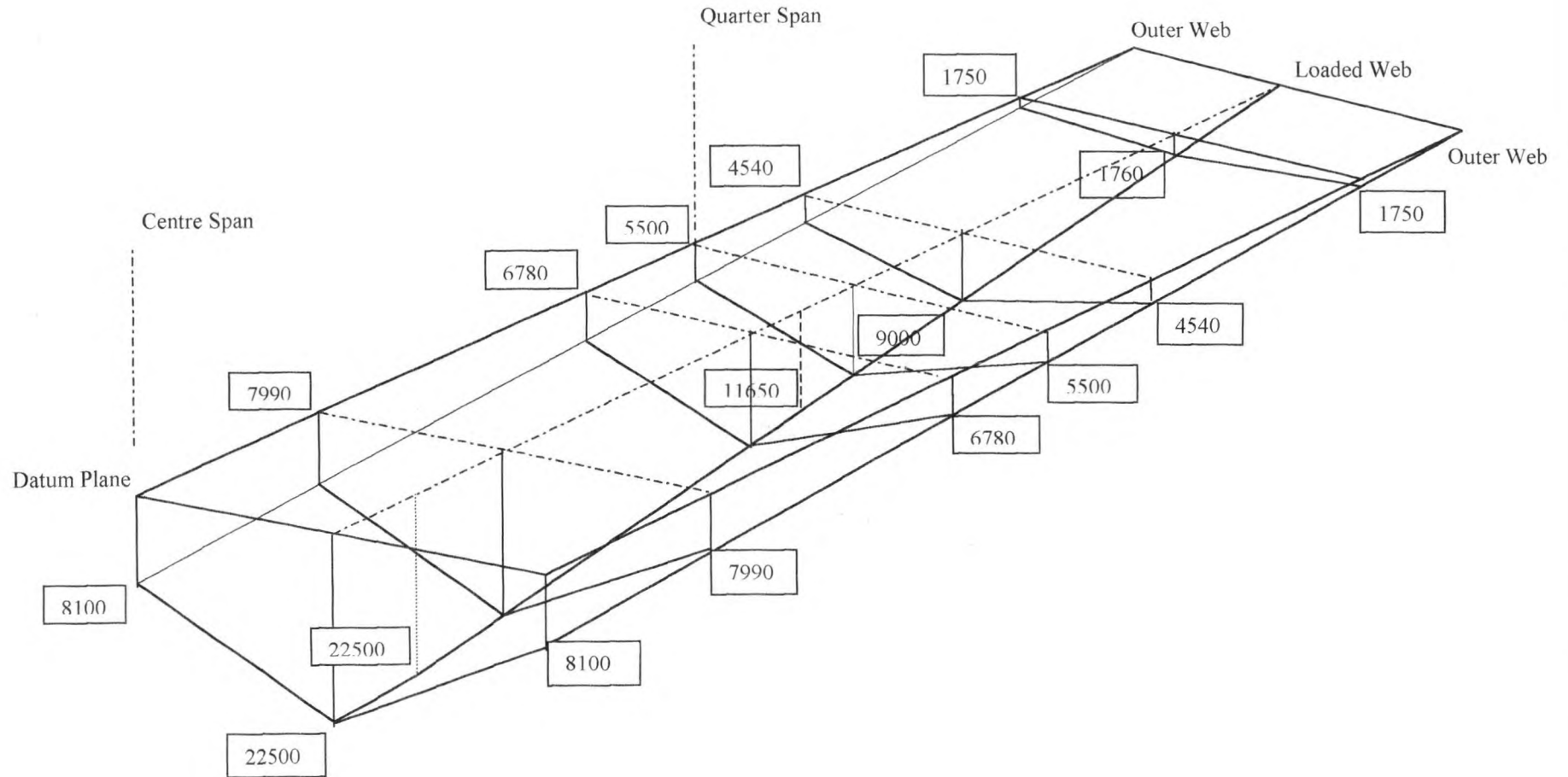


FIGURE 6.5 DEFLECTION PROFILE OF BOTTOM FLANGE BEAM $B1 \times 10^{-3}$ mm LOAD AT 112kN

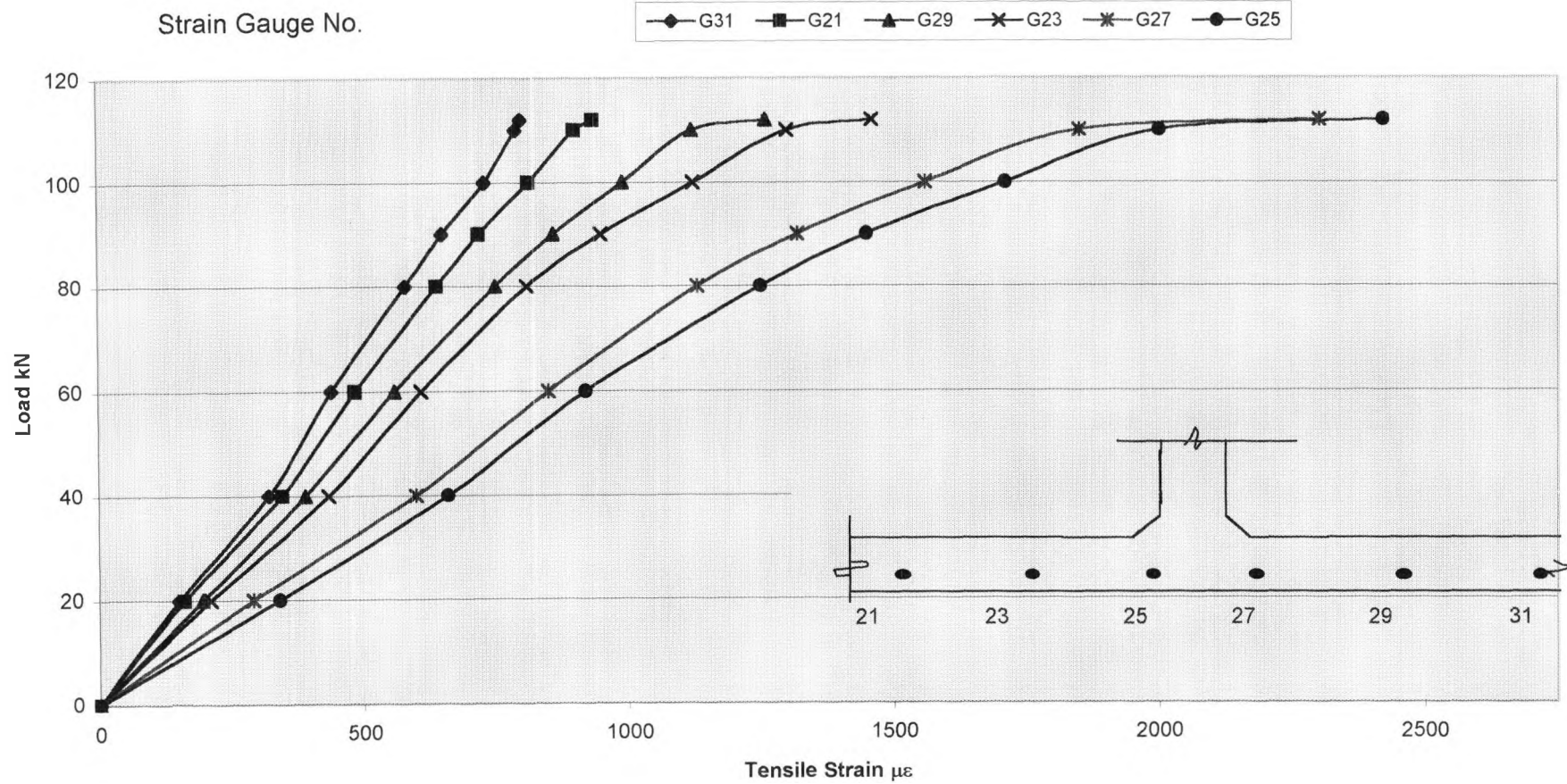


FIGURE 6.6 BOTTOM STEEL STRAIN DISTRIBUTION IN BOTTOM FLANGE NEAR CENTRE OF BOX BEAM B1

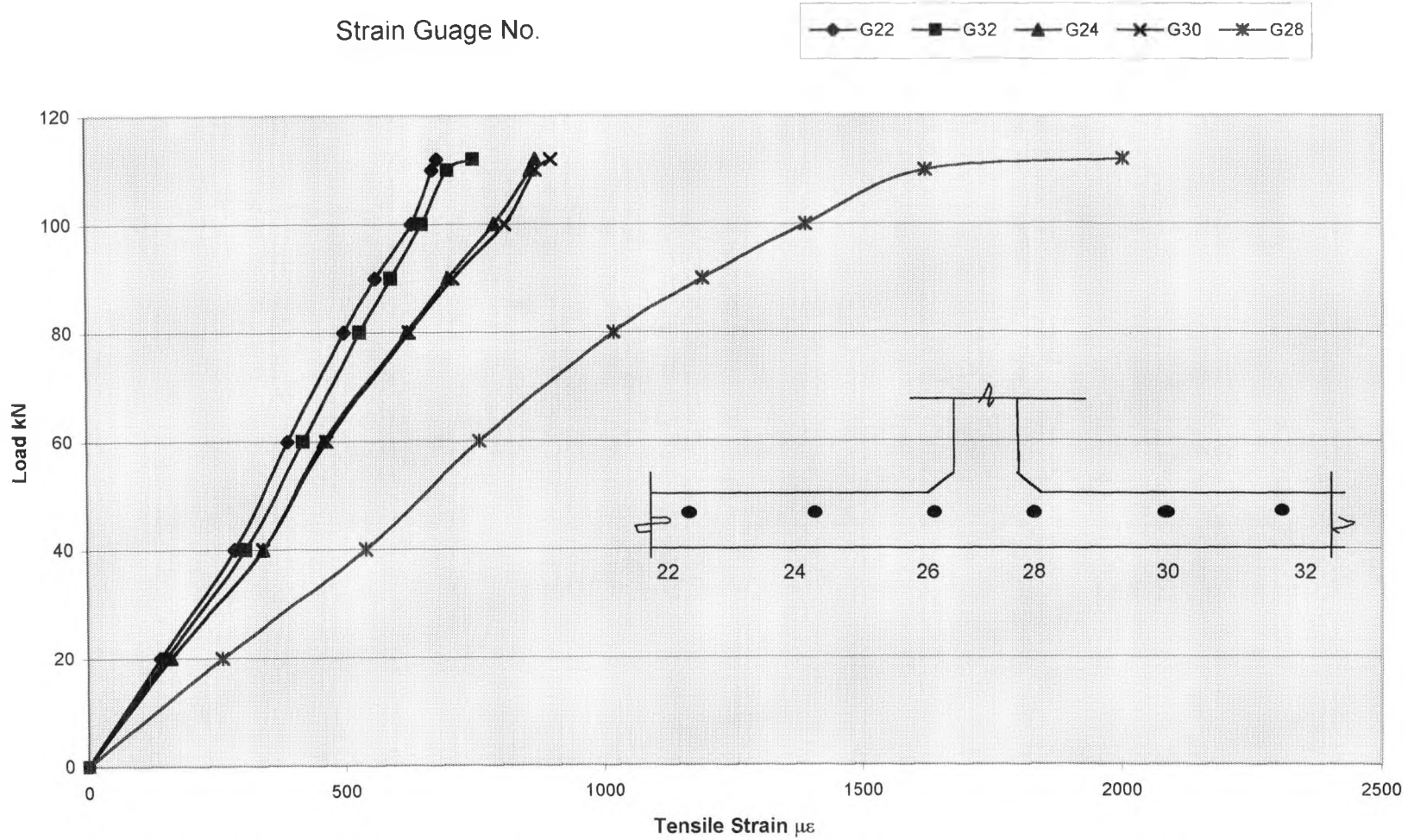


FIGURE 6.7 TOP STEEL STRAIN DISTRIBUTION IN BOTTOM FLANGE NEAR CENTRE OF BOX BEAM

B1

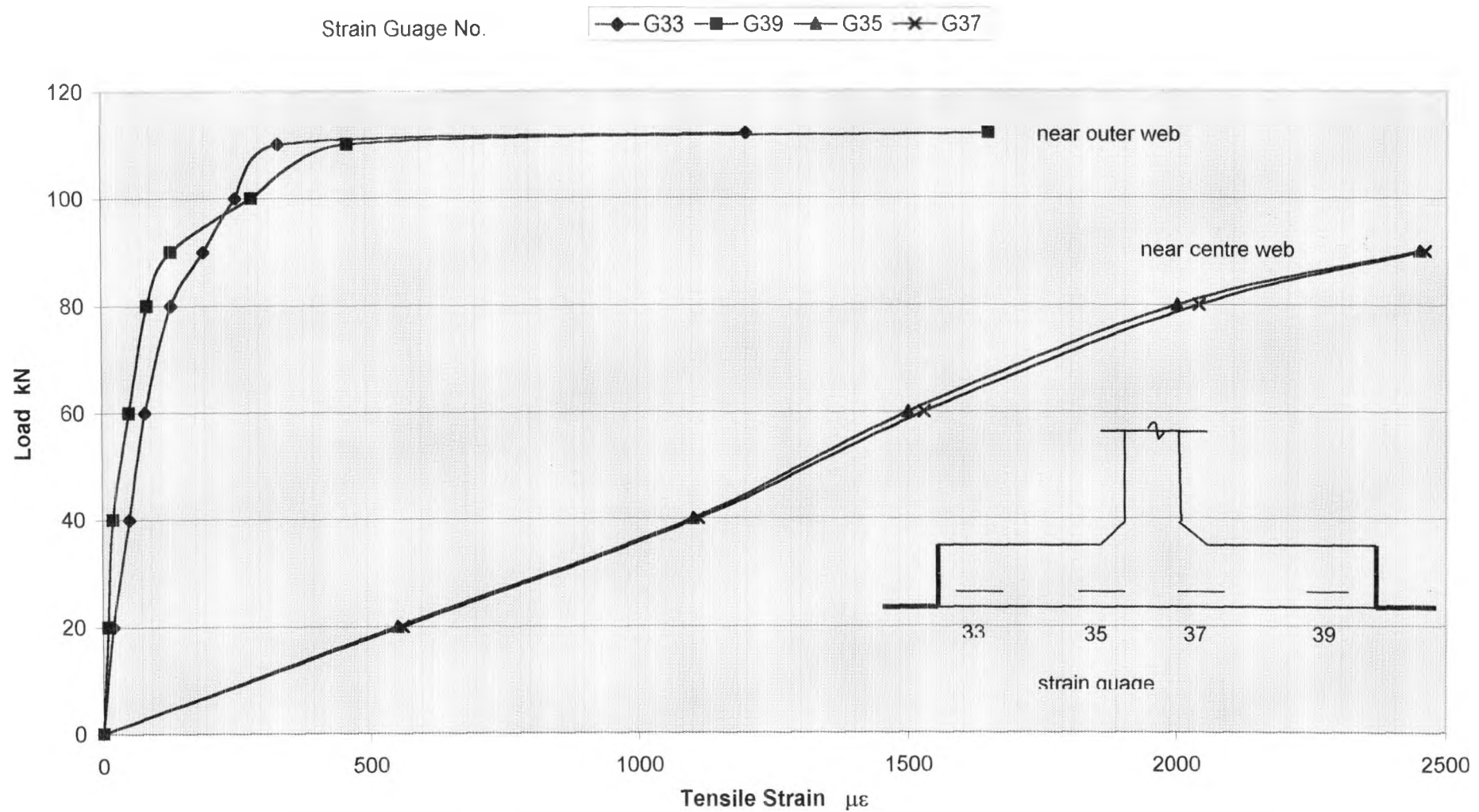


FIGURE 6.8 BOTTOM TRANSVERSE STEEL STRAIN DISTRIBUTION IN BOTTOM FLANGE NEAR CENTRE OF BOX BEAM B1

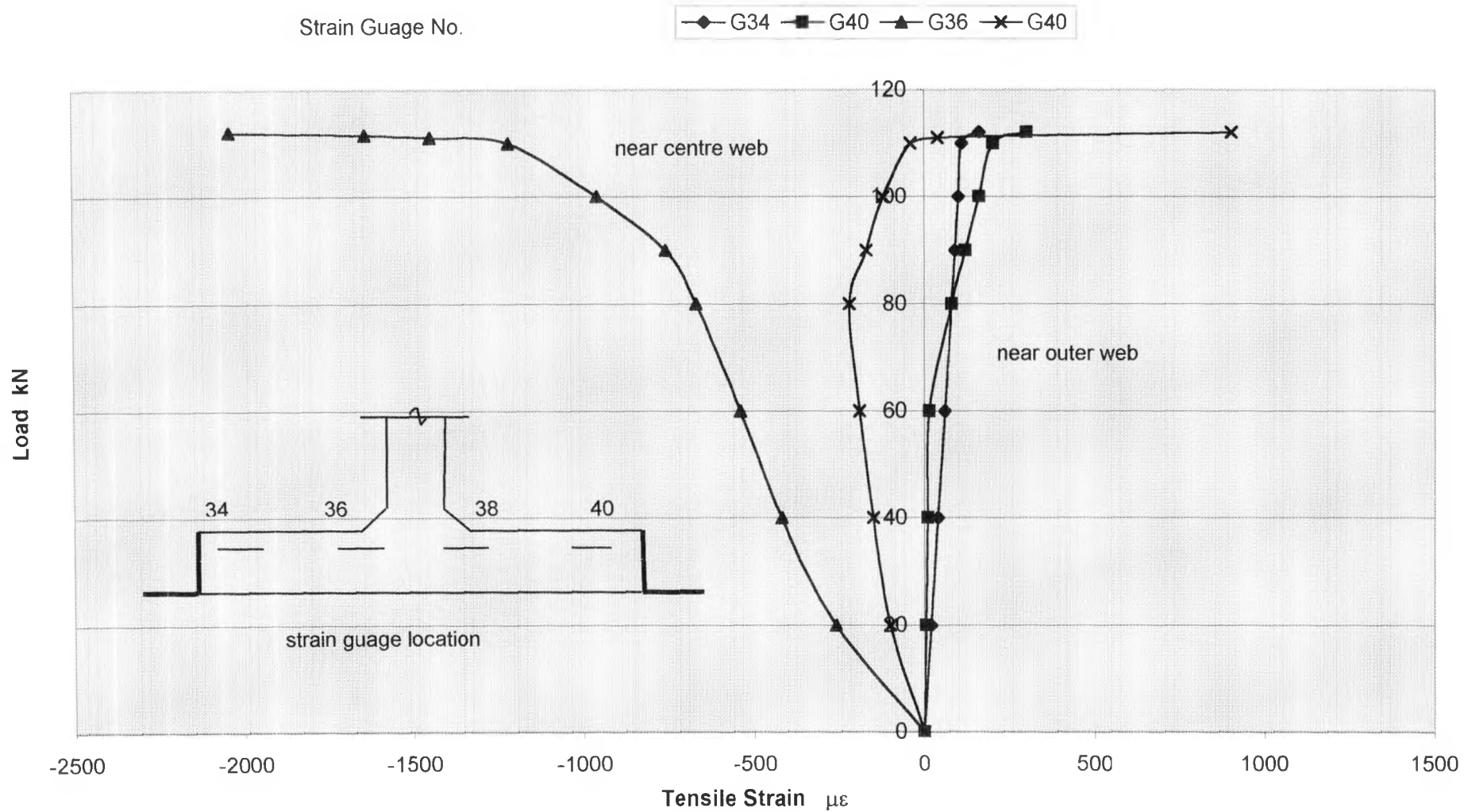


FIGURE 6.9 TOP TRANSVERSE STEEL STRAIN DISTRIBUTION IN BOTTOM FLANGE NEAR CENTRE OF BOX BEAM B1

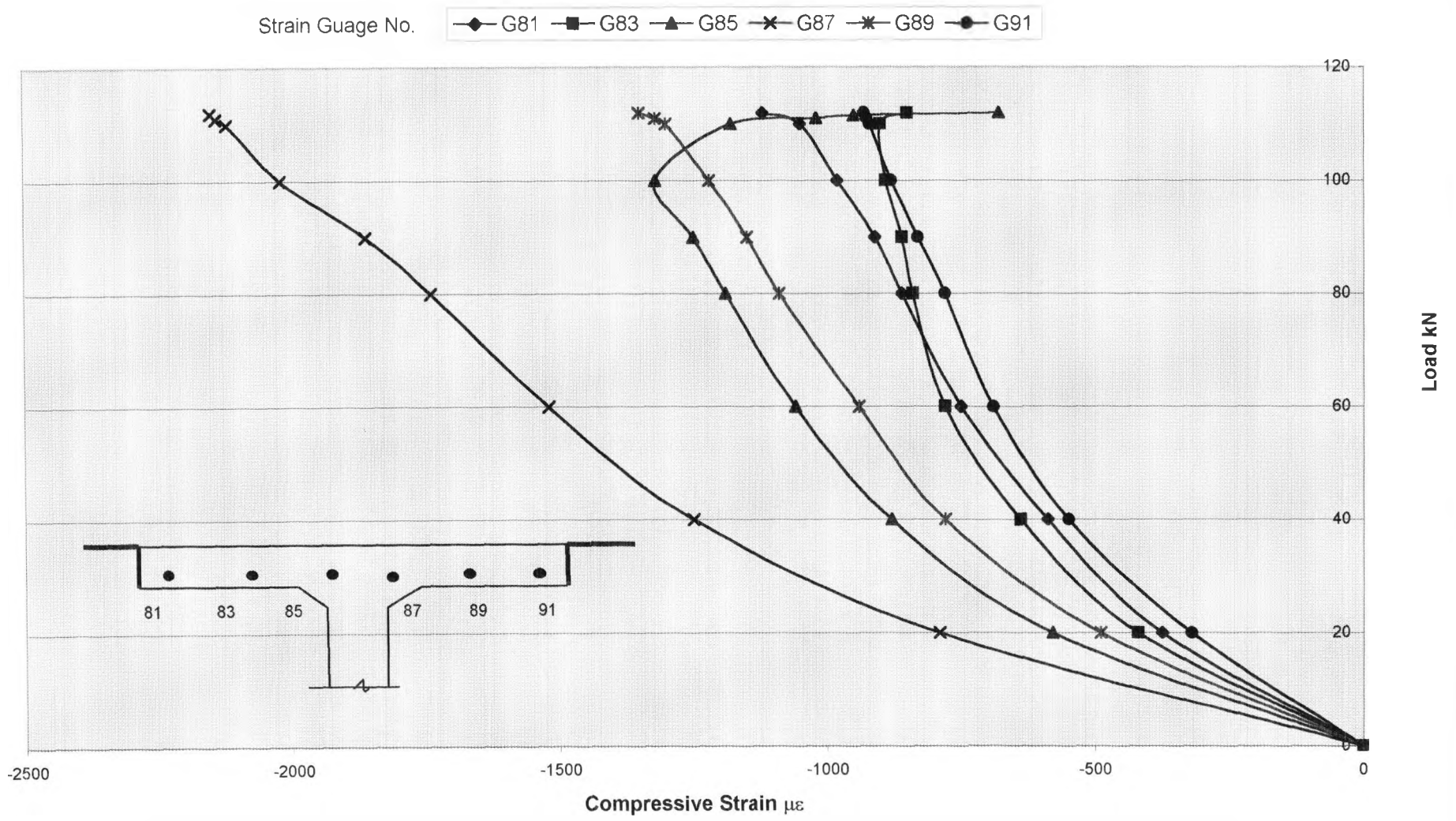


FIGURE 6.10 BOTTOM LONGITUDINAL STEEL STRAIN DISTRIBUTION IN TOP FLANGE NEAR CENTRE OF BOX BEAM B1

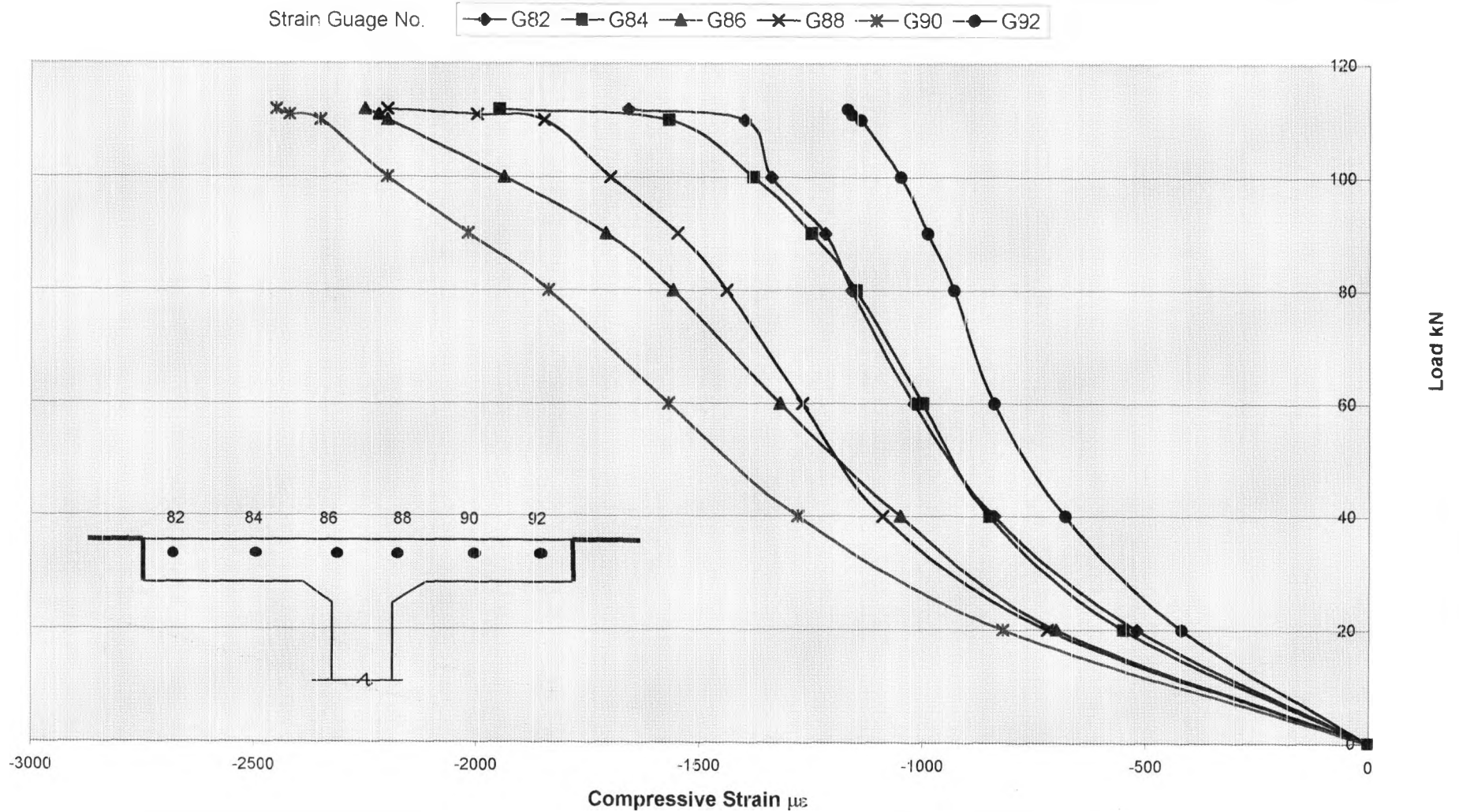


FIGURE 6.11 TOP LONGITUDINAL STEEL STRAIN DISTRIBUTION IN TOP FLANGE NEAR CENTRE OF BOX BEAM B1

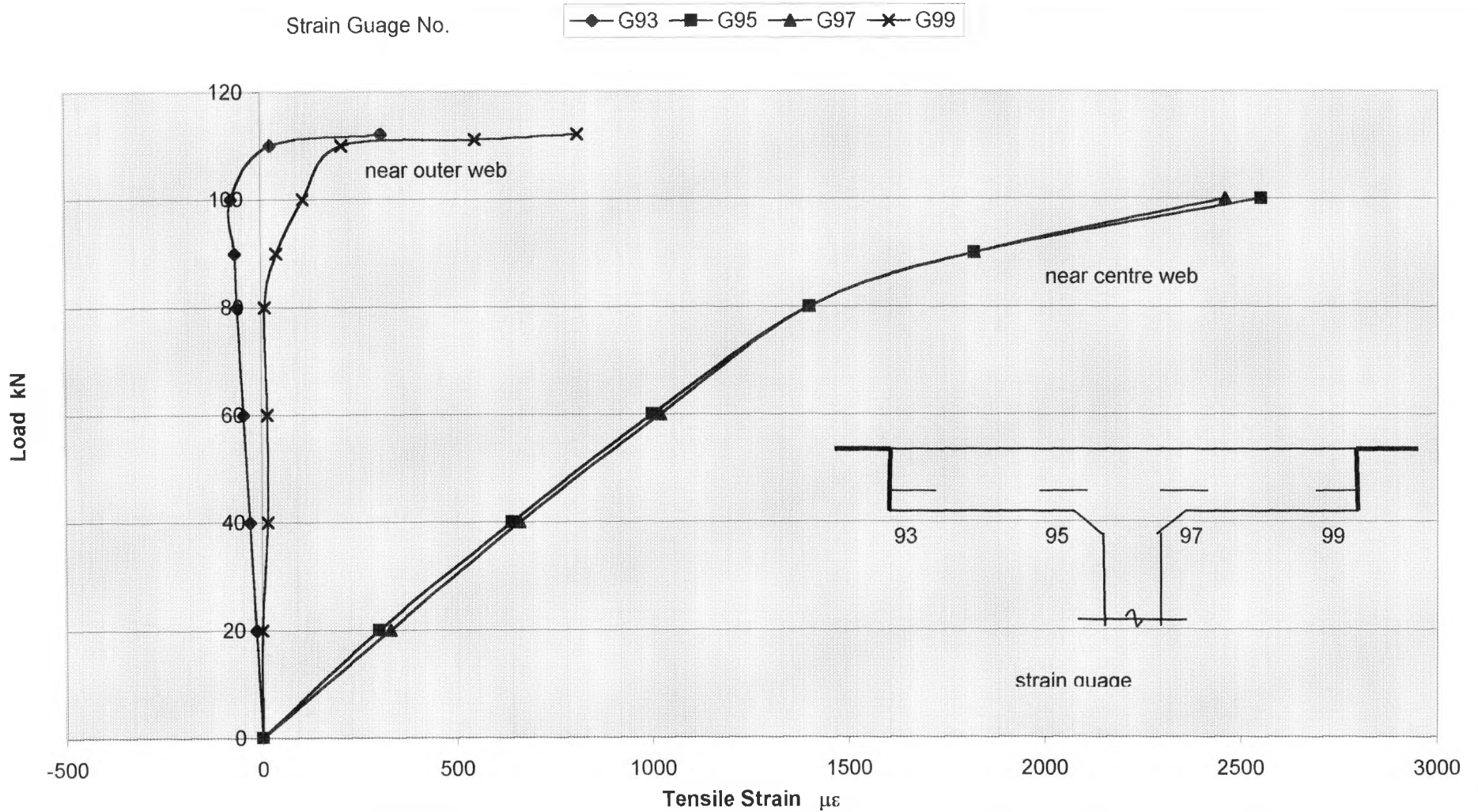


FIGURE 6.12 BOTTOM TRANSVERSE STEEL STRAIN DISTRIBUTION IN TOP FLANGE NEAR CENTRE OF BOX BEAM B1

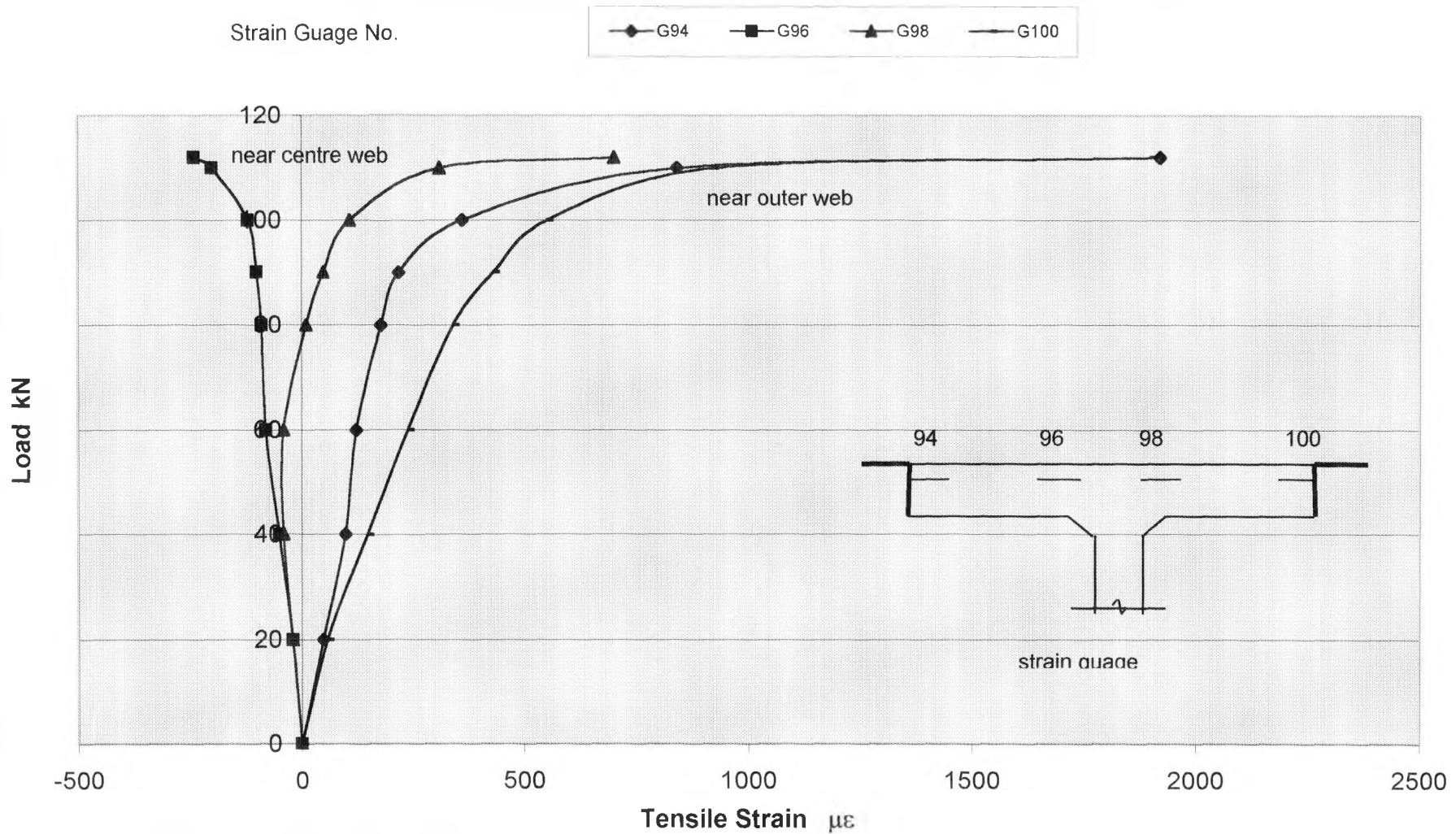


FIGURE 6.13 TOP TRANSVERSE STEEL STRAIN DISTRIBUTION IN TOP FLANGE NEAR CENTRE OF BOX BEAM B1

Strain Gauge No.

—●— G133 —■— G134 —▲— G135 —×— G136 —*— G137 —●— G138

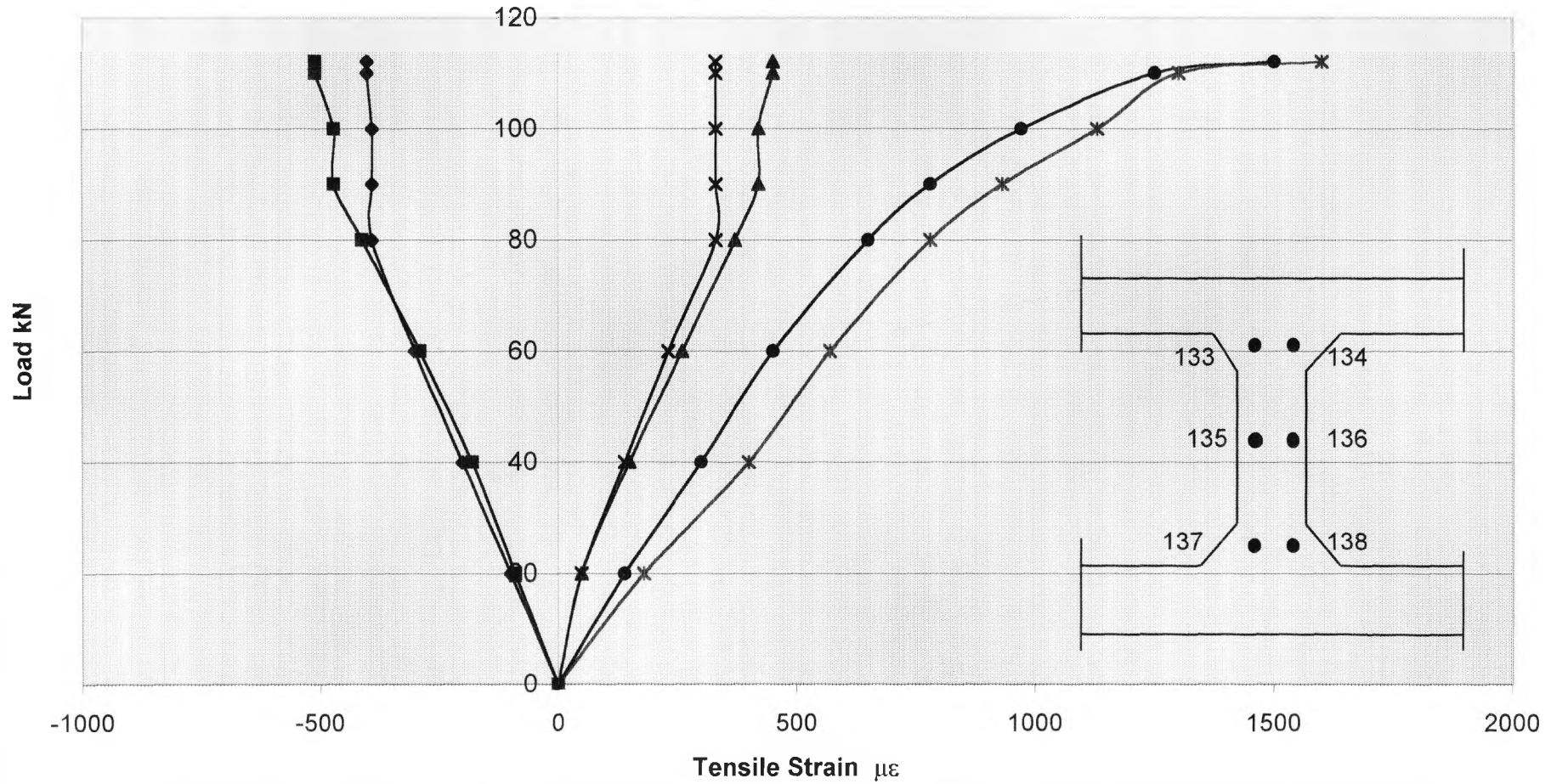


FIGURE 6.14 LONGITUDINAL WEB STEEL STRAIN DISTRIBUTION NEAR CENTRE SECTION OF BOX BEAM B1

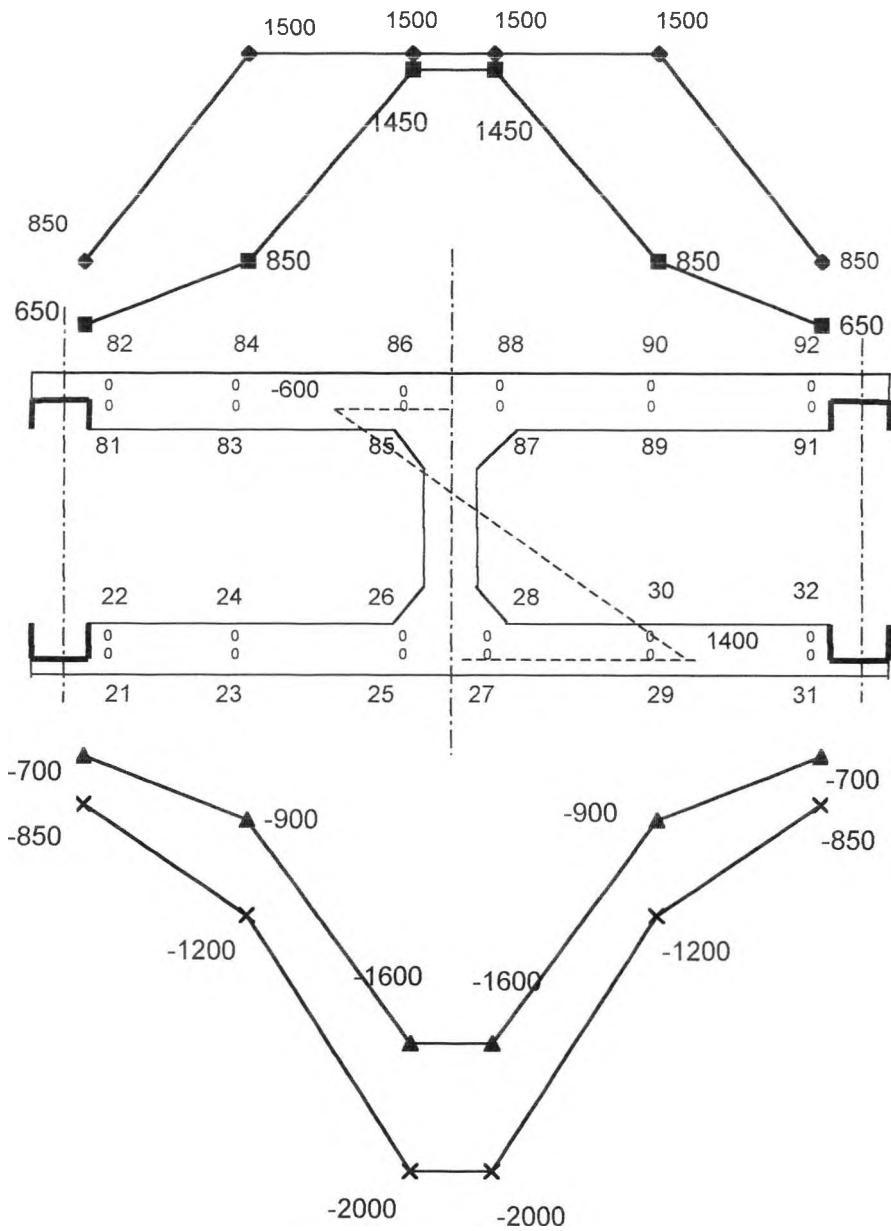


FIGURE 6.15 LONGITUDINAL STEEL STRAIN DISTRIBUTION AT CENTRE SECTION OF BOX BEAM B1 LOAD AT 110kN

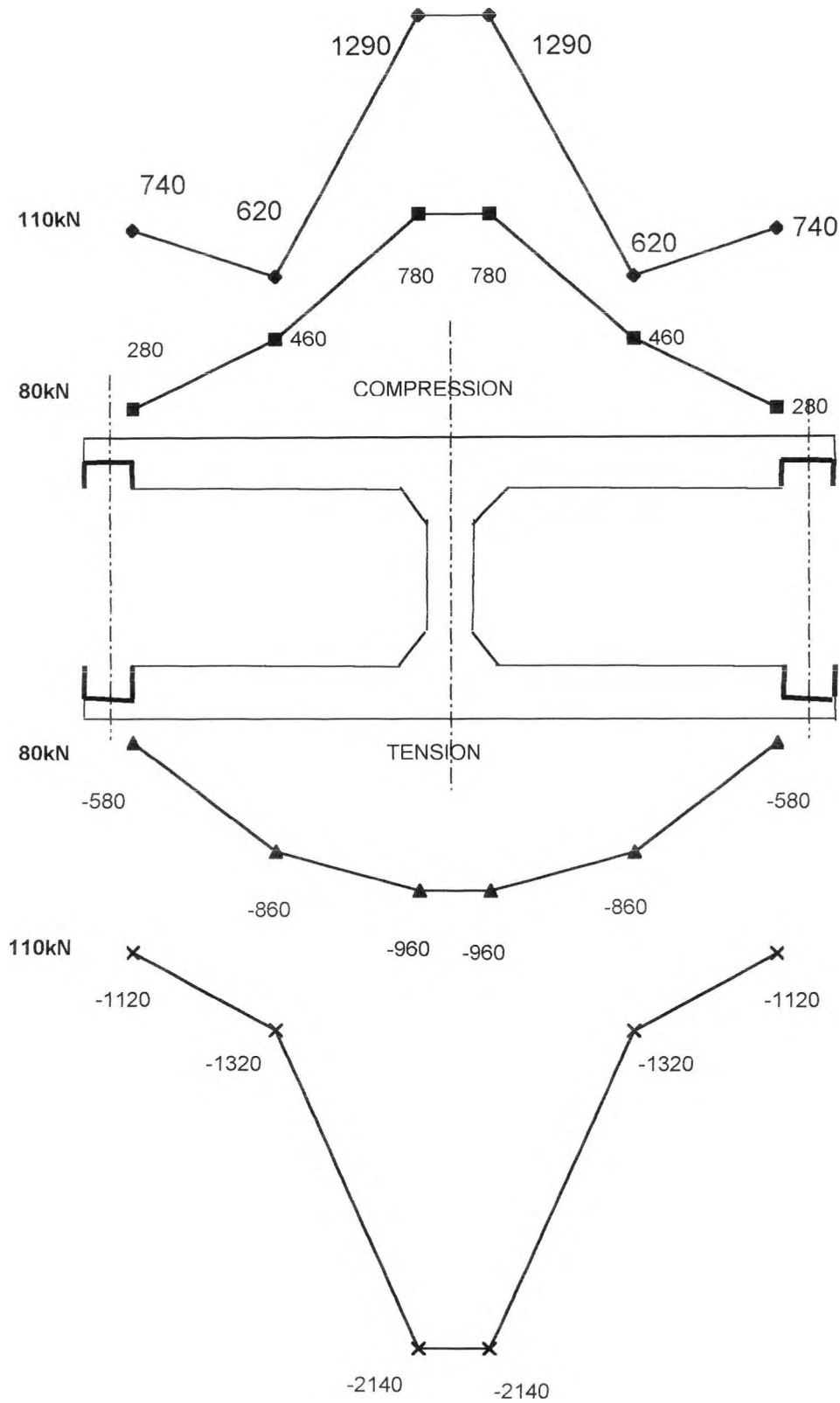


FIGURE 6.16 LONGITUDINAL SURFACE STRAIN DISTRIBUTION AT CENTRE SECTION OF BOX BEAM B1 LOAD AT 80 AND 110kN

BOLD Nos. indicate strain guage numbering

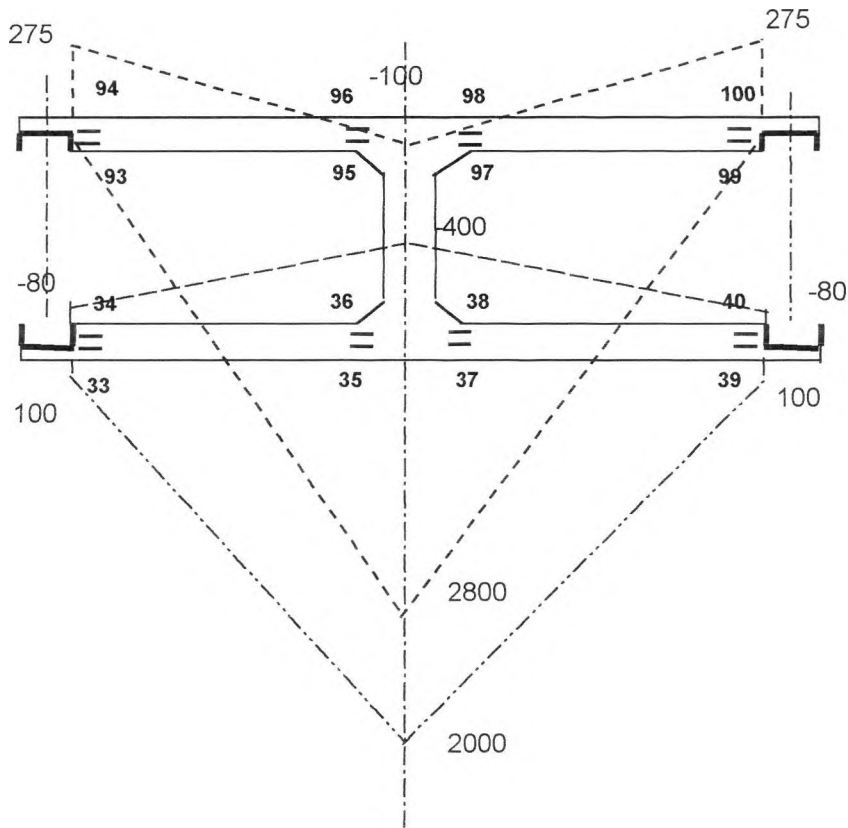


FIGURE 6.17 TRANSVERSE STEEL STRAIN DISTRIBUTION AT CENTRE SECTION OF BOX BEAM B1 LOAD AT 80kN

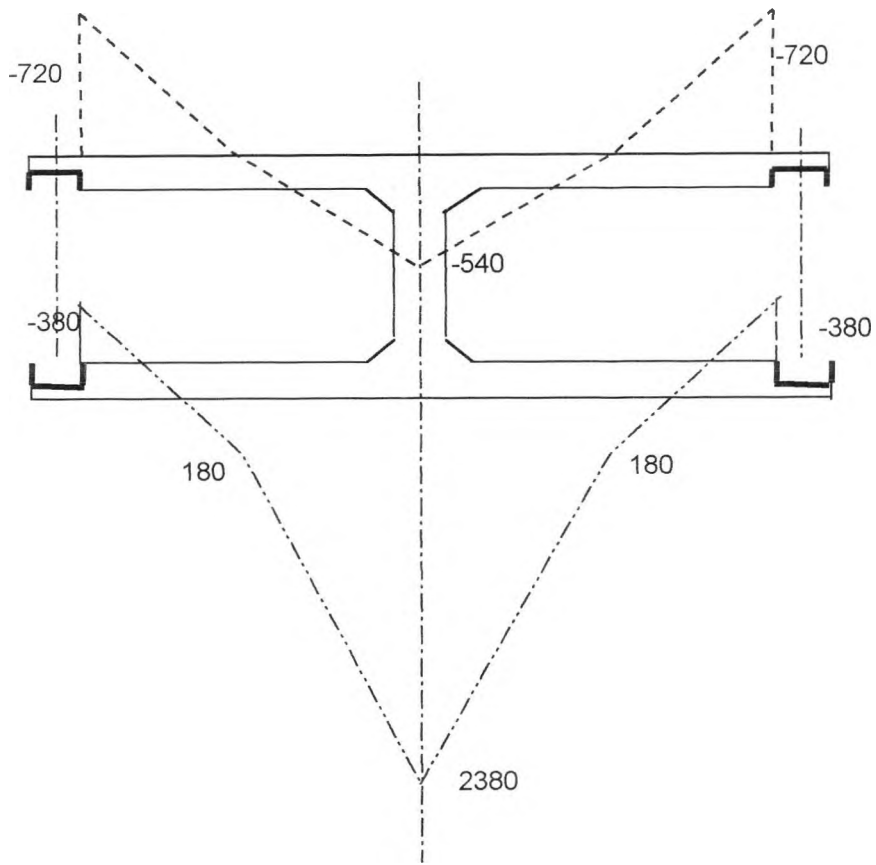


FIGURE 6.18 **TRANSVERSE SURFACE STRAIN DISTRIBUTION AT CENTRE SECTION OF BOX BEAM B1 LOAD AT 80kN**

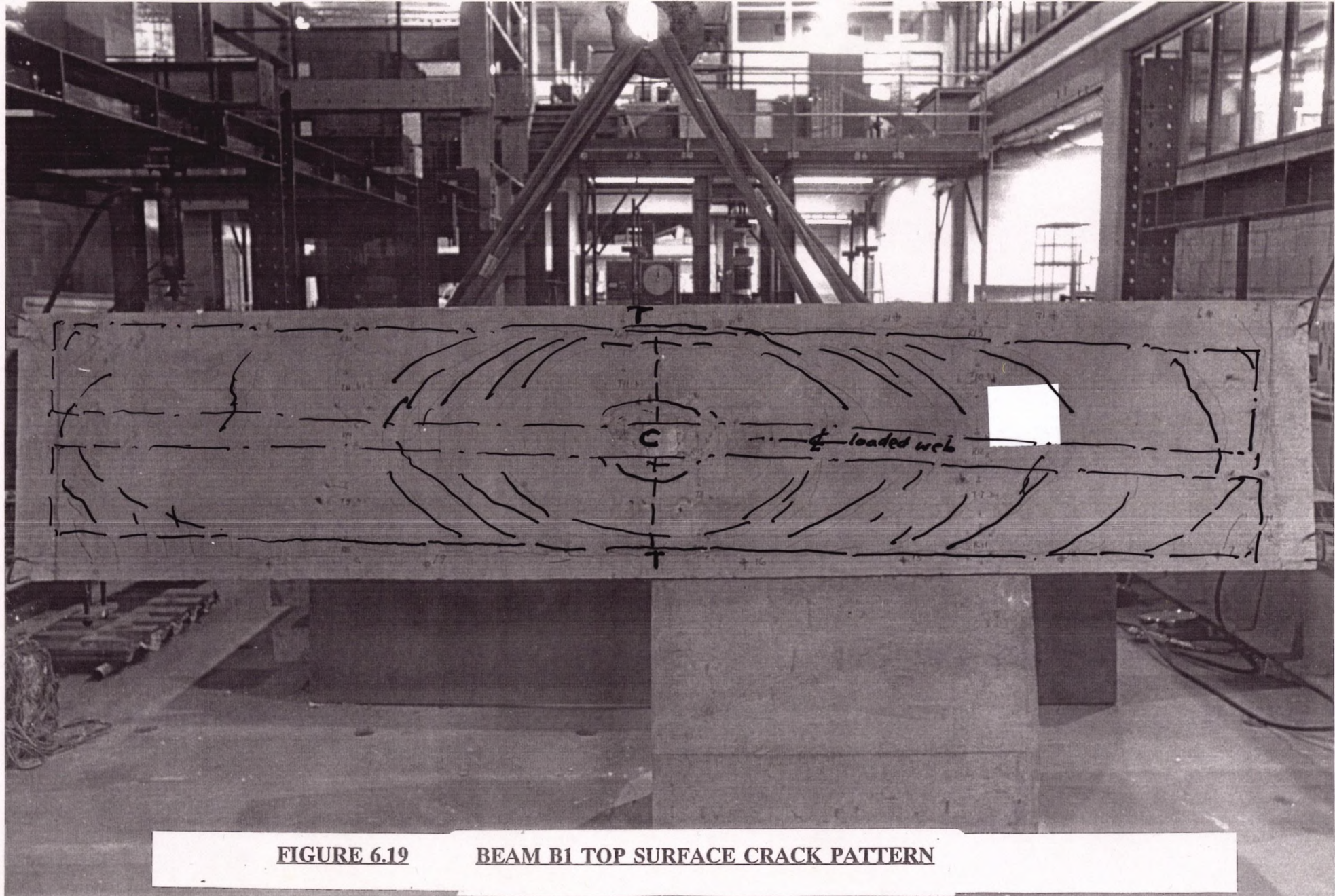


FIGURE 6.19 **BEAM B1 TOP SURFACE CRACK PATTERN**

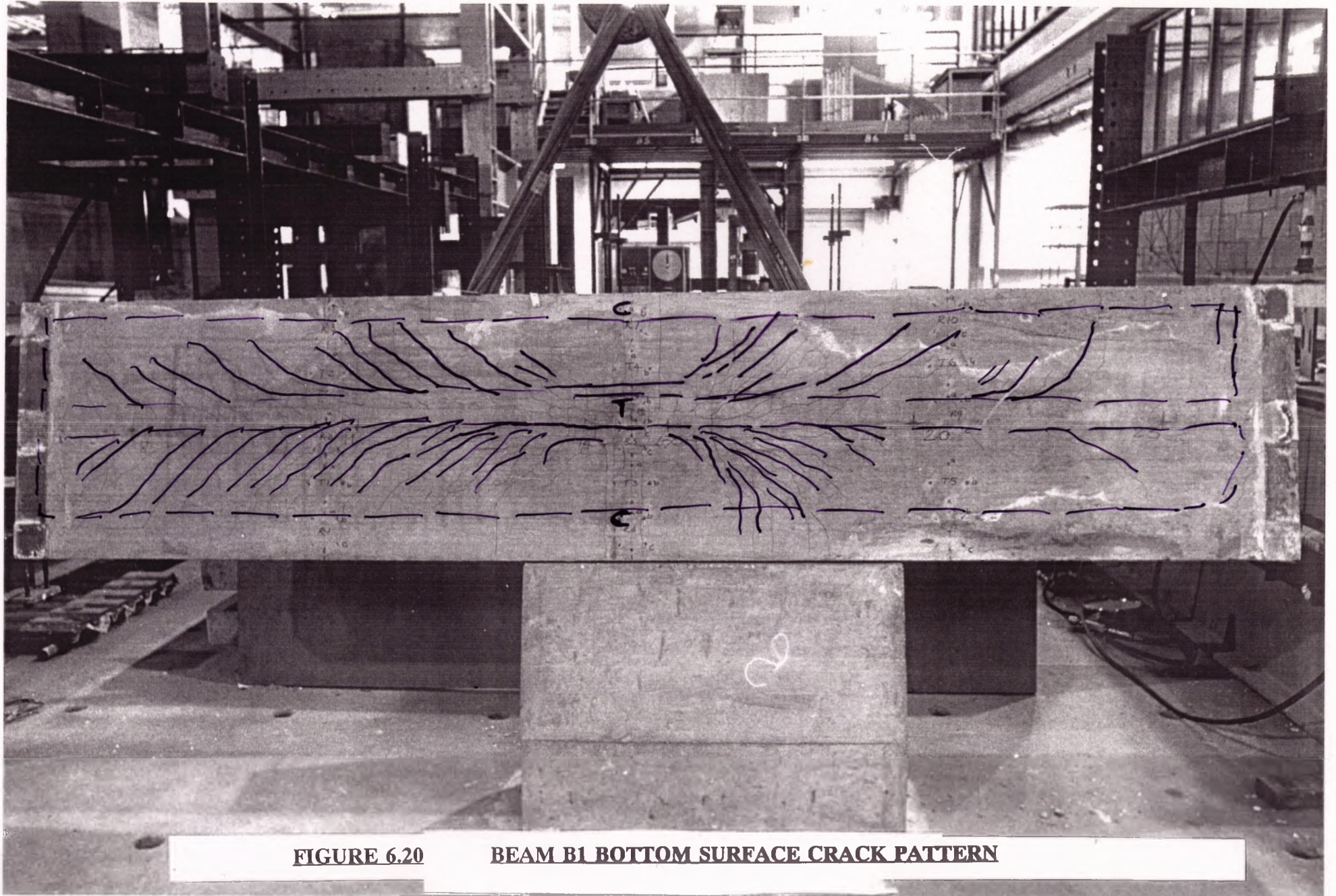


FIGURE 6.20 BEAM B1 BOTTOM SURFACE CRACK PATTERN

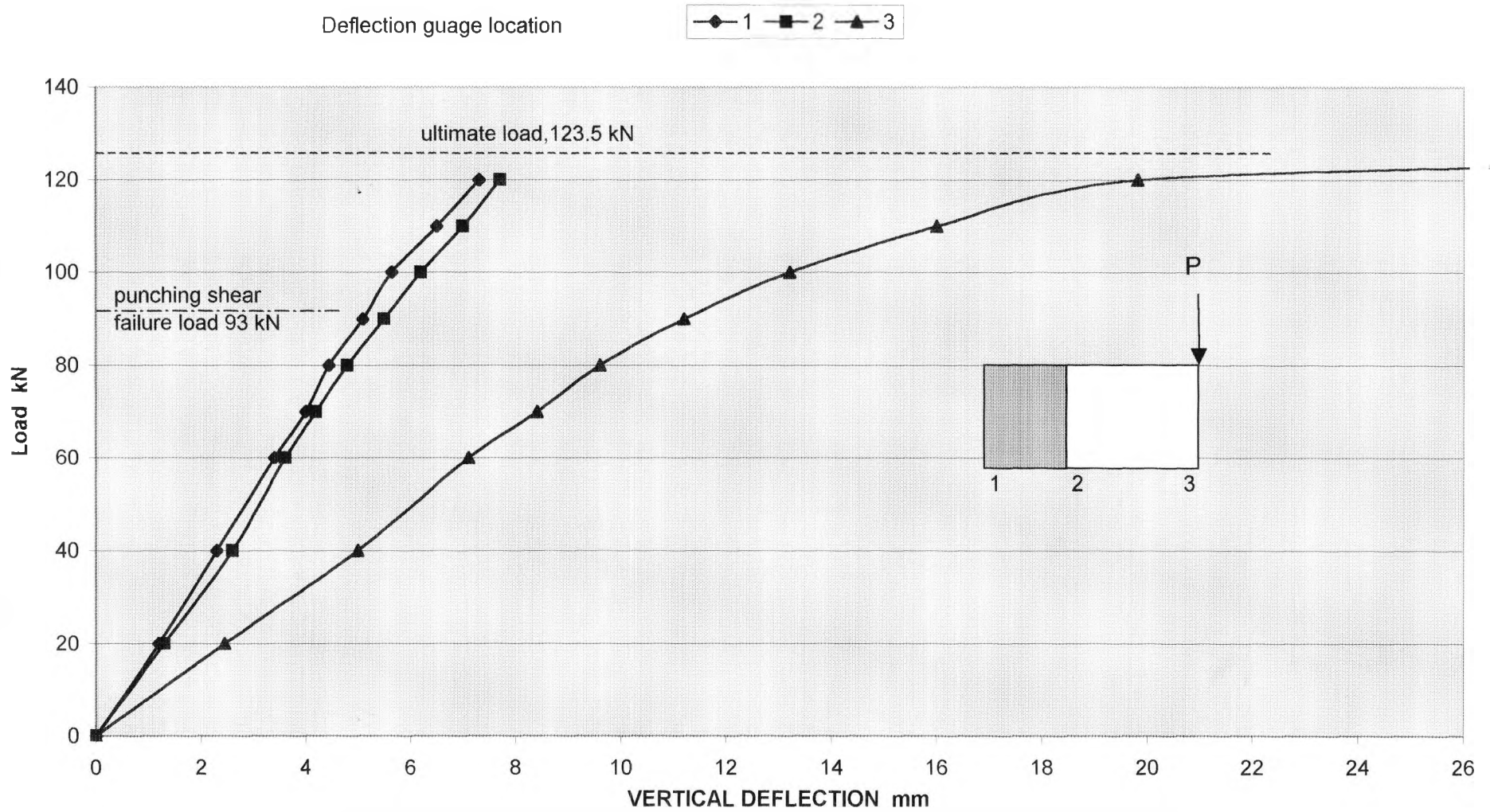


FIGURE 6.21 **LOAD DEFLECTON CURVE AT CENTRE OF BOX BEAM B2**

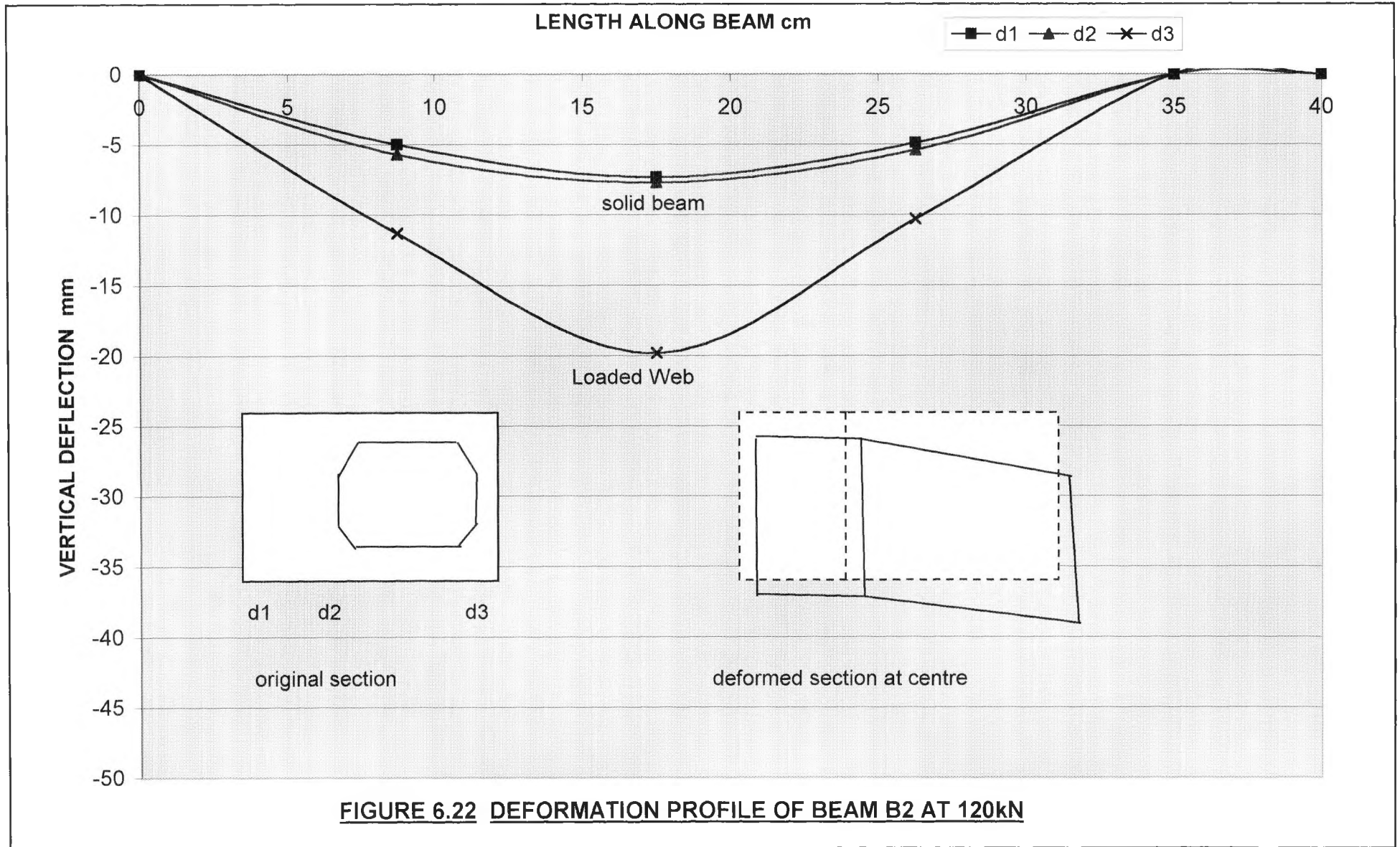




FIGURE 6.23 LOCAL PUNCHING SHEAR FAILURE UNDER POINT LOAD FOR BEAM B2

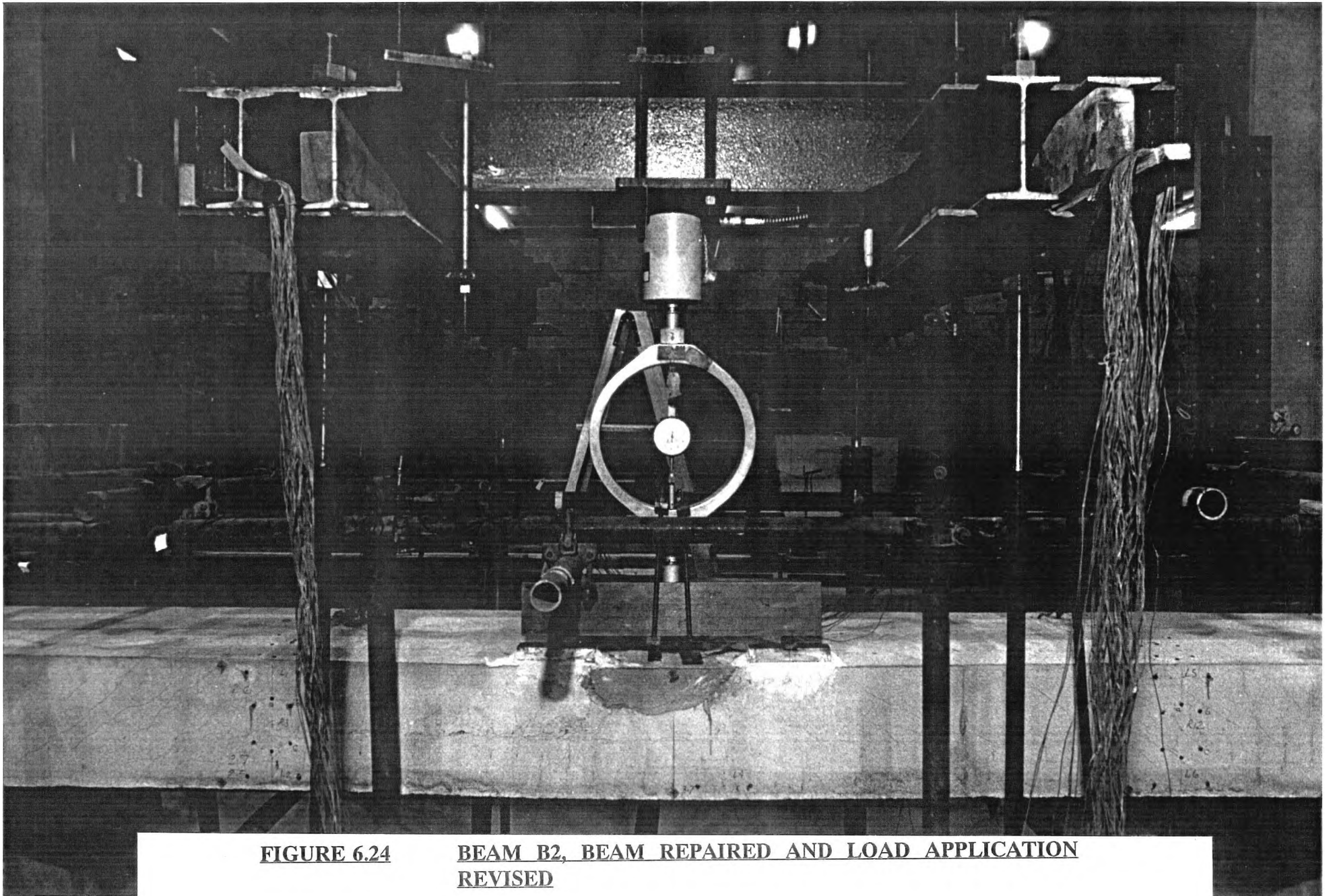


FIGURE 6.24

**BEAM B2, BEAM REPAIRED AND LOAD APPLICATION
REVISED**

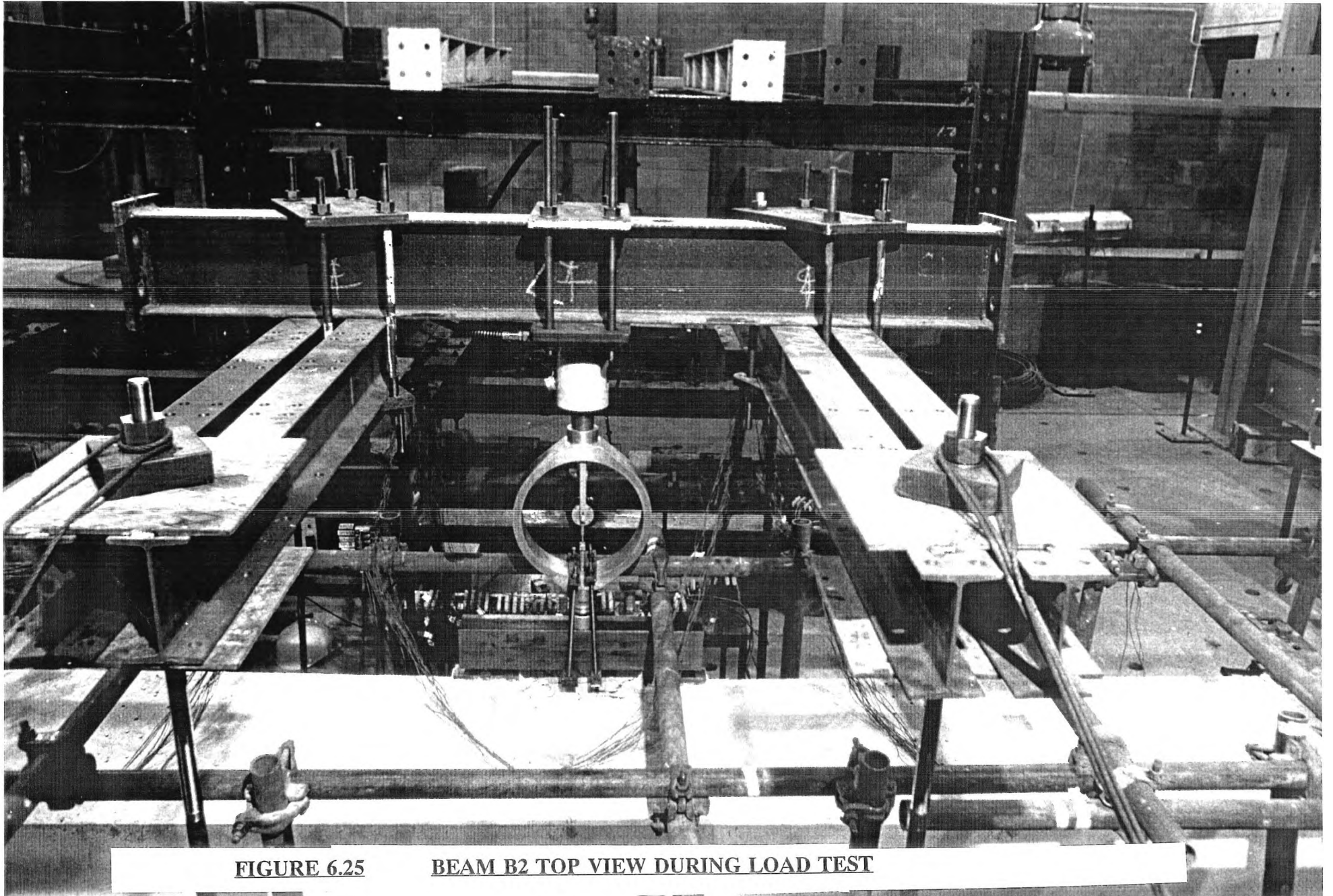


FIGURE 6.25

BEAM B2 TOP VIEW DURING LOAD TEST

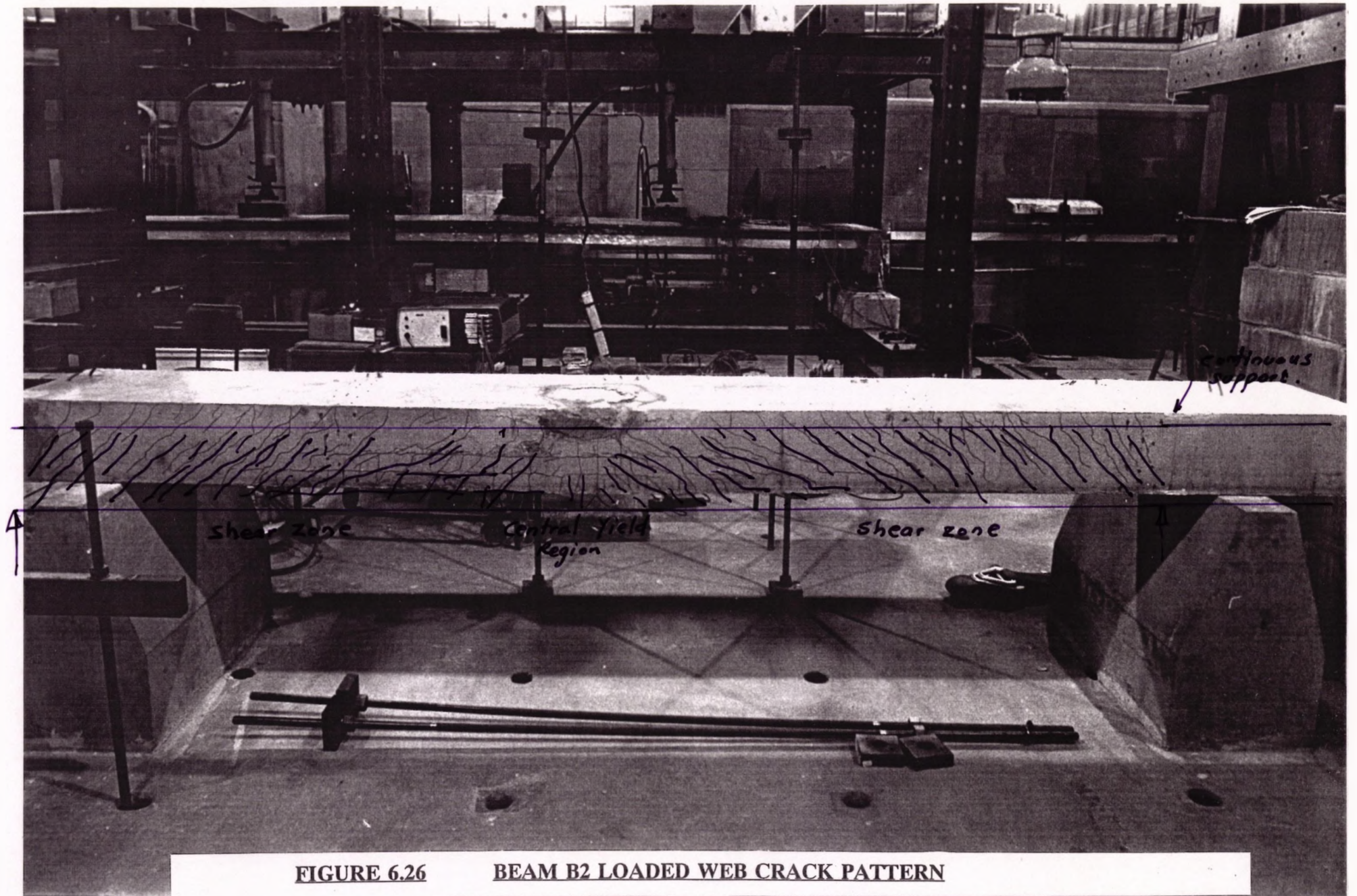


FIGURE 6.26

BEAM B2 LOADED WEB CRACK PATTERN

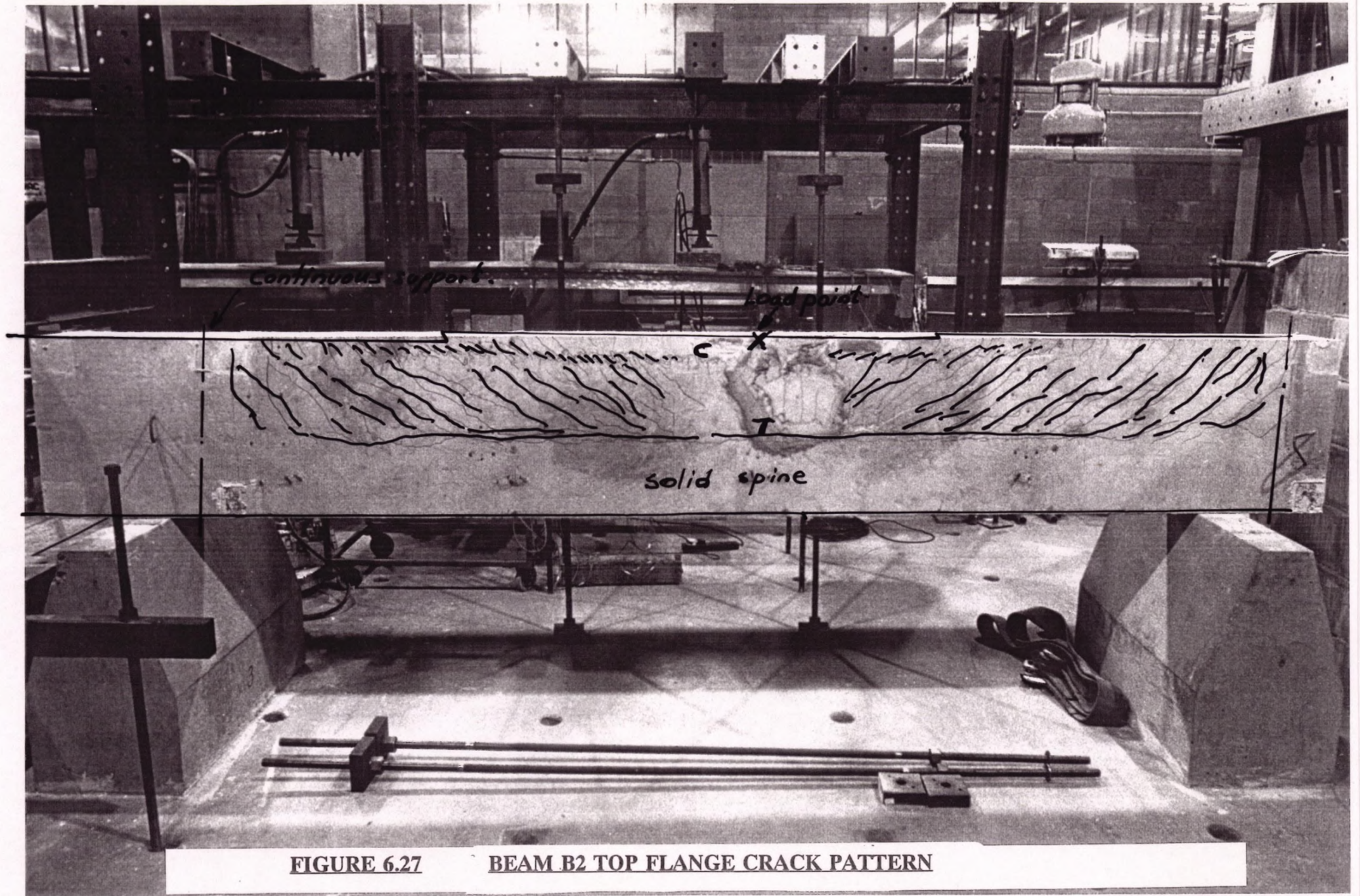
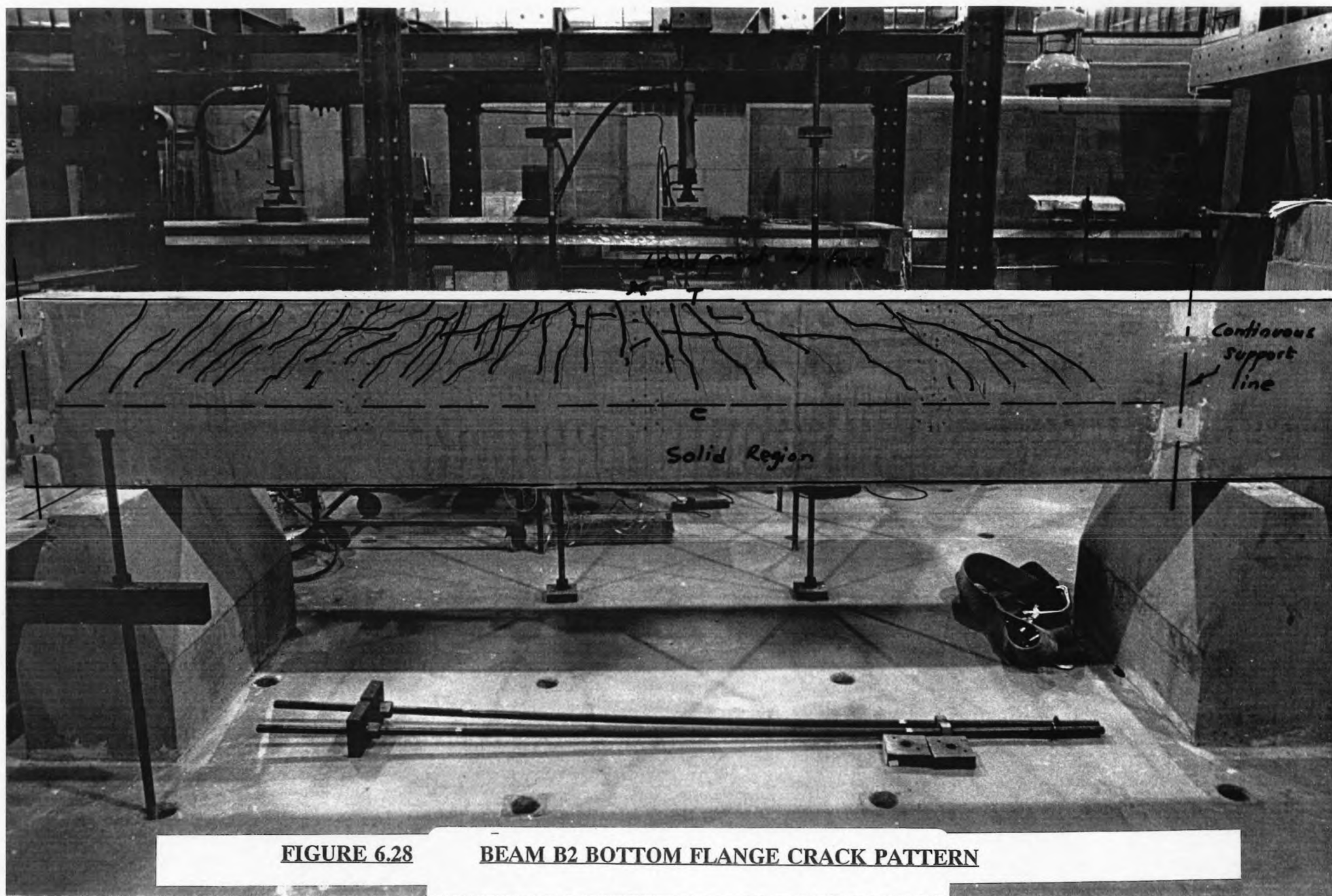


FIGURE 6.27 BEAM B2 TOP FLANGE CRACK PATTERN



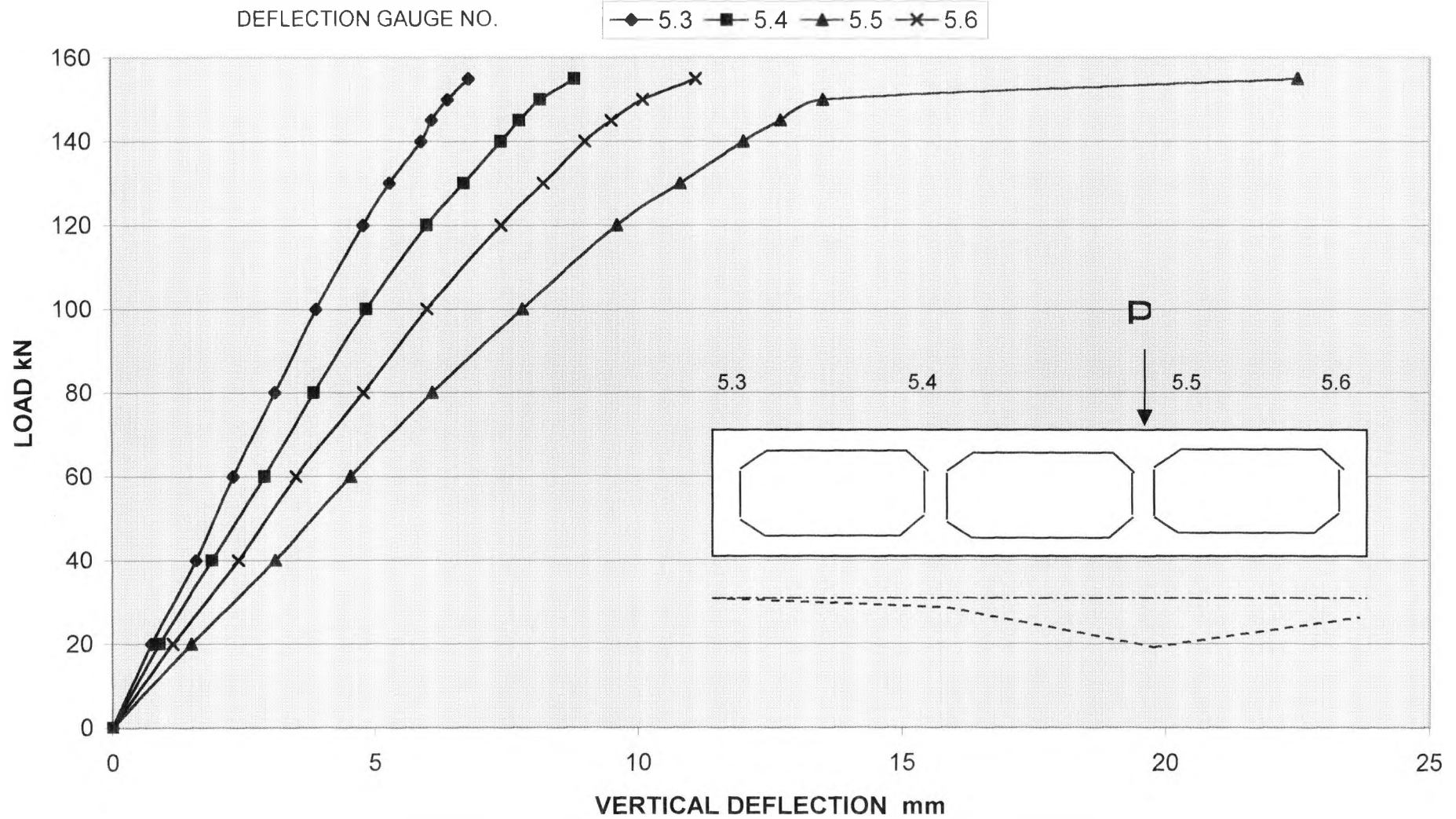


FIGURE 6.29 LOAD DEFLECTION CURVE AT CENTRE SECTION OF BEAM B3

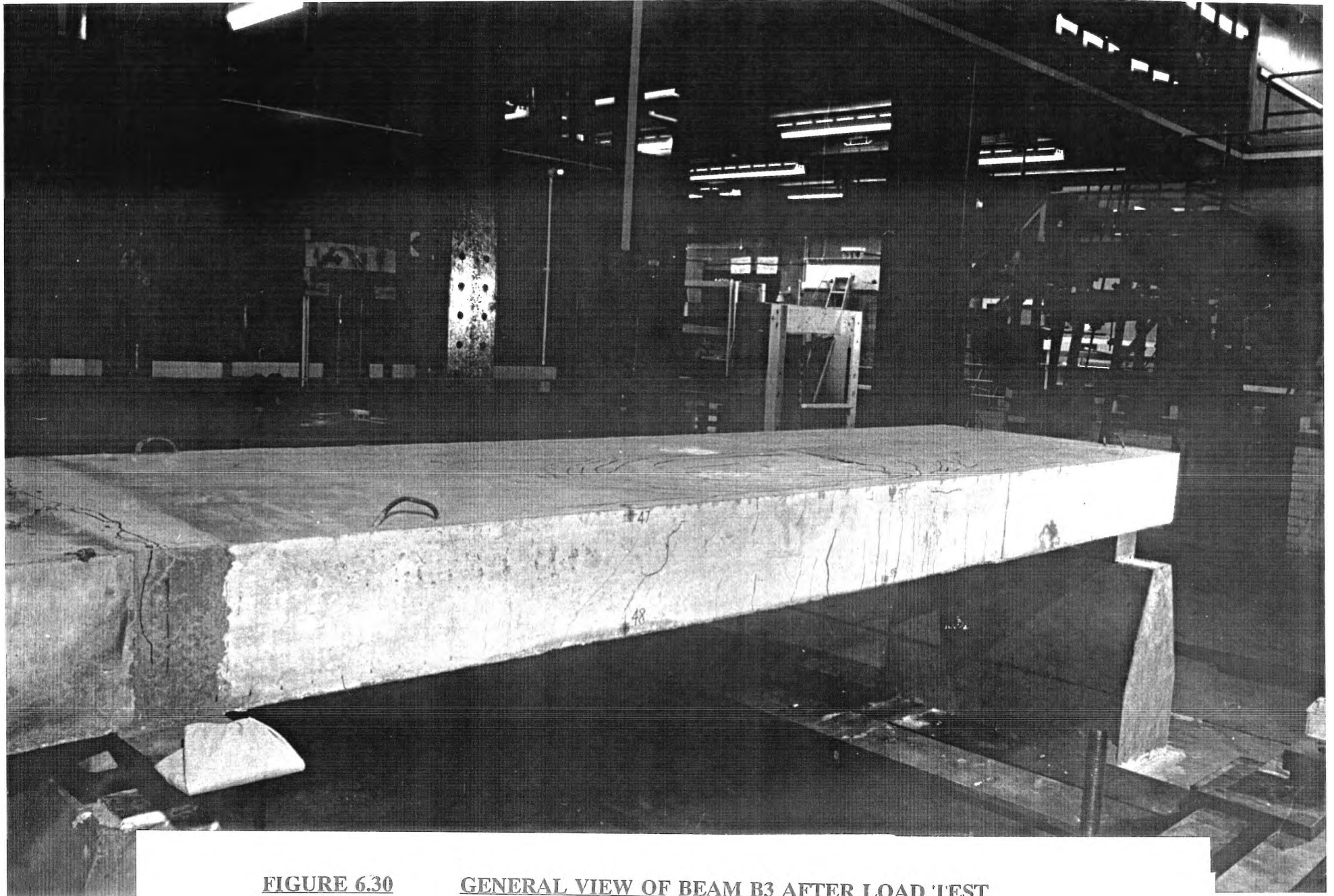


FIGURE 6.30

GENERAL VIEW OF BEAM B3 AFTER LOAD TEST

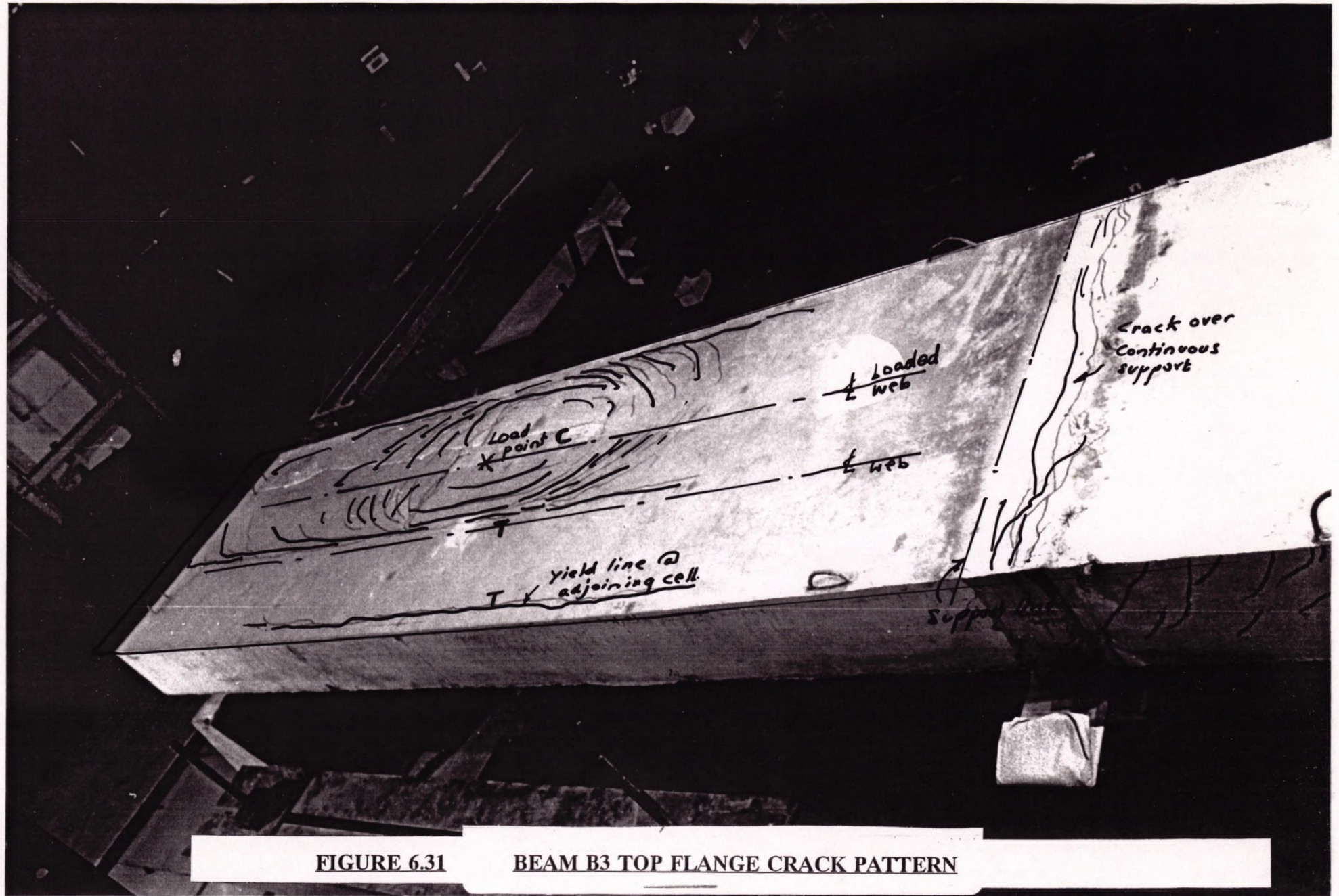


FIGURE 6.31

BEAM B3 TOP FLANGE CRACK PATTERN

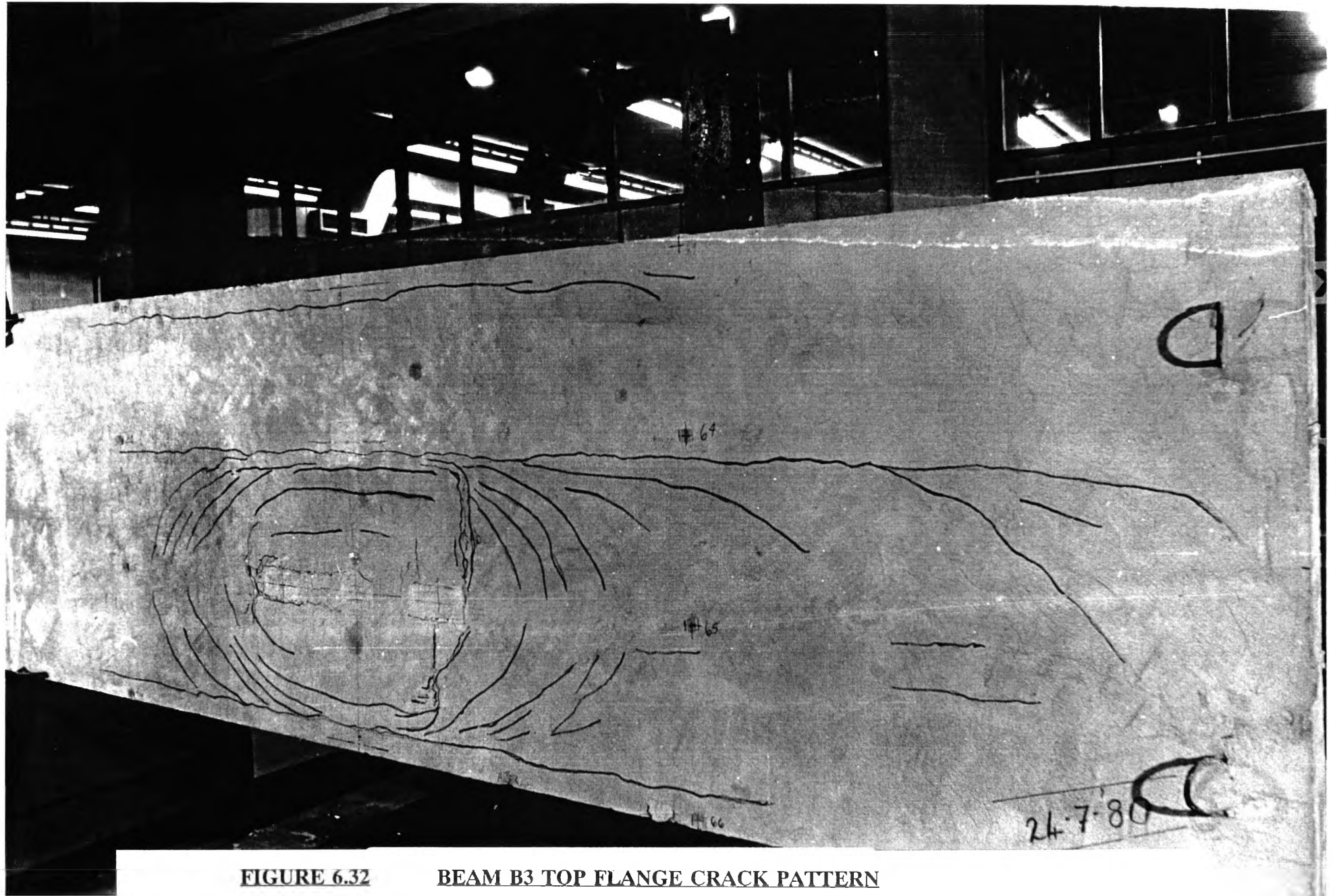


FIGURE 6.32 BEAM B3 TOP FLANGE CRACK PATTERN

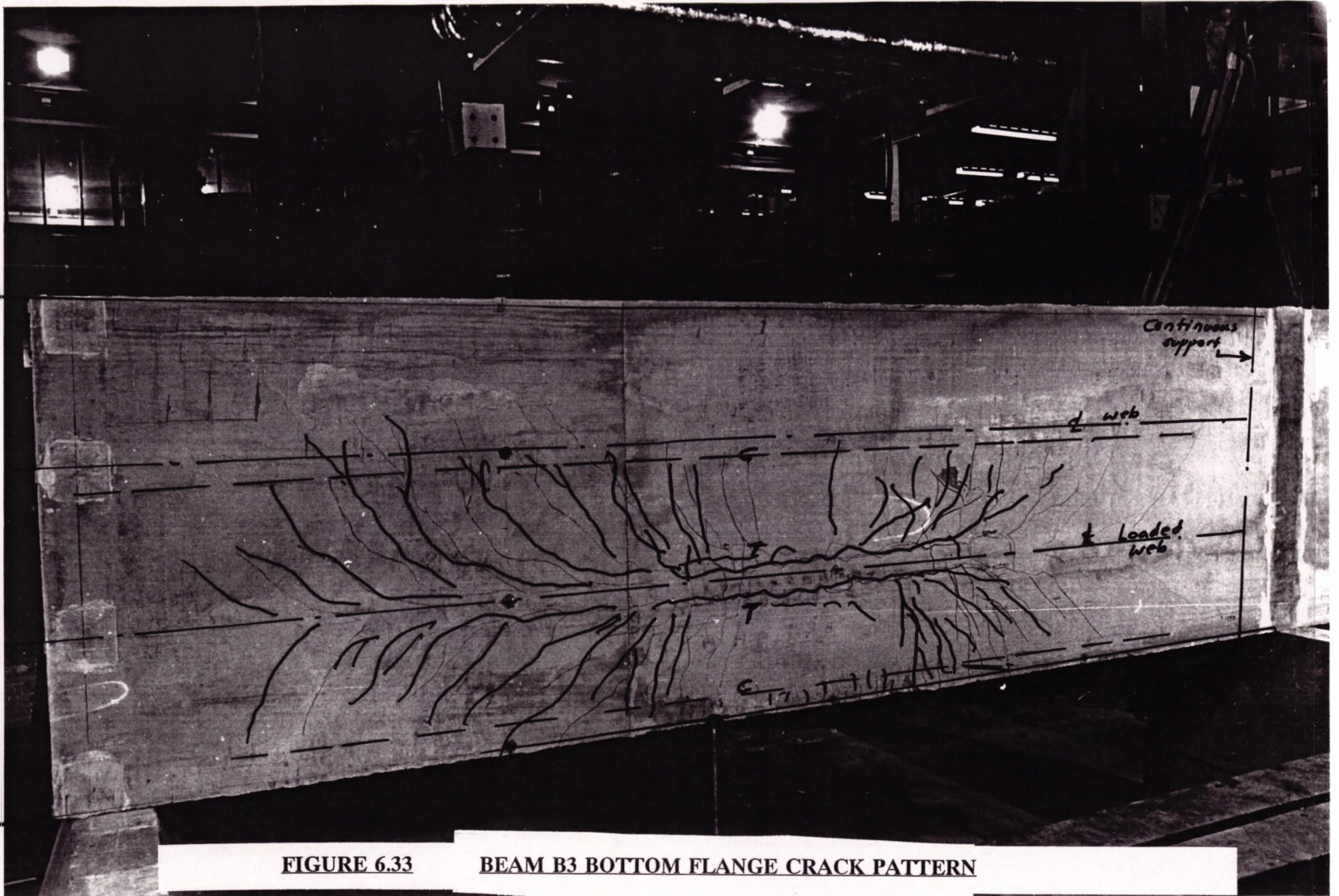


FIGURE 6.33

BEAM B3 BOTTOM FLANGE CRACK PATTERN

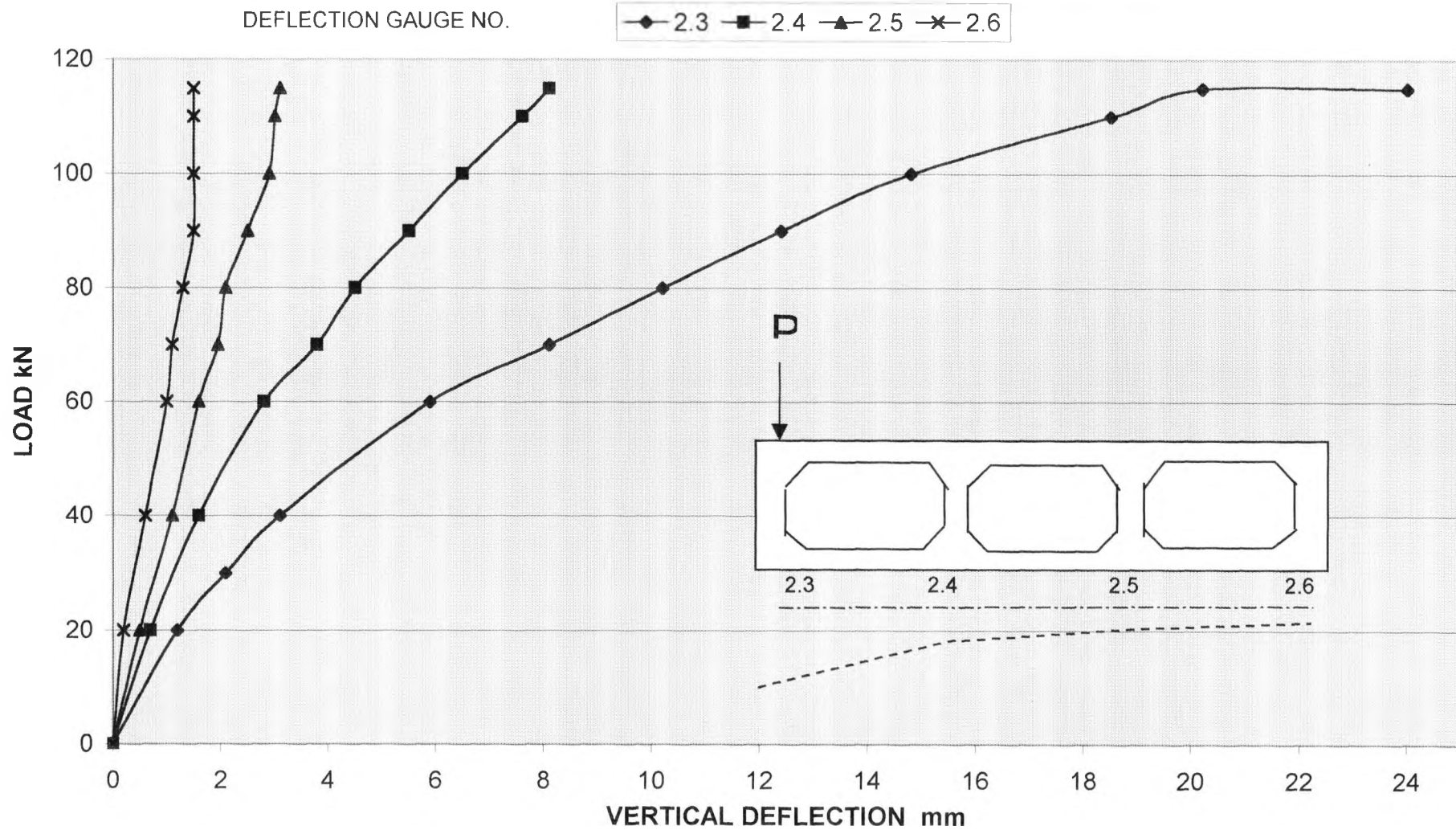


FIGURE 6.34 LOAD DEFLECTION CURVE AT CENTRE SECTION OF BEAM B3 LOAD AT EXTERNAL WEB

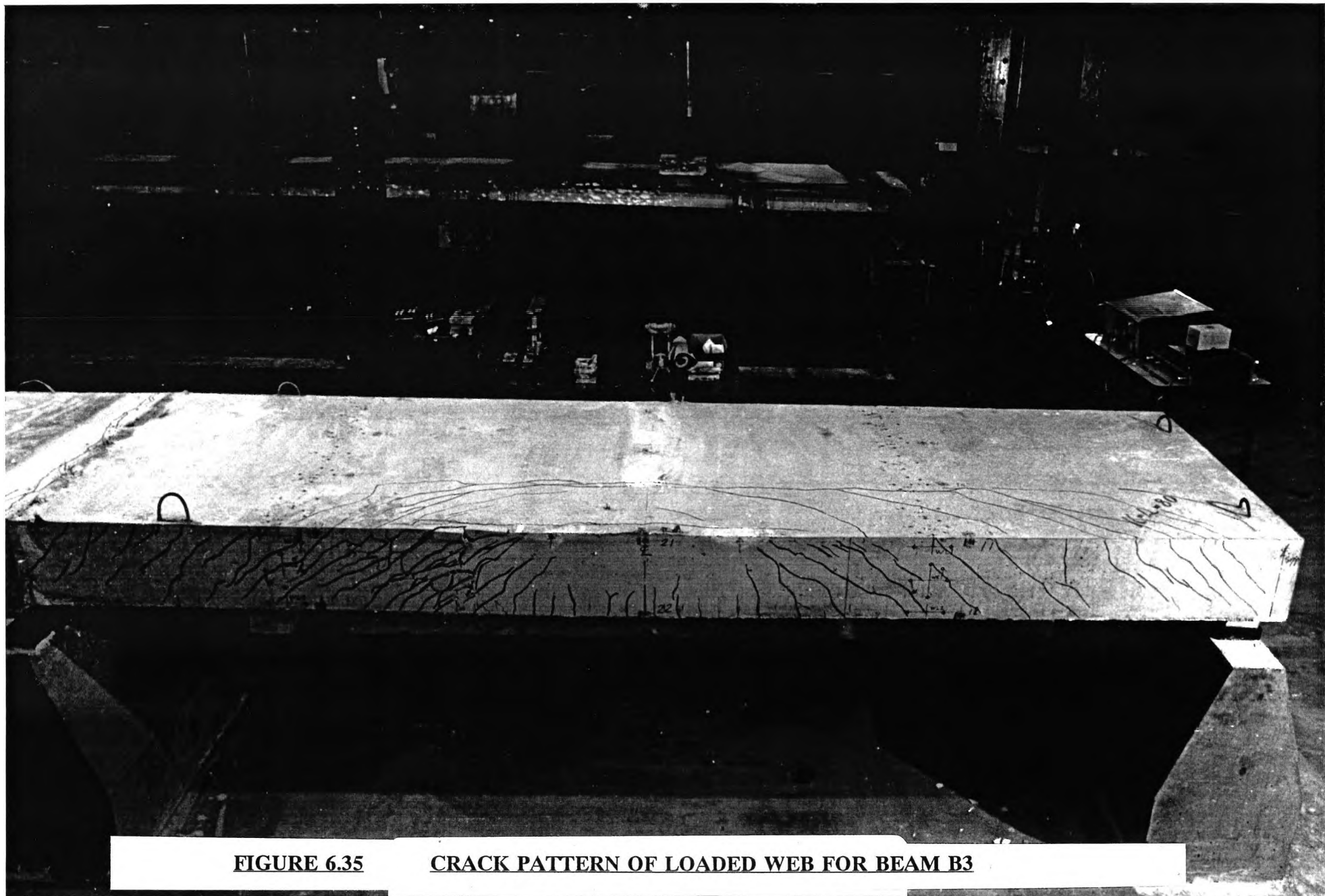


FIGURE 6.35

CRACK PATTERN OF LOADED WEB FOR BEAM B3

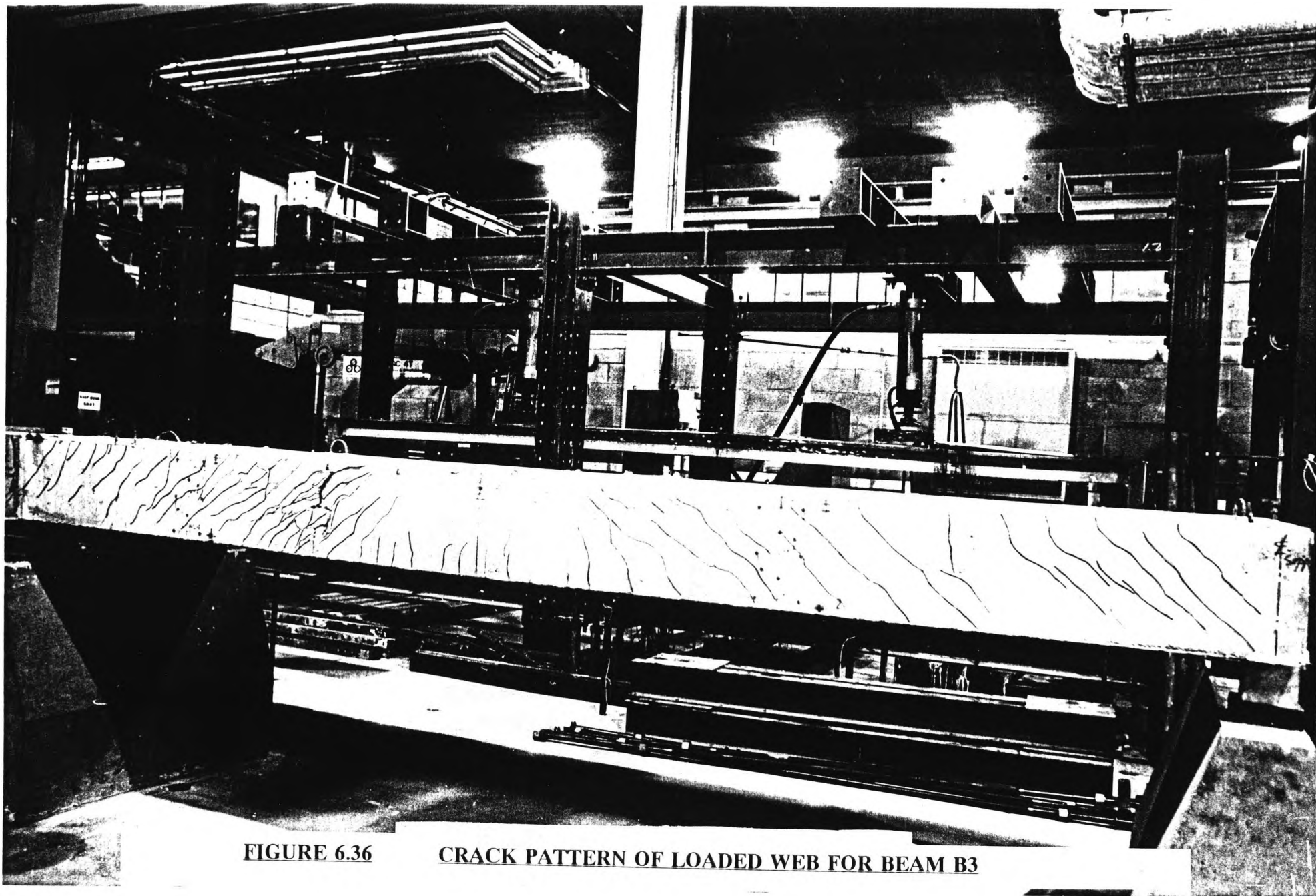


FIGURE 6.36

CRACK PATTERN OF LOADED WEB FOR BEAM B3

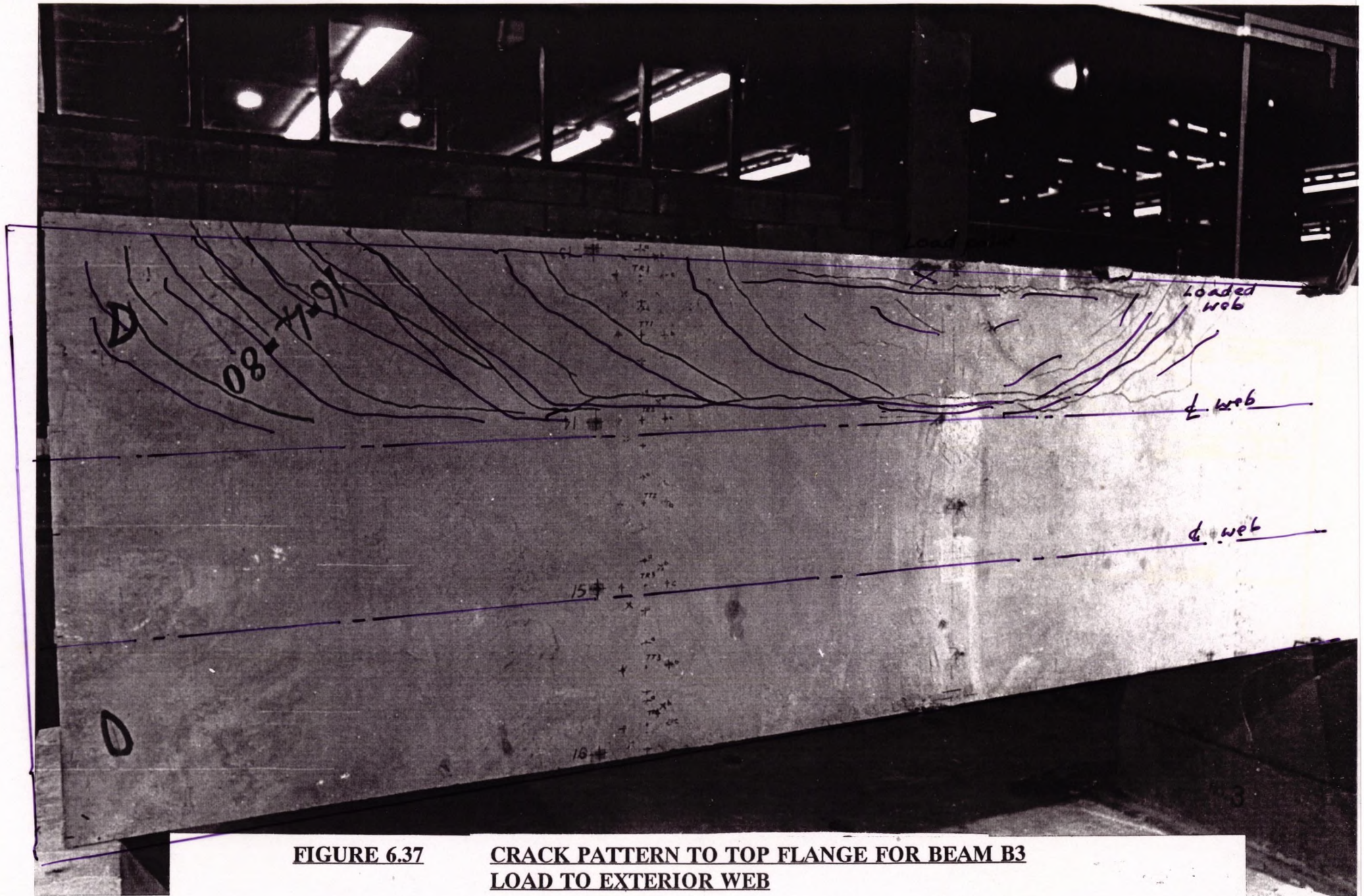


FIGURE 6.37

**CRACK PATTERN TO TOP FLANGE FOR BEAM B3
LOAD TO EXTERIOR WEB**

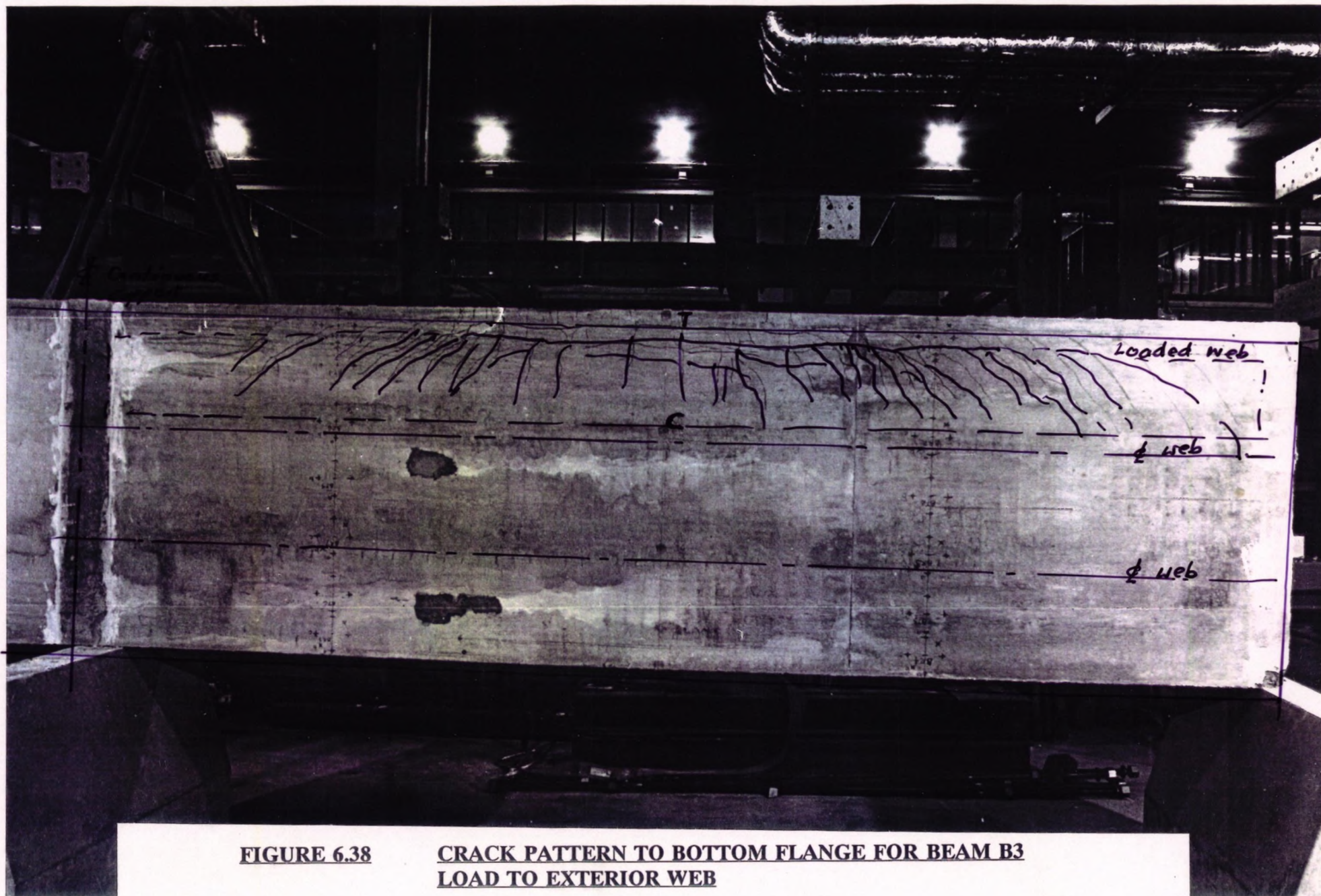


FIGURE 6.38

**CRACK PATTERN TO BOTTOM FLANGE FOR BEAM B3
LOAD TO EXTERIOR WEB**

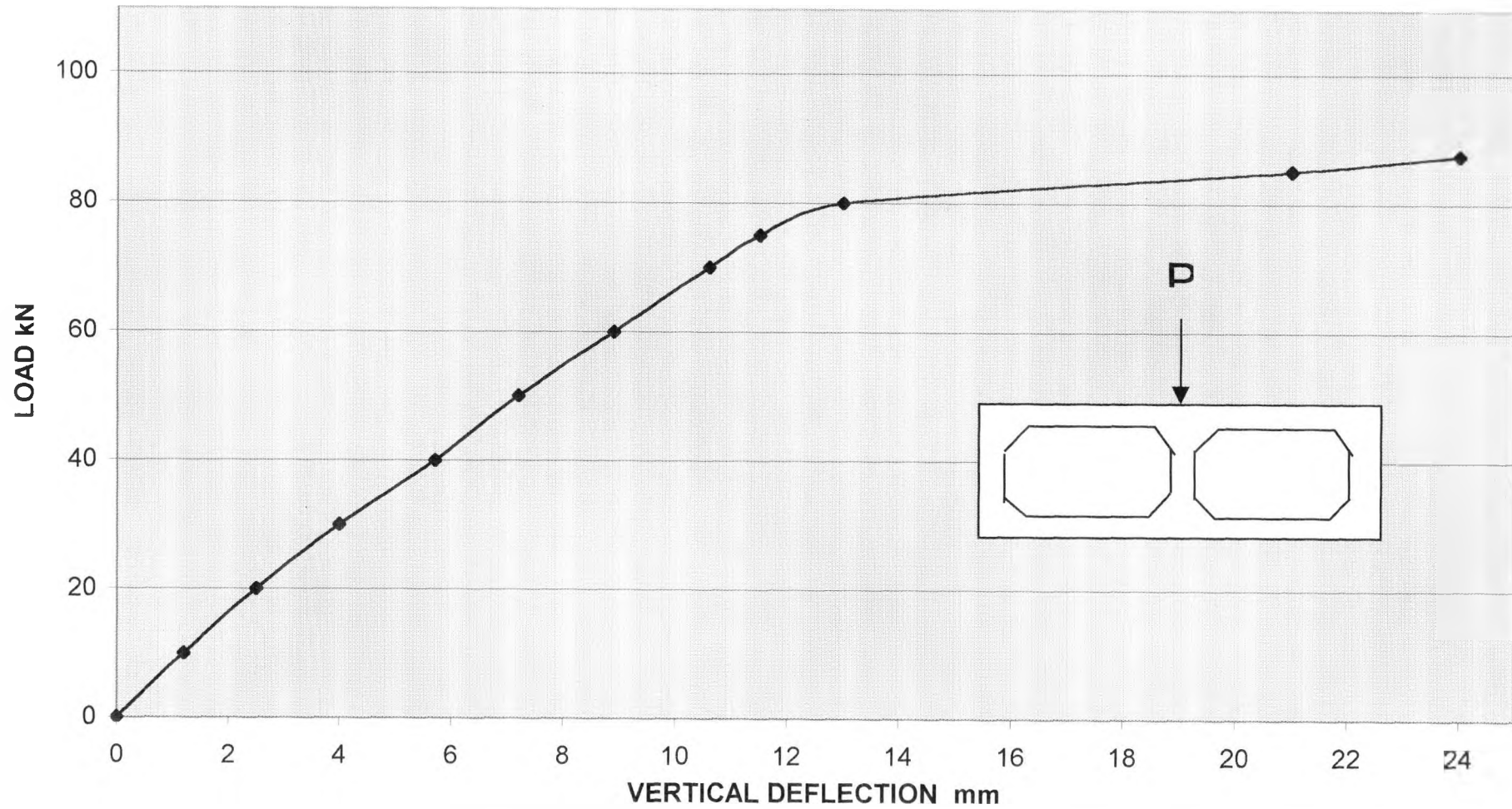


FIGURE 6.39 LOAD DEFLECTION CURVE AT CENTRE SECTION OF BEAM B4

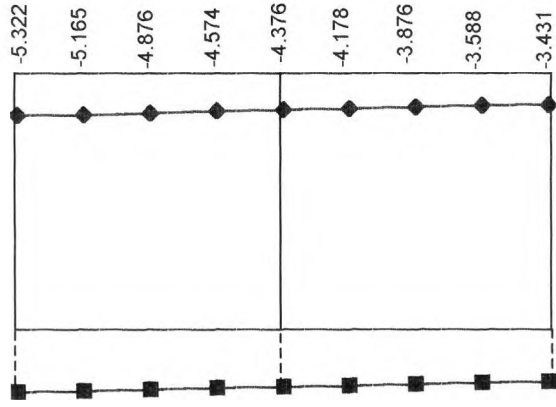
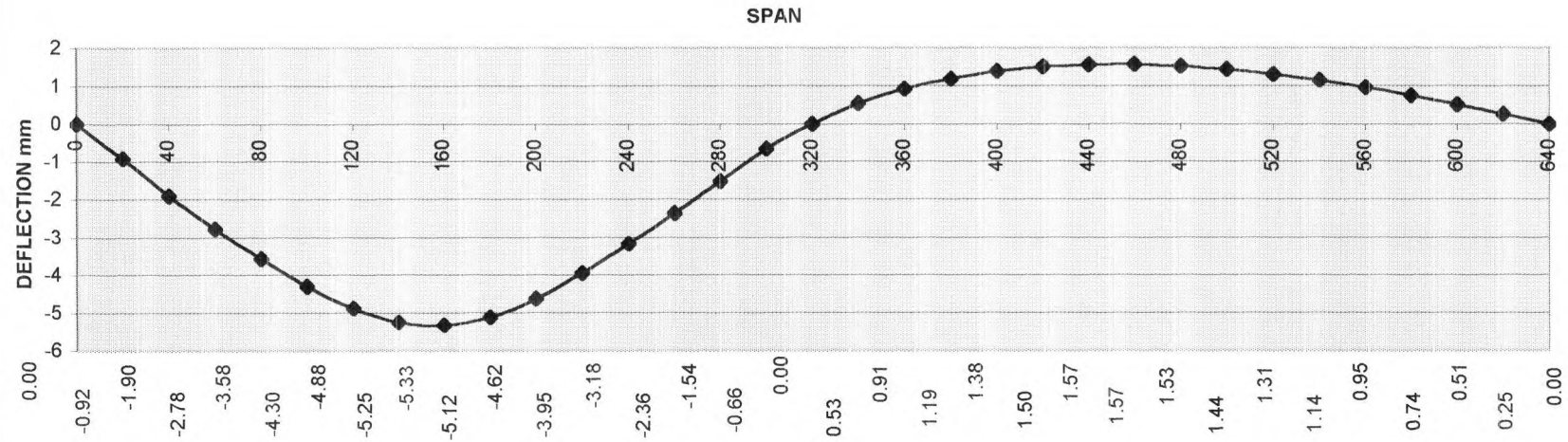


FIGURE 6.40 LONGITUDINAL AND TRANSVERSE DEFORMATION PROFILE OF BOX BEAM B4

Chapter 7 Conclusions

Experiments were carried out to investigate the ductility in shear for ordinary concrete and micro-concrete. The initial tests studied shear specimens subjected to direct shear as well as bending normal to the shear plane. The effects of size of aggregate, reinforcement variation and the size of specimens were studied. Under such stress resultants, shear specimens made from normal aggregates showed a shear strain behaviour that maintained their peak shear stress with considerable shear deformation. Those made from micro-concrete exhibited a peak and residual stress type behaviour. Whilst the peak stress matched that of normal concrete, the effective shear stress reduced to a lower residual value of about 55% of the peak stress after undergoing considerable large shear deformation. This behaviour was explained by the smaller concrete aggregate size limiting the capacity to transfer shear across and along cracks. Hence, a reduction in the effective shear strength could be expected. This aspect would be particularly important for micro-concrete small scale model structures subjected to ultimate load conditions. The effect of the size of the test specimens did not show significant differences except that practical difficulties would be experienced in handling and testing specimens that were too small. Any defects were disproportionately exaggerated and rendered the results unacceptable. The variation of reinforcement across the shear plane could affect the shear strength of the element in proportion to the total yield strength of the reinforcement. The difference of shear strength of the shear specimen when using different bar sizes was small, which confirmed the assumption of dowel action not being significant.

A modification factor was proposed to modify the shear component of a generalised yield criterion developed for concrete slab elements in ultimate load tests in which yield lines underwent large shear deformation.

The modified generalised yield criterion proposed could be applied to a yield line with general deformations that included in plane shear displacement and normal displacement as well as the Johanson's type bending rotation normal to the yield line. In developing the yield condition, both the concrete and reinforcing steel were assumed to be rigid plastic and to follow the flow and the

normality rules. The yield condition was expressed in a non-dimensional parametric form. A refinement of the parametric equation enabled the modified yield criterion to be applied to a wide range of deformation and stress resultants.

The parametric equation was extended to deal with reinforced and prestressed concrete slab elements. Provided that adequate bond and anchorage of the reinforcement were ensured, the effect of reinforcement could be treated as increasing the normal stress capacity of the concrete. This would enhance the resistance against the stress normal to the yield plane. The shear capacity increased as a result of the shear friction from the yielding of the reinforcement. In addition, where reinforcing steel crossed the yield plane at an angle, the component along the yield line would enhance further the shear capacity of the generalised yield line. Dowel action was considered not to contribute significantly to the shear strength in this type of test.

Prestressing was also treated as an increase of the reinforcement content in the ultimate load analysis. Under the rigid plastic rule, the internal work for the reinforcement, and prestressed reinforcement only started after yielding and was concentrated in the yield zones. In reality, prestressing enhanced the load deflection characteristic of the beam. Comparing with reinforced concrete, prestressed concrete elements would have a lower overall ductility. This was because some of the strain in the prestressing steel had already been taken up in the prestressing process.

The rigid plastic theory was used to simplify the computation of the stress resultants and internal work along the yield lines and yield regions. It would however, over estimate the collapse load for mechanisms involving distortion and shear discontinuity. In the final collapse stage, the collapse mechanism deformed along prescribed yield lines and plastic hinges, where the internal work due to the yield stress resultants were established from the yield conditions and the flow rule. The stress levels in the other non-yielding regions would not come into the work equation if the displacement rate rather than total displacement were considered. Hence, it was possible to compute the collapse load using the rigid plastic theory.

Under rigid plastic theory, no deformation occurs until the full mechanism has been developed. For a complex structure such as a box beam, various parts of the structure will be subjected to varying degrees of yielding and deformations prior to the complete formation of the full yield mechanism. Rigid plastic theory, therefore, can not predict the load deflection behaviour of the box beams, because large deformation will have to be experienced in some parts of the structure prior to the assumed complete collapse mechanism. Other collapse mode can develop earlier forming local failure mechanisms, which can give a considerably lower value of the failure load. Local punching shear failure was an example that occurred during some of the tests. This is one of the criticisms for upper bound solutions where it is possible to have other mechanisms that can give a lower collapse load. In order to ensure that the assumed mechanism can develop fully, local areas where high stress concentrations are expected should be reinforced accordingly. However, this can sometimes result in a less economical and impractical or some times even impossible design. In which case, the section size should be increased or geometry revised.

For a more accurate prediction of the deformation characteristic of box beams, materials can be assumed to behave as an elastic plastic medium with stress strain behaviour similar to those proposed in the current design codes for concrete and steel. The process will be much more complicated as the full history of the development of the yield zones have to be traced throughout the loading profile from initial loading to final collapse.

For the ultimate load analysis of the box beams in the experiments, appropriate collapse mechanisms were chosen. Work equations were set up along yield lines and yield zones. Where possible, these were balanced against the external work of the applied load. The self-weight of the structure were ignored for simplicity, but could be included in the work equation. The stress resultants along and across the yield lines could be determined from the parametric equations. However, they may not provide an overall equilibrium condition with the external applied load. If static equilibrium was achieved between the stress resultants and the applied load, the lowest predicted collapse load for the particular mechanism for the structure could be considered to have occurred.

For the multi-span beam experiments, the horizontal restraint offered by the adjoining span was limited since the beams were supported on roller or sliding bearings to allow for shrinkage and thermal movement. In prototype bridges, longitudinal restraint is usually provided at one end of the supports to resist longitudinal forces from vehicle braking and acceleration. A result of the lack of longitudinal restraint is that the arching actions cannot fully develop. The effect of the longitudinal restraining forces from the adjoining spans is usually small and does not influence significantly the overall collapse load. In consequence, for continuous beams, as long as the work equation includes the yield lines over the support regions, the collapse load can be assessed without due regard to the restraining effect.

To maintain geometric compatibility of the collapse mechanism, some of the flange and web elements in the box beams twisted under the collapse condition. The twisting work was relatively small compared to bending and shear. Hence, neglecting the twisting work did not affect significantly the prediction of the collapse load. An alternative is to introduce additional diagonal yield lines to simulate the twisting deformation.

Four multi-box girder models were tested. Upper bound collapse loads for each model were predicted from these collapse mechanisms. The collapse mechanisms proposed were concentrated within the flange and web areas in the cells adjacent to the load point because of the simple concentrated loading applied over one of the web at a time. Hence, two of the models were only idealised structures with local internal and external cells, respectively. The proposed collapse mechanism involved distortion of the local cells and various yield lines and rigid non-yielding regions. The results showed good agreement with the shear distortion mode incorporating the modification for shear ductility. The predicted collapse load for the prestressed beam was low because of poor workmanship in the preparation of the beam model. Its stiffness was much lower than an equivalent reinforced beam. The construction problems that could exist in slabs with a high concentration of reinforcement and prestressing tendons has been demonstrated on the difficulties encountered with testing this specimen. The experiment demonstrated the importance of good workmanship in preparing the beam for prestressing and in the good compaction of concrete around the

prestressing cables and anchorages. A further modification was introduced for the efficiency of prestressing to allow for some correlation of the results.

With the current advancement in computing, further research can be carried out to study the collapse behaviour of complex structures. If the materials are assumed to be perfectly elastic-plastic rather than rigid plastic, deformation could be allowable in the modelling. By discretising the structure into smaller elements, and increasing the load in small increments, the regions where stresses are highest would indicate first yielding. The boundary conditions are then modified to incorporate the new yield hinges or deformation zones. In these yield regions, ignoring strain hardening, the stress resultants would remain at the yield level and not increase under further deformation. The external applied load would be increased to determine the new high stress regions so as to establish the new yield zones. At each stage, except at the region where the material has reached yield, material in all other areas would still behave elastically. This would allow the tracking and the gradual development of the yield regions in the structure. The process can then be repeated until the full collapse mechanism is achieved. At that stage, further increase of load would not be possible whilst allowing continuing deformation of structure.

In conclusion, reasonable collapse loads can be predicted by rigid plastic theory, when the behaviour of the material under large deformation is taken into account. More work needs to be done to provide true collapse behaviour of box girder structures.

References

Birkeland P & Birkeland H, (1966) Connection in Precast Construction (Shear Friction Hypothesis), ACI, Vol 63, March 66, P345-368.

Braestrup M, (1974), Plastic Analysis of Shear in Reinforced Concrete, MCR, Dec 74, Vol 26, p221-228.

Braestrup M, (1970), Yield Line Theory and Limit Analysis of Plates and Slabs, MCR, June 70, Vol 22, p99-105.

Braestrup M, Effect of Main Steel Strength on The Shear Capacity of Reinforced Concrete Beams with Stirrups. Report R 110, Technical University of Denmark.

BS8110: Pt 1, (1985), Structural use of Concrete. British Standard Institution.

Calladine C, Engineering Plasticity, Pergamon Press.

Calladine C, (1973), A Plastic Theory For Collapse of Plate Girders Under Combined Shearing Forces and Bending Moments, I Struct E, Vol 54, April 73, p147-154.

Campbell T, Chitnuyanondh L & Batchelor B de V, (1980), Rigid Plastic Theory Versus Truss Analogy Method for Calculating the Shear Strength of Reinforced Concrete. MCR March 80, p39-44.

Chapman J, Dowlings P, Lim P & Billington C, (1971), The structural Behavior of steel & concrete Box Girder Bridges, I Struct E, Vol 49, March 71, p111-116.

Chen W F, (1975), Limit Analysis and Soil Plasticity. Elsevier Scientific Publishing Co. Amsterdam Netherland, 1975.

Clarke L, (1974), Flexural Crack Similitude in Slabs Spanning One-way, C&CA Report, Oct 74, 42.496

Cook C F, Demountable Portable strain transducers, C & CA internal literature Ref.DR/INST/6.

Cookson P J, (1976), Collapse of Concrete Box Girders Involving Distortion of The Cross Section. PhD Thesis Cambridge University.

Cope P J & Rao P V, (1977), Non-Linear Finite Element Analysis of Concrete Slab Structure, ICE Pt 2, March 77, p159-179.

Davis R E et al, (1972), Model & Prototype Studies of Box Girder Bridges, ASCE ST1, Jan 72, p165-183.

Duncan & Johnarry, (1979), Further Studies On The Constant Stiffness Method of Non-Linear Analysis of Concrete Structure, ICE Pt 2, Dec 79, p951-969.

Dupuch G W, (1979), The Use of Physical Models in The Design of Offshore Structures, Micro-concrete Data Sheet, I Struct E /BRE Seminar, Nov 79.

Edwards A D, (1977), The Structural Behavior of a Prestressed Box Beam with Thin Webs Under Combine Bending & Shear, ICE Pt 2, March 77, p123-135.

Evans H R & Rifaie W N, (1975), An Experimental & Theoretical Investigation of The Behavior of Box Girders Curved in Plan, ICE Pt 2, June 75, p323-353.

Fernando J & Kemp K, (1975), The Strip Method of Slab Design, Unique or Lower Bound Solution ?, MCR, Vol 27, MCR, Vol 27, March 75, p23-29.

Fernando J & Kemp K, (1978), A Generalized Strip Deflection Method of R.C. Slab Design, ICE Pt 2, March 78, p163-174.

Gambarova P G, (1981), On Aggregate Interlock Mechanism In Reinforced Concrete Plates With Extensive Cracking, IABSE, 1981

Gibson J & Mitwally M, (1976), An Experimental and Theoretical Investigation of Model Box Beams In Perspex and Micro-concrete, I Struct E, April 76, p147-151.

Hamadi Y D & Regan P, (1980), Behavior in Shear of Beams With Flexural Cracks. MCR, June 80, p67-78.

Hambly, Pannells, (1975), Grillage Analysis applied to Cellular Bridge Deck, I Struct E, July 75, p267.

Hobbs D, Pomeroy C & Newman J, (1977), Design Stress for Concrete Structure Subject to Multi-axial Stresses, I Struct E, April 77.

Hodge P, Plastic Analysis of Structures, Mcgrall Hill

Hofbeck I, Ibrahim I & Mattock A, (1969), Shear Transfer In Reinforced Concrete, ACI Feb 69, p119-128.

Huslid J & rockey K, (1979), The Influence of End Post Rigidity on the Collapse Behavior of Plate Girders. PICE, June 79, p285-312.

IABSE Colloquium, Kopenhagen 1979, Plasticity in Reinforced Concrete. IABSE.

Ingerslav Age, (1923), The Strength of Rectangular Slab. I Struct E, Vol 1, 1923, p3-14.

Jain S.C. and Kennedy J (1974) Yield Criterion for reinforced slabs, ASCE, Vol.100, ST3 p631.

Janas M, (1968), Large Plastic deformation of R C Slabs, Int J Solid Structures, 1968, Vol 4, p61-74.

Janas M, (1973), Arching Action in Elastic Plastic Plates, J Struct Mec, Jan 73, p277-293.

Janas M, (1963), Limit Analysis of Non-symmetric Plastic Shells by a Generalized Yield Line Method, IASS Symposium, Warsaw, 63.

Janas M, (1967), Kinematically Compatibility Problems in Yield Line Theory, MCR, Vol 19, Mar 67, p33-44.

Janas M & Sawczuk A, (1966), Influence of Position of Lateral Restraints on carrying capacity of Plates. Archiwum.

Johansen K W, Yield Line Theory, English Translation of "Brudlinieteorier", København 1943, C & C A.

Johnson R P, (1962), Strength Test on Scale Down Concrete Suitable For Models With a Note on Mix Design. MCR, Vol 14, 62, p47-53.

Johnson R P & Arneonti C, Punching Shear Strength of Concrete Slab Subjected to In-plane Bi-axial Tension. MCR March 80, p45-50.

Jones L, (1965), The Use of Nodal Forces in Yield Line Analysis, (Recent Developments in Yield Line Theory), MCR, Special Publ. May, 65.

Jones L, (1965), Ultimate Load Analysis of Reinforced and Prestressed Concrete Structures, Chatto & Windus.

Jones L & Wood R H, Yield Line Analysis of Slab, Thames & Hudson, Chatto & Windus.

Kemp K, (1965), The Evaluation of Nodal & Edge Forces in Yield Line Theory. (Recent Developments in Yield Line Theory), MCR, Special Publication, May 65.

Kotsovos M D, (1979), A Mathematical Description of The Strength Properties of Concrete Under Generalized Stress. MCR, Sept 79, p151-158.

Kristek V, (1974), Influence of Actual Physical Characteristic of Material on The Behavior of Box Girders. ACTA Tech 1976.

Kwiencinski, (1965), Test on Yield Criterion of Reinforced Concrete Slab. MCR , Sept 65.

Lampert P, (1972), Torsion & Bending in Reinforced and Prestressed Concrete Members. ICE Pt2, Dec 71, p487-505.

Maisel B & Roll F, Method of Analysis and Design of Concrete Box Beams With Side Cantilevers. C & C A Tech Report, p42-49.

Maisel B, Rowe R & Swann R, (1973), Concrete Box Girder Bridges. I Struct E, Oct 73, Vol 51, p363-376.

Maisel B & Swann R, The Design of Concrete Box Spine Beam Bridges. CIRIA Report 52.

Massonnet C, (1967), Complete Solutions Describing The Limit State of R C Slabs. MCR, Vol 19, No.58, Mar 67, p13-32.

Mattock A H, Chen K C & Soongswang K, (1976), The Behavior of Reinforced Concrete Corbels. PCI Journal, March 76, p52-77.

Mattock A H, Li W K & Wang T C, (1976), Shear Transfer in Lightweight Reinforced Concrete. PCI Jan 76, p20-39.

Mattock A H & Hawkins N, (1972), Shear Transfer in Reinforced Concrete Recent Research. PCI Journal, Mar 72.

Mattock A H , Johal L & Chow H, (1975), Shear Transfer in Reinforced Concrete With Moment or Tension Acting Across the Shear Plane. PCI Journal, July 75.

Mills G, (1975), A Partial Kinking Yield Criterion For Reinforced Concrete Slab. MCR, Vol 27, No 90, Mar 75, p13-22.

Morley C T, (1965), Equilibrium Methods for Least Upper Bounds of Rigid Plastic Plates. MCR, Special Publication, May 65.

Morley C T, (1970), Optimum Reinforcement of Concrete Slab Elements Against Combinations of Moment and Membrane Forces. MCR, Vol 22 Sept 70, p155-162.

Morley C T & Spence R., Ultimate Strength of Cellular Concrete Box Beams. TRRL Supp Report 164 UC, p193-197.

Morley C T & Spence R., (1974), Research on Cellular Concrete Box Beams Tech Report, TR 44 1974, Cambridge University.

Neilsen M P, (1965), A New Nodal-force Theory. MCR, Special Publication, May 65.

Neilsen M P, Limit Analysis of Reinforced Concrete Slab, ACTA, Polytechnica, Scandinavica, C E & Building Construction Series, No. 26.

Neilsen M P, Braestrup M, Jensen B. & Bach F, Concrete Plasticity, Beam Shear, Shear in Joints, Punching Shear. Dennish Society for Structural Science and Engineering. Structure Research Lab.

Neilsen M P & Braestrup M, (1978), Shear Strength of Prestressed Concrete Beams Without Web Reinforcement. MCR, Sept 78.

Park R, (1963), Ultimate Strength of Rectangular Concrete Slab Under Short-term Uniform Loading with Edge Restrained Against Lateral Movement. ICE, May 63.

Prager W, (1952), The General Theory of Limit Design. Proceedings of the 8th International Congress on theoretical and Applied Mechanics, Istanbul, Vol. II 1955, p.65.

Preece B & Davis J, Models for Structural Concrete. CR Books Ltd.

Prince M & Kemp K, (1968), A New Approach to The Yield Criterion for Isotropically Reinforced Concrete slab. MCR, Vol20, March, 68, p13-20.

Regan P & Placas A, (1970), Limit State Design for Shear in Rectangular and T Beams, MCR, Vol 22, No 73, Dec 70, p147-208.

Rajendran S, (1972), The Strength of Reinforced Concrete Slab Elements PhD Thesis, Cambridge, 1972.

Rajendran S & C T Morley, (1974), A General Yield Criterion for Reinforced Concrete Slab Elements, MCR, Vol 26, Dec 74, P212-220.

Raths C H, (1977), Discussion of paper " Design proposal For Reinforced Concrete Corbels" PCI March 77, p93-98.

Richmond B, (1965), Twisting of Thin Wall Box Girders. ICE Vol 33, 1965, p659-675.

Rockey K, Developments in Bridge Design and Construction, Crosby Lockwood.

Rowe R & Base G, (1965), Model Analysis & testing as a Design Tool. ICE 1965.

Roy S & Mukhopadhyay, (1978), Prestressed Concrete T Beams Under Combined Bending, Torsion and Shear. ICE, Sept, 78.

Save M, (1967), A Consistent Limit Analysis Theory for Reinforced Concrete Slab. MCR, Vol 19, No 58, March 67, p3-12

Save M & Massonnet C, Plastic Analysis and Design of Plates Shells & Disks, North Holland Publ. Comp. Amsterdam.

Scordelis A C, (1975), Analytical & Experimental Studies of Multi-cell Concrete Box Girder Bridges. Bulletin of Int. Ass. of Shell & Spatial Structure No 58, April, 75.

Scordelis A C Bouwkamp J & Wasti S, Structural Behavior of a Two Span Reinforced Concrete Box Girder Bridge Model, Vol I, II, III. U C SESM 71.

Scordelis A C, Bouwkamp J & Wasti S, (1973), Structural Response of Concrete Box Girder Bridges, ASCE ST10,73, p2031-2048.

Scordelis A C, Davis & Lo, Load Distribution in Concrete Box Girder Bridges, ACI Publ. SP23 Proceeding 1st Int. Symposium on Concrete Bridges Design, Canada.

Scordelis A C, Larsen P & Elfgren L, (1977), Ultimate Strength of Curved Reinforced Concrete Box Girder Bridge. ASCE ST8, Aug 77, p1507-1524.

Scordelis A C & Larsen P , (1977), Structural Response of Curved Reinforced Concrete Box Girder Bridge, ASCE ST8, Aug 77, p1525-1542.

Shaikh A F, (1978), Proposed Revision to Shear Friction Provision. PCI March 78, p12-21.

Skaloud M, (1974), Failure Mechanism of Webs Loaded in Shear. ACTA Tech. 1974.

Somerville G, Roll F & Galdwell J, Test on a 1/12 Scale Model of The Mancunian Way. C & C A. TRA 394.

Spence R J, (1973), The Strength of Concrete Box Girder Bridge Deck of Deformable Cross-section. PhD Thesis, University of Cambridge, 1973.

Spence R J & Morley C T, (1975), The Strength of Single Cell concrete Box Girders of Deformable Cross Section. ICE Pt 2, Dec 75.

Swann R, (1970), The Construction and Testing of a 1/16 Scale Model For the Prestressed Concrete Super-structure of Section 5, Western Avenue Extension. C & C A TRA, 1970 p441.

Swann R, (1972), A feature survey of concrete box spine beam bridges, C & CA Technical report

Swann R & Williams A, (1973), Combined Loading Tests on Model Prestressed Concrete Box Beams Reinforced With Steel Mesh. C & CA Tech Report 42, 1973.

Taylor H P J, (1970), Investigation of The Forces Carried Across Cracks in Reinforced Concrete Beams in Shear By Interlock of Aggregate. C & C A, Tech Report, Nov 70.

Taylor H P J & Clements S, (1969), Test on a 1/9 Scale Model of a Transverse Section of The West-gate Bridge, Melbourne. C & C A TRA, 1969.

Templement A B & Winterbottom S, (1979), Optimum Design of Concrete Cellular Spine Beam Bridge Deck. PICE, June 79, p389-409.

Trikha D N & Edwards A, (1972), Analysis of Concrete Box Girders Before And After Cracking. ICE Pt2, Dec 72, P515-528.

Walraven J, Vos E & Reinhardt H, (1978), Experiments on Shear Transfer in Cracked Concrete. IASS Symposium, July, 78.

Williams R O, Cassell A & Boswell, (1992), A computer design aid for prestressed concrete box beams. Proceedings of the Institution of Civil Engineers Structures and Buildings Vol. 98 1992.

Wood R H & Armer, (1970), The Strip Method For Designing Slab. BRE Current Paper, Dec 70, CP 39/70.

Wood R H, (1965), New Technique in Nodal Force Theory For Slab. (Recent Developments in Yield Line Theory). MCR Special Report, May 65.

Wood R H, (1978), Plastic Composite Action and Collapse Design of Unreinforced Shear Wall Panels in Frames. ICE Pt 2 June 1978, p381-411.

Wright R, Abdel-Samad S & Robinson A, (1978), Beam on Elastic Foundation, Analogy for Analysis of Box Girders. ASCE ST7, 78. p1719-1743.

Additional reference is included in Appendix C. It is an update of more recent design and research development in shear, yield criteria in reinforced concrete and box girder bridge design.

APPEXDIX A

Summary of parametric stress resultants

| | $\beta \neq \delta$ | $\beta = \delta$ |
|-----------------------------|---|---|
| Normal Force n_n | $\frac{1}{2} \left[\frac{X}{(\beta-\delta)} - 1 \right]$ | $\frac{1}{2} \left[\frac{\beta}{\sqrt{\beta^2 + a^2}} - 1 \right]$ |
| Shear Force n_{nt} | $\frac{a^2 U}{2(\beta-\delta)}$ | $\frac{a^2}{2\sqrt{\beta^2 + a^2}}$ |
| Normal Moment m_n | $\frac{2}{(\beta-\delta)^2} [\phi - U \cdot a^2 - (\beta+\delta) \cdot X]$ | 0 |
| Tangential Force n_t | $\frac{1}{2} \left[\frac{X(1-2a^2)}{(\beta-\delta)} - 1 \right]$ | $\frac{1}{2} \left[\frac{\beta(1-2a^2)}{\sqrt{\beta^2+a^2}} + 1 \right]$ |
| Tangent. Moment m_t | $\frac{2}{(\beta-\delta)^2} [\phi - U \cdot a^2 - (\beta+\delta)X] (1-2a^2)$ | 0 |
| Twisting Moment m_{tw} | $\frac{4a^2}{(\beta-\delta)^2} \left[X - \frac{(\beta+\delta)}{2} \cdot U \right]$ | 0 |

Where: $n_n = N_n / \sigma_{ch}$; $n_{nt} = N_{nt} / \sigma_{ch}$; $m_n = M_n / (\sigma_{ch}^2 / 8)$

$n_t = N_t / \sigma_{ch}$; $m_t = M_t / (\sigma_{ch}^2 / 8)$; $m_{tw} = M_{tw} / (\sigma_{ch}^2 / 8)$

$$X = \sqrt{\beta^2 + a^2} - \sqrt{\delta^2 + a^2}$$

$$U = \log_e \frac{\beta + \sqrt{\beta^2 + a^2}}{\delta + \sqrt{\delta^2 + a^2}}$$

$$\phi = \beta \sqrt{\beta^2 + a^2} - \delta \sqrt{\delta^2 + a^2}$$

$$\beta = \frac{Y_{top} - \varepsilon_n + k_n \cdot h / 2}{2e_{nt}} \quad \text{strain ratio at top.}$$

$$\delta = \frac{Y_{bot} - \varepsilon_n - k_n \cdot h / 2}{2e_{nt}} \quad \text{strain ratio at bottom.}$$

$$\frac{m_n^2}{[4n_n(1+n_n)]^2} + \frac{n_{nt}^2}{-a^2 n_n(1+n_n)} = \Phi_1 \text{ -----3.63}$$

$$\frac{m_n}{-4n_n(1+n_n)} + \frac{n_{nt}^2}{-2a^2 n_n(1+n_n)} = \Phi_3 \text{ -----3.64}$$

$$\frac{m_n^2}{2[-4n_n(1+n_n)]^2} + \frac{n_{nt}}{a\sqrt{[-n_n(1+n_n)]}} = \Phi_4 \text{ -----3.65}$$

$$\frac{m_n^2}{[4n_n(1+n_n)]^2} + \frac{n_{nt}^2}{-a^2 n_n(1+n_n)} + \frac{m_n n_{nt}^2}{48a^2 n_n^3 (1+n_n)^3} = \Phi_2 \text{ -----3.66}$$

$\delta = \text{constant} = \text{Cot } 5^\circ$

| α | θ | β | δ | X | U | ϕ | n_n | n_{nt} | m_n | m_{tw} | n_t | m_t | ϕ_1 | ϕ_2 | ϕ_3 | ϕ_4 |
|----------|----------|---------|----------|--------|-------|---------|-------|----------|-------|----------|-------|-------|----------|----------|----------|----------|
| .55 | 5 | 11.43 | 11.43 | .00 | .00 | .00 | -.001 | .013 | .000 | -.000 | -.303 | .000 | 1.000 | 1.000 | .501 | 1.000 |
| .55 | 10 | 5.67 | 11.43 | -5.75 | -.70 | -98.48 | -.001 | .018 | -.001 | .008 | -.303 | -.000 | 1.013 | .996 | .709 | 1.006 |
| .55 | 15 | 3.73 | 11.43 | -7.67 | -1.11 | -116.72 | -.002 | .022 | -.003 | .016 | -.303 | -.001 | 1.030 | .992 | .808 | 1.014 |
| .55 | 20 | 2.75 | 11.43 | -8.64 | -1.42 | -123.10 | -.002 | .025 | -.004 | .022 | -.303 | -.002 | 1.044 | .989 | .867 | 1.019 |
| .55 | 25 | 2.14 | 11.43 | -9.23 | -1.66 | -126.05 | -.003 | .027 | -.006 | .028 | -.304 | -.002 | 1.056 | .988 | .906 | 1.022 |
| .55 | 30 | 1.73 | 11.43 | -9.63 | -1.86 | -127.65 | -.004 | .029 | -.008 | .034 | -.304 | -.003 | 1.065 | .987 | .935 | 1.024 |
| .55 | 35 | 1.43 | 11.43 | -9.91 | -2.05 | -128.61 | -.004 | .031 | -.011 | .039 | -.304 | -.004 | 1.073 | .987 | .956 | 1.024 |
| .55 | 40 | 1.19 | 11.43 | -10.13 | -2.21 | -129.23 | -.005 | .033 | -.013 | .044 | -.305 | -.005 | 1.079 | .988 | .973 | 1.024 |
| .55 | 45 | 1 | 11.43 | -10.30 | -2.37 | -129.65 | -.006 | .034 | -.016 | .049 | -.305 | -.006 | 1.084 | .989 | .986 | 1.022 |
| .55 | 50 | .84 | 11.43 | -10.44 | -2.52 | -129.95 | -.007 | .036 | -.020 | .054 | -.305 | -.008 | 1.088 | .990 | .997 | 1.019 |
| .55 | 55 | .70 | 11.43 | -10.55 | -2.67 | -130.17 | -.008 | .038 | -.024 | .059 | -.306 | -.009 | 1.091 | .992 | 1.007 | 1.016 |
| .55 | 60 | .58 | 11.43 | -10.65 | -2.81 | -130.34 | -.010 | .039 | -.028 | .064 | -.306 | -.011 | 1.093 | .994 | 1.014 | 1.011 |
| .55 | 65 | .47 | 11.43 | -10.72 | -2.96 | -130.46 | -.011 | .041 | -.033 | .069 | -.307 | -.013 | 1.095 | .996 | 1.021 | 1.006 |
| .55 | 70 | .36 | 11.43 | -10.78 | -3.11 | -130.56 | -.013 | .042 | -.040 | .074 | -.308 | -.016 | 1.096 | .998 | 1.026 | .999 |
| .55 | 75 | .27 | 11.43 | -10.83 | -3.26 | -130.63 | -.015 | .044 | -.047 | .080 | -.308 | -.019 | 1.096 | 1.000 | 1.030 | .992 |
| .55 | 80 | .18 | 11.43 | -10.87 | -3.41 | -130.69 | -.017 | .046 | -.056 | .085 | -.309 | -.022 | 1.095 | 1.002 | 1.033 | .983 |
| .55 | 85 | .09 | 11.43 | -10.89 | -3.57 | -130.75 | -.020 | .048 | -.067 | .091 | -.310 | -.026 | 1.094 | 1.004 | 1.035 | .974 |
| .55 | 90 | 0 | 11.43 | -10.89 | -3.73 | -130.80 | -.023 | .049 | -.079 | .096 | -.312 | -.031 | 1.092 | 1.006 | 1.036 | .963 |
| .55 | 95 | -.09 | 11.43 | -10.89 | -3.89 | -130.84 | -.027 | .051 | -.093 | .102 | -.313 | -.037 | 1.090 | 1.007 | 1.037 | .952 |
| .55 | 100 | -.18 | 11.43 | -10.87 | -4.04 | -130.90 | -.032 | .053 | -.110 | .107 | -.315 | -.043 | 1.087 | 1.009 | 1.037 | .940 |
| .55 | 105 | -.27 | 11.43 | -10.83 | -4.20 | -130.96 | -.037 | .054 | -.128 | .111 | -.317 | -.051 | 1.084 | 1.010 | 1.037 | .928 |
| .55 | 110 | -.36 | 11.43 | -10.78 | -4.35 | -131.04 | -.043 | .056 | -.149 | .116 | -.319 | -.059 | 1.080 | 1.011 | 1.036 | .916 |
| .55 | 115 | -.47 | 11.43 | -10.72 | -4.50 | -131.13 | -.049 | .057 | -.173 | .119 | -.322 | -.068 | 1.077 | 1.012 | 1.035 | .903 |
| .55 | 120 | -.58 | 11.43 | -10.65 | -4.64 | -131.26 | -.057 | .058 | -.199 | .122 | -.325 | -.078 | 1.073 | 1.013 | 1.034 | .891 |
| .55 | 125 | -.70 | 11.43 | -10.55 | -4.79 | -131.42 | -.065 | .060 | -.228 | .125 | -.328 | -.090 | 1.070 | 1.013 | 1.033 | .878 |
| .55 | 130 | -.84 | 11.43 | -10.44 | -4.94 | -131.64 | -.075 | .061 | -.260 | .126 | -.332 | -.103 | 1.066 | 1.013 | 1.031 | .865 |
| .55 | 135 | -1 | 11.43 | -10.30 | -5.09 | -131.94 | -.086 | .062 | -.297 | .127 | -.336 | -.117 | 1.062 | 1.013 | 1.030 | .852 |
| .55 | 140 | -1.19 | 11.43 | -10.13 | -5.24 | -132.36 | -.099 | .063 | -.340 | .127 | -.341 | -.134 | 1.058 | 1.014 | 1.028 | .839 |
| .55 | 145 | -1.43 | 11.43 | -9.91 | -5.41 | -132.98 | -.115 | .064 | -.389 | .125 | -.348 | -.154 | 1.054 | 1.013 | 1.026 | .824 |
| .55 | 150 | -1.73 | 11.43 | -9.63 | -5.59 | -133.94 | -.134 | .064 | -.449 | .122 | -.356 | -.177 | 1.050 | 1.013 | 1.024 | .809 |
| .55 | 155 | -2.14 | 11.43 | -9.23 | -5.80 | -135.54 | -.160 | .065 | -.522 | .116 | -.366 | -.206 | 1.045 | 1.013 | 1.022 | .791 |
| .55 | 160 | -2.75 | 11.43 | -8.64 | -6.04 | -138.49 | -.195 | .064 | -.613 | .106 | -.380 | -.242 | 1.040 | 1.012 | 1.020 | .772 |
| .55 | 165 | -3.73 | 11.43 | -7.67 | -6.34 | -144.87 | -.247 | .063 | -.730 | .088 | -.400 | -.288 | 1.034 | 1.011 | 1.017 | .748 |
| .55 | 170 | -5.67 | 11.43 | -5.75 | -6.76 | -163.11 | -.332 | .060 | -.875 | .057 | -.434 | -.346 | 1.027 | 1.009 | 1.013 | .717 |
| .55 | 175 | -11.43 | 11.43 | .00 | -7.46 | -261.59 | -.500 | .049 | -.993 | -.000 | -.500 | -.392 | 1.017 | 1.007 | 1.009 | .672 |

$\delta = \text{constant} = \text{Cot } 10^\circ$

| α | θ | β | δ | X | U | ϕ | n_n | n_{nt} | m_n | m_{tw} | n_t | m_t | ϕ_1 | ϕ_2 | ϕ_3 | ϕ_4 |
|----------|----------|---------|----------|-------|-------|---------|-------|----------|-------|----------|-------|-------|----------|----------|----------|----------|
| .55 | 5 | 11.43 | 5.67 | 5.75 | .70 | 98.50 | -.001 | .018 | .001 | -.008 | -.303 | .000 | 1.013 | .996 | .709 | 1.006 |
| .55 | 10 | 5.67 | 5.67 | .00 | .00 | .01 | -.002 | .027 | .000 | -.000 | -.303 | .000 | 1.000 | 1.000 | .500 | 1.000 |
| .55 | 15 | 3.73 | 5.67 | -1.92 | -.42 | -18.22 | -.004 | .032 | -.002 | .009 | -.304 | -.001 | 1.005 | .998 | .630 | 1.002 |
| .55 | 20 | 2.75 | 5.67 | -2.89 | -.72 | -24.60 | -.005 | .037 | -.004 | .017 | -.304 | -.002 | 1.013 | .996 | .714 | 1.007 |
| .55 | 25 | 2.14 | 5.67 | -3.48 | -.96 | -27.55 | -.006 | .041 | -.007 | .026 | -.305 | -.003 | 1.023 | .993 | .773 | 1.011 |
| .55 | 30 | 1.73 | 5.67 | -3.88 | -1.16 | -29.15 | -.007 | .045 | -.011 | .033 | -.305 | -.004 | 1.032 | .991 | .818 | 1.015 |
| .55 | 35 | 1.43 | 5.67 | -4.17 | -1.35 | -30.11 | -.009 | .048 | -.015 | .041 | -.306 | -.006 | 1.041 | .989 | .854 | 1.018 |
| .55 | 40 | 1.19 | 5.67 | -4.38 | -1.51 | -30.74 | -.011 | .051 | -.020 | .049 | -.307 | -.008 | 1.049 | .988 | .883 | 1.020 |
| .55 | 45 | 1 | 5.67 | -4.56 | -1.67 | -31.16 | -.012 | .054 | -.025 | .056 | -.307 | -.010 | 1.056 | .987 | .908 | 1.022 |
| .55 | 50 | .84 | 5.67 | -4.69 | -1.82 | -31.46 | -.014 | .057 | -.031 | .064 | -.308 | -.012 | 1.063 | .987 | .929 | 1.024 |
| .55 | 55 | .70 | 5.67 | -4.81 | -1.97 | -31.68 | -.016 | .060 | -.038 | .071 | -.309 | -.015 | 1.070 | .987 | .947 | 1.024 |
| .55 | 60 | .58 | 5.67 | -4.90 | -2.11 | -31.84 | -.019 | .063 | -.046 | .079 | -.310 | -.018 | 1.075 | .988 | .963 | 1.024 |
| .55 | 65 | .47 | 5.67 | -4.98 | -2.26 | -31.96 | -.022 | .066 | -.055 | .087 | -.311 | -.022 | 1.080 | .988 | .977 | 1.023 |
| .55 | 70 | .36 | 5.67 | -5.04 | -2.41 | -32.06 | -.025 | .069 | -.067 | .096 | -.313 | -.026 | 1.085 | .989 | .989 | 1.021 |
| .55 | 75 | .27 | 5.67 | -5.08 | -2.56 | -32.14 | -.029 | .072 | -.080 | .104 | -.314 | -.032 | 1.089 | .991 | 1.000 | 1.018 |
| .55 | 80 | .18 | 5.67 | -5.12 | -2.71 | -32.20 | -.034 | .075 | -.096 | .113 | -.316 | -.038 | 1.092 | .993 | 1.009 | 1.014 |
| .55 | 85 | .09 | 5.67 | -5.14 | -2.87 | -32.25 | -.040 | .078 | -.115 | .121 | -.318 | -.045 | 1.094 | .994 | 1.017 | 1.009 |
| .55 | 90 | 0 | 5.67 | -5.15 | -3.03 | -32.30 | -.046 | .081 | -.137 | .129 | -.321 | -.054 | 1.095 | .997 | 1.023 | 1.003 |
| .55 | 95 | -.09 | 5.67 | -5.14 | -3.19 | -32.35 | -.054 | .084 | -.162 | .137 | -.324 | -.064 | 1.096 | .999 | 1.028 | .995 |
| .55 | 100 | -.18 | 5.67 | -5.12 | -3.34 | -32.40 | -.062 | .087 | -.191 | .144 | -.327 | -.076 | 1.096 | 1.001 | 1.032 | .987 |
| .55 | 105 | -.27 | 5.67 | -5.08 | -3.50 | -32.46 | -.072 | .089 | -.223 | .150 | -.331 | -.088 | 1.095 | 1.003 | 1.034 | .978 |
| .55 | 110 | -.36 | 5.67 | -5.04 | -3.65 | -32.54 | -.083 | .091 | -.259 | .154 | -.335 | -.102 | 1.093 | 1.005 | 1.036 | .968 |
| .55 | 115 | -.47 | 5.67 | -4.98 | -3.80 | -32.64 | -.095 | .094 | -.297 | .158 | -.340 | -.117 | 1.091 | 1.006 | 1.037 | .958 |
| .55 | 120 | -.58 | 5.67 | -4.90 | -3.94 | -32.76 | -.108 | .096 | -.339 | .160 | -.345 | -.134 | 1.089 | 1.008 | 1.037 | .947 |
| .55 | 125 | -.70 | 5.67 | -4.81 | -4.09 | -32.92 | -.123 | .097 | -.384 | .160 | -.351 | -.152 | 1.086 | 1.009 | 1.037 | .936 |
| .55 | 130 | -.84 | 5.67 | -4.69 | -4.24 | -33.14 | -.139 | .098 | -.434 | .158 | -.358 | -.171 | 1.083 | 1.010 | 1.037 | .925 |
| .55 | 135 | -1 | 5.67 | -4.56 | -4.39 | -33.44 | -.159 | .099 | -.487 | .155 | -.365 | -.192 | 1.080 | 1.011 | 1.036 | .912 |
| .55 | 140 | -1.19 | 5.67 | -4.38 | -4.54 | -33.86 | -.181 | .100 | -.546 | .149 | -.374 | -.216 | 1.076 | 1.012 | 1.035 | .899 |
| .55 | 145 | -1.43 | 5.67 | -4.17 | -4.71 | -34.49 | -.207 | .100 | -.611 | .140 | -.384 | -.241 | 1.072 | 1.013 | 1.033 | .885 |
| .55 | 150 | -1.73 | 5.67 | -3.88 | -4.89 | -35.45 | -.238 | .100 | -.682 | .127 | -.396 | -.269 | 1.067 | 1.013 | 1.032 | .869 |
| .55 | 155 | -2.14 | 5.67 | -3.48 | -5.10 | -37.05 | -.277 | .099 | -.761 | .109 | -.412 | -.300 | 1.062 | 1.014 | 1.030 | .851 |
| .55 | 160 | -2.75 | 5.67 | -2.89 | -5.34 | -40.00 | -.328 | .096 | -.845 | .084 | -.432 | -.334 | 1.056 | 1.013 | 1.027 | .830 |
| .55 | 165 | -3.73 | 5.67 | -1.92 | -5.64 | -46.38 | -.398 | .091 | -.926 | .048 | -.460 | -.366 | 1.048 | 1.013 | 1.024 | .805 |
| .55 | 170 | -5.67 | 5.67 | .00 | -6.06 | -64.61 | -.500 | .081 | -.976 | -.000 | -.500 | -.386 | 1.039 | 1.012 | 1.019 | .770 |
| .55 | 175 | -11.43 | 5.67 | 5.75 | -6.76 | -163.10 | -.668 | .060 | -.875 | -.057 | -.566 | -.346 | 1.027 | 1.009 | 1.013 | .717 |

$\delta = \text{constant} = \text{Cot } 15^\circ$

| α | θ | β | δ | X | U | ϕ | n_n | n_{nt} | m_n | m_{tw} | n_t | m_t | ϕ_1 | ϕ_2 | ϕ_3 | ϕ_4 |
|----------|----------|---------|----------|-------|-------|---------|-------|----------|-------|----------|-------|-------|----------|----------|----------|----------|
| .55 | 5 | 11.43 | 3.73 | 7.67 | 1.12 | 116.73 | -.002 | .022 | .003 | -.016 | -.303 | .001 | 1.030 | .992 | .808 | 1.014 |
| .55 | 10 | 5.67 | 3.73 | 1.93 | .42 | 18.25 | -.004 | .032 | .002 | -.009 | -.304 | .001 | 1.005 | .998 | .631 | 1.002 |
| .55 | 15 | 3.73 | 3.73 | .00 | .00 | .02 | -.005 | .040 | .000 | -.000 | -.305 | .000 | 1.000 | 1.000 | .500 | 1.000 |
| .55 | 20 | 2.75 | 3.73 | -.97 | -.30 | -6.36 | -.007 | .046 | -.003 | .009 | -.305 | -.001 | 1.002 | .999 | .596 | 1.001 |
| .55 | 25 | 2.14 | 3.73 | -1.56 | -.54 | -9.32 | -.009 | .052 | -.007 | .018 | -.306 | -.003 | 1.008 | .997 | .667 | 1.004 |
| .55 | 30 | 1.73 | 3.73 | -1.95 | -.75 | -10.92 | -.011 | .057 | -.011 | .027 | -.307 | -.004 | 1.015 | .995 | .722 | 1.007 |
| .55 | 35 | 1.43 | 3.73 | -2.24 | -.93 | -11.88 | -.013 | .061 | -.016 | .036 | -.308 | -.006 | 1.022 | .994 | .767 | 1.010 |
| .55 | 40 | 1.19 | 3.73 | -2.46 | -1.10 | -12.50 | -.016 | .065 | -.022 | .045 | -.309 | -.009 | 1.029 | .992 | .804 | 1.013 |
| .55 | 45 | .1 | 3.73 | -2.63 | -1.25 | -12.92 | -.018 | .069 | -.029 | .054 | -.310 | -.011 | 1.036 | .990 | .836 | 1.016 |
| .55 | 50 | .84 | 3.73 | -2.77 | -1.40 | -13.22 | -.021 | .073 | -.037 | .064 | -.311 | -.015 | 1.044 | .989 | .865 | 1.019 |
| .55 | 55 | .70 | 3.73 | -2.88 | -1.55 | -13.44 | -.025 | .077 | -.046 | .073 | -.312 | -.018 | 1.051 | .988 | .890 | 1.021 |
| .55 | 60 | .58 | 3.73 | -2.97 | -1.70 | -13.60 | -.029 | .081 | -.057 | .083 | -.314 | -.023 | 1.058 | .987 | .912 | 1.023 |
| .55 | 65 | .47 | 3.73 | -3.05 | -1.84 | -13.73 | -.033 | .085 | -.070 | .093 | -.315 | -.028 | 1.064 | .987 | .932 | 1.024 |
| .55 | 70 | .36 | 3.73 | -3.11 | -1.99 | -13.82 | -.038 | .089 | -.086 | .103 | -.317 | -.034 | 1.071 | .987 | .950 | 1.024 |
| .55 | 75 | .27 | 3.73 | -3.16 | -2.14 | -13.90 | -.044 | .094 | -.104 | .114 | -.320 | -.041 | 1.076 | .988 | .966 | 1.024 |
| .55 | 80 | .18 | 3.73 | -3.19 | -2.30 | -13.96 | -.051 | .098 | -.126 | .124 | -.323 | -.050 | 1.082 | .989 | .981 | 1.023 |
| .55 | 85 | .09 | 3.73 | -3.21 | -2.45 | -14.01 | -.059 | .102 | -.151 | .134 | -.326 | -.060 | 1.086 | .990 | .993 | 1.020 |
| .55 | 90 | 0 | 3.73 | -3.22 | -2.61 | -14.06 | -.068 | .106 | -.181 | .144 | -.329 | -.072 | 1.090 | .991 | 1.004 | 1.017 |
| .55 | 95 | -.09 | 3.73 | -3.21 | -2.77 | -14.11 | -.079 | .110 | -.215 | .152 | -.334 | -.085 | 1.093 | .993 | 1.012 | 1.012 |
| .55 | 100 | -.18 | 3.73 | -3.19 | -2.93 | -14.17 | -.091 | .113 | -.253 | .159 | -.339 | -.100 | 1.095 | .995 | 1.019 | 1.007 |
| .55 | 105 | -.27 | 3.73 | -3.16 | -3.08 | -14.23 | -.105 | .117 | -.295 | .165 | -.344 | -.117 | 1.096 | .997 | 1.025 | 1.000 |
| .55 | 110 | -.36 | 3.73 | -3.11 | -3.23 | -14.30 | -.120 | .119 | -.341 | .168 | -.350 | -.135 | 1.096 | .999 | 1.029 | .993 |
| .55 | 115 | -.47 | 3.73 | -3.05 | -3.38 | -14.40 | -.137 | .122 | -.389 | .170 | -.356 | -.154 | 1.096 | 1.001 | 1.032 | .985 |
| .55 | 120 | -.58 | 3.73 | -2.97 | -3.53 | -14.52 | -.155 | .124 | -.440 | .169 | -.364 | -.174 | 1.095 | 1.003 | 1.035 | .976 |
| .55 | 125 | -.70 | 3.73 | -2.88 | -3.67 | -14.69 | -.175 | .125 | -.494 | .166 | -.372 | -.195 | 1.093 | 1.005 | 1.036 | .967 |
| .55 | 130 | -.84 | 3.73 | -2.77 | -3.82 | -14.91 | -.197 | .127 | -.551 | .160 | -.380 | -.218 | 1.091 | 1.007 | 1.037 | .956 |
| .55 | 135 | -.1 | 3.73 | -2.63 | -3.97 | -15.20 | -.222 | .127 | -.610 | .151 | -.390 | -.241 | 1.088 | 1.008 | 1.037 | .945 |
| .55 | 140 | -1.19 | 3.73 | -2.46 | -4.13 | -15.63 | -.250 | .127 | -.672 | .139 | -.401 | -.265 | 1.085 | 1.009 | 1.037 | .933 |
| .55 | 145 | -1.43 | 3.73 | -2.24 | -4.30 | -16.25 | -.283 | .126 | -.736 | .123 | -.414 | -.291 | 1.082 | 1.011 | 1.037 | .920 |
| .55 | 150 | -1.73 | 3.73 | -1.95 | -4.48 | -17.21 | -.321 | .124 | -.801 | .102 | -.429 | -.317 | 1.077 | 1.012 | 1.035 | .905 |
| .55 | 155 | -2.14 | 3.73 | -1.56 | -4.68 | -18.81 | -.368 | .121 | -.865 | .076 | -.448 | -.342 | 1.072 | 1.013 | 1.034 | .887 |
| .55 | 160 | -2.75 | 3.73 | -.97 | -4.92 | -21.76 | -.425 | .115 | -.921 | .042 | -.470 | -.364 | 1.066 | 1.013 | 1.031 | .867 |
| .55 | 165 | -3.73 | 3.73 | .00 | -5.23 | -28.14 | -.500 | .106 | -.954 | -.000 | -.500 | -.377 | 1.059 | 1.014 | 1.028 | .840 |
| .55 | 170 | -5.67 | 3.73 | 1.93 | -5.64 | -46.38 | -.603 | .091 | -.926 | -.049 | -.540 | -.366 | 1.048 | 1.013 | 1.024 | .805 |
| .55 | 175 | -11.43 | 3.73 | 7.67 | -6.34 | -144.86 | -.753 | .063 | -.730 | -.088 | -.600 | -.288 | 1.034 | 1.011 | 1.017 | .748 |

$\delta = \text{constant} = \text{Cot } 20^\circ$

| α | θ | β | δ | χ | U | ϕ | n_n | n_{nt} | m_n | m_{tw} | n_t | m_t | ϕ_1 | ϕ_2 | ϕ_3 | ϕ_4 |
|----------|----------|---------|----------|--------|-------|---------|-------|----------|-------|----------|-------|-------|----------|----------|----------|----------|
| .55 | 5 | 11.43 | 2.75 | 8.64 | 1.42 | 123.08 | -.002 | .025 | .004 | -.022 | -.303 | .002 | 1.044 | .989 | .867 | 1.019 |
| .55 | 10 | 5.67 | 2.75 | 2.89 | .72 | 24.60 | -.005 | .037 | .004 | -.017 | -.304 | .002 | 1.013 | .996 | .714 | 1.006 |
| .55 | 15 | 3.73 | 2.75 | .97 | .30 | 6.37 | -.007 | .046 | .003 | -.009 | -.305 | .001 | 1.002 | .999 | .596 | 1.001 |
| .55 | 20 | 2.75 | 2.75 | -.00 | -.00 | -.01 | -.010 | .054 | -.000 | .000 | -.306 | -.000 | 1.000 | 1.000 | .500 | 1.000 |
| .55 | 25 | 2.14 | 2.75 | -.59 | -.24 | -2.96 | -.012 | .061 | -.004 | .010 | -.307 | -.002 | 1.002 | .999 | .578 | 1.001 |
| .55 | 30 | 1.73 | 2.75 | -.99 | -.45 | -4.56 | -.015 | .067 | -.009 | .019 | -.308 | -.003 | 1.005 | .998 | .640 | 1.003 |
| .55 | 35 | 1.43 | 2.75 | -1.27 | -.63 | -5.53 | -.018 | .072 | -.015 | .029 | -.310 | -.006 | 1.011 | .997 | .691 | 1.005 |
| .55 | 40 | 1.19 | 2.75 | -1.49 | -.80 | -6.15 | -.021 | .077 | -.022 | .039 | -.311 | -.009 | 1.016 | .995 | .734 | 1.008 |
| .55 | 45 | 1 | 2.75 | -1.66 | -.95 | -6.57 | -.025 | .082 | -.030 | .049 | -.312 | -.012 | 1.023 | .993 | .772 | 1.011 |
| .55 | 50 | .84 | 2.75 | -1.80 | -1.10 | -6.87 | -.029 | .087 | -.039 | .059 | -.314 | -.016 | 1.029 | .992 | .806 | 1.013 |
| .55 | 55 | .70 | 2.75 | -1.91 | -1.25 | -7.09 | -.033 | .092 | -.051 | .070 | -.316 | -.020 | 1.036 | .990 | .836 | 1.016 |
| .55 | 60 | .58 | 2.75 | -2.01 | -1.40 | -7.25 | -.038 | .097 | -.064 | .081 | -.318 | -.025 | 1.043 | .989 | .863 | 1.019 |
| .55 | 65 | .47 | 2.75 | -2.08 | -1.54 | -7.38 | -.044 | .102 | -.080 | .092 | -.320 | -.032 | 1.050 | .988 | .888 | 1.021 |
| .55 | 70 | .36 | 2.75 | -2.14 | -1.69 | -7.47 | -.051 | .107 | -.099 | .104 | -.322 | -.039 | 1.057 | .987 | .911 | 1.023 |
| .55 | 75 | .27 | 2.75 | -2.19 | -1.84 | -7.55 | -.058 | .112 | -.121 | .115 | -.326 | -.048 | 1.064 | .987 | .932 | 1.024 |
| .55 | 80 | .18 | 2.75 | -2.23 | -2.00 | -7.61 | -.067 | .117 | -.148 | .127 | -.329 | -.058 | 1.071 | .987 | .951 | 1.024 |
| .55 | 85 | .09 | 2.75 | -2.25 | -2.15 | -7.66 | -.078 | .122 | -.179 | .138 | -.333 | -.071 | 1.077 | .988 | .967 | 1.024 |
| .55 | 90 | 0 | 2.75 | -2.25 | -2.31 | -7.71 | -.090 | .127 | -.215 | .148 | -.338 | -.085 | 1.082 | .989 | .982 | 1.023 |
| .55 | 95 | -.09 | 2.75 | -2.25 | -2.47 | -7.76 | -.104 | .132 | -.256 | .157 | -.344 | -.101 | 1.087 | .990 | .994 | 1.020 |
| .55 | 100 | -.18 | 2.75 | -2.23 | -2.63 | -7.81 | -.120 | .136 | -.301 | .163 | -.350 | -.119 | 1.090 | .992 | 1.004 | 1.017 |
| .55 | 105 | -.27 | 2.75 | -2.19 | -2.78 | -7.88 | -.137 | .139 | -.350 | .167 | -.357 | -.138 | 1.093 | .993 | 1.013 | 1.012 |
| .55 | 110 | -.36 | 2.75 | -2.14 | -2.93 | -7.95 | -.156 | .142 | -.402 | .169 | -.364 | -.159 | 1.095 | .995 | 1.020 | 1.007 |
| .55 | 115 | -.47 | 2.75 | -2.08 | -3.08 | -8.05 | -.176 | .145 | -.456 | .168 | -.372 | -.180 | 1.096 | .997 | 1.025 | 1.000 |
| .55 | 120 | -.58 | 2.75 | -2.01 | -3.23 | -8.17 | -.198 | .147 | -.512 | .164 | -.381 | -.202 | 1.096 | .999 | 1.029 | .993 |
| .55 | 125 | -.70 | 2.75 | -1.91 | -3.37 | -8.34 | -.223 | .148 | -.570 | .157 | -.390 | -.225 | 1.096 | 1.001 | 1.032 | .985 |
| .55 | 130 | -.84 | 2.75 | -1.80 | -3.52 | -8.55 | -.249 | .148 | -.628 | .147 | -.401 | -.248 | 1.095 | 1.003 | 1.034 | .977 |
| .55 | 135 | -1 | 2.75 | -1.66 | -3.67 | -8.85 | -.278 | .148 | -.687 | .133 | -.412 | -.271 | 1.093 | 1.005 | 1.036 | .967 |
| .55 | 140 | -1.19 | 2.75 | -1.49 | -3.83 | -9.28 | -.311 | .147 | -.746 | .116 | -.425 | -.295 | 1.091 | 1.007 | 1.037 | .956 |
| .55 | 145 | -1.43 | 2.75 | -1.27 | -3.99 | -9.90 | -.348 | .145 | -.803 | .095 | -.440 | -.317 | 1.088 | 1.008 | 1.037 | .944 |
| .55 | 150 | -1.73 | 2.75 | -.99 | -4.18 | -10.86 | -.390 | .141 | -.855 | .069 | -.457 | -.338 | 1.084 | 1.010 | 1.037 | .930 |
| .55 | 155 | -2.14 | 2.75 | -.59 | -4.38 | -12.46 | -.440 | .135 | -.900 | .037 | -.476 | -.355 | 1.080 | 1.011 | 1.036 | .913 |
| .55 | 160 | -2.75 | 2.75 | -.00 | -4.62 | -15.41 | -.500 | .127 | -.927 | .000 | -.500 | -.366 | 1.074 | 1.012 | 1.034 | .893 |
| .55 | 165 | -3.73 | 2.75 | .97 | -4.93 | -21.79 | -.575 | .115 | -.921 | -.042 | -.529 | -.364 | 1.066 | 1.013 | 1.031 | .866 |
| .55 | 170 | -5.67 | 2.75 | 2.89 | -5.34 | -40.03 | -.672 | .096 | -.845 | -.084 | -.568 | -.334 | 1.056 | 1.013 | 1.027 | .830 |
| .55 | 175 | -11.43 | 2.75 | 8.64 | -6.04 | -138.51 | -.805 | .064 | -.614 | -.106 | -.620 | -.242 | 1.040 | 1.012 | 1.020 | .772 |

$\delta = \text{constant} = \text{Cot } 25^\circ$

| α | θ | β | δ | X | U | ϕ | n_n | n_{nt} | m_n | m_{tw} | n_t | m_t | ϕ_1 | ϕ_2 | ϕ_3 | ϕ_4 |
|----------|----------|---------|----------|-------|-------|---------|-------|----------|-------|----------|-------|-------|----------|----------|----------|----------|
| .55 | 5 | 11.43 | 2.14 | 9.23 | 1.66 | 126.07 | -.003 | .027 | .006 | -.028 | -.304 | .002 | 1.056 | .988 | .906 | 1.022 |
| .55 | 10 | 5.67 | 2.14 | 3.49 | .96 | 27.59 | -.006 | .041 | .008 | -.026 | -.305 | .003 | 1.023 | .993 | .774 | 1.011 |
| .55 | 15 | 3.73 | 2.14 | 1.56 | .55 | 9.35 | -.009 | .052 | .007 | -.018 | -.306 | .003 | 1.008 | .997 | .668 | 1.004 |
| .55 | 20 | 2.75 | 2.14 | .59 | .24 | 2.97 | -.012 | .061 | .004 | -.010 | -.307 | .002 | 1.002 | .999 | .579 | 1.001 |
| .55 | 25 | 2.14 | 2.14 | .00 | .00 | .02 | -.016 | .068 | .000 | -.000 | -.309 | .000 | 1.000 | 1.000 | .501 | 1.000 |
| .55 | 30 | 1.73 | 2.14 | -.39 | -.20 | -1.58 | -.019 | .075 | -.005 | .010 | -.310 | -.002 | 1.001 | 1.000 | .566 | 1.001 |
| .55 | 35 | 1.43 | 2.14 | -.68 | -.39 | -2.54 | -.023 | .082 | -.011 | .020 | -.312 | -.005 | 1.004 | .999 | .622 | 1.002 |
| .55 | 40 | 1.19 | 2.14 | -.90 | -.55 | -3.16 | -.027 | .088 | -.019 | .031 | -.313 | -.008 | 1.008 | .997 | .670 | 1.004 |
| .55 | 45 | .1 | 2.14 | -1.07 | -.71 | -3.59 | -.031 | .094 | -.028 | .041 | -.315 | -.011 | 1.013 | .996 | .712 | 1.006 |
| .55 | 50 | .84 | 2.14 | -1.21 | -.86 | -3.89 | -.036 | .100 | -.039 | .052 | -.317 | -.015 | 1.019 | .994 | .750 | 1.009 |
| .55 | 55 | .70 | 2.14 | -1.32 | -1.01 | -4.10 | -.042 | .106 | -.052 | .064 | -.319 | -.021 | 1.025 | .993 | .784 | 1.012 |
| .55 | 60 | .58 | 2.14 | -1.41 | -1.15 | -4.27 | -.048 | .111 | -.067 | .076 | -.322 | -.027 | 1.032 | .991 | .816 | 1.014 |
| .55 | 65 | .47 | 2.14 | -1.49 | -1.30 | -4.39 | -.055 | .117 | -.086 | .088 | -.324 | -.034 | 1.039 | .990 | .845 | 1.017 |
| .55 | 70 | .36 | 2.14 | -1.55 | -1.45 | -4.49 | -.064 | .123 | -.107 | .100 | -.328 | -.042 | 1.046 | .989 | .872 | 1.020 |
| .55 | 75 | .27 | 2.14 | -1.60 | -1.60 | -4.56 | -.073 | .129 | -.133 | .113 | -.331 | -.053 | 1.053 | .988 | .897 | 1.022 |
| .55 | 80 | .18 | 2.14 | -1.63 | -1.75 | -4.63 | -.084 | .135 | -.164 | .125 | -.336 | -.065 | 1.060 | .987 | .920 | 1.023 |
| .55 | 85 | .09 | 2.14 | -1.65 | -1.91 | -4.68 | -.097 | .141 | -.200 | .136 | -.341 | -.079 | 1.067 | .987 | .940 | 1.024 |
| .55 | 90 | 0 | 2.14 | -1.66 | -2.07 | -4.73 | -.112 | .146 | -.241 | .146 | -.347 | -.095 | 1.074 | .987 | .958 | 1.024 |
| .55 | 95 | -.09 | 2.14 | -1.65 | -2.23 | -4.78 | -.129 | .151 | -.287 | .154 | -.353 | -.113 | 1.079 | .988 | .974 | 1.023 |
| .55 | 100 | -.18 | 2.14 | -1.63 | -2.38 | -4.83 | -.148 | .156 | -.337 | .160 | -.361 | -.133 | 1.084 | .989 | .988 | 1.022 |
| .55 | 105 | -.27 | 2.14 | -1.60 | -2.54 | -4.89 | -.168 | .159 | -.391 | .162 | -.369 | -.154 | 1.088 | .991 | .999 | 1.019 |
| .55 | 110 | -.36 | 2.14 | -1.55 | -2.69 | -4.97 | -.190 | .162 | -.447 | .162 | -.378 | -.177 | 1.091 | .992 | 1.008 | 1.015 |
| .55 | 115 | -.47 | 2.14 | -1.49 | -2.84 | -5.06 | -.214 | .165 | -.505 | .158 | -.387 | -.199 | 1.094 | .994 | 1.015 | 1.010 |
| .55 | 120 | -.58 | 2.14 | -1.41 | -2.98 | -5.19 | -.240 | .166 | -.563 | .151 | -.397 | -.222 | 1.095 | .996 | 1.021 | 1.005 |
| .55 | 125 | -.70 | 2.14 | -1.32 | -3.13 | -5.35 | -.268 | .167 | -.621 | .140 | -.408 | -.245 | 1.096 | .998 | 1.026 | .998 |
| .55 | 130 | -.84 | 2.14 | -1.21 | -3.28 | -5.57 | -.298 | .166 | -.678 | .126 | -.420 | -.268 | 1.096 | 1.000 | 1.030 | .991 |
| .55 | 135 | -.1 | 2.14 | -1.07 | -3.43 | -5.87 | -.330 | .165 | -.733 | .109 | -.433 | -.290 | 1.095 | 1.002 | 1.033 | .982 |
| .55 | 140 | -1.19 | 2.14 | -.90 | -3.58 | -6.29 | -.365 | .163 | -.785 | .087 | -.447 | -.310 | 1.094 | 1.004 | 1.035 | .973 |
| .55 | 145 | -1.43 | 2.14 | -.68 | -3.75 | -6.91 | -.405 | .159 | -.832 | .062 | -.462 | -.329 | 1.092 | 1.006 | 1.037 | .961 |
| .55 | 150 | -1.73 | 2.14 | -.39 | -3.93 | -7.88 | -.449 | .154 | -.871 | .033 | -.480 | -.344 | 1.089 | 1.008 | 1.037 | .948 |
| .55 | 155 | -2.14 | 2.14 | .00 | -4.14 | -9.48 | -.501 | .146 | -.896 | -.000 | -.500 | -.354 | 1.085 | 1.010 | 1.037 | .933 |
| .55 | 160 | -2.75 | 2.14 | .59 | -4.38 | -12.43 | -.561 | .136 | -.899 | -.037 | -.524 | -.355 | 1.080 | 1.011 | 1.036 | .913 |
| .55 | 165 | -3.73 | 2.14 | 1.56 | -4.68 | -18.81 | -.633 | .121 | -.864 | -.076 | -.553 | -.341 | 1.072 | 1.013 | 1.034 | .888 |
| .55 | 170 | -5.67 | 2.14 | 3.49 | -5.10 | -37.04 | -.723 | .099 | -.760 | -.109 | -.588 | -.300 | 1.062 | 1.014 | 1.030 | .852 |
| .55 | 175 | -11.43 | 2.14 | 9.23 | -5.80 | -135.53 | -.840 | .065 | -.521 | -.116 | -.634 | -.206 | 1.045 | 1.013 | 1.022 | .792 |

$\delta = \text{constant} = \text{Cot } 30^\circ$

| α | θ | β | δ | X | U | ϕ | n_n | n_{nt} | m_n | m_{tw} | n_t | m_t | ϕ_1 | ϕ_2 | ϕ_3 | ϕ_4 |
|----------|----------|---------|----------|-------|-------|---------|-------|----------|-------|----------|-------|-------|----------|----------|----------|----------|
| .55 | 5 | 11.43 | 1.73 | 9.63 | 1.86 | 127.66 | -.004 | .029 | .008 | -.034 | -.304 | .003 | 1.065 | .987 | .935 | 1.024 |
| .55 | 10 | 5.67 | 1.73 | 3.88 | 1.17 | 29.17 | -.007 | .045 | .011 | -.033 | -.305 | .004 | 1.032 | .991 | .819 | 1.015 |
| .55 | 15 | 3.73 | 1.73 | 1.96 | .75 | 10.94 | -.011 | .057 | .011 | -.027 | -.307 | .004 | 1.015 | .995 | .723 | 1.007 |
| .55 | 20 | 2.75 | 1.73 | .99 | .45 | 4.56 | -.015 | .067 | .009 | -.019 | -.308 | .003 | 1.005 | .998 | .640 | 1.003 |
| .55 | 25 | 2.14 | 1.73 | .40 | .21 | 1.61 | -.019 | .075 | .005 | -.010 | -.310 | .002 | 1.001 | 1.000 | .567 | 1.001 |
| .55 | 30 | 1.73 | 1.73 | .00 | .00 | .01 | -.023 | .083 | .000 | -.000 | -.312 | .000 | 1.000 | 1.000 | .500 | 1.000 |
| .55 | 35 | 1.43 | 1.73 | -.28 | -.18 | -.95 | -.028 | .091 | -.007 | .010 | -.314 | -.003 | 1.001 | 1.000 | .559 | 1.000 |
| .55 | 40 | 1.19 | 1.73 | -.50 | -.35 | -1.58 | -.033 | .098 | -.015 | .021 | -.316 | -.006 | 1.003 | .999 | .610 | 1.002 |
| .55 | 45 | 1 | 1.73 | -.67 | -.50 | -2.00 | -.038 | .104 | -.025 | .032 | -.318 | -.010 | 1.007 | .998 | .656 | 1.003 |
| .55 | 50 | .84 | 1.73 | -.81 | -.65 | -2.30 | -.044 | .111 | -.036 | .044 | -.320 | -.014 | 1.011 | .996 | .698 | 1.006 |
| .55 | 55 | .70 | 1.73 | -.92 | -.80 | -2.52 | -.051 | .118 | -.051 | .056 | -.323 | -.020 | 1.017 | .995 | .736 | 1.008 |
| .55 | 60 | .58 | 1.73 | -1.02 | -.95 | -2.68 | -.058 | .124 | -.067 | .068 | -.326 | -.027 | 1.022 | .993 | .771 | 1.011 |
| .55 | 65 | .47 | 1.73 | -1.09 | -1.09 | -2.80 | -.067 | .131 | -.088 | .081 | -.329 | -.035 | 1.029 | .992 | .804 | 1.013 |
| .55 | 70 | .36 | 1.73 | -1.16 | -1.24 | -2.90 | -.077 | .138 | -.112 | .094 | -.333 | -.044 | 1.036 | .990 | .834 | 1.016 |
| .55 | 75 | .27 | 1.73 | -1.20 | -1.39 | -2.98 | -.088 | .144 | -.141 | .107 | -.337 | -.056 | 1.043 | .989 | .863 | 1.019 |
| .55 | 80 | .18 | 1.73 | -1.24 | -1.55 | -3.04 | -.102 | .151 | -.175 | .119 | -.343 | -.069 | 1.051 | .988 | .889 | 1.021 |
| .55 | 85 | .09 | 1.73 | -1.26 | -1.71 | -3.09 | -.117 | .157 | -.214 | .131 | -.349 | -.085 | 1.058 | .987 | .913 | 1.023 |
| .55 | 90 | 0 | 1.73 | -1.27 | -1.86 | -3.14 | -.134 | .163 | -.259 | .140 | -.356 | -.102 | 1.065 | .987 | .935 | 1.024 |
| .55 | 95 | -.09 | 1.73 | -1.26 | -2.02 | -3.19 | -.154 | .168 | -.309 | .147 | -.363 | -.122 | 1.072 | .987 | .953 | 1.024 |
| .55 | 100 | -.18 | 1.73 | -1.24 | -2.18 | -3.24 | -.175 | .173 | -.363 | .151 | -.372 | -.144 | 1.078 | .988 | .970 | 1.024 |
| .55 | 105 | -.27 | 1.73 | -1.20 | -2.33 | -3.30 | -.199 | .177 | -.420 | .152 | -.381 | -.166 | 1.083 | .989 | .984 | 1.022 |
| .55 | 110 | -.36 | 1.73 | -1.16 | -2.48 | -3.38 | -.224 | .179 | -.479 | .149 | -.391 | -.189 | 1.087 | .990 | .995 | 1.020 |
| .55 | 115 | -.47 | 1.73 | -1.09 | -2.63 | -3.48 | -.251 | .181 | -.538 | .143 | -.402 | -.212 | 1.090 | .992 | 1.005 | 1.016 |
| .55 | 120 | -.58 | 1.73 | -1.02 | -2.78 | -3.60 | -.279 | .182 | -.596 | .133 | -.413 | -.235 | 1.093 | .993 | 1.013 | 1.012 |
| .55 | 125 | -.70 | 1.73 | -.92 | -2.93 | -3.76 | -.310 | .182 | -.652 | .119 | -.425 | -.258 | 1.095 | .995 | 1.019 | 1.007 |
| .55 | 130 | -.84 | 1.73 | -.81 | -3.07 | -3.98 | -.342 | .181 | -.706 | .102 | -.438 | -.279 | 1.096 | .997 | 1.025 | 1.001 |
| .55 | 135 | -1 | 1.73 | -.67 | -3.22 | -4.28 | -.377 | .179 | -.755 | .082 | -.451 | -.298 | 1.096 | .999 | 1.029 | .994 |
| .55 | 140 | -1.19 | 1.73 | -.50 | -3.38 | -4.70 | -.414 | .175 | -.799 | .058 | -.466 | -.316 | 1.096 | 1.001 | 1.032 | .985 |
| .55 | 145 | -1.43 | 1.73 | -.28 | -3.55 | -5.33 | -.455 | .170 | -.836 | .030 | -.482 | -.330 | 1.094 | 1.003 | 1.035 | .975 |
| .55 | 150 | -1.73 | 1.73 | .00 | -3.73 | -6.29 | -.500 | .163 | -.861 | -.000 | -.500 | -.340 | 1.092 | 1.006 | 1.036 | .963 |
| .55 | 155 | -2.14 | 1.73 | .40 | -3.93 | -7.89 | -.551 | .154 | -.870 | -.034 | -.520 | -.344 | 1.089 | 1.008 | 1.037 | .948 |
| .55 | 160 | -2.75 | 1.73 | .99 | -4.18 | -10.84 | -.610 | .141 | -.855 | -.069 | -.544 | -.338 | 1.084 | 1.010 | 1.037 | .930 |
| .55 | 165 | -3.73 | 1.73 | 1.96 | -4.48 | -17.22 | -.679 | .124 | -.801 | -.102 | -.571 | -.316 | 1.077 | 1.012 | 1.035 | .905 |
| .55 | 170 | -5.67 | 1.73 | 3.88 | -4.89 | -35.45 | -.762 | .100 | -.682 | -.127 | -.604 | -.269 | 1.067 | 1.013 | 1.032 | .869 |
| .55 | 175 | -11.43 | 1.73 | 9.63 | -5.59 | -133.94 | -.866 | .064 | -.449 | -.122 | -.644 | -.177 | 1.050 | 1.013 | 1.024 | .809 |

$\delta = \text{constant} = \text{Cot } 45^\circ$

| α | θ | β | δ | X | U | ϕ | n_n | n_{nt} | m_n | m_{tw} | n_t | m_t | ϕ_1 | ϕ_2 | ϕ_3 | ϕ_4 |
|----------|----------|---------|----------|-------|-------|---------|---------|----------|---------|----------|---------|---------|----------|----------|----------|----------|
| .55 | 5 | 11.43 | 1 | 10.30 | 2.37 | 129.66 | -.006 | .034 | .016 | -.049 | -.305 | .006 | 1.084 | .989 | .986 | 1.022 |
| .55 | 10 | 5.67 | 1 | 4.56 | 1.67 | 31.17 | -.012 | .054 | .025 | -.056 | -.307 | .010 | 1.056 | .987 | .908 | 1.022 |
| .55 | 15 | 3.73 | 1 | 2.63 | 1.25 | 12.94 | -.018 | .069 | .029 | -.054 | -.310 | .011 | 1.036 | .990 | .837 | 1.016 |
| .55 | 20 | 2.75 | 1 | 1.66 | .95 | 6.56 | -.025 | .082 | .030 | -.049 | -.312 | .012 | 1.023 | .993 | .772 | 1.011 |
| .55 | 25 | 2.14 | 1 | 1.07 | .71 | 3.61 | -.031 | .094 | .028 | -.041 | -.315 | .011 | 1.013 | .996 | .712 | 1.006 |
| .55 | 30 | 1.73 | 1 | .68 | .51 | 2.01 | -.038 | .104 | .025 | -.032 | -.318 | .010 | 1.007 | .998 | .657 | 1.003 |
| .55 | 35 | 1.43 | 1 | .39 | .32 | 1.04 | -.046 | .114 | .019 | -.022 | -.321 | .007 | 1.003 | .999 | .603 | 1.001 |
| .55 | 40 | 1.19 | 1 | .17 | .16 | .42 | -.053 | .124 | .011 | -.012 | -.324 | .004 | 1.001 | 1.000 | .551 | 1.000 |
| .55 | 45 | 1 | 1 | 0 | 0 | -.00 | #VALUE! | #DIV/0! | #DIV/0! | #DIV/0! | #VALUE! | #DIV/0! | #VALUE! | #VALUE! | #VALUE! | #VALUE! |
| .55 | 50 | .84 | 1 | -.14 | -.15 | -.30 | -.071 | .141 | -.013 | .012 | -.331 | -.005 | 1.001 | 1.000 | .549 | 1.000 |
| .55 | 55 | .70 | 1 | -.25 | -.30 | -.52 | -.082 | .150 | -.030 | .025 | -.335 | -.012 | 1.002 | .999 | .595 | 1.001 |
| .55 | 60 | .58 | 1 | -.34 | -.44 | -.68 | -.093 | .159 | -.050 | .038 | -.339 | -.020 | 1.005 | .998 | .639 | 1.003 |
| .55 | 65 | .47 | 1 | -.42 | -.59 | -.81 | -.106 | .167 | -.074 | .051 | -.344 | -.029 | 1.009 | .997 | .680 | 1.005 |
| .55 | 70 | .36 | 1 | -.48 | -.74 | -.90 | -.121 | .176 | -.103 | .065 | -.350 | -.041 | 1.014 | .996 | .720 | 1.007 |
| .55 | 75 | .27 | 1 | -.53 | -.89 | -.98 | -.138 | .184 | -.138 | .078 | -.357 | -.054 | 1.020 | .994 | .757 | 1.010 |
| .55 | 80 | .18 | 1 | -.56 | -1.04 | -1.04 | -.158 | .192 | -.179 | .090 | -.365 | -.071 | 1.027 | .992 | .793 | 1.012 |
| .55 | 85 | .09 | 1 | -.58 | -1.20 | -1.09 | -.180 | .199 | -.225 | .100 | -.374 | -.089 | 1.034 | .991 | .826 | 1.015 |
| .55 | 90 | 0 | 1 | -.59 | -1.36 | -1.14 | -.204 | .206 | -.278 | .107 | -.383 | -.110 | 1.042 | .989 | .857 | 1.018 |
| .55 | 95 | -.09 | 1 | -.58 | -1.52 | -1.19 | -.231 | .211 | -.334 | .111 | -.394 | -.132 | 1.049 | .988 | .884 | 1.021 |
| .55 | 100 | -.18 | 1 | -.56 | -1.67 | -1.24 | -.260 | .215 | -.393 | .110 | -.405 | -.155 | 1.057 | .987 | .909 | 1.023 |
| .55 | 105 | -.27 | 1 | -.53 | -1.83 | -1.31 | -.291 | .218 | -.453 | .105 | -.418 | -.179 | 1.064 | .987 | .930 | 1.024 |
| .55 | 110 | -.36 | 1 | -.48 | -1.98 | -1.38 | -.323 | .220 | -.512 | .096 | -.430 | -.202 | 1.070 | .987 | .949 | 1.024 |
| .55 | 115 | -.47 | 1 | -.42 | -2.13 | -1.48 | -.357 | .220 | -.567 | .083 | -.443 | -.224 | 1.076 | .988 | .965 | 1.024 |
| .55 | 120 | -.58 | 1 | -.34 | -2.28 | -1.60 | -.391 | .218 | -.617 | .067 | -.457 | -.244 | 1.081 | .988 | .979 | 1.023 |
| .55 | 125 | -.70 | 1 | -.25 | -2.42 | -1.76 | -.426 | .215 | -.662 | .047 | -.471 | -.262 | 1.085 | .990 | .990 | 1.021 |
| .55 | 130 | -.84 | 1 | -.14 | -2.57 | -1.98 | -.462 | .211 | -.700 | .025 | -.485 | -.277 | 1.089 | .991 | 1.001 | 1.018 |
| .55 | 135 | -1 | 1 | 0 | -2.72 | -2.28 | -.500 | .206 | -.730 | 0 | -.500 | -.288 | 1.092 | .993 | 1.010 | 1.014 |
| .55 | 140 | -1.19 | 1 | .17 | -2.88 | -2.71 | -.539 | .198 | -.751 | -.026 | -.515 | -.297 | 1.094 | .995 | 1.017 | 1.009 |
| .55 | 145 | -1.43 | 1 | .39 | -3.04 | -3.33 | -.580 | .189 | -.760 | -.054 | -.532 | -.300 | 1.096 | .997 | 1.024 | 1.002 |
| .55 | 150 | -1.73 | 1 | .68 | -3.22 | -4.29 | -.624 | .178 | -.755 | -.082 | -.549 | -.298 | 1.096 | .999 | 1.029 | .993 |
| .55 | 155 | -2.14 | 1 | 1.07 | -3.43 | -5.89 | -.671 | .165 | -.733 | -.109 | -.567 | -.290 | 1.095 | 1.002 | 1.033 | .982 |
| .55 | 160 | -2.75 | 1 | 1.66 | -3.67 | -8.84 | -.722 | .148 | -.687 | -.133 | -.588 | -.272 | 1.093 | 1.005 | 1.036 | .967 |
| .55 | 165 | -3.73 | 1 | 2.63 | -3.97 | -15.22 | -.778 | .127 | -.610 | -.151 | -.610 | -.241 | 1.088 | 1.008 | 1.037 | .945 |
| .55 | 170 | -5.67 | 1 | 4.56 | -4.39 | -33.46 | -.842 | .099 | -.487 | -.155 | -.635 | -.192 | 1.080 | 1.011 | 1.036 | .912 |
| .55 | 175 | -11.43 | 1 | 10.30 | -5.09 | -131.94 | -.914 | .062 | -.297 | -.127 | -.664 | -.117 | 1.062 | 1.013 | 1.030 | .852 |

$\delta = \text{constant} = \text{Cot } 60^\circ$

| α | θ | β | δ | X | U | ϕ | n_n | n_{nt} | m_n | m_{tw} | n_t | m_t | ϕ_1 | ϕ_2 | ϕ_3 | ϕ_4 |
|----------|----------|---------|----------|-------|-------|---------|-------|----------|-------|----------|-------|-------|----------|----------|----------|----------|
| .55 | 5 | 11.43 | .58 | 10.64 | 2.81 | 130.33 | -.009 | .039 | .028 | -.064 | -.306 | .011 | 1.093 | .994 | 1.014 | 1.011 |
| .55 | 10 | 5.67 | .58 | 4.90 | 2.11 | 31.85 | -.019 | .063 | .046 | -.079 | -.310 | .018 | 1.075 | .988 | .963 | 1.024 |
| .55 | 15 | 3.73 | .58 | 2.97 | 1.69 | 13.62 | -.028 | .081 | .057 | -.083 | -.314 | .022 | 1.058 | .987 | .912 | 1.023 |
| .55 | 20 | 2.75 | .58 | 2.00 | 1.39 | 7.23 | -.038 | .097 | .064 | -.081 | -.318 | .025 | 1.043 | .989 | .863 | 1.019 |
| .55 | 25 | 2.14 | .58 | 1.41 | 1.15 | 4.28 | -.048 | .111 | .067 | -.075 | -.321 | .026 | 1.032 | .991 | .816 | 1.014 |
| .55 | 30 | 1.73 | .58 | 1.02 | .95 | 2.68 | -.058 | .124 | .067 | -.068 | -.325 | .026 | 1.022 | .993 | .770 | 1.011 |
| .55 | 35 | 1.43 | .58 | .73 | .76 | 1.72 | -.069 | .136 | .064 | -.059 | -.330 | .025 | 1.015 | .995 | .726 | 1.007 |
| .55 | 40 | 1.19 | .58 | .51 | .60 | 1.10 | -.081 | .147 | .058 | -.049 | -.334 | .023 | 1.009 | .997 | .682 | 1.005 |
| .55 | 45 | 1 | .58 | .34 | .44 | .68 | -.093 | .158 | .049 | -.038 | -.339 | .019 | 1.005 | .998 | .638 | 1.003 |
| .55 | 50 | .84 | .58 | .20 | .29 | .38 | -.106 | .169 | .037 | -.026 | -.345 | .014 | 1.002 | .999 | .593 | 1.001 |
| .55 | 55 | .70 | .58 | .09 | .14 | .16 | -.121 | .179 | .020 | -.013 | -.350 | .008 | 1.001 | 1.000 | .547 | 1.000 |
| .55 | 60 | .58 | .58 | -.00 | -.00 | -.00 | -.138 | .189 | -.001 | .000 | -.357 | -.000 | 1.000 | 1.000 | .501 | 1.000 |
| .55 | 65 | .47 | .58 | -.08 | -.15 | -.13 | -.156 | .199 | -.026 | .014 | -.364 | -.010 | 1.001 | 1.000 | .549 | 1.000 |
| .55 | 70 | .36 | .58 | -.14 | -.30 | -.22 | -.176 | .209 | -.058 | .027 | -.372 | -.023 | 1.002 | .999 | .595 | 1.001 |
| .55 | 75 | .27 | .58 | -.19 | -.45 | -.30 | -.200 | .218 | -.095 | .039 | -.381 | -.038 | 1.005 | .998 | .641 | 1.003 |
| .55 | 80 | .18 | .58 | -.22 | -.60 | -.36 | -.225 | .226 | -.139 | .050 | -.392 | -.055 | 1.010 | .997 | .684 | 1.005 |
| .55 | 85 | .09 | .58 | -.24 | -.76 | -.41 | -.254 | .234 | -.189 | .058 | -.403 | -.074 | 1.015 | .995 | .725 | 1.007 |
| .55 | 90 | 0 | .58 | -.25 | -.92 | -.46 | -.285 | .240 | -.243 | .062 | -.415 | -.096 | 1.021 | .994 | .764 | 1.010 |
| .55 | 95 | -.09 | .58 | -.24 | -1.08 | -.51 | -.318 | .244 | -.300 | .063 | -.428 | -.119 | 1.028 | .992 | .800 | 1.013 |
| .55 | 100 | -.18 | .58 | -.22 | -1.23 | -.57 | -.353 | .247 | -.358 | .058 | -.442 | -.141 | 1.036 | .990 | .833 | 1.016 |
| .55 | 105 | -.27 | .58 | -.19 | -1.39 | -.63 | -.389 | .248 | -.414 | .049 | -.456 | -.163 | 1.043 | .989 | .862 | 1.019 |
| .55 | 110 | -.36 | .58 | -.14 | -1.54 | -.70 | -.426 | .247 | -.466 | .036 | -.471 | -.184 | 1.050 | .988 | .888 | 1.021 |
| .55 | 115 | -.47 | .58 | -.08 | -1.69 | -.80 | -.463 | .244 | -.512 | .020 | -.485 | -.202 | 1.057 | .987 | .911 | 1.023 |
| .55 | 120 | -.58 | .58 | -.00 | -1.84 | -.92 | -.499 | .240 | -.551 | .000 | -.500 | -.217 | 1.064 | .987 | .931 | 1.024 |
| .55 | 125 | -.70 | .58 | .09 | -1.98 | -1.09 | -.536 | .234 | -.582 | -.021 | -.514 | -.230 | 1.070 | .987 | .949 | 1.024 |
| .55 | 130 | -.84 | .58 | .20 | -2.13 | -1.31 | -.572 | .227 | -.605 | -.043 | -.528 | -.239 | 1.076 | .988 | .965 | 1.024 |
| .55 | 135 | -1 | .58 | .34 | -2.28 | -1.60 | -.608 | .218 | -.618 | -.066 | -.543 | -.244 | 1.081 | .988 | .979 | 1.023 |
| .55 | 140 | -1.19 | .58 | .51 | -2.44 | -2.03 | -.645 | .208 | -.623 | -.089 | -.557 | -.246 | 1.086 | .990 | .992 | 1.021 |
| .55 | 145 | -1.43 | .58 | .73 | -2.60 | -2.65 | -.682 | .196 | -.616 | -.112 | -.572 | -.243 | 1.090 | .991 | 1.003 | 1.017 |
| .55 | 150 | -1.73 | .58 | 1.02 | -2.78 | -3.61 | -.720 | .182 | -.597 | -.133 | -.587 | -.236 | 1.093 | .993 | 1.013 | 1.012 |
| .55 | 155 | -2.14 | .58 | 1.41 | -2.99 | -5.21 | -.760 | .166 | -.564 | -.151 | -.603 | -.223 | 1.095 | .996 | 1.022 | 1.004 |
| .55 | 160 | -2.75 | .58 | 2.00 | -3.23 | -8.16 | -.801 | .147 | -.514 | -.164 | -.619 | -.203 | 1.096 | .999 | 1.029 | .993 |
| .55 | 165 | -3.73 | .58 | 2.97 | -3.53 | -14.54 | -.845 | .124 | -.441 | -.169 | -.636 | -.174 | 1.094 | 1.003 | 1.035 | .976 |
| .55 | 170 | -5.67 | .58 | 4.90 | -3.95 | -32.78 | -.892 | .096 | -.340 | -.160 | -.655 | -.134 | 1.089 | 1.008 | 1.037 | .947 |
| .55 | 175 | -11.43 | .58 | 10.64 | -4.65 | -131.26 | -.943 | .059 | -.199 | -.122 | -.675 | -.079 | 1.073 | 1.013 | 1.034 | .891 |

$\delta = \text{constant} = \text{Cot } 75^\circ$

| α | θ | β | δ | X | U | ϕ | n_n | n_{nt} | m_n | m_{tw} | n_t | m_t | ϕ_1 | ϕ_2 | ϕ_3 | ϕ_4 |
|----------|----------|---------|----------|-------|-------|---------|-------|----------|-------|----------|-------|-------|----------|----------|----------|----------|
| .55 | 5 | 11.43 | .27 | 10.83 | 3.25 | 130.63 | -.015 | .044 | .047 | -.080 | -.308 | .019 | 1.096 | 1.000 | 1.030 | .992 |
| .55 | 10 | 5.67 | .27 | 5.09 | 2.56 | 32.15 | -.029 | .072 | .080 | -.104 | -.314 | .032 | 1.089 | .991 | 1.000 | 1.018 |
| .55 | 15 | 3.73 | .27 | 3.16 | 2.14 | 13.91 | -.044 | .094 | .104 | -.113 | -.320 | .041 | 1.076 | .988 | .966 | 1.024 |
| .55 | 20 | 2.75 | .27 | 2.19 | 1.84 | 7.53 | -.058 | .112 | .121 | -.115 | -.325 | .048 | 1.064 | .987 | .931 | 1.024 |
| .55 | 25 | 2.14 | .27 | 1.60 | 1.60 | 4.58 | -.073 | .129 | .133 | -.112 | -.331 | .052 | 1.053 | .988 | .897 | 1.022 |
| .55 | 30 | 1.73 | .27 | 1.20 | 1.39 | 2.98 | -.088 | .144 | .140 | -.107 | -.337 | .055 | 1.043 | .989 | .862 | 1.019 |
| .55 | 35 | 1.43 | .27 | .92 | 1.21 | 2.02 | -.104 | .158 | .143 | -.099 | -.344 | .057 | 1.034 | .991 | .828 | 1.015 |
| .55 | 40 | 1.19 | .27 | .70 | 1.04 | 1.40 | -.120 | .171 | .142 | -.089 | -.350 | .056 | 1.027 | .992 | .793 | 1.012 |
| .55 | 45 | 1 | .27 | .53 | .89 | .98 | -.138 | .184 | .137 | -.078 | -.357 | .054 | 1.020 | .994 | .756 | 1.009 |
| .55 | 50 | .84 | .27 | .39 | .74 | .68 | -.157 | .196 | .127 | -.065 | -.364 | .050 | 1.014 | .996 | .719 | 1.007 |
| .55 | 55 | .70 | .27 | .28 | .59 | .46 | -.177 | .207 | .113 | -.052 | -.373 | .045 | 1.009 | .997 | .680 | 1.005 |
| .55 | 60 | .58 | .27 | .18 | .44 | .29 | -.200 | .218 | .094 | -.039 | -.381 | .037 | 1.005 | .998 | .639 | 1.003 |
| .55 | 65 | .47 | .27 | .11 | .30 | .17 | -.224 | .228 | .069 | -.025 | -.391 | .027 | 1.002 | .999 | .595 | 1.001 |
| .55 | 70 | .36 | .27 | .05 | .15 | .07 | -.251 | .238 | .037 | -.012 | -.402 | .015 | 1.001 | 1.000 | .548 | 1.000 |
| .55 | 75 | .27 | .27 | -.00 | -.00 | -.00 | -.280 | .247 | -.001 | .000 | -.413 | -.000 | 1.000 | 1.000 | .501 | 1.000 |
| .55 | 80 | .18 | .27 | -.04 | -.16 | -.06 | -.313 | .255 | -.045 | .010 | -.426 | -.018 | 1.001 | 1.000 | .551 | 1.000 |
| .55 | 85 | .09 | .27 | -.06 | -.31 | -.12 | -.347 | .261 | -.095 | .017 | -.440 | -.037 | 1.003 | .999 | .600 | 1.001 |
| .55 | 90 | 0 | .27 | -.06 | -.47 | -.17 | -.384 | .265 | -.148 | .019 | -.454 | -.058 | 1.006 | .998 | .647 | 1.003 |
| .55 | 95 | -.09 | .27 | -.06 | -.63 | -.21 | -.422 | .267 | -.203 | .017 | -.469 | -.080 | 1.011 | .997 | .691 | 1.005 |
| .55 | 100 | -.18 | .27 | -.04 | -.79 | -.27 | -.461 | .267 | -.256 | .011 | -.484 | -.101 | 1.016 | .995 | .732 | 1.008 |
| .55 | 105 | -.27 | .27 | -.00 | -.94 | -.33 | -.499 | .265 | -.305 | .000 | -.500 | -.121 | 1.022 | .993 | .770 | 1.010 |
| .55 | 110 | -.36 | .27 | .05 | -1.09 | -.41 | -.537 | .261 | -.349 | -.014 | -.515 | -.138 | 1.029 | .992 | .804 | 1.013 |
| .55 | 115 | -.47 | .27 | .11 | -1.24 | -.50 | -.574 | .255 | -.385 | -.030 | -.529 | -.152 | 1.036 | .990 | .834 | 1.016 |
| .55 | 120 | -.58 | .27 | .18 | -1.39 | -.63 | -.609 | .248 | -.415 | -.049 | -.543 | -.164 | 1.043 | .989 | .862 | 1.019 |
| .55 | 125 | -.70 | .27 | .28 | -1.54 | -.79 | -.643 | .239 | -.436 | -.067 | -.557 | -.172 | 1.050 | .988 | .887 | 1.021 |
| .55 | 130 | -.84 | .27 | .39 | -1.68 | -1.01 | -.676 | .229 | -.449 | -.087 | -.570 | -.177 | 1.057 | .987 | .910 | 1.023 |
| .55 | 135 | -1 | .27 | .53 | -1.83 | -1.31 | -.708 | .218 | -.455 | -.105 | -.582 | -.180 | 1.064 | .987 | .931 | 1.024 |
| .55 | 140 | -1.19 | .27 | .70 | -1.99 | -1.73 | -.739 | .206 | -.452 | -.123 | -.595 | -.179 | 1.071 | .987 | .950 | 1.024 |
| .55 | 145 | -1.43 | .27 | .92 | -2.16 | -2.35 | -.770 | .192 | -.441 | -.139 | -.607 | -.174 | 1.077 | .988 | .967 | 1.024 |
| .55 | 150 | -1.73 | .27 | 1.20 | -2.34 | -3.31 | -.801 | .177 | -.422 | -.152 | -.619 | -.166 | 1.083 | .989 | .984 | 1.022 |
| .55 | 155 | -2.14 | .27 | 1.60 | -2.54 | -4.91 | -.832 | .159 | -.392 | -.162 | -.631 | -.155 | 1.088 | .991 | .999 | 1.019 |
| .55 | 160 | -2.75 | .27 | 2.19 | -2.78 | -7.86 | -.863 | .140 | -.351 | -.167 | -.643 | -.139 | 1.093 | .993 | 1.013 | 1.012 |
| .55 | 165 | -3.73 | .27 | 3.16 | -3.09 | -14.24 | -.895 | .117 | -.296 | -.165 | -.656 | -.117 | 1.096 | .997 | 1.025 | 1.000 |
| .55 | 170 | -5.67 | .27 | 5.09 | -3.50 | -32.48 | -.928 | .089 | -.224 | -.150 | -.669 | -.088 | 1.095 | 1.003 | 1.034 | .978 |
| .55 | 175 | -11.43 | .27 | 10.83 | -4.20 | -130.96 | -.963 | .054 | -.129 | -.111 | -.683 | -.051 | 1.084 | 1.010 | 1.037 | .928 |

$\delta = \text{constant} = \text{Cot } 90^\circ$

| α | θ | β | δ | X | U | ϕ | n_n | n_{nt} | m_n | m_{tw} | n_t | m_t | ϕ_1 | ϕ_2 | ϕ_3 | ϕ_4 |
|----------|----------|---------|----------|-------|-------|---------|---------|----------|---------|----------|---------|---------|----------|----------|----------|----------|
| .55 | 5 | 11.43 | 0 | 10.89 | 3.73 | 130.80 | -.023 | .049 | .079 | -.096 | -.312 | .031 | 1.092 | 1.006 | 1.036 | .963 |
| .55 | 10 | 5.67 | 0 | 5.15 | 3.03 | 32.31 | -.046 | .081 | .137 | -.129 | -.321 | .054 | 1.095 | .997 | 1.023 | 1.003 |
| .55 | 15 | 3.73 | 0 | 3.22 | 2.61 | 14.08 | -.068 | .106 | .181 | -.144 | -.329 | .072 | 1.090 | .991 | 1.004 | 1.017 |
| .55 | 20 | 2.75 | 0 | 2.25 | 2.31 | 7.70 | -.090 | .127 | .215 | -.148 | -.338 | .085 | 1.082 | .989 | .982 | 1.023 |
| .55 | 25 | 2.14 | 0 | 1.66 | 2.07 | 4.75 | -.112 | .146 | .241 | -.146 | -.347 | .095 | 1.074 | .987 | .959 | 1.024 |
| .55 | 30 | 1.73 | 0 | 1.27 | 1.86 | 3.15 | -.134 | .163 | .259 | -.140 | -.355 | .102 | 1.065 | .987 | .935 | 1.024 |
| .55 | 35 | 1.43 | 0 | .98 | 1.68 | 2.19 | -.157 | .178 | .271 | -.131 | -.364 | .107 | 1.057 | .987 | .910 | 1.023 |
| .55 | 40 | 1.19 | 0 | .76 | 1.52 | 1.56 | -.180 | .192 | .277 | -.120 | -.374 | .110 | 1.049 | .988 | .884 | 1.021 |
| .55 | 45 | 1 | 0 | .59 | 1.36 | 1.14 | -.204 | .206 | .278 | -.107 | -.383 | .110 | 1.042 | .989 | .857 | 1.018 |
| .55 | 50 | .84 | 0 | .45 | 1.21 | .84 | -.230 | .218 | .272 | -.093 | -.393 | .108 | 1.034 | .991 | .828 | 1.015 |
| .55 | 55 | .70 | 0 | .34 | 1.06 | .62 | -.257 | .229 | .261 | -.078 | -.404 | .103 | 1.028 | .992 | .797 | 1.013 |
| .55 | 60 | .58 | 0 | .25 | .92 | .46 | -.286 | .240 | .243 | -.062 | -.415 | .096 | 1.021 | .994 | .764 | 1.010 |
| .55 | 65 | .47 | 0 | .17 | .77 | .34 | -.317 | .250 | .218 | -.047 | -.428 | .086 | 1.015 | .995 | .728 | 1.007 |
| .55 | 70 | .36 | 0 | .11 | .62 | .24 | -.350 | .258 | .186 | -.032 | -.441 | .073 | 1.010 | .997 | .689 | 1.005 |
| .55 | 75 | .27 | 0 | .06 | .47 | .16 | -.385 | .265 | .147 | -.019 | -.454 | .058 | 1.006 | .998 | .646 | 1.003 |
| .55 | 80 | .18 | 0 | .03 | .32 | .10 | -.422 | .270 | .102 | -.009 | -.469 | .040 | 1.003 | .999 | .601 | 1.001 |
| .55 | 85 | .09 | 0 | .01 | .16 | .05 | -.460 | .274 | .052 | -.002 | -.484 | .021 | 1.001 | 1.000 | .552 | 1.000 |
| .55 | 90 | 0 | 0 | 0 | 0 | 0 | #VALUE! | #DIV/0! | #DIV/0! | #DIV/0! | #VALUE! | #DIV/0! | #VALUE! | #VALUE! | #VALUE! | #VALUE! |
| .55 | 95 | -.09 | 0 | .01 | -.16 | -.05 | -.540 | .274 | -.052 | -.002 | -.516 | -.021 | 1.001 | 1.000 | .552 | 1.000 |
| .55 | 100 | -.18 | 0 | .03 | -.32 | -.10 | -.578 | .270 | -.102 | -.009 | -.531 | -.040 | 1.003 | .999 | .601 | 1.001 |
| .55 | 105 | -.27 | 0 | .06 | -.47 | -.16 | -.615 | .265 | -.147 | -.019 | -.546 | -.058 | 1.006 | .998 | .646 | 1.003 |
| .55 | 110 | -.36 | 0 | .11 | -.62 | -.24 | -.650 | .258 | -.186 | -.032 | -.559 | -.073 | 1.010 | .997 | .689 | 1.005 |
| .55 | 115 | -.47 | 0 | .17 | -.77 | -.34 | -.683 | .250 | -.218 | -.047 | -.572 | -.086 | 1.015 | .995 | .728 | 1.007 |
| .55 | 120 | -.58 | 0 | .25 | -.92 | -.46 | -.714 | .240 | -.243 | -.062 | -.585 | -.096 | 1.021 | .994 | .764 | 1.010 |
| .55 | 125 | -.70 | 0 | .34 | -1.06 | -.62 | -.743 | .229 | -.261 | -.078 | -.596 | -.103 | 1.028 | .992 | .797 | 1.013 |
| .55 | 130 | -.84 | 0 | .45 | -1.21 | -.84 | -.770 | .218 | -.272 | -.093 | -.607 | -.108 | 1.034 | .991 | .828 | 1.015 |
| .55 | 135 | -.91 | 0 | .59 | -1.36 | -1.14 | -.796 | .206 | -.278 | -.107 | -.617 | -.110 | 1.042 | .989 | .857 | 1.018 |
| .55 | 140 | -1.19 | 0 | .76 | -1.52 | -1.56 | -.820 | .192 | -.277 | -.120 | -.626 | -.110 | 1.049 | .988 | .884 | 1.021 |
| .55 | 145 | -1.43 | 0 | .98 | -1.68 | -2.19 | -.843 | .178 | -.271 | -.131 | -.636 | -.107 | 1.057 | .987 | .910 | 1.023 |
| .55 | 150 | -1.73 | 0 | 1.27 | -1.86 | -3.15 | -.866 | .163 | -.259 | -.140 | -.645 | -.102 | 1.065 | .987 | .935 | 1.024 |
| .55 | 155 | -2.14 | 0 | 1.66 | -2.07 | -4.75 | -.888 | .146 | -.241 | -.146 | -.653 | -.095 | 1.074 | .987 | .959 | 1.024 |
| .55 | 160 | -2.75 | 0 | 2.25 | -2.31 | -7.70 | -.910 | .127 | -.215 | -.148 | -.662 | -.085 | 1.082 | .989 | .982 | 1.023 |
| .55 | 165 | -3.73 | 0 | 3.22 | -2.61 | -14.08 | -.932 | .106 | -.181 | -.144 | -.671 | -.072 | 1.090 | .991 | 1.004 | 1.017 |
| .55 | 170 | -5.67 | 0 | 5.15 | -3.03 | -32.31 | -.954 | .081 | -.137 | -.129 | -.679 | -.054 | 1.095 | .997 | 1.023 | 1.003 |
| .55 | 175 | -11.43 | 0 | 10.89 | -3.73 | -130.80 | -.977 | .049 | -.079 | -.096 | -.688 | -.031 | 1.092 | 1.006 | 1.036 | .963 |

$\delta = \text{constant} = \text{Cot } 120^\circ$

| α | θ | β | δ | χ | U | ϕ | n_n | n_{nt} | m_n | m_{tw} | n_t | m_t | ϕ_1 | ϕ_2 | ϕ_3 | ϕ_4 |
|----------|----------|---------|----------|--------|-------|---------|-------|----------|-------|----------|-------|-------|----------|----------|----------|----------|
| .55 | 5 | 11.43 | -.58 | 10.64 | 4.65 | 131.26 | -.057 | .059 | .199 | -.122 | -.325 | .079 | 1.073 | 1.013 | 1.034 | .891 |
| .55 | 10 | 5.67 | -.58 | 4.90 | 3.95 | 32.78 | -.108 | .096 | .340 | -.160 | -.345 | .134 | 1.089 | 1.008 | 1.037 | .947 |
| .55 | 15 | 3.73 | -.58 | 2.97 | 3.53 | 14.54 | -.155 | .124 | .441 | -.169 | -.364 | .174 | 1.094 | 1.003 | 1.035 | .976 |
| .55 | 20 | 2.75 | -.58 | 2.00 | 3.23 | 8.16 | -.199 | .147 | .514 | -.164 | -.381 | .203 | 1.096 | .999 | 1.029 | .993 |
| .55 | 25 | 2.14 | -.58 | 1.41 | 2.99 | 5.21 | -.240 | .166 | .564 | -.151 | -.397 | .223 | 1.095 | .996 | 1.022 | 1.004 |
| .55 | 30 | 1.73 | -.58 | 1.02 | 2.78 | 3.61 | -.280 | .182 | .597 | -.133 | -.413 | .236 | 1.093 | .993 | 1.013 | 1.012 |
| .55 | 35 | 1.43 | -.58 | .73 | 2.60 | 2.65 | -.318 | .196 | .616 | -.112 | -.428 | .243 | 1.090 | .991 | 1.003 | 1.017 |
| .55 | 40 | 1.19 | -.58 | .51 | 2.44 | 2.03 | -.355 | .208 | .623 | -.089 | -.443 | .246 | 1.086 | .990 | .992 | 1.021 |
| .55 | 45 | 1 | -.58 | .34 | 2.28 | 1.60 | -.392 | .218 | .618 | -.066 | -.457 | .244 | 1.081 | .988 | .979 | 1.023 |
| .55 | 50 | .84 | -.58 | .20 | 2.13 | 1.31 | -.428 | .227 | .605 | -.043 | -.472 | .239 | 1.076 | .988 | .965 | 1.024 |
| .55 | 55 | .70 | -.58 | .09 | 1.98 | 1.09 | -.464 | .234 | .582 | -.021 | -.486 | .230 | 1.070 | .987 | .949 | 1.024 |
| .55 | 60 | .58 | -.58 | -.00 | 1.84 | .92 | -.501 | .240 | .551 | .000 | -.500 | .217 | 1.064 | .987 | .931 | 1.024 |
| .55 | 65 | .47 | -.58 | -.08 | 1.69 | .80 | -.537 | .244 | .512 | .020 | -.515 | .202 | 1.057 | .987 | .911 | 1.023 |
| .55 | 70 | .36 | -.58 | -.14 | 1.54 | .70 | -.574 | .247 | .466 | .036 | -.529 | .184 | 1.050 | .988 | .888 | 1.021 |
| .55 | 75 | .27 | -.58 | -.19 | 1.39 | .63 | -.611 | .248 | .414 | .049 | -.544 | .163 | 1.043 | .989 | .862 | 1.019 |
| .55 | 80 | .18 | -.58 | -.22 | 1.23 | .57 | -.647 | .247 | .358 | .058 | -.558 | .141 | 1.036 | .990 | .833 | 1.016 |
| .55 | 85 | .09 | -.58 | -.24 | 1.08 | .51 | -.682 | .244 | .300 | .063 | -.572 | .119 | 1.028 | .992 | .800 | 1.013 |
| .55 | 90 | 0 | -.58 | -.25 | .92 | .46 | -.715 | .240 | .243 | .062 | -.585 | .096 | 1.021 | .994 | .764 | 1.010 |
| .55 | 95 | -.09 | -.58 | -.24 | .76 | .41 | -.746 | .234 | .189 | .058 | -.597 | .074 | 1.015 | .995 | .725 | 1.007 |
| .55 | 100 | -.18 | -.58 | -.22 | .60 | .36 | -.775 | .226 | .139 | .050 | -.608 | .055 | 1.010 | .997 | .684 | 1.005 |
| .55 | 105 | -.27 | -.58 | -.19 | .45 | .30 | -.800 | .218 | .095 | .039 | -.619 | .038 | 1.005 | .998 | .641 | 1.003 |
| .55 | 110 | -.36 | -.58 | -.14 | .30 | .22 | -.824 | .209 | .058 | .027 | -.628 | .023 | 1.002 | .999 | .595 | 1.001 |
| .55 | 115 | -.47 | -.58 | -.08 | .15 | .13 | -.844 | .199 | .026 | .014 | -.636 | .010 | 1.001 | 1.000 | .549 | 1.000 |
| .55 | 120 | -.58 | -.58 | -.00 | .00 | .00 | -.862 | .189 | .001 | .000 | -.643 | .000 | 1.000 | 1.000 | .501 | 1.000 |
| .55 | 125 | -.70 | -.58 | .09 | -.14 | -.16 | -.879 | .179 | -.020 | -.013 | -.650 | -.008 | 1.001 | 1.000 | .547 | 1.000 |
| .55 | 130 | -.84 | -.58 | .20 | -.29 | -.38 | -.894 | .169 | -.037 | -.026 | -.655 | -.014 | 1.002 | .999 | .593 | 1.001 |
| .55 | 135 | -.91 | -.58 | .34 | -.44 | -.68 | -.907 | .158 | -.049 | -.038 | -.661 | -.019 | 1.005 | .998 | .638 | 1.003 |
| .55 | 140 | -1.19 | -.58 | .51 | -.60 | -1.10 | -.919 | .147 | -.058 | -.049 | -.666 | -.023 | 1.009 | .997 | .682 | 1.005 |
| .55 | 145 | -1.43 | -.58 | .73 | -.76 | -1.72 | -.931 | .136 | -.064 | -.059 | -.670 | -.025 | 1.015 | .995 | .726 | 1.007 |
| .55 | 150 | -1.73 | -.58 | 1.02 | -.95 | -2.68 | -.942 | .124 | -.067 | -.068 | -.675 | -.026 | 1.022 | .993 | .770 | 1.011 |
| .55 | 155 | -2.14 | -.58 | 1.41 | -1.15 | -4.28 | -.952 | .111 | -.067 | -.075 | -.679 | -.026 | 1.032 | .991 | .816 | 1.014 |
| .55 | 160 | -2.75 | -.58 | 2.00 | -1.39 | -7.23 | -.962 | .097 | -.064 | -.081 | -.682 | -.025 | 1.043 | .989 | .863 | 1.019 |
| .55 | 165 | -3.73 | -.58 | 2.97 | -1.69 | -13.62 | -.972 | .081 | -.057 | -.083 | -.686 | -.022 | 1.058 | .987 | .912 | 1.023 |
| .55 | 170 | -5.67 | -.58 | 4.90 | -2.11 | -31.85 | -.981 | .063 | -.046 | -.079 | -.690 | -.018 | 1.075 | .988 | .963 | 1.024 |
| .55 | 175 | -11.43 | -.58 | 10.64 | -2.81 | -130.33 | -.991 | .039 | -.028 | -.064 | -.694 | -.011 | 1.093 | .994 | 1.014 | 1.011 |

$\delta = \text{constant} = \text{Cot } 150^\circ$

| α | θ | β | δ | X | U | ϕ | n_n | n_{nt} | m_n | m_{tw} | n_t | m_t | ϕ_1 | ϕ_2 | ϕ_3 | ϕ_4 |
|----------|----------|---------|----------|-------|-------|---------|-------|----------|-------|----------|-------|-------|----------|----------|----------|----------|
| .55 | 5 | 11.43 | -1.73 | 9.63 | 5.59 | 133.94 | -.134 | .064 | .449 | -.122 | -.356 | .177 | 1.050 | 1.013 | 1.024 | .809 |
| .55 | 10 | 5.67 | -1.73 | 3.88 | 4.89 | 35.45 | -.238 | .100 | .682 | -.127 | -.396 | .269 | 1.067 | 1.013 | 1.032 | .869 |
| .55 | 15 | 3.73 | -1.73 | 1.96 | 4.48 | 17.22 | -.321 | .124 | .801 | -.102 | -.429 | .316 | 1.077 | 1.012 | 1.035 | .905 |
| .55 | 20 | 2.75 | -1.73 | .99 | 4.18 | 10.84 | -.390 | .141 | .855 | -.069 | -.456 | .338 | 1.084 | 1.010 | 1.037 | .930 |
| .55 | 25 | 2.14 | -1.73 | .40 | 3.93 | 7.89 | -.449 | .154 | .870 | -.034 | -.480 | .344 | 1.089 | 1.008 | 1.037 | .948 |
| .55 | 30 | 1.73 | -1.73 | .00 | 3.73 | 6.29 | -.500 | .163 | .861 | -.000 | -.500 | .340 | 1.092 | 1.006 | 1.036 | .963 |
| .55 | 35 | 1.43 | -1.73 | -.28 | 3.55 | 5.33 | -.545 | .170 | .836 | .030 | -.518 | .330 | 1.094 | 1.003 | 1.035 | .975 |
| .55 | 40 | 1.19 | -1.73 | -.50 | 3.38 | 4.70 | -.586 | .175 | .799 | .058 | -.534 | .316 | 1.096 | 1.001 | 1.032 | .985 |
| .55 | 45 | .9 | -1.73 | -.67 | 3.22 | 4.28 | -.623 | .179 | .755 | .082 | -.549 | .298 | 1.096 | .999 | 1.029 | .994 |
| .55 | 50 | .84 | -1.73 | -.81 | 3.07 | 3.98 | -.658 | .181 | .706 | .102 | -.562 | .279 | 1.096 | .997 | 1.025 | 1.001 |
| .55 | 55 | .70 | -1.73 | -.92 | 2.93 | 3.76 | -.690 | .182 | .652 | .119 | -.575 | .258 | 1.095 | .995 | 1.019 | 1.007 |
| .55 | 60 | .58 | -1.73 | -1.02 | 2.78 | 3.60 | -.721 | .182 | .596 | .133 | -.587 | .235 | 1.093 | .993 | 1.013 | 1.012 |
| .55 | 65 | .47 | -1.73 | -1.09 | 2.63 | 3.48 | -.749 | .181 | .538 | .143 | -.598 | .212 | 1.090 | .992 | 1.005 | 1.016 |
| .55 | 70 | .36 | -1.73 | -1.16 | 2.48 | 3.38 | -.776 | .179 | .479 | .149 | -.609 | .189 | 1.087 | .990 | .995 | 1.020 |
| .55 | 75 | .27 | -1.73 | -1.20 | 2.33 | 3.30 | -.801 | .177 | .420 | .152 | -.619 | .166 | 1.083 | .989 | .984 | 1.022 |
| .55 | 80 | .18 | -1.73 | -1.24 | 2.18 | 3.24 | -.825 | .173 | .363 | .151 | -.628 | .144 | 1.078 | .988 | .970 | 1.024 |
| .55 | 85 | .09 | -1.73 | -1.26 | 2.02 | 3.19 | -.846 | .168 | .309 | .147 | -.637 | .122 | 1.072 | .987 | .953 | 1.024 |
| .55 | 90 | 0 | -1.73 | -1.27 | 1.86 | 3.14 | -.866 | .163 | .259 | .140 | -.644 | .102 | 1.065 | .987 | .935 | 1.024 |
| .55 | 95 | -.09 | -1.73 | -1.26 | 1.71 | 3.09 | -.883 | .157 | .214 | .131 | -.651 | .085 | 1.058 | .987 | .913 | 1.023 |
| .55 | 100 | -.18 | -1.73 | -1.24 | 1.55 | 3.04 | -.898 | .151 | .175 | .119 | -.657 | .069 | 1.051 | .988 | .889 | 1.021 |
| .55 | 105 | -.27 | -1.73 | -1.20 | 1.39 | 2.98 | -.912 | .144 | .141 | .107 | -.663 | .056 | 1.043 | .989 | .863 | 1.019 |
| .55 | 110 | -.36 | -1.73 | -1.16 | 1.24 | 2.90 | -.923 | .138 | .112 | .094 | -.667 | .044 | 1.036 | .990 | .834 | 1.016 |
| .55 | 115 | -.47 | -1.73 | -1.09 | 1.09 | 2.80 | -.933 | .131 | .088 | .081 | -.671 | .035 | 1.029 | .992 | .804 | 1.013 |
| .55 | 120 | -.58 | -1.73 | -1.02 | .95 | 2.68 | -.942 | .124 | .067 | .068 | -.674 | .027 | 1.022 | .993 | .771 | 1.011 |
| .55 | 125 | -.70 | -1.73 | -.92 | .80 | 2.52 | -.949 | .118 | .051 | .056 | -.677 | .020 | 1.017 | .995 | .736 | 1.008 |
| .55 | 130 | -.84 | -1.73 | -.81 | .65 | 2.30 | -.956 | .111 | .036 | .044 | -.680 | .014 | 1.011 | .996 | .698 | 1.006 |
| .55 | 135 | -.9 | -1.73 | -.67 | .50 | 2.00 | -.962 | .104 | .025 | .032 | -.682 | .010 | 1.007 | .998 | .656 | 1.003 |
| .55 | 140 | -1.19 | -1.73 | -.50 | .35 | 1.58 | -.967 | .098 | .015 | .021 | -.684 | .006 | 1.003 | .999 | .610 | 1.002 |
| .55 | 145 | -1.43 | -1.73 | -.28 | .18 | .95 | -.972 | .091 | .007 | .010 | -.686 | .003 | 1.001 | 1.000 | .559 | 1.000 |
| .55 | 150 | -1.73 | -1.73 | .00 | -.00 | -.01 | -.977 | .083 | -.000 | -.000 | -.688 | -.000 | 1.000 | 1.000 | .500 | 1.000 |
| .55 | 155 | -2.14 | -1.73 | .40 | -.21 | -1.61 | -.981 | .075 | -.005 | -.010 | -.690 | -.002 | 1.001 | 1.000 | .567 | 1.001 |
| .55 | 160 | -2.75 | -1.73 | .99 | -.45 | -4.56 | -.985 | .067 | -.009 | -.019 | -.692 | -.003 | 1.005 | .998 | .640 | 1.003 |
| .55 | 165 | -3.73 | -1.73 | 1.96 | -.75 | -10.94 | -.989 | .057 | -.011 | -.027 | -.693 | -.004 | 1.015 | .995 | .723 | 1.007 |
| .55 | 170 | -5.67 | -1.73 | 3.88 | -1.17 | -29.17 | -.993 | .045 | -.011 | -.033 | -.695 | -.004 | 1.032 | .991 | .819 | 1.015 |
| .55 | 175 | -11.43 | -1.73 | 9.63 | -1.86 | -127.66 | -.996 | .029 | -.008 | -.034 | -.696 | -.003 | 1.065 | .987 | .935 | 1.024 |

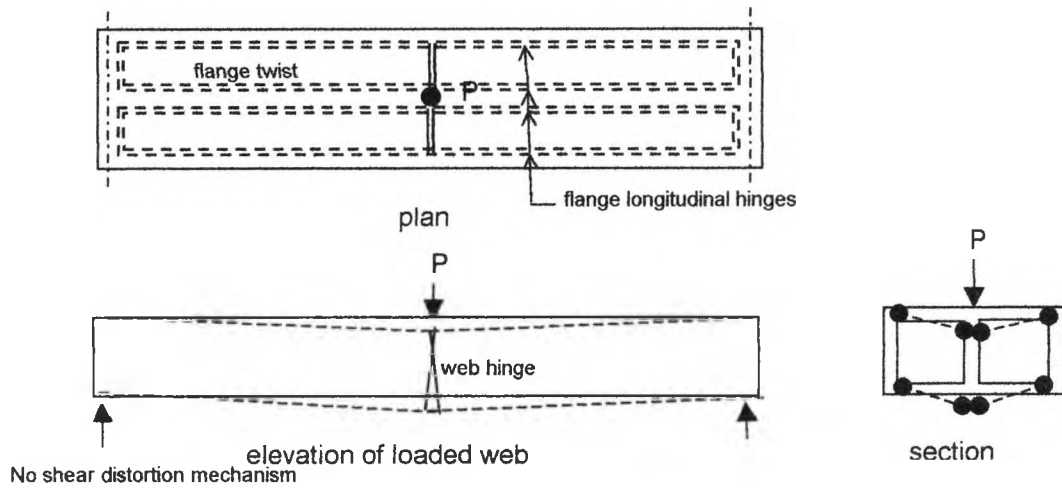
$\delta = \text{constant} = \text{Cot } 175^\circ$

| α | θ | β | δ | χ | U | ϕ | n_n | n_{nt} | m_n | m_{tw} | n_t | m_t | ϕ_1 | ϕ_2 | ϕ_3 | ϕ_4 |
|----------|----------|---------|----------|--------|------|--------|-------|----------|-------|----------|-------|-------|----------|----------|----------|----------|
| .55 | 5 | 11.43 | -11.43 | .00 | 7.46 | 261.59 | -.500 | .049 | .993 | -.000 | -.500 | .392 | 1.017 | 1.007 | 1.009 | .672 |
| .55 | 10 | 5.67 | -11.43 | -5.75 | 6.76 | 163.11 | -.668 | .060 | .875 | .057 | -.566 | .346 | 1.027 | 1.009 | 1.013 | .717 |
| .55 | 15 | 3.73 | -11.43 | -7.67 | 6.34 | 144.87 | -.753 | .063 | .730 | .088 | -.600 | .288 | 1.034 | 1.011 | 1.017 | .748 |
| .55 | 20 | 2.75 | -11.43 | -8.64 | 6.04 | 138.49 | -.805 | .064 | .613 | .106 | -.620 | .242 | 1.040 | 1.012 | 1.020 | .772 |
| .55 | 25 | 2.14 | -11.43 | -9.23 | 5.80 | 135.54 | -.840 | .065 | .522 | .116 | -.634 | .206 | 1.045 | 1.013 | 1.022 | .791 |
| .55 | 30 | 1.73 | -11.43 | -9.63 | 5.59 | 133.94 | -.866 | .064 | .449 | .122 | -.644 | .177 | 1.050 | 1.013 | 1.024 | .809 |
| .55 | 35 | 1.43 | -11.43 | -9.91 | 5.41 | 132.98 | -.885 | .064 | .389 | .125 | -.652 | .154 | 1.054 | 1.013 | 1.026 | .824 |
| .55 | 40 | 1.19 | -11.43 | -10.13 | 5.24 | 132.36 | -.901 | .063 | .340 | .127 | -.659 | .134 | 1.058 | 1.014 | 1.028 | .839 |
| .55 | 45 | .9 | -11.43 | -10.30 | 5.09 | 131.94 | -.914 | .062 | .297 | .127 | -.664 | .117 | 1.062 | 1.013 | 1.030 | .852 |
| .55 | 50 | .84 | -11.43 | -10.44 | 4.94 | 131.64 | -.925 | .061 | .260 | .126 | -.668 | .103 | 1.066 | 1.013 | 1.031 | .865 |
| .55 | 55 | .70 | -11.43 | -10.55 | 4.79 | 131.42 | -.935 | .060 | .228 | .125 | -.672 | .090 | 1.070 | 1.013 | 1.033 | .878 |
| .55 | 60 | .58 | -11.43 | -10.65 | 4.64 | 131.26 | -.943 | .058 | .199 | .122 | -.675 | .078 | 1.073 | 1.013 | 1.034 | .891 |
| .55 | 65 | .47 | -11.43 | -10.72 | 4.50 | 131.13 | -.951 | .057 | .173 | .119 | -.678 | .068 | 1.077 | 1.012 | 1.035 | .903 |
| .55 | 70 | .36 | -11.43 | -10.78 | 4.35 | 131.04 | -.957 | .056 | .149 | .116 | -.681 | .059 | 1.080 | 1.011 | 1.036 | .916 |
| .55 | 75 | .27 | -11.43 | -10.83 | 4.20 | 130.96 | -.963 | .054 | .128 | .111 | -.683 | .051 | 1.084 | 1.010 | 1.037 | .928 |
| .55 | 80 | .18 | -11.43 | -10.87 | 4.04 | 130.90 | -.968 | .053 | .110 | .107 | -.685 | .043 | 1.087 | 1.009 | 1.037 | .940 |
| .55 | 85 | .09 | -11.43 | -10.89 | 3.89 | 130.84 | -.973 | .051 | .093 | .102 | -.687 | .037 | 1.090 | 1.007 | 1.037 | .952 |
| .55 | 90 | 0 | -11.43 | -10.89 | 3.73 | 130.80 | -.977 | .049 | .079 | .096 | -.688 | .031 | 1.092 | 1.006 | 1.036 | .963 |
| .55 | 95 | -.09 | -11.43 | -10.89 | 3.57 | 130.75 | -.980 | .048 | .067 | .091 | -.690 | .026 | 1.094 | 1.004 | 1.035 | .974 |
| .55 | 100 | -.18 | -11.43 | -10.87 | 3.41 | 130.69 | -.983 | .046 | .056 | .085 | -.691 | .022 | 1.095 | 1.002 | 1.033 | .983 |
| .55 | 105 | -.27 | -11.43 | -10.83 | 3.26 | 130.63 | -.985 | .044 | .047 | .080 | -.692 | .019 | 1.096 | 1.000 | 1.030 | .992 |
| .55 | 110 | -.36 | -11.43 | -10.78 | 3.11 | 130.56 | -.987 | .042 | .040 | .074 | -.692 | .016 | 1.096 | .998 | 1.026 | .999 |
| .55 | 115 | -.47 | -11.43 | -10.72 | 2.96 | 130.46 | -.989 | .041 | .033 | .069 | -.693 | .013 | 1.095 | .996 | 1.021 | 1.006 |
| .55 | 120 | -.58 | -11.43 | -10.65 | 2.81 | 130.34 | -.990 | .039 | .028 | .064 | -.694 | .011 | 1.093 | .994 | 1.014 | 1.011 |
| .55 | 125 | -.70 | -11.43 | -10.55 | 2.67 | 130.17 | -.992 | .038 | .024 | .059 | -.694 | .009 | 1.091 | .992 | 1.007 | 1.016 |
| .55 | 130 | -.84 | -11.43 | -10.44 | 2.52 | 129.95 | -.993 | .036 | .020 | .054 | -.695 | .008 | 1.088 | .990 | .997 | 1.019 |
| .55 | 135 | -.9 | -11.43 | -10.30 | 2.37 | 129.65 | -.994 | .034 | .016 | .049 | -.695 | .006 | 1.084 | .989 | .986 | 1.022 |
| .55 | 140 | -1.19 | -11.43 | -10.13 | 2.21 | 129.23 | -.995 | .033 | .013 | .044 | -.695 | .005 | 1.079 | .988 | .973 | 1.024 |
| .55 | 145 | -1.43 | -11.43 | -9.91 | 2.05 | 128.61 | -.996 | .031 | .011 | .039 | -.696 | .004 | 1.073 | .987 | .956 | 1.024 |
| .55 | 150 | -1.73 | -11.43 | -9.63 | 1.86 | 127.65 | -.996 | .029 | .008 | .034 | -.696 | .003 | 1.065 | .987 | .935 | 1.024 |
| .55 | 155 | -2.14 | -11.43 | -9.23 | 1.66 | 126.05 | -.997 | .027 | .006 | .028 | -.696 | .002 | 1.056 | .988 | .906 | 1.022 |
| .55 | 160 | -2.75 | -11.43 | -8.64 | 1.42 | 123.10 | -.998 | .025 | .004 | .022 | -.697 | .002 | 1.044 | .989 | .867 | 1.019 |
| .55 | 165 | -3.73 | -11.43 | -7.67 | 1.11 | 116.72 | -.998 | .022 | .003 | .016 | -.697 | .001 | 1.030 | .992 | .808 | 1.014 |
| .55 | 170 | -5.67 | -11.43 | -5.75 | .70 | 98.48 | -.999 | .018 | .001 | .008 | -.697 | .000 | 1.013 | .996 | .709 | 1.006 |
| .55 | 175 | -11.43 | -11.43 | .00 | -.00 | -.00 | -.999 | .013 | -.000 | -.000 | -.697 | -.000 | 1.000 | 1.000 | .500 | 1.000 |

Appendix B Collapse load computation

Beam B1

Idealised internal flange and web study



| | | | |
|---------------------------------------|----------|----------------------|----------|
| concrete strength | f_{cu} | 40 N/mm ² | |
| 3mm mesh yield force | F_{ym} | 3.5 kN/wire | 50mm c/c |
| 4mm add wire | F_{yw} | 6.1 kN/wire | 20mm c/c |
| effective flange width between fillet | b | 262 mm | |
| flange thickness | t_f | 25 mm | |
| web depth | d | 250 mm | |
| web thickness | t_w | 30 mm | |

top flange

| | |
|-----------------------------|---------------------------|
| long reinf. Top 3mm mesh | 0.141 mm ² /mm |
| reinf. Parameter | 0.117 |
| dist of layer from top | 8.5 mm |
| long reinf bottom 3mm mesh | 0.141 mm ² /mm |
| reinf para | 0.117 |
| distance of layer from top | 16.5 mm |
| trans reinf. top 3mm mesh | 0.141 mm ² /mm |
| reinf. Parameter | 0.117 |
| distance of layer from top | 5.5 mm |
| trans reinf bottom 3mm mesh | 0.141 mm ² /mm |
| reinf para | 0.117 |
| distance of layer from top | 19.5 mm |

Moment capacity can be derived from equation 3.80, in all cases for the long. and transverse yield lines; strain rates are limited to normal strain and rotation only

| | | | |
|---|----------------|------------------|-------------|
| longitudinal sagging & hogging moment | $\rho = 0.117$ | $d = 12.5 - 8.5$ | |
| transverse sagging & hogging moment | $\rho = 0.117$ | $d = 12.5 - 5.5$ | |
| long. sagg yield moment of top flange = | | | 560 N-mm/mm |
| long. hogg yield moment of top flange = | | | 560 N-mm/mm |
| trans sagg yield moment of top flange = | | | 980 N-mm/mm |
| trans hogg yield moment of top flange = | | | 980 N-mm/mm |
| average for twisting moment by top flange | | | 770 N-mm/mm |

bottom flange

| | |
|---------------------------------------|---------------------------|
| long reinf. Top 3mm mesh + 4.1mm wire | 0.8 mm ² /mm |
| reinf. Parameter | 0.625 |
| dist of layer from top | 8.5 mm |
| long reinf bot 3mm mesh + 4.1mm wire | 0.8 mm ² /mm |
| reinf para | 0.625 |
| dist of layer from top | 16.5 mm |
| trans reinf. Top 3mm mesh | 0.141 mm ² /mm |
| reinf. Parameter | 0.117 |
| dist of layer from top | 5.5 mm |
| trans reinf bot 3mm mesh | 0.141 mm ² /mm |
| reinf para | 0.117 |
| dist of layer from top | 19.5 mm |

Similarly

Moment capacity can be derived from equation 3.80, in all cases for the long. and transverse yield lines; strain rates are limited to normal strain and rotation only

| | | |
|---------------------------------------|----------------|------------------|
| longitudinal sagging & hogging moment | $\rho = 0.625$ | $d = 12.5 - 8.5$ |
| transverse hogging and sagging moment | $\rho = 0.117$ | $d = 12.5 - 5.5$ |

| | |
|--|--------------|
| long. sagg yield moment of bottom flange = | 2900 N-mm/mm |
| long. hogg yield moment of bottom flange = | 2900 N-mm/mm |
| trans sagg yield moment of bottom flange = | 980 N-mm/mm |
| trans hogg yield moment of bottom flange = | 980 N-mm/mm |
| average for twisting moment by bottom flange | 1940 N-mm/mm |

web yield hinge

(simplified calculation taking into account local equilibrium condition)

| | | |
|--|----|------------|
| web reinforcement 3mm mesh each face | | |
| effective flange width for web bending | b | 330 mm |
| effective bottom flange reinforcement yield force | | 217 kN |
| effective top flange compression due to concrete | | 198 kN |
| capacity of top flange steel in compression | | 23.1 kN |
| effective top flange reinforcement in compression | | 19 kN |
| average yield force due to web reinforcement | | 28 kN |
| neutral axis depth for web resisting sagging moment | | 12.5 mm |
| lever arm for moment calculation | | 225 mm |
| effective bending capacity of web due to flange | | 48.83 kN-m |
| additional bending capacity due to web reinforcement | | 3.5 kN-m |
| total bending capacity due to web hinge | Mw | 52.33 kN-m |

Internal work due to top flange longitudinal hinges

$$\begin{aligned}
 &= \text{total transverse moment capacity } M_c \times \text{average rotation of flange web hinge} \\
 &= M_c \times (1/b) / 2 \times 4 L \quad (4 \text{ No. longitudinal hinge lines}) \\
 &= 980 \times 1/262 / 2 \times 4 \times 3500 / 1000000 = 0.026183 \text{ kN-m}
 \end{aligned}$$

Internal work due to top flange transverse hinges

$$\begin{aligned}
 &= \text{total longitudinal moment capacity } M_c \times \text{average rotation of flange hinge} \\
 &= M_c \times (1/(L/2)) / 2 \times 2 \times b \times 2 \quad (1 \text{ No. transverse hinge}) \\
 &= 560 \times 1 \times 2 / 3500 / 2 \times 2 \times 262 \times 2 / 1000000 = 0.000168 \text{ kN-m}
 \end{aligned}$$

Internal work due to bottom flange longitudinal hinges
 = total transverse moment capacity M_c x average rotation of flange web hinge
 = $M_c \times (1/b) / 2 \times 4 L$ (4 No. longitudinal hinge lines)
 = $980 \times 1/262 / 2 \times 4 \times 3500 / 1000000 = 0.026183 \text{ kN-m}$

Internal work due to bottom flange transverse hinges
 = total longitudinal moment capacity M_c x average rotation of flange hinge
 = $M_c \times (1/(L/2)) / 2 \times 2 \times b \times 2$ (1 No. transverse hinge)
 = $2900 / 1750 / 2 \times 2 \times 262 \times 2 / 1000000 = 0.000868 \text{ kN-m}$

internal work due to web hinge
 = web moment capacity M_w x rotation of web hinge
 = $M_w \times (1/(L/2)) \times 2$ (1 No. web hinge)
 = $M_w \times 1 \times 2 / 3500 \times 2 = 0.0598 \text{ kN-m}$

twisting work due to top flange
 = average yield moment x K x area
 = Average $M_c \times (1/b/(L/2)) \times b \times (L/2) \times 4 = 0.00308 \text{ kN-m}$
 = $770 \times (1/262/1750) \times 262 \times 1750 \times 4 =$

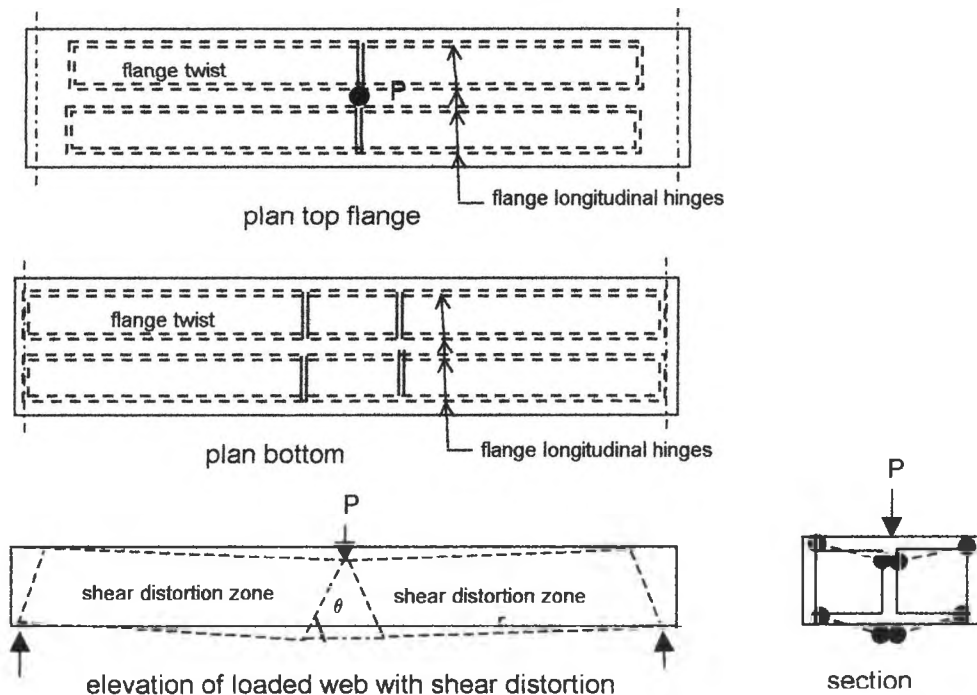
twisting work due to bottom flange
 = average yield moment x K x area
 = Average $M_c \times (1/b/(L/2)) \times b \times (L/2) \times 4 = 0.00776 \text{ kN-m}$
 = $1940 \times (1/262/1750) \times 262 \times 1750 \times 4 =$

Total internal work due to unit deflection 0.124042 kN-m

External work due to point load = $P \times 1\text{mm} / 1000 = 0.001P \text{ kN-m}$

equating Internal and external work $P = 124.04 \text{ kN}$

Shear distortion mechanism



Internal work of web due to shear mechanism from equation 4.9-4.11

due to web reinforcement $\text{try } \theta = 45$ $r = 1500.00$
 $2 \times A_s \times F_y \times \cot \theta \times (1/r) \times h \times r = 0.0700 \text{ kN-m}$

due to web in shear
 $2 \times \sigma_c / 2 / \sin \theta \times (1 - \cos \theta) \times t \times (1/r) \times h \times r = 0.0497 \text{ kN-m}$

Internal work from top flange

longitudinal hinges

$= M_c \times 1/b / 2 \times 8 \times r$ (4 No. longitudinal hinge lines)
 $= 980 \times 1 / 262 / 2 \times 8 \times r / 1000000 = 0.022443 \text{ kN-m}$

transverse hinges

$= M_c \times 1/r / 2 \times 4 \times b \times 2$
 $= 560 \times 1 / r / 2 \times 4 \times 262 \times 2 / 1000000 = 0.000391 \text{ kN-m}$

Internal work from bottom flange

longitudinal hinges

$= 2 \times M_c \times (4 \times r / b / 2 + 1 / b \times 2 \times h \times \cot \theta)$
 $= 2 \times 980 \times (2 \times r / 262 + 1 / 262 \times 2 \times 250 \cot \theta) / 1000000 = 0.022483 \text{ kN-m}$

transverse hinges

$= M_c \times (1 / r) / 2 \times 4 \times b$ (4 No. transverse hinge)
 $= 2900 / r / 2 \times 4 \times 262 / 1000000 = 0.001013 \text{ kN-m}$

twisting work due to top flange

$= \text{average yield moment} \times K \times \text{area}$
 $= \text{Average } M_c \times (1/b/r) \times b \times r \times 4 =$
 $= 770 \times (1/262/r) \times 262 \times r \times 4 = 0.00308 \text{ kN-m}$

twisting work due to bottom flange

$= \text{average yield moment} \times K \times \text{area}$
 $= \text{Average } M_c \times (1/b/r) \times b \times r \times 4 =$
 $= 1940 \times (1/262/r) \times 262 \times r \times 4 = 0.00776 \text{ kN-m}$

Total internal work due to unit deflection 0.1769 kN-m

External work due to point load $= P \times 1 \text{ mm} / 1000 = 0.001P \text{ kN-m}$

equating internal and external work $P_{sd} = 176.9 \text{ kN}$

by numerical method, minimum occur when θ is about 62 degrees

$P_{sd \text{ min}} = 169.8 \text{ kN}$

With shear modification

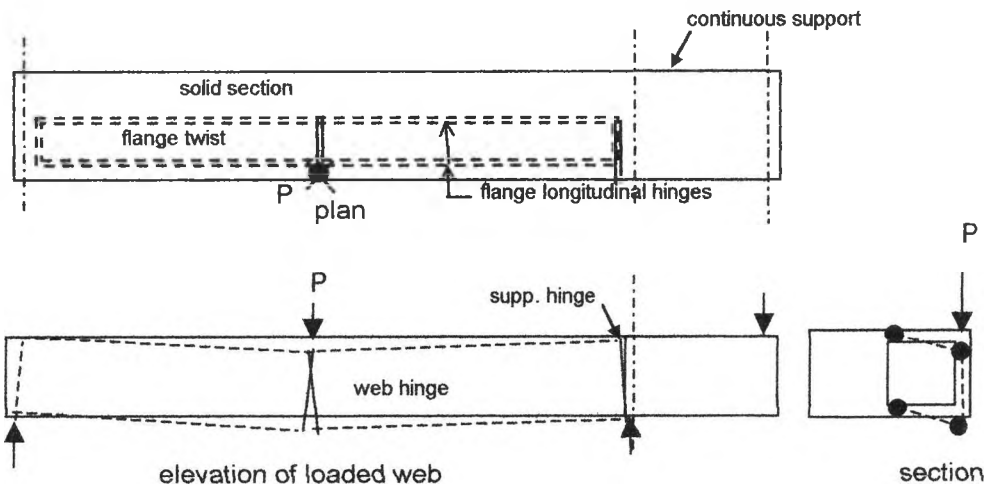
the shear capacity of web is reduced to

$.55 \times 2 \times \sigma_c / 2 / \sin q \times (1 - \cos q) \times t \times (r) \times h \times r \times 1000 = 39.66 \text{ kN}$

modified collapse load

$P' = P - 72.1 + 39.66$ $P_{sd}' \text{ min} = 137.36 \text{ kN}$

Beam B2 Idealised external flange web continuous box beam



No shear distortion mechanism

| | | | |
|--|-----|----------------------|----------|
| concrete strength | fcu | 45 N/mm ² | |
| 3mm mesh yield force | Fym | 3.5 kN/wire | 50mm c/c |
| 4mm add wire | Fyw | 6.1 kN/wire | 20mm c/c |
| flange width clear width between fillets | b | 270 mm | |
| flange thickness | tf | 25 mm | |
| web depth | d | 250 mm | |
| web thickness | tw | 30 mm | |

top flange

| | |
|--|---------------------------|
| long reinf. Top 3mm mesh mid span | 0.141 mm ² /mm |
| reinf. Parameter | 0.104 |
| dist of layer from top | 8.5 mm |
| long reinf bot 3mm mesh mid span | 0.141 mm ² /mm |
| reinf para | 0.104 |
| dist of layer from top | 16.5 mm |
| long reinf. Top 3mm mesh + 4mm support | 0.8 mm ² /mm |
| reinf. Parameter | 0.560 |
| dist of layer from top | 8.5 mm |
| long reinf bot 3mm mesh + 4mm support | 0.8 mm ² /mm |
| reinf para | 0.560 |
| dist of layer from top | 16.5 mm |
| trans reinf. Top 3mm mesh | 0.141 mm ² /mm |
| reinf. Parameter | 0.104 |
| dist of layer from top | 5.5 mm |
| trans reinf bot 3mm mesh | 0.141 mm ² /mm |
| reinf para | 0.104 |
| dist of layer from top | 19.5 mm |

Moment capacity can be derived from equation 3.80, in all cases for the long. and transverse yield lines; strain rates are limited to normal strain and rotation only

| | | |
|--|----------------|------------------|
| longitudinal sagging & hogging moment mid span | $\rho = 0.104$ | $d = 12.5 - 8.5$ |
| longitudinal sagging & hogging moment support | $\rho = 0.56$ | $d = 12.5 - 8.5$ |
| transverse sagging & hogging moment | $\rho = 0.104$ | $d = 12.5 - 5.5$ |

| | |
|---|--------------|
| long. sagg yield moment of top flange mid span= | 560 N-mm/mm |
| long. hogg yield moment of top flange mid span= | 560 N-mm/mm |
| long. sagg yield moment of top flange support= | 3000 N-mm/mm |
| long. hogg yield moment of top flange support= | 3000 N-mm/mm |
| trans sagg yield moment of top flange= | 980 N-mm/mm |
| trans hogg yield moment of top flange= | 980 N-mm/mm |
| average for twisting moment by top flange near end span | 770 N-mm/mm |
| average for twisting moment by top flange adj cont. support | 1990 N-mm/mm |

bottom flange

| | |
|---|---------------------------|
| long reinf. Top 3mm mesh + 4.1mm mid span | 0.8 mm ² /mm |
| reinf. Parameter | 0.56 |
| dist of layer from top | 8.5 mm |
| long reinf bot 3mm mesh + 4.1mm wire mid span | 0.8 mm ² /mm |
| reinf para | 0.56 |
| dist of layer from top | 16.5 mm |
| long reinf. Top 3mm mesh + 4.1mm near cont. support | 0.471 mm ² /mm |
| reinf. Parameter | 0.33 |
| dist of layer from top | 8.5 mm |
| long reinf bot 3mm mesh + 4.1mm near cont. support | 0.8 mm ² /mm |
| reinf para | 0.33 |
| dist of layer from top | 16.5 mm |
| trans reinf. Top 3mm mesh | 0.141 mm ² /mm |
| reinf. Parameter | 0.104 |
| dist of layer from top | 5.5 mm |
| trans reinf bot 3mm mesh | 0.141 mm ² /mm |
| reinf para | 0.104 |
| dist of layer from top | 19.5 |

Similarly

Moment capacity can be derived from equation 3.80, in all cases for the long. and transverse yield lines; strain rates are limited to normal strain and rotation only

| | | |
|--|----------------|------------------|
| longitudinal sagging & hogging moment mid span | $\rho = 0.56$ | $d = 12.5 - 8.5$ |
| longitudinal sagging & hogging moment support | $\rho = 0.33$ | $d = 12.5 - 8.5$ |
| transverse sagging & hogging moment | $\rho = 0.104$ | $d = 12.5 - 5.5$ |

| | |
|--|--------------|
| long. sagg yield moment of bott flange mid span= | 3000 N-mm/mm |
| long. hogg yield moment of bottom flange mid span= | 3000 N-mm/mm |
| long. sagg yield moment of bottom flange support= | 1780 N-mm/mm |
| long. hogg yield moment of bottom flange support= | 1780 N-mm/mm |
| trans sagg yield moment of bottom flange= | 980 N-mm/mm |
| trans hogg yield moment of bottom flange= | 980 N-mm/mm |

average for twisting moment by bottom flange near end span 1990 N-mm/mm
 average for twisting moment by bottom flange adj cont. support 1380 N-mm/mm

web yield hinge mid span and at support

(simplified calculation taking into account local equilibrium condition)

web reinforcement 3mm mesh each face

effective flange width for web bending 300 mm

effective bottom flange reinforcement yield force 237.2 kN

effective top flange compression due to concrete 202.5 kN

capacity of top flange steel in compression 21 kN

effective top flange reinforcement in compression 34.7 kN

average yield force due to web reinforcement 28 kN

neutral axis depth for web resisting sagging moment 12.5 mm

lever arm for moment calculation 225 mm

effective bending capacity of web due to flange 53.37 kN-m

additional bending capacity due to web reinforcement 3.5 kN-m

total bending capacity due to web hinge **Mw** 56.87 kN-m

Internal work due to top flange longitudinal hinges

= transverse moment capacity M_c x average rotation of flange web hinge

= $M_c \times (1/b) / 2 \times 2 L$ (2 No. longitudinal hinge lines)

= $980 \times 1/b / 2 \times 2 \times 3500 / 1000000 = 0.0127 \text{ kN-m}$

Internal work due to top flange transverse hinge at mid span

= long. moment capacity M_c x average rotation of flange hinge at mid span

= $M_c \times (1/(L/2)) / 2 \times 2 \times b$ (1 No. transverse hinge)

= $560 \times 1750 / 2 \times 2 \times b / 1000000 = 0.0001 \text{ kN-m}$

Internal work due to top flange transverse hinge at support

= long. moment capacity M_c x average rotation of flange hinge at support

= $M_c \times (1/(L/2)) / 2 \times b$ (1 No. transverse hinge)

= $1780 \times 1 / 1750 / 2 \times b / 1000000 = 0.0001 \text{ kN-m}$

Internal work due to bottom flange longitudinal hinges

= total transverse moment capacity M_c x average rotation of flange web hinge

= $M_c \times (1/b) / 2 \times 2 L$ (2 No. longitudinal hinge lines)

= $980 \times 1/b / 2 \times 2 \times 3500 / 1000000 = 0.0127 \text{ kN-m}$

Internal work due to bottom flange transverse hinges at mid span

= long. moment capacity M_c x average rotation of flange hinge at mid span

= $M_c \times (1/(L/2)) / 2 \times 2 \times b$ (1 No. transverse hinge)

= $3000 / 1750 / 2 \times 2 \times b / 1000000 = 0.0005 \text{ kN-m}$

Internal work due to bottom flange transverse hinges at support

= long. moment capacity M_c x average rotation of flange hinge at cont. support

= $M_c \times (1/(L/2)) / 2 \times b$ (1 No. transverse hinge)

= $3000 / 1750 / 2 \times b / 1000000 = 0.0002 \text{ kN-m}$

internal work due to web hinge at mid span

= web moment capacity M_w x rotation of web hinge at mid span

= $M_w \times (1/(L/2)) \times 2$ (1 No. web hinge)

= $M_w \times 1 \times 2 / 3500 \times 2 = 0.0650 \text{ kN-m}$

internal work due to web hinge at cont. support

= web moment capacity M_w x rotation of web hinge at cont. support
 = $M_w \times (1/(L/2))$ (1 No. web hinge)
 = $M_w \times 1 \times 2 / 3500 =$ 0.0325 kN-m

twisting work due to top flange near end span and support
 = total average yield moment x K x area
 = Average $M_c \times (1/b/(L/2)) \times b \times (L/2) =$
 = $(770+1990) \times (1/b/1750) \times b \times 1750 =$ 0.0028 kN-m

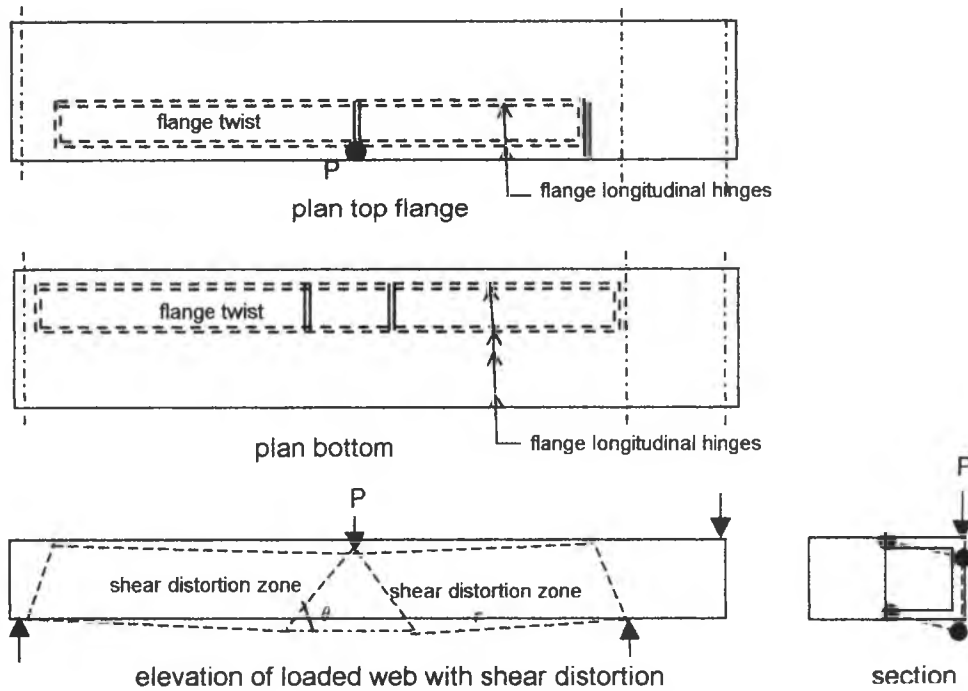
twisting work due to bottom flange
 =total average yield moment x K x area
 =Average $M_c \times (1/b/(L/2)) \times b \times (L/2) =$
 = $(1990+1380) \times (1/b/1750) \times b \times 1750 =$ 0.0034 kN-m

Total internal work due to unit deflection 0.1299 kN-m

External work due to point load = $P \times 1\text{mm} / 1000$ 0.001P kN-m

equating internal and external work **P= 129.9 kN**

Shear distortion mechanism



Internal work of web due to shear mechanism from equation 4.9-4.11

due to web reinforcement $2 \times A_s \times F_y \times \cot \theta \times (1/r) \times h \times r$ try $\theta = 45$ $r = 1500.00$
 = $980 \times 1 / 270 / 2 \times 4 \times r / 1000000 = 0.0700 \text{ kN-m}$

due to web in shear $2 \times \sigma_c / 2 / \sin \theta \times (1 - \cos \theta) \times t \times (1/r) \times h \times r$ = 0.0559 kN-m

Internal work from top flange longitudinal hinges
 = $M_c \times 1/b / 2 \times 4 \times r$ (2 No. longitudinal hinge lines)
 = $980 \times 1 / 270 / 2 \times 4 \times r / 1000000 = 0.010889 \text{ kN-m}$

transverse top hinge mid span
 = $M_c \times 1 / r / 2 \times b \times 2$
 = $560 \times 1 / r / 2 \times 270 \times 2 / 1000000 = 0.000391 \text{ kN-m}$

transverse top hinge near end support and cont support
 = $M_c \times 1 / r / 2 \times b \times 2$
 = $(560 + 3000) \times 1 / r / 2 \times 270 / 1000000 = 0.00032 \text{ kN-m}$

Internal work from bottom flange longitudinal hinges
 = $M_c \times (4 \times r / b / 2 + 1 / b \times 2 \times h \times \cot \theta)$
 = $980 \times (2 \times r / 270 + 1 / 270 \times 2 \times 250 \cot \theta) / 1000000 = 0.011242 \text{ kN-m}$

transverse hinges
 = $M_c \times (1 / r) / 2 \times 4 \times b$ (4 No. transverse hinge)
 = $(3000 + 1780) \times 1 / r / 2 \times 270 \times 2 / 1000000 = 0.00086 \text{ kN-m}$

twisting work due to top flange
 = average yield moment x K x area
 = Average $M_c \times (1/b/r) \times b \times r =$
 = $(770+1990) \times (1/270/r) \times 270 \times r =$ 0.00276 kN-m

twisting work due to bottom flange
 = average yield moment x K x area
 = Average $M_c \times (1/b/r) \times b \times r =$
 = $(1990+1380) \times (1/262/r) \times 262 \times r =$ 0.00337 kN-m

Total internal work due to unit deflection 0.1558 kN-m

External work due to point load = $P \times 1\text{mm} / 1000$ 0.001P kN-m

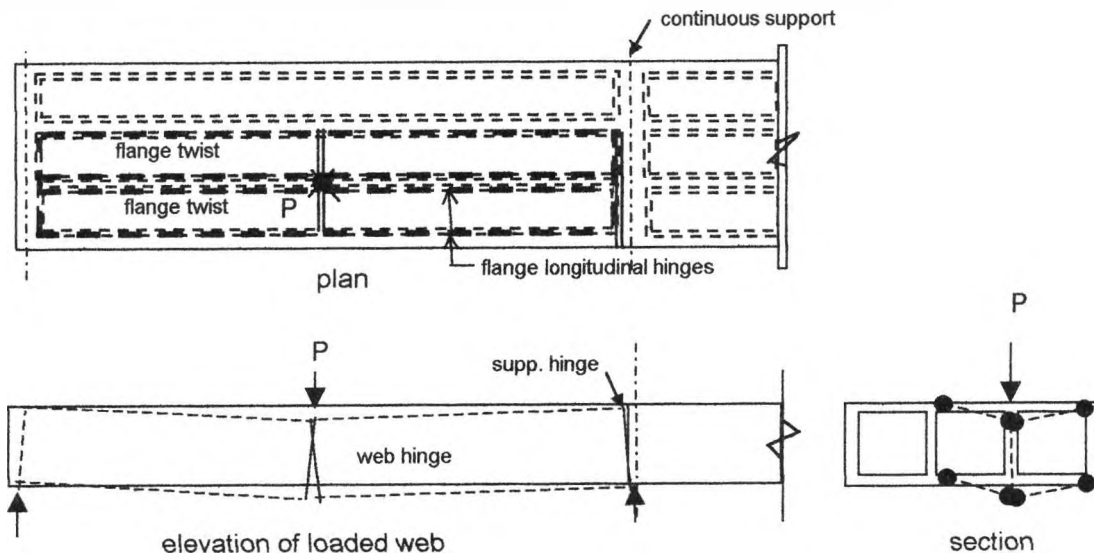
equating Internal and external work $P_{sd} =$ 155.8 kN

by numerical method, minimum occur when
 θ is about 61degrees $P_{sd} \text{ min} =$ 149.7 kN

With shear modification
 the shear capacity of web is reduced to
 $.55 \times 2 \times sc/2/\sin q \times (1-\cos q) \times t \times (r) \times h \times r \times 1000$ 43.74 kN

modified collapse load
 $P' = P - 79.5 + 43.7$ $P_{sd}' \text{ min} =$ 113.90 kN

Beam B3 Three-cell continuous box beam internal web loaded



No shear distortion mechanism

| | | | |
|----------------------|-----|----------------------|----------|
| concrete strength | fcu | 57 N/mm ² | |
| 3mm mesh yield force | Fym | 3.5 kN/wire | 50mm c/c |
| 4mm add wire | Fyw | 6.1 kN/wire | 20mm c/c |

| | | |
|------------------------------|----|--------|
| flange width between fillets | b | 270 mm |
| flange thickness | tf | 25 mm |
| web depth | d | 250 mm |
| web thickness | tw | 30 mm |

top flange

| | |
|--|---------------------------|
| long reinf. Top 3mm mesh mid span | 0.141 mm ² /mm |
| reinf. Parameter | 0.082 |
| dist of layer from top | 8.5 mm |
| long reinf bot 3mm mesh mid span | 0.141 mm ² /mm |
| reinf para | 0.082 |
| dist of layer from top | 16.5 mm |
| long reinf. Top 3mm mesh + 4mm support | 0.8 mm ² /mm |
| reinf. Parameter | 0.439 |
| dist of layer from top | 8.5 mm |
| long reinf bot 3mm mesh + 4mm support | 0.8 mm ² /mm |
| reinf para | 0.439 |
| dist of layer from top | 16.5 mm |
| trans reinf. Top 3mm mesh | 0.141 mm ² /mm |
| reinf. Parameter | 0.082 |
| dist of layer from top | 5.5 mm |
| trans reinf bot 3mm mesh | 0.141 mm ² /mm |
| reinf para | 0.082 |
| dist of layer from top | 19.5 mm |

Moment capacity can be derived from equation 3.80, in all cases for the long. and transverse yield lines; strain rates are limited to normal strain and rotation only

| | | |
|--|----------------|------------------|
| longitudinal sagging & hogging moment mid span | $\rho = 0.082$ | $d = 12.5 - 8.5$ |
| longitudinal sagging & hogging moment support | $\rho = 0.44$ | $d = 12.5 - 8.5$ |
| transverse sagging & hogging moment | $\rho = 0.082$ | $d = 12.5 - 5.5$ |

| | |
|---|--------------|
| long. sagg yield moment of top flange mid span= | 560 N-mm/mm |
| long. hogg yield moment of top flange mid span= | 560 N-mm/mm |
| long. sagg yield moment of top flange support= | 3000 N-mm/mm |
| long. hogg yield moment of top flange support= | 3000 N-mm/mm |
| trans sagg yield moment of top flange= | 980 N-mm/mm |
| trans hogg yield moment of top flange= | 980 N-mm/mm |
| average for twisting moment by top flange near end span | 770 N-mm/mm |
| average for twisting moment by top flange adj cont. support | 1990 N-mm/mm |

bottom flange

| | |
|---|---------------------------|
| long reinf. Top 3mm mesh + 4.1mm mid span | 0.8 mm ² /mm |
| reinf. Parameter | 0.44 |
| dist of layer from top | 8.5 mm |
| long reinf bot 3mm mesh + 4.1mm wire mid span | 0.8 mm ² /mm |
| reinf para | 0.44 |
| dist of layer from top | 16.5 mm |
| long reinf. Top 3mm mesh + 4.1mm near cont. support | 0.471 mm ² /mm |
| reinf. Parameter | 0.26 |
| dist of layer from top | 8.5 mm |
| long reinf bot 3mm mesh + 4.1mm near cont. support | 0.471 mm ² /mm |
| reinf para | 0.26 |
| dist of layer from top | 16.5 mm |
| trans reinf. Top 3mm mesh | 0.141 mm ² /mm |
| reinf. Parameter | 0.082 |
| dist of layer from top | 5.5 mm |
| trans reinf bot 3mm mesh | 0.141 mm ² /mm |
| reinf para | 0.082 |
| dist of layer from top | 19.5 |

Moment capacity can be derived from equation 3.80, in all cases for the long. and transverse yield lines; strain rates are limited to normal strain and rotation only

| | | |
|--|----------------|------------------|
| longitudinal sagging & hogging moment mid span | $\rho = 0.44$ | $d = 12.5 - 8.5$ |
| longitudinal sagging & hogging moment support | $\rho = 0.26$ | $d = 12.5 - 8.5$ |
| transverse sagging & hogging moment | $\rho = 0.082$ | $d = 12.5 - 5.5$ |

| | |
|--|--------------|
| long. sagg yield moment of bott flange mid span= | 3000 N-mm/mm |
| long. hogg yield moment of bottom flange mid span= | 3000 N-mm/mm |
| long. sagg yield moment of bottom flange support= | 1780 N-mm/mm |
| long. hogg yield moment of bottom flange support= | 1780 N-mm/mm |
| trans sagg yield moment of bottom flange= | 980 N-mm/mm |
| trans hogg yield moment of bottom flange= | 980 N-mm/mm |
| average for twisting moment by bottom flange near end span | 1990 N-mm/mm |
| average for twisting moment by bottom flange adj cont. support | 1380 N-mm/mm |

| | |
|---|----------------------|
| web yield hinge mid span and at support (simplified calculation taking into account local equilibrium condition) | |
| web reinforcement 3mm mesh each face | |
| effective flange width for web bending | 330 mm |
| effective bottom flange reinforcement yield force | 241.4 kN |
| effective top flange compression due to concrete | 282.15 kN |
| capacity of top flange steel in compression | 23.1 kN |
| effective top flange reinforcement in compression | -40.75 kN |
| average yield force due to web reinforcement | 28 kN |
| neutral axis depth for web resisting sagging moment | 22 mm |
| lever arm for moment calculation | 215.5 mm |
| effective bending capacity of web due to flange | 52.02 kN-m |
| additional bending capacity due to web reinforcement | 3.5 kN-m |
| total bending capacity due to web hinge | Mw 55.52 kN-m |

Internal work due to top flange longitudinal hinges
= transverse moment capacity M_c x average rotation of flange web hinge
= $M_c \times (1/b) / 2 \times 4 \times L$ (4 No. longitudinal hinge lines)
= $980 \times 1/b / 2 \times 4 \times 3500 / 1000000 = 0.0254 \text{ kN-m}$

Internal work due to top flange transverse hinge at mid span
= long. moment capacity M_c x average rotation of flange hinge at mid span
= $M_c \times (1/(L/2)) / 2 \times 4 \times b$ (1 No. transverse hinge)
= $560 \times 1750 / 2 \times 4 \times b / 1000000 = 0.0002 \text{ kN-m}$

Internal work due to top flange transverse hinge at support
= long. moment capacity M_c x average rotation of flange hinge at support
= $M_c \times (1/(L/2)) / 2 \times b \times 2$ (1 No. transverse hinge)
= $1780 \times 1 / 1750 / 2 \times b \times 2 / 1000000 = 0.0003 \text{ kN-m}$

Internal work due to bottom flange longitudinal hinges
= total transverse moment capacity M_c x average rotation of flange web hinge
= $M_c \times (1/b) / 2 \times 4 \times L$ (4 No. longitudinal hinge lines)
= $980 \times 1/b / 2 \times 4 \times 3500 / 1000000 = 0.0254 \text{ kN-m}$

Internal work due to bottom flange transverse hinges at mid span
= long. moment capacity M_c x average rotation of flange hinge at mid span
= $M_c \times (1/(L/2)) / 2 \times 4 \times b$ (2 No. transverse hinge)
= $3000 / 1750 / 2 \times 4 \times b / 1000000 = 0.0009 \text{ kN-m}$

Internal work due to bottom flange transverse hinges at support
= long. moment capacity M_c x average rotation of flange hinge at cont. support
= $M_c \times (1/(L/2)) / 2 \times b \times 2$ (2 No. transverse hinge)
= $3000 / 1750 / 2 \times 2 \times b / 1000000 = 0.0005 \text{ kN-m}$

internal work due to web hinge at mid span
= web moment capacity M_w x rotation of web hinge at mid span
= $M_w \times (1/(L/2)) \times 2$ (1 No. web hinge)
= $M_w \times 1 \times 2 / 3500 \times 2 = 0.0635 \text{ kN-m}$

internal work due to web hinge at cont. support
= web moment capacity M_w x rotation of web hinge at cont. support
= $M_w \times (1/(L/2))$ (1 No. web hinge)
= $M_w \times 1 \times 2 / 3500 = 0.0317 \text{ kN-m}$

twisting work due to top flange near end span and support

= total average yield moment x K x area

=Average Mc x (1/b/(L/2)) x b x (L/2) x 2 =

$$= (770+1990) \times (1/270/1750) \times 270 \times 1750 \times 2 = 0.0055 \text{ kN-m}$$

twisting work due to bottom flange

=total average yield moment x K x area

=Average Mc x (1/b/(L/2)) x b x (L/2) x 2 =

$$= (1990+1380) \times (1/b/1750) \times b \times 1750 \times 2 = 0.0067 \text{ kN-m}$$

Total internal work due to unit deflection

0.1601 kN-m

External work due to point load = P x 1mm /1000

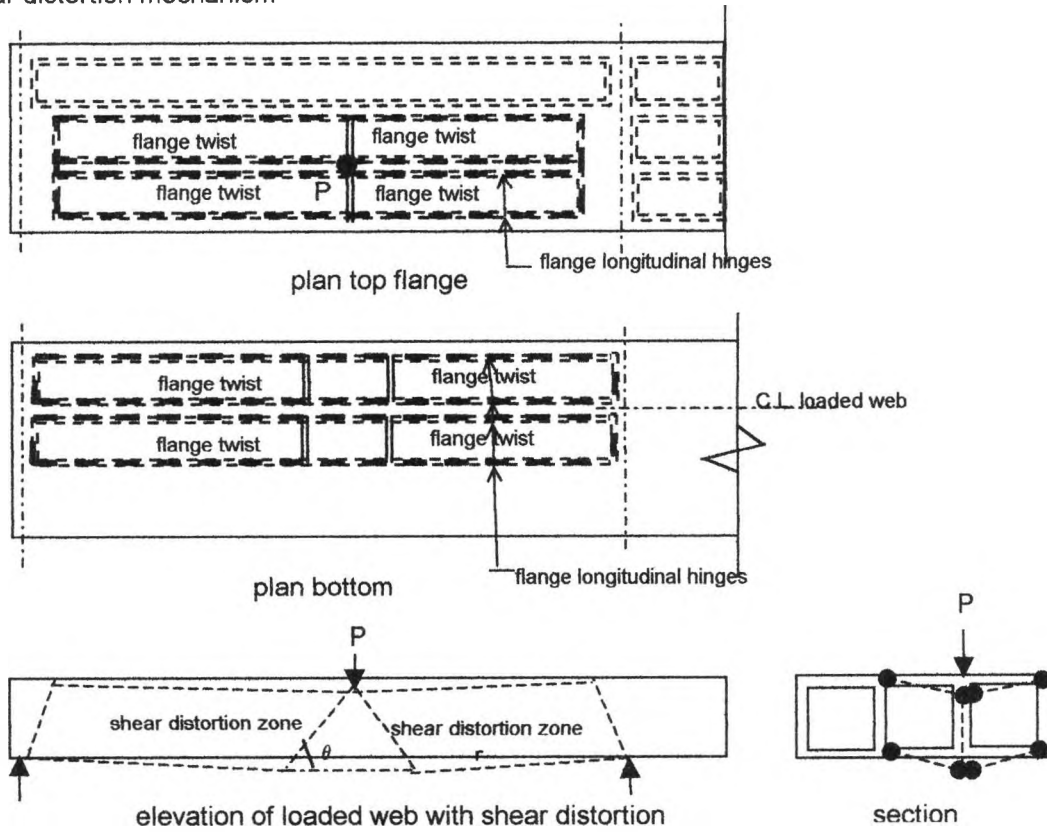
0.001P kN-m

equating Internal and external work

P=

160.1 kN

Shear distortion mechanism



Internal work of web due to shear mechanism from equation 4.9-4.11

| | | | | |
|--|----------------|----|-------|-------------|
| due to web reinforcement | try $\theta =$ | 45 | $r =$ | 1500.00 |
| $2 \times A_s \times F_y \times \cot \theta \times (1/r) \times h \times r$ | | | | 0.0700 kN-m |
| due to web in shear | | | | 0.0708 kN-m |
| $2 \times \sigma_c / 2 / \sin \theta \times (1 - \cos \theta) \times t \times (1/r) \times h \times r$ | | | | |

Internal work from top flange longitudinal hinges
 $= Mc \times 1/b / 2 \times 4 \times 2 \times r \times (4 \text{ No. longitudinal hinge lines})$
 $= 980 \times 1 / 270 / 2 \times 4 \times 2 \times r / 1000000 = 0.021778 \text{ kN-m}$

transverse top hinge mid span
 $= Mc \times 1 / r / 2 \times b \times 4$
 $= 560 \times 1 / r / 2 \times 270 \times 4 / 1000000 = 0.000806 \text{ kN-m}$

transverse top hinge near end support and cont support
 $= Mc \times 1 / r / 2 \times b \times 2$
 $= (560 + 3000) \times 1 / r / 2 \times 270 \times 2 / 1000000 = 0.000641 \text{ kN-m}$

Internal work from bottom flange longitudinal hinges
 $= 2 \times Mc \times (4 \times r / b / 2 + 1 / b \times 2 \times h \times \cot \theta)$
 $= 2 \times 980 \times (2 \times r / 270 + 1 / 270 \times 2 \times 250 \cot \theta) / 1000000 = 0.022483 \text{ kN-m}$

transverse hinges
 $= 2 \times Mc \times (1 / r) / 2 \times 4 \times b \times (8 \text{ No. transverse hinge})$
 $= 2 \times (3000 + 1780) \times 1 / r / 2 \times 270 \times 2 / 1000000 = 0.001721 \text{ kN-m}$

twisting work due to top flange
 = average yield moment x K x area
 =Average Mc x (1/b/(r)) x b x (r) x2 =
 = (770+1990) x (1/270/r) x 270 x r x2 = 0.00552 kN-m

twisting work due to bottom flange
 = average yield moment x K x area
 =Average Mc x (1/b/r) x b x r x2 =
 = 2x(1990+1380) x (1/262/r) x 270 x r = 0.00674 kN-m

Total internal work due to unit deflection 0.2005 kN-m

External work due to point load = P x 1mm /1000 0.001P kN-m

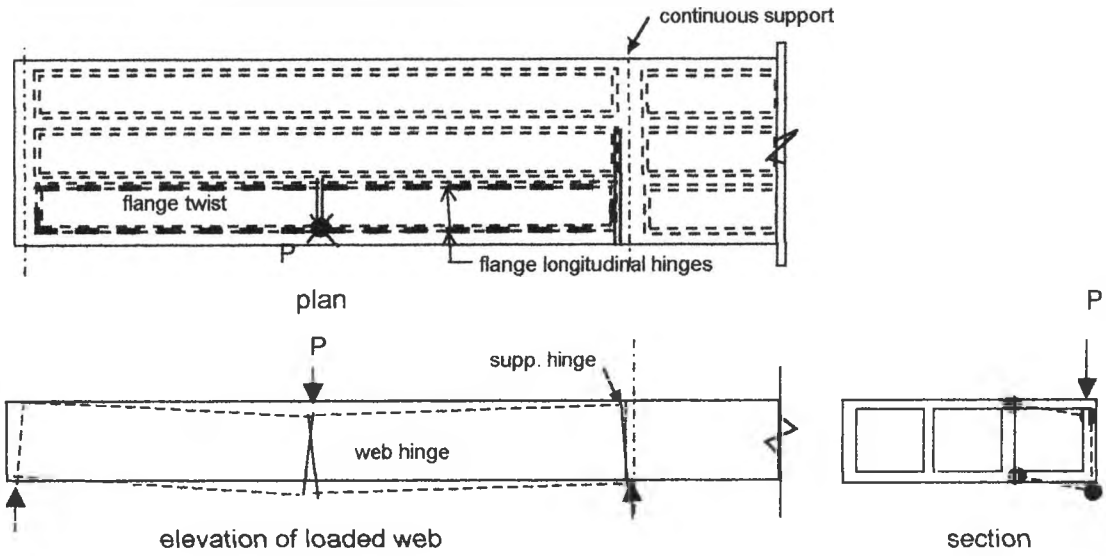
equating internal and external work $P_{sd} = 200.5 \text{ kN}$

by numerical method, minimum occur when θ is about 50degrees
 $P_{sd \text{ min}} = 199 \text{ kN}$

With shear modification
 the shear capacity of web is reduced to
 $.55 \times 2 \times sc/2/\sin q * (1-\cos q) * t * (r) \times h \times r * 1000$ 43.86 kN

modified collapse load
 $P' = P - 79.7 + 43.9$ $P_{sd}' \text{ min} = 163.20 \text{ kN}$

Beam B3 Three-cell continuous box beam external web loaded



No shear distortion mechanism

| | | | |
|----------------------|-----|----------------------|----------|
| concrete strength | fcu | 57 N/mm ² | |
| 3mm mesh yield force | Fym | 3.5 kN/wire | 50mm c/c |
| 4mm add wire | Fyw | 6.1 kN/wire | 20mm c/c |

| | | |
|------------------------------|----|--------|
| flange width between fillets | b | 270 mm |
| flange thickness | tf | 25 mm |
| web depth | d | 250 mm |
| web thickness | tw | 30 mm |

top flange

| | |
|--|---------------------------|
| long reinf. Top 3mm mesh mid span | 0.141 mm ² /mm |
| reinf. Parameter | 0.082 |
| dist of layer from top | 8.5 mm |
| long reinf bot 3mm mesh mid span | 0.141 mm ² /mm |
| reinf para | 0.082 |
| dist of layer from top | 16.5 mm |
| long reinf. Top 3mm mesh + 4mm support | 0.8 mm ² /mm |
| reinf. Parameter | 0.439 |
| dist of layer from top | 8.5 mm |
| long reinf bot 3mm mesh + 4mm support | 0.8 mm ² /mm |
| reinf para | 0.439 |
| dist of layer from top | 16.5 mm |
| trans reinf. Top 3mm mesh | 0.141 mm ² /mm |
| reinf. Parameter | 0.082 |
| dist of layer from top | 5.5 mm |
| trans reinf bot 3mm mesh | 0.141 mm ² /mm |
| reinf para | 0.082 |
| dist of layer from top | 19.5 mm |

Moment capacity can be derived from equation 3.80, in all cases for the long. and transverse yield lines; strain rates are limited to normal strain and rotation only

| | | |
|--|----------------|------------------|
| longitudinal sagging & hogging moment mid span | $\rho = 0.082$ | $d = 12.5 - 8.5$ |
| longitudinal sagging & hogging moment support | $\rho = 0.44$ | $d = 12.5 - 8.5$ |
| transverse sagging & hogging moment | $\rho = 0.082$ | $d = 12.5 - 5.5$ |

| | |
|---|--------------|
| long. sagg yield moment of top flange mid span= | 560 N-mm/mm |
| long. hogg yield moment of top flange mid span= | 560 N-mm/mm |
| long. sagg yield moment of top flange support= | 3000 N-mm/mm |
| long. hogg yield moment of top flange support= | 3000 N-mm/mm |
| trans sagg yield moment of top flange= | 980 N-mm/mm |
| trans hogg yield moment of top flange= | 980 N-mm/mm |
| average for twisting moment by top flange near end span | 770 N-mm/mm |
| average for twisting moment by top flange adj cont. support | 1990 N-mm/mm |

bottom flange

| | |
|---|---------------------------|
| long reinf. Top 3mm mesh + 4.1mm mid span | 0.8 mm ² /mm |
| reinf. Parameter | 0.44 |
| dist of layer from top | 8.5 mm |
| long reinf bot 3mm mesh + 4.1mm wire mid span | 0.8 mm ² /mm |
| reinf para | 0.44 |
| dist of layer from top | 16.5 mm |
| long reinf. Top 3mm mesh + 4.1mm near cont. support | 0.471 mm ² /mm |
| reinf. Parameter | 0.26 |
| dist of layer from top | 8.5 mm |
| long reinf bot 3mm mesh + 4.1mm near cont. support | 0.471 mm ² /mm |
| reinf para | 0.26 |
| dist of layer from top | 16.5 mm |
| trans reinf. Top 3mm mesh | 0.141 mm ² /mm |
| reinf. Parameter | 0.082 |
| dist of layer from top | 5.5 mm |
| trans reinf bot 3mm mesh | 0.141 mm ² /mm |
| reinf para | 0.082 |
| dist of layer from top | 19.5 |

Moment capacity can be derived from equation 3.80, in all cases for the long. and transverse yield lines; strain rates are limited to normal strain and rotation only

| | | |
|--|----------------|------------------|
| longitudinal sagging & hogging moment mid span | $\rho = 0.44$ | $d = 12.5 - 8.5$ |
| longitudinal sagging & hogging moment support | $\rho = 0.26$ | $d = 12.5 - 8.5$ |
| transverse sagging & hogging moment | $\rho = 0.082$ | $d = 12.5 - 5.5$ |

| | |
|--|--------------|
| long. sagg yield moment of bott flange mid span= | 3000 N-mm/mm |
| long. hogg yield moment of bottom flange mid span= | 3000 N-mm/mm |
| long. sagg yield moment of bottom flange support= | 1780 N-mm/mm |
| long. hogg yield moment of bottom flange support= | 1780 N-mm/mm |
| trans sagg yield moment of bottom flange= | 980 N-mm/mm |
| trans hogg yield moment of bottom flange= | 980 N-mm/mm |
| average for twisting moment by bottom flange near end span | 1990 N-mm/mm |
| average for twisting moment by bottom flange adj cont. support | 1380 N-mm/mm |

web yield hinge mid span and at support
(simplified calculation taking into account local equilibrium condition)

web reinforcement 3mm mesh each face

| | |
|--|------------------|
| effective flange width for web bending | 300 mm |
| effective bottom flange reinforcement yield force | 237.2 kN |
| effective top flange compression due to concrete | 256.5 kN |
| capacity of top flange steel in compression | 21 kN |
| effective top flange reinforcement in compression | -19.3 kN |
| average yield force due to web reinforcement | 28 kN |
| neutral axis depth for web resisting sagging moment | 23 mm |
| lever arm for moment calculation | 226 mm |
| effective bending capacity of web due to flange | 53.61 kN-m |
| additional bending capacity due to web reinforcement | 3.5 kN-m |
| total bending capacity due to web hinge | M_w 57.11 kN-m |

Internal work due to top flange longitudinal hinges

= transverse moment capacity M_c x average rotation of flange web hinge

= $M_c \times (1/b) / 2 \times 2 \times L$ (2 No. longitudinal hinge lines)

= $980 \times 1/b / 2 \times 2 \times 3500 / 1000000 = 0.0127 \text{ kN-m}$

Internal work due to top flange transverse hinge at mid span

= long. moment capacity M_c x average rotation of flange hinge at mid span

= $M_c \times (1/(L/2)) / 2 \times 2 \times b$ (1 No. transverse hinge)

= $560 \times 1750 / 2 \times 2 \times b / 1000000 = 0.0001 \text{ kN-m}$

Internal work due to top flange transverse hinge at support

= long. moment capacity M_c x average rotation of flange hinge at support

= $M_c \times (1/(L/2)) / 2 \times b$ (1 No. transverse hinge)

= $1780 \times 1 / 1750 / 2 \times b / 1000000 = 0.0001 \text{ kN-m}$

Internal work due to bottom flange longitudinal hinges

= total transverse moment capacity M_c x average rotation of flange web hinge

= $M_c \times (1/b) / 2 \times 2 \times L$ (2 No. longitudinal hinge lines)

= $980 \times 1/b / 2 \times 2 \times 3500 / 1000000 = 0.0127 \text{ kN-m}$

Internal work due to bottom flange transverse hinges at mid span

= long. moment capacity M_c x average rotation of flange hinge at mid span

= $M_c \times (1/(L/2)) / 2 \times 2 \times b$ (1 No. transverse hinge)

= $3000 / 1750 / 2 \times 2 \times b / 1000000 = 0.0005 \text{ kN-m}$

Internal work due to bottom flange transverse hinges at support

= long. moment capacity M_c x average rotation of flange hinge at cont. support

= $M_c \times (1/(L/2)) / 2 \times b$ (1 No. transverse hinge)

= $3000 / 1750 / 2 \times b / 1000000 = 0.0002 \text{ kN-m}$

internal work due to web hinge at mid span

= web moment capacity M_w x rotation of web hinge at mid span

= $M_w \times (1/(L/2)) \times 2$ (1 No. web hinge)

= $M_w \times 1 \times 2 / 3500 \times 2 = 0.0653 \text{ kN-m}$

internal work due to web hinge at cont. support

= web moment capacity M_w x rotation of web hinge at cont. support

= $M_w \times (1/(L/2))$ (1 No. web hinge)

= $M_w \times 1 \times 2 / 3500 = 0.0326 \text{ kN-m}$

twisting work due to top flange near end span and support

= total average yield moment x K x area

= Average $M_c \times (1/b/(L/2)) \times b \times (L/2) =$

= $(770+1990) \times (1/270/1750) \times 270 \times 1750 =$

0.0028 kN-m

twisting work due to bottom flange

= total average yield moment x K x area

= Average $M_c \times (1/b/(L/2)) \times b \times (L/2) =$

= $(1990+1380) \times (1/b/1750) \times b \times 1750 =$

0.0034 kN-m

Total internal work due to unit deflection

0.1304 kN-m

External work due to point load = $P \times 1\text{mm} / 1000$

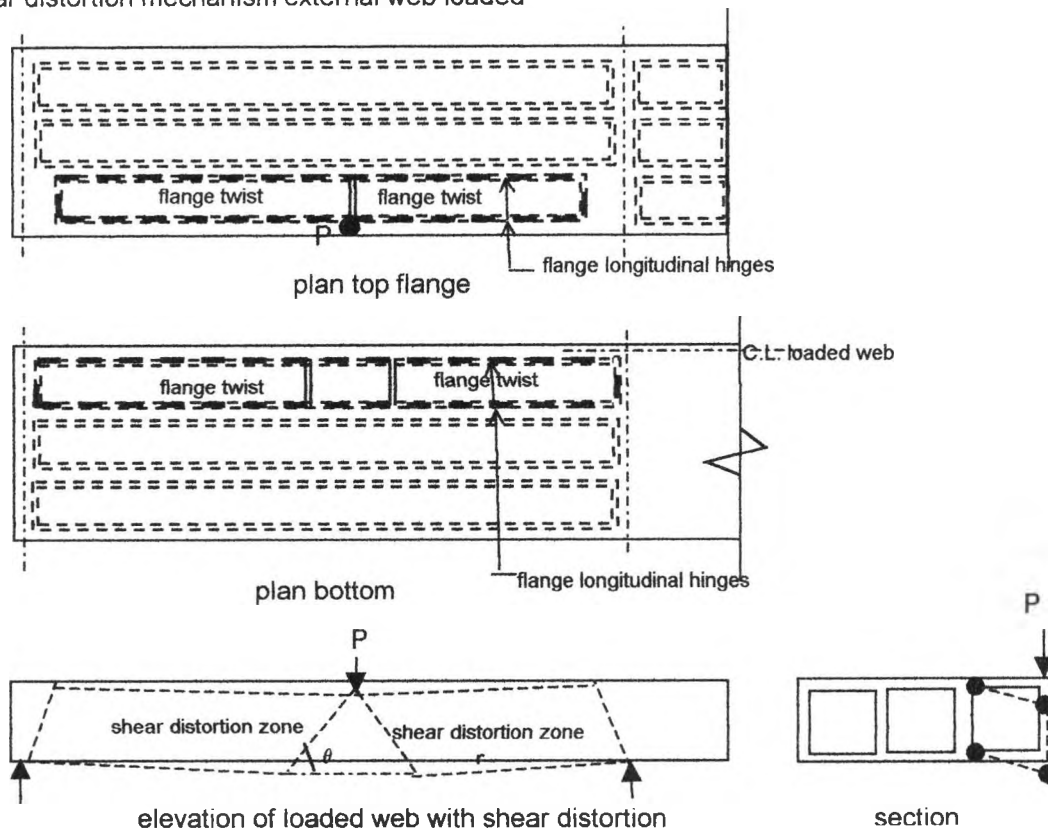
0.001P kN-m

equating Internal and external work

P=

130.4 kN

Shear distortion mechanism external web loaded



Internal work of web due to shear mechanism from equation 4.9-4.11

due to web reinforcement try $\theta = 45$ $r = 1500.00$
 $2 \times A_s \times F_y \times \cot \theta \times (1/r) \times h \times r$ 0.0700 kN-m

due to web in shear 0.0708 kN-m
 $2 \times \sigma_c / 2 \sin \theta \times (1 - \cos \theta) \times t \times (1/r) \times h \times r$

Internal work from top flange longitudinal hinges
 $= M_c \times 1/b / 2 \times 4 \times r$ (2 No. longitudinal hinge lines)
 $= 980 \times 1 / b / 2 \times 4 \times r / 1000000 = 0.010889 \text{ kN-m}$

transverse top hinge mid span
 $= M_c \times 1 / r / 2 \times b \times 2$
 $= 560 \times 1 / r / 2 \times 270 \times 2 / 1000000 = 0.000403 \text{ kN-m}$

transverse top hinge near end support and cont support
 $= M_c \times 1 / r / 2 \times b$
 $= (560 + 3000) \times 1 / r / 2 \times 270 / 1000000 = 0.00032 \text{ kN-m}$

Internal work from bottom flange longitudinal hinges
 $= M_c \times (4 \times r / b / 2 + 1 / b \times 2 \times h \times \cot \theta)$
 $= 980 \times (2 \times r / 270 + 1 / 270 \times 2 \times 250 \cot \theta) / 1000000 = 0.011242 \text{ kN-m}$

transverse hinges
 $= M_c \times (1 / r) / 2 \times 4 \times b$ (4 No. transverse hinge)
 $= (3000 + 1780) \times 1 / r / 2 \times 270 \times 2 / 1000000 = 0.00086 \text{ kN-m}$

twisting work due to top flange
 = average yield moment x K x area
 = Average $M_c \times (1/b/r) \times b \times r =$
 = $(770+1990) \times (1/270/r) \times 270 \times r =$ 0.00276 kN-m

twisting work due to bottom flange
 = average yield moment x K x area
 = Average $M_c \times (1/b/r) \times b \times r =$
 = $(1990+1380) \times (1/262/r) \times 270 \times r =$ 0.00337 kN-m

Total internal work due to unit deflection 0.1707 kN-m

External work due to point load = $P \times 1 \text{ mm} / 1000$ 0.001P kN-m

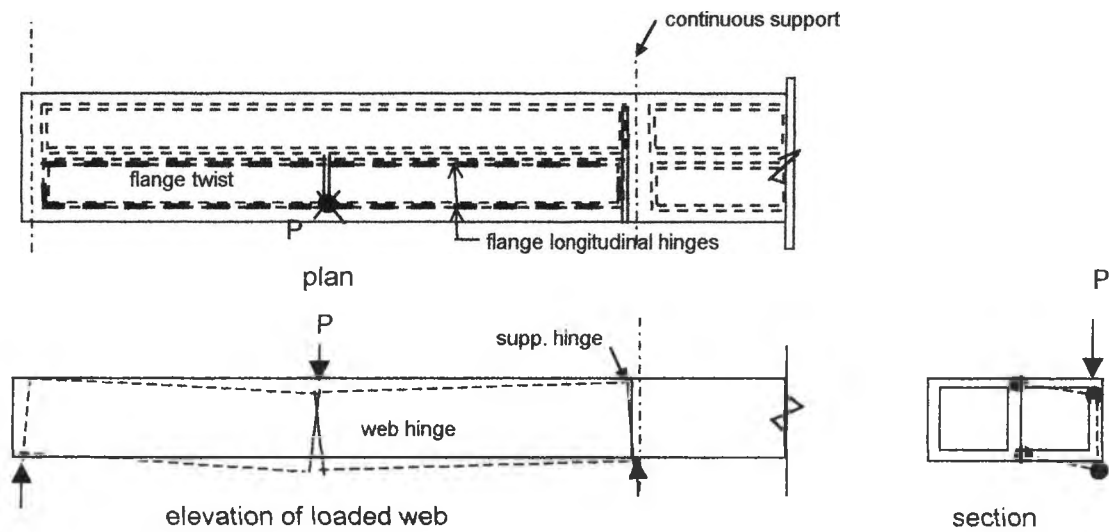
equating Internal and external work $P_{sd} =$ 170.7 kN

by numerical method, minimum occur when
 θ is about 50degrees $P_{sd} \text{ min} =$ 168.7 kN

With shear modification
 the shear capacity of web is reduced to
 $.55 \times 2 \times sc/2/\sin q \times (1 - \cos q) \times t \times (r) \times h \times r \times 1000$ 43.86 kN

modified collapse load
 $P' = P - 79.7 + 43.9$ $P_{sd}' \text{ min} =$ 132.90 kN

Beam B4 Two-cell prestressed continuous box beam external web loaded



No shear distortion mechanism

| | | | |
|--|----------|----------------------|----------|
| concrete strength pour compaction use 50% say | f_{cu} | 30 N/mm ² | |
| 3mm mesh yield force | F_{ym} | 3.5 kN/wire | 50mm c/c |
| 4mm add wire | F_{yw} | 6.1 kN/wire | 20mm c/c |
| prestressed wires 5mm 70% Ultimate 50% effective | F_p | 11.3 kN/wire | |
| flange width between fillets | b | 270 mm | |
| flange thickness | t_f | 25 mm | |
| web depth | d | 250 mm | |
| web thickness | t_w | 30 mm | |

top flange

| | | |
|--|--|---------------------------|
| long reinf. Top 3mm mesh mid span | | 0.141 mm ² /mm |
| reinf. Parameter | | 0.156 |
| dist of layer from top | | 8.5 mm |
| long reinf bot 3mm mesh mid span | | 0.141 mm ² /mm |
| reinf para | | 0.156 |
| dist of layer from top | | 16.5 mm |
| long reinf. Top 3mm mesh + 4mm support | | 0.47 mm ² /mm |
| reinf. Parameter | | 0.833 |
| dist of layer from top | | 8.5 mm |
| long reinf bot 3mm mesh | | 0.141 mm ² /mm |
| reinf para | | 0.083 |
| dist of layer from top | | 16.5 mm |
| trans reinf. Top 3mm mesh | | 0.141 mm ² /mm |
| reinf. Parameter | | 0.156 |
| dist of layer from top | | 5.5 mm |
| trans reinf bot 3mm mesh | | 0.141 mm ² /mm |
| reinf para | | 0.156 |
| dist of layer from top | | 19.5 mm |

Moment capacity can be derived from equation 3.80, in all cases for the long. and transverse yield lines; strain rates are limited to normal strain and rotation only

| | | |
|--|----------------|------------------|
| longitudinal sagging & hogging moment mid span | $\rho = 0.083$ | $d = 12.5 - 8.5$ |
| longitudinal sagging & hogging moment support | $\rho = 0.44$ | $d = 12.5 - 8.5$ |
| transverse sagging & hogging moment | $\rho = 0.083$ | $d = 12.5 - 5.5$ |

| | |
|---|--------------|
| long. sagg yield moment of top flange mid span= | 560 N-mm/mm |
| long. hogg yield moment of top flange mid span= | 560 N-mm/mm |
| long. sagg yield moment of top flange support= | 560 N-mm/mm |
| long. hogg yield moment of top flange support= | 3000 N-mm/mm |
| trans sagg yield moment of top flange= | 980 N-mm/mm |
| trans hogg yield moment of top flange= | 980 N-mm/mm |
| average for twisting moment by top flange near end span | 770 N-mm/mm |
| average for twisting moment by top flange adj cont. support | 1275 N-mm/mm |

bottom flange

| | |
|--|---------------------------|
| long reinf. Top 3mm mesh | 0.141 mm ² /mm |
| reinf. Parameter | 0.156 |
| dist of layer from top | 8.5 mm |
| long reinf bot 3mm mesh + 4.1mm wire mid span | 0.8 mm ² /mm |
| reinf para | 0.833 |
| dist of layer from top | 16.5 mm |
| long reinf. Top 3mm mesh near cont. support | 0.141 mm ² /mm |
| reinf. Parameter | 0.49 |
| dist of layer from top | 8.5 mm |
| long reinf bot 3mm mesh + 4.1mm near cont. support | 0.471 mm ² /mm |
| reinf para | 0.49 |
| dist of layer from top | 16.5 mm |
| trans reinf. Top 3mm mesh | 0.141 mm ² /mm |
| reinf. Parameter | 0.156 |
| dist of layer from top | 5.5 mm |
| trans reinf bot 3mm mesh | 0.141 mm ² /mm |
| reinf para | 0.156 |
| dist of layer from top | 19.5 |

Moment capacity can be derived from equation 3.80, in all cases for the long. and transverse yield lines; strain rates are limited to normal strain and rotation only

| | | |
|--|----------------|------------------|
| longitudinal sagging & hogging moment mid span | $\rho = 0.44$ | $d = 12.5 - 8.5$ |
| longitudinal sagging & hogging moment support | $\rho = 0.26$ | $d = 12.5 - 8.5$ |
| transverse sagging & hogging moment | $\rho = 0.082$ | $d = 12.5 - 5.5$ |

| | |
|--|--------------|
| long. sagg yield moment of bott flange mid span= | 3000 N-mm/mm |
| long. hogg yield moment of bottom flange mid span= | 560 N-mm/mm |
| long. sagg yield moment of bottom flange support= | 1780 N-mm/mm |
| long. hogg yield moment of bottom flange support= | 560 N-mm/mm |
| trans sagg yield moment of bottom flange= | 980 N-mm/mm |
| trans hogg yield moment of bottom flange= | 980 N-mm/mm |
| average for twisting moment by bottom flange near end span | 1380 N-mm/mm |
| average for twisting moment by bottom flange adj cont. support | 1825 N-mm/mm |

web yield hinge mid span and at support
(simplified calculation taking into account local equilibrium condition)

web reinforcement 3mm mesh each face

| | |
|--|----------------------|
| effective flange width for web bending | 300 mm |
| effective bottom flange reinforcement yield force | 127.4 kN |
| effective top flange compression due to concrete | 135 kN |
| capacity of top flange steel in compression | 21 kN |
| effective top flange reinforcement in compression | -7.6 kN |
| average yield force due to web reinforcement | 28 kN |
| prestressing force at 100, 175 and 200 from top | 22.6 kN |
| neutral axis depth for web resisting sagging moment | 8.5 mm |
| lever arm for moment calculation | 233 mm |
| effective bending capacity of web due to flange | 29.68 kN-m |
| additional bending capacity due to web reinforcement | 3.5 kN-m |
| additional bending capacity due to prestressing | 4.38 kN-m |
| total bending capacity due to web hinge | Mw 37.56 kN-m |

Internal work due to top flange longitudinal hinges

$$\begin{aligned}
 &= \text{transverse moment capacity } M_c \times \text{average rotation of flange web hinge} \\
 &= M_c \times (1/b) / 2 \times 2 L \quad (2 \text{ No. longitudinal hinge lines}) \\
 &= 980 \times 1/b / 2 \times 2 \times 3500 / 1000000 = 0.0127 \text{ kN-m}
 \end{aligned}$$

Internal work due to top flange transverse hinge at mid span

$$\begin{aligned}
 &= \text{long. moment capacity } M_c \times \text{average rotation of flange hinge at mid span} \\
 &= M_c \times (1/(L/2)) / 2 \times 2 \times b \quad (1 \text{ No. transverse hinge}) \\
 &= 560 \times 1750 / 2 \times 2 \times b / 1000000 = 0.0001 \text{ kN-m}
 \end{aligned}$$

Internal work due to top flange transverse hinge at support

$$\begin{aligned}
 &= \text{long. moment capacity } M_c \times \text{average rotation of flange hinge at support} \\
 &= M_c \times (1/(L/2)) / 2 \times b \quad (1 \text{ No. transverse hinge}) \\
 &= 3000 \times 1 / 1750 / 2 \times b / 1000000 = 0.0002 \text{ kN-m}
 \end{aligned}$$

Internal work due to bottom flange longitudinal hinges

$$\begin{aligned}
 &= \text{total transverse moment capacity } M_c \times \text{average rotation of flange web hinge} \\
 &= M_c \times (1/b) / 2 \times 2 L \quad (2 \text{ No. longitudinal hinge lines}) \\
 &= 980 \times 1/b / 2 \times 2 \times 3500 / 1000000 = 0.0127 \text{ kN-m}
 \end{aligned}$$

Internal work due to bottom flange transverse hinges at mid span

$$\begin{aligned}
 &= \text{long. moment capacity } M_c \times \text{average rotation of flange hinge at mid span} \\
 &= M_c \times (1/(L/2)) / 2 \times 2 \times b \quad (1 \text{ No. transverse hinge}) \\
 &= 3000 / 1750 / 2 \times 2 \times b / 1000000 = 0.0005 \text{ kN-m}
 \end{aligned}$$

Internal work due to bottom flange transverse hinges at support

$$\begin{aligned}
 &= \text{long. moment capacity } M_c \times \text{average rotation of flange hinge at cont. support} \\
 &= M_c \times (1/(L/2)) / 2 \times b \quad (1 \text{ No. transverse hinge}) \\
 &= 560 / 1750 / 2 \times b / 1000000 = 0.0002 \text{ kN-m}
 \end{aligned}$$

internal work due to web hinge at mid span

$$\begin{aligned}
 &= \text{web moment capacity } M_w \times \text{rotation of web hinge at mid span} \\
 &= M_w \times (1/(L/2)) \times 2 \quad (1 \text{ No. web hinge}) \\
 &= M_w \times 1 \times 2 / 3500 \times 2 = 0.0429 \text{ kN-m}
 \end{aligned}$$

internal work due to web hinge at cont. support

$$= \text{web moment capacity } M_w \times \text{rotation of web hinge at cont. support}$$

$$= Mw \times (1/(L/2)) \quad (1 \text{ No. web hinge})$$

$$= Mw \times 1 \times 2 / 3500 = 0.0215 \text{ kN-m}$$

twisting work due to top flange near end span and support

$$= \text{total average yield moment} \times K \times \text{area}$$

$$= \text{Average } M_c \times (1/b/(L/2)) \times b \times (L/2) =$$

$$= (770+1275) \times (1/270/1750) \times 270 \times 1750 = 0.0020 \text{ kN-m}$$

twisting work due to bottom flange

$$= \text{total average yield moment} \times K \times \text{area}$$

$$= \text{Average } M_c \times (1/b/(L/2)) \times b \times (L/2) =$$

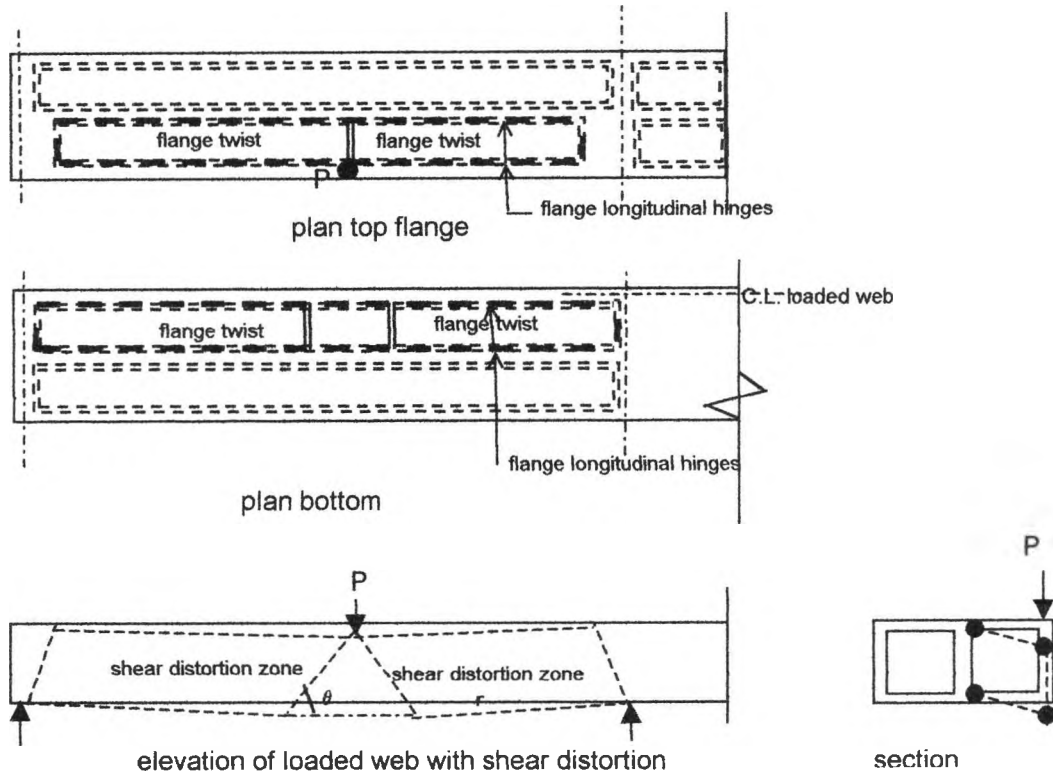
$$= (1380+1825+1380) \times (1/b/1750) \times b \times 1750 = 0.0032 \text{ kN-m}$$

$$\text{Total internal work due to unit deflection} = 0.0961 \text{ kN-m}$$

$$\text{External work due to point load} = P \times 1 \text{ mm} / 1000 = 0.001P \text{ kN-m}$$

$$\text{equating Internal and external work} \quad P = \quad \mathbf{96.1 \text{ kN}}$$

Shear distortion mechanism external web loaded



Internal work of web due to shear mechanism from equation 4.9-4.11

| | | | | |
|---|----------------|----|-------|-------------|
| due to web reinforcement | try $\theta =$ | 45 | $r =$ | 1500.00 |
| $2 \times A_s \times F_y \times \cot \theta \times (1/r) \times h \times r$ | | | | 0.0700 kN-m |
| due to prestressing wire | | | | |
| $2 \times (A_p \times F_y \times \sin \theta \times \cos \theta) \times \cot \theta \times 1/r \times h \times r$ | | | | 0.0339 kN-m |
| due to web in shear | | | | |
| $2 \times \sigma_c / 2 / \sin \theta \times (1 - \cos \theta) \times t \times (1/r) \times h \times r$ | | | | 0.0373 kN-m |

Internal work from top flange longitudinal hinges
 $= M_c \times 1/b / 2 \times 4 \times r \times (2 \text{ No. longitudinal hinge lines})$
 $= 980 \times 1/b / 2 \times 4 \times r / 1000000 = 0.010889 \text{ kN-m}$

transverse top hinge mid span
 $= M_c \times 1/r / 2 \times b \times 2$
 $= 560 \times 1/r / 2 \times 270 \times 2 / 1000000 = 0.000403 \text{ kN-m}$

transverse top hinge near end support and cont support
 $= M_c \times 1/r / 2 \times b$
 $= (560 + 3000) \times 1/r / 2 \times 270 / 1000000 = 0.00032 \text{ kN-m}$

Internal work from bottom flange longitudinal hinges
 $= M_c \times (4 \times r / b / 2 + 1/b \times 2 \times h \times \cot \theta)$
 $= 980 \times (2 \times r / 270 + 1/270 \times 2 \times 250 \cot \theta) / 1000000 = 0.011242 \text{ kN-m}$

transverse hinges
 $= M_c \times (1/r) / 2 \times 4 \times b \times (4 \text{ No. transverse hinge})$
 $= (560 + 1780) \times 1/r / 2 \times 270 \times 2 / 1000000 = 0.000421 \text{ kN-m}$

twisting work due to top flange
 = average yield moment x K x area
 = Average $M_c \times (1/b/r) \times b \times r =$
 = $(770+1990) \times (1/270/r) \times 270 \times r =$ 0.00276 kN-m

twisting work due to bottom flange
 = average yield moment x K x area
 = Average $M_c \times (1/b/r) \times b \times r =$
 = $(1990+1380) \times (1/262/r) \times 270 \times r =$ 0.00337 kN-m

Total internal work due to unit deflection 0.1706 kN-m

External work due to point load = $P \times 1\text{mm} / 1000$ 0.001P kN-m

equating Internal and external work $P_{sd} =$ 170.6 kN

by numerical method, minimum occur when θ is about 84degrees
 $P_{sd} \text{ min} =$ 121.6 kN

With shear modification
 the shear capacity of web is reduced to
 $.55 \times 2 \times sc/2/\sin q \times (1-\cos q) \times t \times (r) \times h \times r \times 1000$ 44.60 kN

modified collapse load
 $P' = P - 81 + 44.6$ $P_{sd}' \text{ min} =$ 85.20 kN

Appendix C Further Literature Review

A further research of literature has been conducted to review more recent design and research development in shear, yield criteria in reinforced concrete and box girder design.

Although there were a lot of research work on shear in concrete in recent years, most dealt with deep beam shears and punching shears. No significant development has been made on the aggregate size effect on shear.

Bortolli L (1990) presented a theoretical solution for the punching shear strength of concrete slab assuming rigid plastic material and theory of plasticity. He included the effect strain softening in tension as well as compression in concrete during failure to obtain a minimum upper bound solution.

Tan, Kong and Weng (1997) studied the shear strength characteristic of deep beams reinforced with different patterns of web reinforcement in which the ultimate shear strength of various tests were found to be independent of the loading condition imposed on the beams.

Morgan, Niwa and Tanabe (1997) studied the size effect in flexure and shear strength for different concrete and reinforced concrete beam sizes subjected to various loading conditions. They successfully predicted the behaviour of the model after cracking using non-linear fracture mechanics through their constitutive model to simulate the crack paths and the localised crack zones.

On the yield criterion of concrete, Labbane, Saha and Ting (1993) tried to develop a rational plasticity based numerical model for the response and failure load prediction of concrete structures. They used a computer model and finite element technique to evaluate the effect of yield criterion and loading function on several plasticity fracture models. They have established the importance of accurately modelling the stress-strain relationship in predicting structural failure.

Ashour and Morley (1994) used a numerical technique to predict upper bound collapse load for concrete beams in

shear. They used a modified Coulomb failure criterion and assuming a rigid-perfectly plastic material with tension cut-off. By varying the geometry of the yield lines, rigid moving non-yielding regions and plastic zones, a minimum collapse load for the assumed mechanism could be developed. It could be used to improve the prediction of collapse load contributed by the webs in the box beam involving similar yield mechanism.

Feenstra and De Borst (1996) used a composite yield function to describe the behaviour of plain and reinforced concrete in biaxial stress under monotonic loading condition. They used different criteria to describe the tension and compression condition. This elasto-plastic approach is extremely useful for the numerical analysis and to predicting the elastic-plastic behaviour of reinforced concrete structures. It is interesting that their approach is quite similar to that proposed by the author in Chapter 7 as a recommendation for future work.

Bensalem and Bhatt (1996) presented a yield criteria for reinforced concrete in plate structure. Using the technique of non-linear finite element program and an elasto-plastic material assumption, they predicted the collapse behaviour of three reinforced concrete deep beams and found that their experimental and theoretical values were in good agreement.

Beeby (1997) described the possibility of a lower ductility in reinforcement than the general assumed view. He described the shear bond-slip characteristic of reinforcement in reinforced concrete and how it could affect the ductility assumption of tensile reinforcement. It is interesting to note that unless the bond between concrete and reinforcement can be fully developed, the limit strength would not be governed by the yield strength of reinforcement but the shear bond-slip strength between the surface of the two constituent materials. In area where reinforcement laps are not confined by link reinforcement, bond-slip strength may be more appropriate. It would be interesting to study and compare the effect of using different aggregate including micro concrete on the bond slip behaviour. The bond slip surface for a strong aggregate concrete would likely to

be rougher than that using a micro concrete. For micro concrete the residual shear strength could affect the bond-slip strength in determining yield forces in reinforcement for such models.

There were a considerable amount of experimental and theoretical work carried out on box girders, most deal with elastic methods of analysis whilst some also studied the ultimate collapse condition.

Dansei and Edwards (1982) studied the behaviour of three large-scale prestressed segmental bridge models of deformable cross section. These models were tested in service load conditions under concentric and eccentric loading. They used finite element method and modified simple beam theory to predict the deflections and stresses in the section with good correlation.

Perry, Waldron and Pinkley (1985) designed and constructed a 1:12 scale concrete model of a four lane carriageway bifurcated junction. It was of typical single and double box girder construction highly curved on plan with cantilever extending from both edges. The highly complex prestressed model was made up of up to 11 different segments. It described the difficulties in the construction and instrumentation of the model. In an accompanying paper, Pinkney, Perry and Waldron (1985) presented the results for the elastic loading tests as well as an ultimate load test. The elastic test results compared well with established grillage analysis and thin wall beam theory. The collapse behaviour under increasing uniform load showed a sudden explosive collapse after sustaining almost four times the normal dead load intensity. Such collapse behaviour is typical of prestressed boxes that have lower ductility as a result of prestressing.

Kermani and Waldron (1993) studied the behaviour of single-cell box girder bridge models with deformable cross section. They developed a method of elastic analysis based on finite element and stiffness approach. Their experimental results compared well with theoretical prediction.

Yang and Fu (1997) developed a new torsional analysis method for multicell box based on the Softened Truss Model Theory. This elastic method models the shear and torsional effect associated with straight multi-cell box beams.

Additional Reference:

Ashour A, Morley C (1994) The numerical determination of Shear Failure Mechanisms in reinforced concrete beams. The Structural Engineer (UK), Vol. 72 No 23 & 24 Dec 1994, pp 395-400

Beeby A (1997) Ductility in reinforced concrete: why is needed and how is it achieved. The Structural Engineer (UK), Vol. 75, No. 18, 1997

Bensalem A, Bhatt P (1996) Yield Criteria for Reinforced Concrete under Plane Stress. Advances in analysis and Design of Composites, Publ. Civil Comp Press (GB), 1996, pp137-142.

Dansei R F, Edwards A D (1982) Bending torsion and distortion of prestressed concrete box beams of deformable cross section: a comparison of experimental and theoretical results. Proceeding Institution of Civil Engineers Pt 2 Vol 73, Dec. 1982.

Feenstra P H and De Borst R. (1996) A composite Plasticity model for concrete. International Journal of Solids and Structures (UK), Vol. 33, No. 5, Feb 1996, pp. 707-730.

Kermani B and Waldron P (1993) Behaviour of concrete box girder bridges of deformable cross-section. Proceeding of Institution of Civil Engineers, Struct. & bldgs, Vol. 99 May 1993.

Labbane M, Saha N K, Ting EC (1993) Yield Criterion and Loading Function for Concrete Plasticity. International J Solids & Struct. (UK), Vol. 30, No. 9, 1993, pp1269-1288.

Morgan A, Niwa J and Tanabe T (1997) Detecting the size effect in concrete beams using non-linear fracture mechanics. Engineering Structures (GB) Vol. 19 No 8 Aug 1997 pp605-616

Perry S H, Waldron P and Pinkney M (1985) Design and construction of a model prestressed concrete bifurcated box girder bridge. Proceeding of Institution of Civil Engineers, Pt 2 Vol. 79 Sept 85.

Pinkney M, Perry S and Waldron P (1985). Elastic analysis and experimental behaviour to collapse of a 1:12 scale prestressed concrete bifurcated bridge. Proceeding of Institution of Civil Engineers, Pt 2 Vol. 79 Sept 85.

Yang D, Fu C. (1997) Torsional Analysis for Multiple box cells using soften-truss model. Structural Engineering and Mechanics (Korea) Vol. 5, No 1, 1997, pp 21-32